Physico-chemical and Toxicological Characterization of Regulated and Unregulated Emissions of Diesel and Advanced Dual-fuel Engines

A Thesis Submitted

In Partial Fulfillment of the Requirements

for the Degree of

Doctor of Philosophy

by

Neeraj Kumar Yadav 2018MEZ0024



DEPARTMENT OF MECHANICAL ENGINEERING INDIAN INSTITUTE OF TECHNOLOGY ROPAR

July 2024

Copyright © "Year" by Indian Institute of Technology Ropar

DEDICATED

TO

FAMILY AND FRIENDS

DECLARATION

I hereby declare that the work which is being presented in the thesis entitled "Physico-chemical

and Toxicological Characterization of Regulated and Unregulated Emissions of Diesel and

Advanced Dual-fuel Engines" has been solely authored by me. It presents the result of my own

independent investigation/research conducted during the time period from January 2019 to July

2024 under the supervision of Dr. Rakesh Kumar Maurya, Associate Professor Department of

Mechanical Engineering IIT Ropar. To the best of my knowledge, it is an original work, both in

terms of research content and narrative, and has not been submitted or accepted elsewhere, in part

or in full, for the award of any degree, diploma, fellowship, associateship, or similar title of any

university or institution. Further, due credit has been attributed to the relevant state-of-the-art and

collaborations (if any) with appropriate citations and acknowledgments, in line with established

ethical norms and practices. I also declare that any idea/data/fact/source stated in my thesis has not

been fabricated/ falsified/ misrepresented. All the principles of academic honesty and integrity

have been followed. I fully understand that if the thesis is found to be unoriginal, fabricated, or

plagiarized, the Institute reserves the right to withdraw the thesis from its archive and revoke the

associated Degree conferred. Additionally, the Institute also reserves the right to appraise all

concerned sections of society of the matter for their information and necessary action (if any). If

accepted, I hereby consent to my thesis to be available online in the Institute's Open Access

repository, inter-library loan, and the title & abstract to be made available to outside organizations.

Signature

Name: Neeraj Kumar Yadav

Roll ID: 2018MEZ0024

Date: July 2024

٧

ACKNOWLEDGMENTS

First and foremost, I would like to express my sincere gratitude to my PhD advisor, Dr. Rakesh Kumar Maurya, Associate Professor, Department of Mechanical Engineering, IIT Ropar, for his continuous support, patience, and guidance throughout my research journey. His insightful feedback and encouragement have been invaluable to my research and the completion of this thesis. I am deeply thankful to the members of my dissertation committee, Dr. Ekta Singla (Chairperson), Dr. Himanshu Tyagi, Dr. Ranjan Das, and Dr. S.C. Martha, for their time, effort, and their valuable suggestions during the semester evaluations. Their contributions have significantly improved my work.

I extend my gratitude to my colleagues in the Advanced Engine and Fuel Research Lab (AEFRL) at IIT Ropar. Their camaraderie, collaboration, and support made my PhD experience enjoyable and enriching. Special thanks to Dr. Mohit Raj Saxena, Dr. Ajay Singh, Dr. Sahil Rana, Ratnesh Yadav and Saket Kumar for their assistance during experimentation. I would also like to extend my heartfelt gratitude to my friends, whose support and companionship have been a source of strength throughout my PhD journey. Special thanks to Neha, Gopal, Vivek, Raushan, Anand, Rakesh, Mainak, Amit, Suraj, Devendra, Dilip, Harsh, Praveen, Akhilesh and Nitish for their encouragement, understanding, and for providing much-needed breaks and laughter.

I am profoundly grateful to my parents, Jeetani Devi and my late father, Indradeo Yadav. Your unwavering support, endless love, and sacrifices have been the foundation of my success. Words cannot express how much your belief in me has meant throughout this journey. Thank you for always being my pillars of strength and for instilling in me the values of perseverance and dedication. I hope to make you proud. To my dear sisters and brothers, Mandakini, Anupma, Sunidhi, Narendra, Jainendra and Gyanendra your constant encouragement, understanding, and love have been my greatest motivation. You have celebrated my achievements and lifted me up during the challenging times. I am blessed to have such a wonderful family, and I dedicate this accomplishment to all of you. Finally, I want to thank all the individuals and organizations who have indirectly contributed to my research. Your support has been greatly appreciated. I extend my gratefulness to IIT Ropar fraternity for providing me with such a wonderful environment to work and grow.

CERTIFICATE

This is to certify that the thesis entitled "Physico-chemical and Toxicological Characterization of Regulated and Unregulated Emissions of Diesel and Advanced Dual-fuel Engines" submitted by Neeraj Kumar Yadav (2018MEZ0024) for the award of the degree of Doctor of Philosophy of Indian Institute of Technology Ropar, is a record of bonafide research work carried out under our guidance and supervision. To the best of my knowledge and belief, the work presented in this thesis is original and has not been submitted, either in part or full, for the award of any other degree, diploma, fellowship, associateship or similar title of any university or institution.

In our opinion, the thesis has reached the standard fulfilling the requirements of the regulations relating to the degree.

Dr. Rakesh Kumar Maurya

Associate Professor, Department of Mechanical Engineering

Indian Institute of Technology, Ropar

LAY SUMMARY

The transportation sector is crucial to modern society as it facilitates the movement of goods, people, and services. Currently, a significant portion of the transport sector relies on internal combustion engines (ICEs) fueled with petroleum-based fossil fuels. As the world population grows and lifestyles geared towards easy accessibility, the demand for vehicles is increasing significantly. The increased number of vehicles leads to a rise in local and global air pollution, climate change and depletion of fossil fuel resources. The increased vehicular air pollution forces government bodies to implement stringent emission norms. Because of these associated challenges, there is growing adoption of high-efficiency advanced combustion engines and renewable low and zero-carbon alternative fuels such as methanol and hydrogen in future technologies. However, the current engine technology is designed to run on fossil fuels and welloptimized conventional combustion strategies such as diesel and SI engines. Adopting alternative fuels and advanced combustion modes changes the combustion process inside the combustion chamber, leading to changes in the formation and emission of gas and particle phase engine emissions, which are chemically distinct from conventional combustion-emitted pollutants. Hence, before the widespread adoption of advanced combustion technology and alternative fuels in the market, it is essential to conduct a comprehensive analysis of emission species to predict their impact on human health and the environment. This study conducted a comparative comprehensive assessment of physical, chemical and toxicological characterization of engine exhaust emission of conventional and advanced dual fuel combustion engines fueled with conventional (diesel and gasoline) and low and zero carbon (methanol and hydrogen) alternative fuels. The study is conducted for both light-duty and heavy-duty applications. A light-duty single-cylinder diesel engine presently used as a mini truck in India was modified to operate in advanced dual-fuel mode by integrating a port fuel injection system with modification in the intake manifold. Numerical investigation was performed on a Cummins N-14 series research engine for heavy-duty application. This engine was simulated for conventional and hydrogen-diesel dual-fuel engines to predict the exhaust species and their chemical compositions. The study focused on regulated (emissions on which the government imposes norms) and unregulated (not regulated by the government) emissions and their effects on human health and environment.

The study found that adding methanol in advanced combustion engines reduces particle emission by mass and number compared to conventional diesel and gasoline-diesel advanced dual-fuel engines. The transition from conventional to methanol-diesel and gasoline diesel in an advanced dual fuel mode leads to higher emissions from unregulated species. Among all the unregulated species, the formaldehyde (cancer-causing pollutant) emission was highest in methanol-diesel dual fuel. The particle retention in the human lung region due to inhalation was lowest in the methanol-diesel advanced dual fuel compared to conventional and gasoline-diesel dual fuel. The unregulated emissions were lower than low load operations at moderate engine load operations. The addition of hydrogen in diesel engines significantly reduces the toxicity potential. The study concludes that adding methanol and hydrogen as alternative fuels in diesel engines significantly reduces inhalation particle toxicity, cytotoxicity, global warming potential, acidification potential, and eutrophication potential at moderate load conditions. However, the cancer risk potential associated with formaldehyde emissions is higher in methanol-diesel dual fuel mode than other combustion modes. The study highlights the need for after-treatment devices to mitigate formaldehyde emissions to fully realize human health and environmental benefits.

Abstract

At present, the transportation sector predominantly utilizes conventional engines fueled by petroleum-based fossil fuels. However, with concerns over decreasing fossil fuel reserves, stringent emission norms, energy security, and the adverse environmental impact of combustiongenerated pollutants and carbon-containing compound emissions, there is a growing momentum towards adopting low-carbon alternative fuels and advanced combustion mode engine technologies. Before adopting new engine technologies and alternative fuels, assessing their potential adverse effects on human health and the environment is essential. Introducing alternative fuels or advanced dual fuel combustion methods alters the combustion processes within the engine, leading to changes in the exhaust species formation and emission characteristics compared to conventional fuels and combustion modes. Analyzing the physical and chemical properties of regulated and unregulated emissions provides a better estimate and more precise understanding of their impact on human health and the environment. The present study aims to ensure that emerging technologies support environmental goals and safeguard public health. This study is also in accordance with the US-EPA charter that states that any new technology must not emit more toxic pollutants than existing ones. Experimental and numerical investigations are conducted to meet the proposed objectives. The experimental investigation was conducted on a single-cylinder automotive diesel engine representing light-duty applications. The engine was modified to run on advanced dual-fuel combustion mode utilizing gasoline and methanol as low reactive fuel and diesel as high reactive fuel. To modify the conventional engine to operate in advanced dual fuel mode, the intake port is modified to install a port fuel injection system to deliver low-reactive fuel during the intake stroke. Numerical investigation was done on an experimentally validated Cummin N-14 series engine for heavy-duty applications, using diesel and hydrogen-diesel dualfuel modes. A detailed reaction mechanism is used to predict the exhaust emission species for hydrogen-diesel dual-fuel combustion in numerical simulation.

Regulated and unregulated gas phase emissions were measured using an AVL-manufactured FTIR emission analyzer. Nanoparticle emissions were measured using a DMS 500 (Manufacturer: CAMBUSTION) particle analyzer. For the physicochemical and toxicological characterization of PM samples, the aggregate PM sample was collected in a partial flow dilution tunnel using a preconditioned filter paper. The physical characterization of PM emission includes nanoparticle size

distribution, number concentration, mass distribution, and aggregate PM surface morphology analysis using SEM imaging. Chemical characterization encompasses gas phase unregulated (saturated, unsaturated, carbonyl and aromatic) emissions, soluble organic fractions associated with PM, and traces of heavy metals in the PM samples.

The study found that methanol-diesel dual fuel (MD-RCCI) combustion mode reduces total particle number (TPN), nucleation mode particle number (NMPs) and accumulation mode particle number (AMPs) emissions significantly compared to conventional diesel combustion (CDC) and gasoline-diesel dual fuel (GD-RCCI) mode. The concentration of nucleation mode particles (NMPs) decreases as engine load increases, while accumulation mode particles (AMPs) increase for both CDC and MD-RCCI combustion modes. With increased fuel premixing ratio (RP), the NMPs in the MD-RCCI and gasoline diesel dual fuel GD-RCCI engines are increased. The chemical characterization results found that as the combustion mode transitioned to the RCCI, the saturated, unsaturated, carbonyl, aromatic (toluene) and soluble organic fraction emissions increases. Formaldehyde emissions are observed to be highest in MD-RCCI engines. The metal trace emission is significantly lower in RCCI than in CDC. The forecast for lung loading reveals that nanoparticles emitted by the CDC show a higher lung retention than MD-RCCI. RCCI combustion demonstrates lower lung retention in all tested conditions compared to CDC. The lung loading of particles of MD-RCCI decreases significantly with an increase in the premixing ratio for a constant load compared to GD-RCCI. The MD-RCCI engine shows higher cancer risk potential at a lower engine load than CDC and GD-RCCI engines due to higher formaldehyde emissions. Interestingly, cytotoxicity potential varies with engine load; medium engine loads decrease toxicity potential in MD-RCCI engines but increase it in GD-RCCI and CDC engines. PM cytotoxicity increases with increased RP in both RCCI engine types. Methanol reduces cytotoxicity and particle inhalation toxicity at medium engine load. The transitions of combustion mode from CDC to RCCI significantly decrease global warming, acidification, eutrophication and ozone-forming potential. Adding hydrogen in diesel engines decreases the carcinogenicity and mutagenicity potential under all the simulated conditions. Alternative fuels such as methanol and hydrogen have the potential of enhancing environmental sustainability and public health. However, careful consideration and additional exhaust after-treatment are essential to fully realize the benefit of the MD-RCCI engine across all operational conditions.

List of Publication

- 1. **Neeraj Kumar Yadav**, Mohit Raj Saxena and Rakesh Kumar Maurya, "Inhalation Toxicity Characterization of Nanoparticle and Carbonyl Emission from Conventional Diesel and Methanol/Gasoline-Diesel RCCI Engine". **Fuel**
- 2. **Neeraj Kumar Yadav** and Rakesh Kumar Maurya. "Experimental Investigation on Metal, PM and Unregulated Emissions Along with their Toxicity from Conventional Diesel and RCCI Engines Employing Gasoline and Methanol as Low Reactivity Fuels" **Fuel**
- 3. **Neeraj Kumar Yadav** and Rakesh Kumar Maurya, "Numerical Investigation on Hydrogen Enrichment and EGR on In-Cylinder Soot and NOx Formation in Dual-Fuel CI-Engine", SAE 2024-01-2098, **SAE Technical Paper** 2024. [Link].
- 4. **Neeraj Kumar Yadav**, Mohit Raj Saxena and Rakesh Kumar Maurya, "Environmental and cancer risk potential assessment of unregulated emissions from Methanol-Diesel dual fuel engine", SAE 2024-26-0152, **SAE Technical Paper** 2024. [Link]
- Neeraj Kumar Yadav, Mohit Raj Saxena and Rakesh Kumar Maurya, "Numerical Investigation for carcinogenicity and mutagenicity potential of PAHs emitted from hydrogen/diesel dual-fuel engine" SAE 2023-32-0049 SAE Technical Paper 2023 [Link].
- 6. **Neeraj Kumar Yadav**, Mohit Raj Saxena, and Rakesh Kumar Maurya, "A Review of Toxicity analysis of particulate emissions from conventional and advanced low-temperature combustion engines", SAE 2021-01-0617, **SAE Technical Paper** 2021. [Link].
- 7. **Neeraj Kumar Yadav**, Mohit Raj Saxena, and Rakesh Kumar Maurya. Numerical Investigation on Toxicity Potential of PAHs Emitted from Hydrogen-Diesel Fueled Dual-Fuel Engine (**under review**)
- 8. **Neeraj Kumar Yadav** and Rakesh Kumar Maurya. Risk Assessment of Particle and Gaseous Emissions from Diesel and Methanol-Diesel Advanced Dual-Fuel Engines (**Under review**)
- 9. **Neeraj Kumar Yadav**, Rakesh Kumar Maurya and Vatan Chawla. Toxicological Assessment of Particulate and Unregulated Emissions from Methanol and Gasoline Fueled Reactivity Controlled Compression Ignition Engines (**under review**)

Table of Contents:

DECLARATION	V
ACKNOWLEDGMENTS	VI
CERTIFICATE	VII
LAY SUMMARY	VIII
ABSTRACT	X
LIST OF PUBLICATION	XII
LIST OF FIGURES	XIX
LIST OF TABLES	XXII
CHAPTER 1:	1
INTRODUCTION	1
1.1 MOTIVATION FOR ENGINE RESEARCH	2
1.1.1 ENVIRONMENTAL AND HEALTH IMPLICATIONS	3
1.1.2 EMISSION REGULATIONS	5
1.1.3 FUEL CHALLENGES	7
1.2 CONVENTIONAL AND ADVANCED DUAL-FUEL ENGINES	7
1.2.1 CONVENTIONAL DIESEL ENGINE	7
1.2.2 ADVANCED DUAL-FUEL ENGINE	11
1.3 AUTOMOTIVE FUELS	14

1.2.1 DIESEL FUEL	15
1.2.2 GASOLINE FUEL	17
1.2.3 METHANOL FUEL	18
1.2.4 HYDROGEN FUEL:	21
1.4 ENGINE EMISSION	23
1.4.1 REGULATED EMISSION	23
1.4.1.1 THC EMISSION	23
1.4.1.2 CO EMISSIONS	24
1.4.1.3 NOX EMISSIONS	25
1.4.1.4 PM EMISSION	27
1.4.2 UNREGULATED EMISSIONS	29
1.4.2.1 SATURATED HC EMISSIONS	29
1.4.2.2 UNSATURATED HC EMISSIONS	30
1.4.2.3 CARBONYL COMPOUND EMISSION	30
1.4.2.4 AROMATIC EMISSION	31
1.5 PHYSICO-CHEMICAL AND TOXICOLOGICAL PROPERTIES OF ENGINE EMISSIONS	32
1.5.1 PHYSICO-CHEMICAL PROPERTIES	32
1.5.1.2 PARTICULATE MASS AND MORPHOLOGY	34
1513 SOLURI F ORGANIC FRACTION	34

1.5.1.4 HEAVY METAL EMISSION	34
1.5.2 TOXICOLOGICAL PROPERTIES	35
1.5.2.1 TOXICITY MECHANISM OF PM	36
1.5.2.2 MUTAGENICITY AND CYTOTOXICITY OF PM	37
1.5.2.3 LUNG RETENTION OF PM PARTICLES	39
1.5.3 ENVIRONMENTAL RISK FACTORS	39
1.5.3.1 GLOBAL WARMING POTENTIAL (GWP)	40
1.5.3.2 ACIDIFICATION POTENTIAL (ACP)	41
1.5.3.3 EUTROPHICATION POTENTIAL (EUP)	41
1.5.3.4 OZONE FORMING POTENTIAL (OFP)	42
1.6 MOTIVATION FOR THE PRESENT RESEARCH	42
1.7 MAIN GOAL AND OBJECTIVE OF THESIS	44
1.8 THESIS ORGANIZATION	45
CHAPTER 2 LITERATURE REVIEW	47
2.1 COMBUSTION AND EMISSION CHARACTERISTICS OF CONVENTIONAL AND DUAL FUEL ENGINES	47
2.1.1 COMBUSTION CHARACTERISTICS OF DIESEL AND DUAL FUEL ENGINES	48
2.1.2 REGULATED EMISSION CHARACTERISTICS	49
2.1.3 UNREGULATED EMISSIONS	56
2.2 PHYSICO-CHEMICAL CHARACTERISTICS OF DIESEL AND DUAL-FUEL ENGIN	NES 57

2.2.1 PARTICLE EMISSION CHARACTERISTICS	57
2.2.2 SOLUBLE ORGANIC FRACTION AND PAHS EMISSION	59
2.2.3 HEAVY METAL EMISSION	61
2.3 TOXICOLOGICAL CHARACTERISTICS OF DIESEL AND DUAL FUEL ENGINES	62
2.3.1 CYTOTOXICITY AND MUTAGENICITY OF PM AND GASEOUS EMISSIONS	64
2.3.2 NANOPARTICLE INHALATION TOXICITY	66
2.4 ENVIRONMENTAL RISK ASSESSMENT OF EMISSIONS	68
2.5 GAPS IN THE LITERATURE	68
CHAPTER 3	71
3.1 TEST SETUP AND INSTRUMENTATION	71
3.1.1 LIGHT-DUTY ENGINE SETUP	72
3.1.1.1 EXPERIMENTAL METHODOLOGY	72
3.1.1.2 IN-CYLINDER PRESSURE MEASUREMENT	78
3.1.1.3 COMBUSTION CHARACTERISTICS CALCULATIONS	80
3.1.1.4. EMISSION MEASUREMENTS	81
3.1.1.5 PARTICULATE SAMPLING METHODOLOGY	83
3.1.1.6 PHYSICO-CHEMICAL CHARACTERIZATION METHOD	86
3.1.1.7 TOXICOLOGICAL CHARACTERISTICS	9(
3.1.1.7.2 CARCINOGENICITY AND MUTAGENICITY CALCULATIONS	91
3 1 1 7 A ENVIRONMENTAL RISK ASSESSMENT	06

3.1.2 HEAVY DUTY ENGINE TEST SETUP	97
3.1.2.1 NUMERICAL METHODOLOGIES	98
3.1.2.1.1 GOVERNING EQUATIONS AND SIMULATION SETUP	98
3.1.2.1.2 COMPUTATIONAL DOMAIN, SUB MODELS AND OPERATING MATRIX	100
3.1.1.2.3 MODEL VALIDATION	105
3.1.3 UNCERTAINTY AND ACCURACY	108
3.1.3.1 UNCERTAINTY ANALYSIS OF COMBUSTION PARAMETERS	108
3.1.3.3 ACCURACY OF THE INSTRUMENTS	111
CHAPTER 4 RESULT AND DISCUSSION	113
4.1 COMBUSTION ANALYSIS	113
4.2 EMISSION ANALYSIS	120
4.2.1 REGULATED EMISSIONS	120
4.2.1.1 THC, CO AND NO_X EMISSION	121
4.2.1.2 PARTICULATE EMISSIONS	123
4.2.2 UNREGULATED EMISSION ANALYSIS	124
4.2.2.1 SATURATED HYDROCARBON EMISSIONS	124
4.2.2.2 UNSATURATED HYDROCARBON EMISSIONS	127
4.2.2.3 CARBONYL COMPOUND EMISSIONS	129
4.2.2.4 AROMATIC EMISSIONS	131
4.3 PHYSICO-CHEMICAL CHARACTERIZATION AND ANALYSIS	133

4.3.1 PARTICLE SIZE DISTRIBUTION	133
4.3.2 PARTICLE SIZE AND MASS LOBES	137
4.3.3 PARTICULATE VISUALIZATION AND MORPHOLOGY	139
4.4 TOXICOLOGICAL CHARACTERISTICS AND ANALYSIS	144
4.4.1 CYTOTOXICITY AND REACTIVE OXYGEN SPECIES ANALYSIS	144
4.4.2 CANCER RISK POTENTIAL DUE TO CARBONYL AND METAL EMISSIONS	146
4.4.3 CARCINOGENIC AND MUTAGENIC POTENTIAL DUE TO AROMATIC EMISS	ION 148
4.4.5 PM PARTICLE LUNG RETENTION ANALYSIS	149
4.5 ENVIRONMENTAL RISK ASSESSMENT	156
CHAPTER 5 CONCLUSIONS AND FUTURE SCOPE	161
5.1 REGULATED AND UNREGULATED EMISSION CHARACTERISTICS	161
5.2 PHYSICOCHEMICAL CHARACTERISTICS OF PM	162
5.3 TOXICOLOGICAL CHARACTERISTICS OF EMISSIONS	163
5.4 ENVIRONMENTAL RISK ASSESSMENT OF EMISSIONS	164
5.5 SOCIETAL IMPLICATIONS OF THE PRESENT WORK	165
5.6 FUTURE DIRECTIONS FOR RESEARCH	165
CHAPTER 6: REFERENCES	166

List of Figures

FIGURE 1.1: ENGINE EMISSION ADVERSE EFFECT ON HUMAN HEALTH AND THE ENVIRONMENT	4
FIGURE 1.2: HEAT RELEASE RATE DIAGRAM FOR A DIRECT INJECTION (DI) DIESEL ENGINE ILLUSTRATING THE DIST	ΓINCT
PHASES OF COMBUSTION.	
FIGURE 1.3 HEAT RELEASE RATE CURVE OF RCCI COMBUSTION [1.58]	13
FIGURE 1.4: SCHEMATIC REPRESENTATION OF PARTICULATE MATTER	28
FIGURE 1.5: PM PARTICLE CONSTITUENTS AND THEIR IMPACT ON ENVIRONMENT AND HUMAN HEALTH [1.78]	32
FIGURE 1.6 HYPOTHETICAL PATHWAY FOR PARTICLE-INDUCED OXIDATIVE STRESS AND DEATH OR HOSPITALIZATION	ON OF
CANCER AND CARDIOVASCULAR DISEASE [1.99].	37
FIGURE 1.7. THE PROCEDURE OF AMES TEST [1.100].	38
FIGURE 3.1 (A-D): ACTUAL IMAGES OF (A) SINGLE CYLINDER ENGINE, (B) DYNAMOMETER, (C) PORT-FUEL INJECT	ION
SYSTEM AND (D) CRDI SYSTEM.	74
FIGURE 3.2: MODIFIED INTAKE MANIFOLD OF THE ENGINE FOR CONDUCTING RCCI EXPERIMENTS	74
FIGURE 3.3: DIFFERENTIAL PRESSURE TRANSMITTER FOR FUEL AND AIR FLOW MEASUREMENTS	76
FIGURE 3.4: EXPERIMENTAL SET UP SCHEMATIC	78
FIGURE 3.5: (A) PRESSURE SENSOR, (B) PRESSURE SENSOR SLOT IN ENGINE HEAD AND (C) INSTALLED PRESSURE	
SENSOR.	79
FIGURE 3.6: WORKING PRINCIPLE OF DMS 500 [3.12]	
FIGURE 3.7: WORKING PRINCIPAL OF FTIR	
FIGURE 3.8. ACTUAL IMAGE OF DILUTION TUNNEL AND SAMPLING PROCESS.	85
FIGURE 3.9: MOISTURE REMOVAL BEFORE AND AFTER THE SAMPLING OF PM ON FILTER PAPER.	86
FIGURE 3.10: PHYSICAL CHARACTERIZATION METHOD.	
FIGURE 3.11: CHEMICAL CHARACTERIZATION METHOD	
FIGURE 3.12: ACTUAL SOXHLET EXTRACTOR IMAGE	
FIGURE 3.13: STEP BY STEP PROCEDURE TO DETERMINE THE SOLUBLE ORGANIC FRACTION	
FIGURE: 3.14: TOXICOLOGICAL CHARACTERIZATION OF EMISSIONS	
FIGURE 3.15: LUNG COMPARTMENT MODEL FOR THE DIESEL PARTICLE RETENTION [3.16]	94
FIGURE 3.16: SIMULATION PROCEDURE TO SET-UP THE SIMULATION CASE.	
FIGURE 3.17: DETAILED DESCRIPTION OF 450 SECTOR COMPUTATIONAL DOMAIN AT BDC (WITH 80,000 CELLS)	
FIGURE 3.18: DETAIL DESCRIPTION OF TEST CONDITIONS.	104
FIGURE 3.19: VALIDATION OF (A) IN-CYLINDER PRESSURE AND AHRR, (B) NORMALIZED SOOT [3.35], AND (C) GI	RID
INDEPENDENCE TEST FOR VARYING THE CELL SIZE (SHOWN NUMBERS ARE AT TDC)	106
FIGURE: 4.1 (A-D) EFFECT OF COMBUSTION MODE AND ENGINE LOAD ON IN-CYLINDER PRESSURE, HRR, CA ₁₀ , CA	
AND CA ₁₀₋₉₀ .	115
FIGURE 4.2 (A-D): EFFECT OF FUEL PREMIXING RATIO (RP) ON IN-CYLINDER PRESSURE, HRR, CA ₁₀ , CA ₅₀ AND CA	A_{10-90}
IN METHANOL DIESEL AND GASOLINE DIESEL RCCI ENGINES	116
FIGURE 4.3 (A-D): EFFECT OF HYDROGEN ENERGY SHARE AND ENGINE LOAD ON IN-CYLINDER PRESSURE, AVG.	
TEMPERATURE AND HRR.	119
FIGURE 4.4 (A, B): EFFECT OF HYDROGEN ENERGY SHARES ON IN-CYLINDER COMBUSTION OF H2 FUEL AND EVOL	UTION
OF OH RADICAL AT BOTH LOW AND MEDIUM LOAD CONDITIONS	120
FIGURE 4.5 (A-D): EFFECT OF ENGINE LOAD, COMBUSTION MODE AND RP ON THE EMISSION OF THC, CO AND NC) χ
FROM CDC AND RCCI COMBUSTION ENGINES, (E, F) EFFECT OF ENGINE LOAD AND HYDROGEN ENERGY SHA	ARE
ON THE EMISSION OF CO, NOX AND SOOT EMISSIONS.	
FIGURE 4.6 (A): EFFECT OF ENGINE LOAD, COMBUSTION MODE ON PM MASS EMISSION FROM CDC, MD-RCCI AT	
GD-RCCI ENGINES	124
FIGURE 4.7 (A-D): EFFECT OF ENGINE LOAD, COMBUSTION MODE AND RP ON SATURATED EMISSIONS FROM MD-F	RCCI
AND GD-RCCI ENGINES. (E) EFFECT OF HYDROGEN ENERGY SHARE ON THE EMISSION OF SATURATED HCs	FROM
HYDROGEN-DIESEL DUAL FUEL ENGINE	126

FIGURE 4.8 (A-D): EFFECT OF ENGINE LOAD, COMBUSTION MODE AND RP ON SATURATED EMISSIONS FROM MD-RCCI AND GD-RCCI ENGINES. (E) EFFECT OF HYDROGEN ENERGY SHARE ON THE EMISSION OF SATURATED HCS FROM HYDROGEN-DIESEL DUAL FUEL ENGINE
FIGURE 4.9 (A-D): EFFECT OF ENGINE LOAD, COMBUSTION MODE AND RP ON CARBONYL EMISSIONS FROM CDC, MD-RCCI AND GD-RCCI ENGINES. (E) EFFECT OF HYDROGEN ENERGY SHARE ON THE EMISSION OF CARBONYL
COMPOUNDS FROM HYDROGEN-DIESEL DUAL FUEL ENGINE.
FIGURE 4.10 (A, B): EFFECT OF ENGINE LOAD, COMBUSTION MODE AND RP ON TOLUENE EMISSIONS FROM CDC, MD-
RCCI AND GD-RCCI ENGINES. (C, D) EFFECT OF HYDROGEN ENERGY SHARE ON THE EMISSION OF PAHS FROM HYDROGEN-DIESEL DUAL FUEL ENGINE
FIGURE 4.11: (A) EFFECT OF ENGINE LOAD ON PARTICLE SIZE NUMBER DISTRIBUTION IN CDC ENGINE, (B) EFFECT OF
ENGINE LOAD ON PARTICLE SIZE NUMBER DISTRIBUTION IN MD-RCCI ENGINE, (C) EFFECT OF ENGINE LOAD ON
PARTICLE SIZE NUMBER DISTRIBUTION IN GD-RCCI ENGINE, (D) EFFECT OF PREMIXING RATIO (RP) ON PARTICLE SIZE NUMBER DISTRIBUTION IN MD-RCCI ENGINE, (E) EFFECT OF PREMIXING RATIO (RP) ON PARTICLE SIZE
NUMBER DISTRIBUTION IN GD-RCCI ENGINE
FIGURE 4.12: (A) EFFECT OF ENGINE LOAD ON TPN, NMPS AND AMPS NUMBER CONCENTRATION IN CDC ENGINE, (B)
EFFECT OF ENGINE LOAD ON TPN, NMPS AND AMPS NUMBER CONCENTRATION IN MD-RCCI ENGINE AND (C)
EFFECT OF ENGINE LOAD ON TPN, NMPS AND AMPS NUMBER CONCENTRATION IN GD-RCCI ENGINE (D)
EFFECT OF PREMIXING RATIO (RP) ON TPN, NMPS AND AMPS NUMBER CONCENTRATION IN MD-RCCI ENGINE
AND (E) EFFECT OF PREMIXING RATIO RP ON TPN, NMPS AND AMPS NUMBER CONCENTRATION IN GD-RCCI
ENGINE
FIGURE 4.13: (A) EFFECT OF ENGINE LOAD ON PARTICLE NUMBER AND MASS CORRELATION IN CDC, (B) EFFECT OF
ENGINE LOAD ON PARTICLE NUMBER AND MASS CORRELATION IN MD-RCCI (C) EFFECT OF ENGINE LOAD ON
PARTICLE NUMBER AND MASS CORRELATION IN GD-RCCI, AND (D) EFFECT OF PREMIXING RATIO (R_P) ON
PARTICLE NUMBER AND MASS CORRELATION IN MD-RCCI
FIGURE 4.14: IMAGES OF SAMPLED FILTER PAPER FOR CDC AND MD-RCCI COMBUSTION MODE140
FIGURE 4.15: SEM IMAGES OF PM SAMPLES FROM CDC, MD-RCCI AND GD-RCCI AT LOW AND MODERATE ENGINE
LOADS141
FIGURE 4.16 (A-D) INFLUENCE OF COMBUSTION MODE AND ENGINE LOAD ON THE EMISSION LEVELS OF NON-
CARCINOGENIC TRACE METALS
FIGURE: 4.17 (A-D) INFLUENCE OF COMBUSTION MODE AND ENGINE LOAD ON THE EMISSION LEVELS OF CARCINOGENIC TRACE METALS
FIGURE: 4.18 (A, B) INFLUENCE OF COMBUSTION MODE, ENGINE LOAD AND RP ON THE PM ASSOCIATED SOLUBLE
ORGANIC FRACTION
FIGURE 4.19: (A) IMPACT OF LOAD AND COMBUSTION MODE ON CYTOTOXICITY OF PM EMITTED FROM RCCI ENGINES,
(B) EFFECT OF RP ON CYTOTOXICITY OF PM EMITTED FROM MD-RCCI, (C) INFLUENCE OF RP ON CYTOTOXICITY
OF PM EMITTED FROM GD-RCCI AND (D) EFFECT OF COMBUSTION MODE ON OXIDATIVE STRESS INDUCED BY PM IN CELLS
FIGURE: 4.20 (A-D) INFLUENCE OF COMBUSTION MODE, ENGINE LOAD AND RP ON THE CANCER RISK POTENTIAL
ASSOCIATED WITH METAL AND CARBONYL EMISSION
FIGURE: 4.21 (A, B) INFLUENCE OF ENGINE LOAD AND HYDROGEN ENERGY SHARE ON THE CARCINOGENICITY AND
MUTAGENICITY POTENTIAL OF PAHS EMISSION
FIGURE 4.22: EFFECT OF ENGINE LOAD ON REGIONAL AND TOTAL LUNG LOAD DUE TO THE INHALATION OF SOOT
NANOPARTICLES EMITTED FROM CDC, GD-RCCI AND MD-RCCI WITH RESPECT TO AVERAGE CONCENTRATION
AND AN EXPOSURE TIME OF 13 YEARS
FIGURE 4.23: EFFECT OF ENGINE LOAD ON REGIONAL AND TOTAL LUNG LOAD DUE TO THE INHALATION OF SOOT
NANOPARTICLES EMITTED FROM CDC, GD-RCCI AND MD-RCCI WITH RESPECT TO AVERAGE CONCENTRATION
AND AN EXPOSURE TIME OF 13 YEARS. 152
FIGURE 4.24: EFFECT OF PREMIXING RATIO (RP) ON REGIONAL AND TOTAL LUNG LOAD FOR GD/MD -RCCI ENGINE
FIGURE 4.25: REGIONAL LUNG LOADING WITH RESPECT TO PARTICLE DIAMETER FOR CDC GD-RCCI AND MD-RCCI
ENGINE. 155

FIGURE 4.26: REGIONAL LUNG LOADING WITH RESPECT TO PARTICLE DIAMETER AT DIFFERENT PREMIXING RA	ATIO (RP)
FOR MD-RCCI ENGINE.	150
FIGURE 4.27 (A-D): EFFECT OF COMBUSTION MODE AND ENGINE LOAD ON ENVIRONMENTAL RISK MARKERS	15′
FIGURE 4.28: EFFECT OF RP ENVIRONMENTAL RISK MARKERS FROM MD-RCCI AND GD-RCCI ENGINES	159

List of Tables

TABLE 1.1: EURO 5 AND EURO 6 VEHICLE EMISSION STANDARDS FOR HEAVY DUTY DIESEL ENGINES [1.22]	6
TABLE 1.2: DIESEL FUEL PROPERTIES [1.39].	15
TABLE 1.3 GASOLINE FUEL PROPERTIES AND TEST METHOD [1.43]	
TABLE 1.4: PHYSICAL AND CHEMICAL PROPERTIES OF METHANOL [1.45]	19
TABLE 1.5: PROPERTIES OF HYDROGEN FUEL [1.58].	21
Table 1.6. Effect of NO _x emission on human health [1.84-1.89]	35
TABLE 1.7 EFFECT OF CO EMISSION ON HUMAN HEALTH [1.90-1.93].	35
TABLE 1.8. EFFECT OF HYDROCARBON SPECIES EMISSION ON HUMAN HEALTH [1.94]	36
TABLE 3.1: SPECIFICATIONS OF THE AUTOMOTIVE DIESEL ENGINE	73
Table 3.2: Governing differential equation:	95
TABLE 3.3: ENGINE SETUP SANDIA CUMMINS [3.23].	97
Table 3.4: Governing equations	98
Table 3.5: Validated Operating condition of the Cummins N-14 engine [15]	107
Table 3.6: Initial and Boundary Conditions [3.35].	107
TABLE 3.7 TECHNICAL DETAILS OF MEASURED PARAMETERS	
TABLE 3.8 UNCERTAINTIES OF PARTICLE EMISSIONS PARAMETERS	110
TABLE 3.9 ACCURACY OF PARTICLE SIZER	110
TABLE 3.10: ACCURACY AND TECHNICAL DETAILS OF MEASURED PARAMETERS IN EXPERIMENT [3.43]	111



Chapter 1:

Introduction

As civilization progresses, so does its technology, leaving behind noticeable markers for future generations in advantageous and disadvantageous forms. The transport sector stands as a cornerstone in this evolutionary journey. The transport sector's growth drives the efficient movement of goods and services, significantly contributing to the national GDP [1.1]. This sector not only enhances the average living standard but also brings a multitude of other benefits, driving economic progress and improving quality of life. While the transport sector drives progress and prosperity, it also harbors a hidden downside when powered by fossil fuels. This includes rising air pollution and accelerating climate change due to global warming, acidification, eutrophication, and ground-level ozone formation in the environment [1.2]. The reciprocating internal combustion engine is a crucial and essential component of the automotive sector. An Internal combustion engine (ICE) is a device that converts the chemical energy of fuel into shaft work. Fuel combustion with an oxidizer converts chemical energy into thermal energy in an internal combustion engine. This thermal energy increases the temperature and pressure of the in-cylinder combustion products, pushing the piston downward and producing useful work [1.3]. Currently, two types of ICEs are in use: compression ignition and spark ignition engines. Compression ignition engines, which run on fossil fuels like diesel, are known as diesel engines. Spark ignition engines, which use gasoline as fuel, are called petrol engines. Diesel engines are preferred over SI engines due to their superior torque, power output, thermal efficiency, robustness and durability. However, they are associated with high particulate matter (PM) and oxides of nitrogen (NO_x) emissions [1.3]. These pollutants are categorized as criterion pollutants by USEPA due to their adverse effect on human health and the environment [1.4]. The rapid increase in vehicles results in a significant rise in pollutant emissions into our atmosphere. This increase in engine-related emissions, coupled with the brisk depletion of fossil fuel reserves, necessitates the development of more efficient and cleaner engines.

According to the International Transport Forum, the demand for transportation will double or even quadruple by 2050, leading to a higher need for fossil fuels in the coming years [1.5]. In response to the environmental impacts of transportation-related pollution, the world is increasingly shifting

towards decarbonizing this sector. This involves adopting alternative fuels that are low or zero carbon, such as methanol and hydrogen, and the development of advanced combustion concepts, such as advanced dual-fuel combustion engines. The present chapter discusses the motivation of engine research, conventional and advanced dual fuel combustion concepts, methanol and hydrogen as automotive alternative fuels, regulated and unregulated emissions, and their impact on human health and the environment. This chapter is divided into different sections to elucidate the explanation.

1.1 Motivation for engine research

The growth of the global economy and society depends on the efficient transport infrastructure. Transport sector development is crucial to achieving this growth [1.6, 1.7]. Throughout history, transportation has evolved and expanded, helping in the trade and movement of people. Internal combustion engines (ICEs) are the primary power sources for engine-equipped vehicles, ships, construction equipment, and agricultural equipment. Most of these engines are reciprocating ICEs fueled by petroleum-based fossil fuels [1.8]. A forecast suggests that ICEs utilizing petroleum-based fuels will likely power most of the transportation, with an estimated 90% share in the near future by 2030. The global rise in automation has significantly increased the demand for fossil fuels and the number of automotive vehicles [1.7, 1.8]. Currently, the transportation sector accounts for 20% of global energy consumption and a 40% increase in energy usage within this sector, especially in non-OECD countries like India and China [1.7].

The global demand for energy utilized in the transport sector is projected to be 40-50% higher than today [1.7, 1.8]. The IEO predicts that fuel demand will continue to increase over the next three decades, with fossil fuels comprising 78% of energy use by 2040 [1.9, 1.10]. The growing demand for energy in the transport sector will substantially increase air pollution and GHG emissions. It will result in more stringent emission regulations worldwide [1.11]. Additionally, the rise in oil prices in the coming decades is inevitable due to limited fossil fuel reserves on Earth.

Consequently, due to strict emission regulations and rising oil prices, reciprocating ICE-powered vehicles are expected to become more efficient and environmentally friendly [1.11, 1.12]. Recently, energy topography in the transport sector has advanced with the introduction of fuel cells, battery electric vehicles (BEVs), and hybrid electric vehicles (HEVs) [1.13, 1.14]. These

advanced technologies aim to mitigate emissions from the transport sector, which has a share of 16% of total GHG emissions [1.15]. While BEVs offer local zero-pollution benefits, their dependence on coal for electricity production (for charging the BEVs) in certain regions can contribute to global pollution [1.15, 1.14]. Thus, before promoting BEVs, it is essential to decarbonize the power generation units used to charge the BEVs [1.16]. Despite decarbonized power sources, BEVs still pose significant challenges related to freshwater ecotoxicity, mainly due to the production processes for battery elements [1.16]. Furthermore, modern batteries still exhibit lower volumetric and gravimetric energy densities than gasoline and diesel used in ICEs [1.17].

Therefore, combustion engines are expected to remain prominent for several decades unless more fuel-efficient and cleaner alternatives become widely available [1.17]. Hence, research focused on enhancing fuel conversion efficiency and reducing harmful emissions from ICEs is justified and necessary in the current context [1.17]. Over the years, improving fuel conversion efficiency and power density in IC engines has been a primary driving force for research and development. The identification of automobile exhaust emissions as a significant contributor to urban air pollution dates back to the 1950s (California). Today, users of IC engines are increasingly aware of vehicular air pollution, leading to demands for compliance with environmental considerations and regulatory standards worldwide. The key factors governing engine research are discussed in the following subsections.

1.1.1 Environmental and health implications

According to the World Health Organization (WHO), 9 out of 10 people breathe polluted air. Nearly the entire global population (99%) is exposed to air that exceeds the pollutant concentration limits recommended by the WHO [1.18, 1.19]. The air pollutants identified by the WHO as concerning for public health include particulate matter (PM), carbon monoxide (CO), ground-level ozone (O₃), nitrogen oxides (NO_x), and sulfur oxides (SO_x) [1.20]. Traces of these pollutants are either directly emitted by ICEs or formed during the atmospheric transport of primary pollutants. For example, ICEs do not directly emit O₃. However, volatile organic compounds (VOCs) emitted from engines undergo atmospheric transport processes in the presence of sunlight and NOx, forming ground-level O₃ [1.21]. Individual pollutants have different effects on human health and the environment. Several markers made by international organizations represent the adverse effects of engine-emitted pollutants on human health and the environment [1.21]. The environmental risk

markers are global warming, acidification, eutrophication and ozone-forming potential equivalent. Global warming represents a significant environmental challenge and drives the regulatory bodies to decarbonize the energy sectors. Global warming results from a thermal energy imbalance caused by heat trapping in the Earth's atmosphere by greenhouse gases. Photochemical smog or ground-level ozone is a mixture of pollutants formed when NOx and volatile organic compounds (VOCs) react in sunlight, creating a brown haze above cities [1.22]. Acid rain occurs when sulfur dioxide (SO₂) and nitrogen oxides (NO_x) are emitted into the atmosphere and transported by wind and air currents, causing acidification. This phenomenon adversely affects soil, forests, streams, and lakes. The combustion of fossil fuels is a significant source of sulfur dioxide and NO_x emissions, contributing significantly to the formation of acid rain [1.22]. The excessive formation of nutrients, particularly nitrogen-containing compounds emitted from internal combustion engines (ICEs), in water bodies is identified as the potential for eutrophication.

The adverse effects of engine-emitted pollutants on human health have been studied extensively. Figure 1.1 shows the effect of engine emissions on human health and the environment.

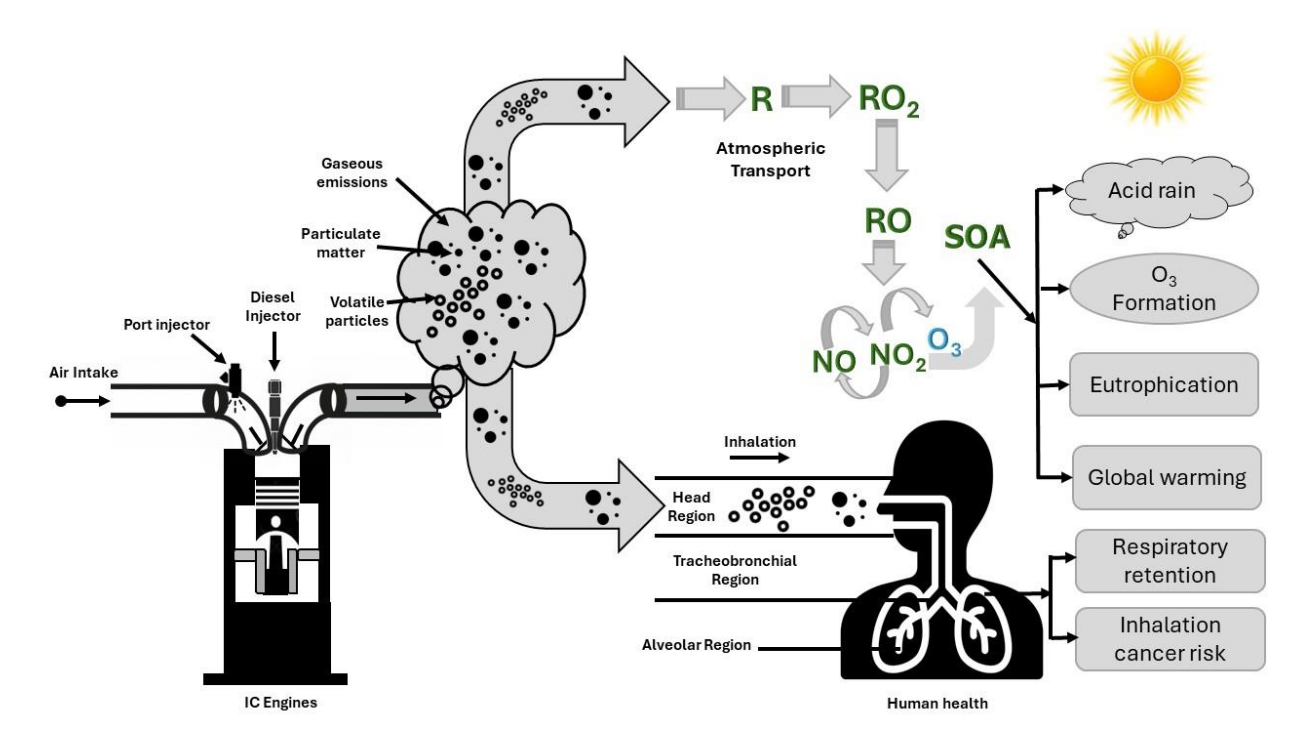


Figure 1.1: Adverse effects of engine emissions on human health and the environment

Once the pollutants enter the human body, they undergo chemical transformation and affect the biological mechanisms [1.21]. Even at lower concentrations of vehicular emissions, susceptible individuals can experience adverse health impacts. Short-term exposure to air pollutants is closely linked to COPD (Chronic Obstructive Pulmonary Disease), coughing, shortness of breath, wheezing, asthma, respiratory diseases, and high hospitalization rates, a measure of morbidity. Long-term effects associated with air pollution include chronic asthma, pulmonary insufficiency, cardiovascular diseases, and cardiovascular mortality [1.21]. Several chemical compounds with different toxicity potential have been identified to quantify the effect of gas phase emissions on human health. The markers used by the US Environmental Protection Agency (EPA) to assess cancer risk potential are called inhalation unit risk (IUR). Following extensive testing and analysis of large datasets, the US EPA assigns numerical values of IUR to pollutants [1.23]. PM emissions from the engines have a more pronounced impact on human health due to their diverse physical and chemical properties. The California Air Resources Board (CARB) has classified diesel PM as an 'air toxic' and estimated that in 2003, diesel PM was responsible for approximately 70% of the cancer cases attributed to all air toxics [1.114]. The PM is emitted in the form of nanoparticles from diesel engines. Particles are classified based on their size by aerodynamic diameter: nanoparticles (aerodynamic diameter < 50 nm), ultrafine particles (aerodynamic diameter < 100 nm), and fine particles (aerodynamic diameter < 2.5 μm, designated as PM 2.5) [1.24]. Depending on their size, particles can reach different regions of the lungs after inhalation. The body's nasal defense mechanisms typically filter out large particles and do not reach deeper lung regions. However, nanoparticles can penetrate into the lower regions of the lungs, where their clearance is slow. Once nanoparticles reach these areas, depending on their chemical composition, they can induce adverse effects that contribute to long-term diseases. Several studies have investigated the chemical composition of diesel particulate matter (PM) particles and reported that they contain several carcinogenic compounds recognized by the International Agency for Research on Cancer (IARC), such as polycyclic aromatic hydrocarbons (PAHs) [1.25].

1.1.2 Emission regulations

Government bodies enforce regulatory emission norms on vehicles to mitigate the adverse effects of engine emissions on human health and the environment. These norms set limits on the concentration of pollutants that vehicles can emit. Over the last few decades, these emission norms

have become increasingly stringent, motivating researchers to develop cleaner combustion engines. Generally, for light-duty vehicular exhaust emission, the emission is expressed in norms as mass per kilometer distance travelled (g/km) [1.22]. For heavy-duty engines, emission limits are specified in terms of mass of emissions per unit of work output (g/kWh) [1.26, 1.27]. Newly produced vehicles and engines undergo testing for compliance with emission standards in a government-approved laboratory. For emission certification, vehicles and engines are tested on a specified driving cycle. The test-driving cycle includes a cold start period, idling, moderate acceleration, deceleration, and cruise mode [1.28]. For heavy-duty vehicles, engines undergo testing under various load and speed conditions using steady-state and transient test cycles. Emission legislation encompasses pollutant species such as NOx, unburned hydrocarbons (UHC), CO, and particulate matter (PM) [1.28]. These are called regulated emissions due to the imposed regulation on their emission. Among the regulated emissions, CO, HC and NOx are regulated on a mass basis, whereas PM is regulated on a mass and number basis in the present regulations. Particulate number (PN) standard was introduced in 2011 with Euro V(b) for diesel engines and in 2014 with Euro VI for petrol engines. In Europe the current emissions standard is EURO VI and in India it is BS VI. The emission norms and limit for the pollutant is presented in Table 1.1.

Table 1.1: Euro 5 and Euro 6 vehicle emission standards for heavy duty diesel engines [1.22]

Pollutant	Euro V	Euro VI	
CO (g/kwh)	1.5	1.5	4.0
HC(g/kwh)	0.46	0.13	0.16
CH ₄ (g/kwh)	-	-	0.5
NOx(g/kwh)	2.0	0.4	0.46
PM(g/kwh)	0.02	0.01	0.01
PN (#/kwh)	-	8.0×10^{11}	8.0×10^{11}
Smoke (1/m)	0.5	-	-
Ammonia (ppm)	-	10	10
Test cycle	ESC and ELR	WHSC	WHTC

The achievement in the field of emission reduction can be understood through the significant reduction achieved in particulate mass emissions. For instance, the particulate mass standard in Euro VI for diesel engines has been reduced by 96% compared to Euro I emission standards. As

the world moves towards more stringent regulations, researchers are motivated to explore new combustion concepts along with alternative fuels to meet future emission norms.

1.1.3 Energy security and fuel challenges

The acceleration of decarbonization in the transport sector motivates researchers to investigate low and zero-carbon alternative fuels. Currently, the transport sector relies heavily on liquid fuels due to their high energy density, ease of transport and storage, and extensive infrastructure. The annual global demand for transport fuel is immense, with approximately 23 million barrels of oil equivalent per day (MBODE) for gasoline and 26 MBODE for diesel, equating to around 1.6 trillion liters each per year [1.6, 1.7, 1.8]. This heavy consumption of fossil fuels results in the emission of large quantities of CO₂, which is identified as a greenhouse gas. ICEs operating on fossil fuels provide 25% of the world's power and produce 10% of the total GHGs emissions. To address this issue, the International Energy Agency's (IEA) roadmap calls for new road vehicles worldwide to consume 30 to 50 % less fuel per kilometer by 2030 [1.28]. To achieve the IEA roadmap, researchers have identified zero and low-carbon alternative fuels as a promising solution. The use of alternative fuels in existing engines can be achieved through dual-fuel combustion modes. The present research focuses on this approach.

1.2 Conventional and advanced dual-fuel engines

Conventional engines by name indicates that those internal combustion engines which operates on fossil fuel such as diesel and gasoline with conventional combustion strategy such as mixing controlled in diesel engine and premixed combustion using ignition source in case of SI engines. This section discusses the history, evolution, combustion phenomena challenges and advantages of conventional and advanced combustion engines.

1.2.1 Conventional diesel Engine

A German engineer, named 'Rudolf diesel' invented the diesel engine in the late 19th century. The engine design was patented by him in 1892, pointing to creating a more efficient alternative to existing steam engines. In the early 20th century, diesel engines were beginning to be commercialized. The efficiency and ability to run on a variety of fuels made them attractive for

industrial applications, marine propulsion, and transportation [1.29]. Throughout the 20th century, significant advancements in diesel engine design occurred. Improvements included improved fuel injection systems, turbocharging to increased power output, and material durability and reliability [1.28]. During World War II, diesel engines played a crucial role in military vehicles, submarines, and ships. This period encouraged further developments in diesel technology. Post-World War II, diesel engines became increasingly prevalent in transportation, particularly in heavy-duty transport vehicles like trucks, buses, and locomotives. The ability of diesel engines to haul heavy loads efficiently made it popular in industrial sectors. In the latter half of the 20th century and into the 21st century, environmental concerns led to stricter emissions regulations for diesel engines. This drove advancements in emissions control technologies such as diesel particulate filters (DPF) and selective catalytic reduction (SCR) [1.30]. Diesel engines have been adopted globally across various sectors, including agriculture, construction, mining, and stationary power generation. In recent decades, advancements in diesel combustion have been driven by improvements in highpressure common rail direct injection (CRDI) systems. Modern diesel engines equipped with CRDI high pressure systems which exhibit a reduction in premixed heat release because of enhanced fuel-air mixing and a shortened ignition delay period. As already discussed, diesel engines are preferred over SI engines due to their high torque and power output. This attribute comes in diesel engines due to the nature of their design and combustion.

Combustion in diesel engine

In diesel engines, fuel is injected at high pressure directly into the combustion chamber at the end of the compression stroke, where it ignites by mixing with the hot air resulting from compression. The injection occurs at the end of the compression stroke using a direct injection type fuel injector that delivers diesel into the hot, dense air [1.26]. Combustion observations, including photographic analysis and pressure-time history measurements ana analysis, indicate that the diesel combustion process take in three distinct phases: ignition delay, premixed combustion, and mixing-controlled combustion or diffusion combustion. Ignition delay is often divided into physical delay and chemical delay, although it is understood that these two components cannot be solely observed. Physical delay is the time lags within the injection system and the duration required for heat and mass transfer processes to create a combustible mixture of fuel vapor and air. Chemical delay arises from the time necessary for pre-flame reactions to step up and initiate the ignition of a combustible

mixture of fuel vapor and air [1.26]. Figure 1.2 presents the heat release curve for conventional diesel, describing these phases. After injection, due to dense air ambient and high-pressure liquid fuel undergoes atomization into fine droplets, vaporization, mixing with hot air, and chain initiation reactions, resulting in autoignition that initiates combustion. The time interval between the start of injection and the onset of combustion is termed the ignition delay [1.26]. Combustion originates at multiple sites within the rich premixed region of the spray and propagates rapidly along the periphery, burning the fuel vapor mixture around the spray core during the ignition delay period. During the premixed combustion phase, cylinder pressure and temperature increases rapidly. Fuel injection continues even after the onset of combustion based on the power requirement [1.26].

The combustion rate after the onset of combustion is dictated by the rates of atomization, vaporization, and air-fuel mixing. Increased in-cylinder temperatures and pressures following combustion initiation accelerate fuel droplet vaporization, making air-fuel mixing the primary control factor for combustion. This phase is referred to as mixing-controlled or diffusion combustion [1.26]. Combustion continues beyond the end of fuel injection, extending the overall combustion duration past the injection period. The heat release rate reduces rapidly and gradually approaches zero due to the dissipation of spray-induced turbulence. Fuel distribution within the cylinder is non-uniform, with local fuel-air ratios ranging from rich at the spray center to lean at the edges. At high combustion temperatures (2000-2500°C), carbon particles in the diffusion flames achieve sufficient luminosity, appearing as yellow regions [1.26].

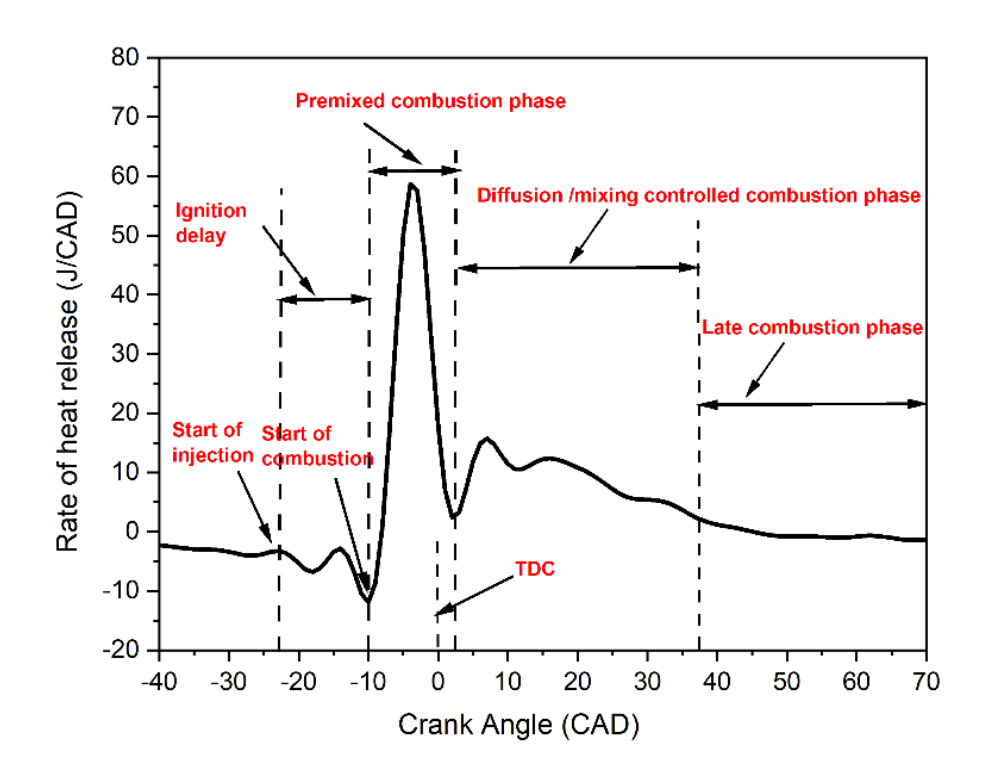


Figure 1.2: Heat release rate diagram for a direct injection (DI) diesel engine illustrating the distinct phases of combustion.

Merits and Demerits of conventional diesel engines [1.28, 1.31]

Merits of diesel engines

- Higher thermal efficiency compared to gasoline engines mainly due to higher compression ratio, overall lean combustion, higher specific heat and no pumping loss
- Diesel engines are very robust and reliable
- No requirement of external ignition source such as spark plug or ignition coil in case of gasoline engines.
- Lower CO₂ emission as compared to gasoline engines.
- In diesel engines, overheating during extended idling is less frequent due to lower heat losses. These engines can sustain idle speeds for prolonged periods, making them suitable for sectors such as agriculture, marine applications, and trains.
- Diesel engines can achieve substantial intake pressure boosts through turbocharging without encountering knock limitations, thereby enhancing both efficiency and power density.

Demerits of diesel engines [1.28, 1.31]

- Particulate matter emission: one of the major undesirable combustion products in diesel engines is particulate matter which ais one of the criterion pollutants.
- PAHs emission: diesel engines also emit gas phase PAHs in trace amount which are recognized as carcinogenic by IARC
- Comparable NOx emissions with gasoline counterparts due to higher operating temperature and overall lean combustion
- Particulate and NOx tradeoff limits
- After-treatment systems impose significant operational and maintenance demands, contributing to elevated vehicle production costs, increased operational expenses, higher fuel consumption, and enhanced system complexity.

1.2.2 Advanced dual-fuel engine

To address challenges inherent in conventional diesel and gasoline engines, researchers have explored new combustion modes termed advanced combustion modes [1.31]. These engines combine the advantages of both diesel and gasoline engines while significantly reducing particulate matter (PM) and nitrogen oxides (NOx) emissions to ultra-low levels. The charge preparation strategy in advanced combustion engines is like that of SI engines, while the ignition strategy of compression ignition engines [1.31]. The premixed charge preparation strategy eliminates locally rich zones within the combustion chamber, thereby minimizing particulate matter (PM) formation. Compression ignition of the charge eliminates flame front zones or hightemperature zones, reducing the formation of thermal NOx. Additionally, the use of an excessively lean charge significantly lowers combustion temperatures (lowering NOx), reducing heat loss and increasing efficiency [1.32]. Due to lower operating temperatures these engines are also recognized as low temperature combustion (LTCs) engines. Homogeneous Charge Compression Ignition (HCCI) engines were the initial type of advanced combustion engines. However, HCCI engines lack direct control over the combustion process, resulting in limited power density. The simultaneous autoignition of the entire charge in HCCI engines constrains their high-load operation due to the risk of excessive pressure rise rates and potential knock [1.32]. This issue in HCCI engines arises from the very short combustion duration, as the entire charge ignites simultaneously. To address these challenges, researchers have proposed two types of stratification

within the combustion chamber: thermal stratification and composition stratification. Thermal stratification aims to create a temperature gradient inside the combustion chamber, while composition stratification focuses on creating a gradient in the fuel-air mixture. Both approaches are intended to extend the combustion duration and improve control over the combustion process. Composition stratification has an advantage over thermal stratification because it is easier to implement. One effective method to achieve composition stratification is by adjusting the injection timing, making it a more practical approach compared to creating a thermal gradient within the combustion chamber. Composition stratification can be of two types one is single fuel partial premixed charge compression ignition (PPCI) engine, and the other is dual fuel reactivity charge compression ignition (RCCI) engines [1.31].

Reactivity Controlled Compression Ignition (RCCI) engines, also known as advanced dual fuel combustion engines, stand out due to their wider operating range, fuel flexibility, improved combustion control, and lower cyclic variability compared to other low-temperature combustion (LTC) strategies [1.33]. RCCI engines achieve these benefits by utilizing two fuels with different reactivities, typically injected at different stages of the engine cycle. This dual-fuel approach allows for precise control over the combustion process, enabling better management of ignition timing and combustion phasing. As a result, RCCI engines can operate efficiently across a broader range of conditions, achieve higher thermal efficiency, and produce lower emissions of NOx and particulate matter compared to conventional engines. Additionally, RCCI engines can leverage renewable and alternative fuels, further enhancing their environmental benefits and adaptability to future energy landscapes. [1.33]

Combustion in advanced dual fuel (RCCI) engines

In a Reactivity Controlled Compression Ignition (RCCI) engine, combustion is carefully controlled using two fuels with different reactivities, typically gasoline (low reactivity) and diesel (high reactivity). The process begins with the low-reactivity fuel being injected into the intake manifold via a port fuel injector, where it mixes with the intake air during the engine's intake stroke to create a homogeneous air-fuel mixture within the combustion chamber. Concurrently, the high-reactivity fuel is injected directly into the combustion chamber during the compression stroke. Early injections of the high-reactivity fuel target specific regions, such as the squish area, to create zones of higher reactivity, while later injections serve as ignition sources [1.33]. To control the

combustion process, exhaust gas recirculation (EGR) is employed to manage in-cylinder reactivity and temperature, optimizing the timing of combustion and reducing peak temperatures. Multiple injection strategies are used to fine-tune the quantity and timing of fuel injection, ensuring efficient and clean combustion. The ignition process begins with low-temperature heat release (LTHR), characterized by cool flame reactions from the high-reactivity fuel, leading to a moderate rise in temperature and pressure. This is followed by high-temperature heat release (HTHR), driven by the high-temperature oxidation of CO and the breakdown products of both fuels, resulting in the main combustion event and the release of most of the energy. Figure 1.3 shows the rate of heat release (ROHR) profile for a RCCI combustion [1.33]. The stratified reactivity within the cylinder ensures a controlled and increased combustion event, leading to a smoother pressure rise and broader heat release profile. This precise control over combustion dynamics enhances thermal efficiency and significantly reduces NOx and soot emissions compared to conventional combustion methods, making RCCI an effective strategy for achieving efficient and clean engine performance [1.33].

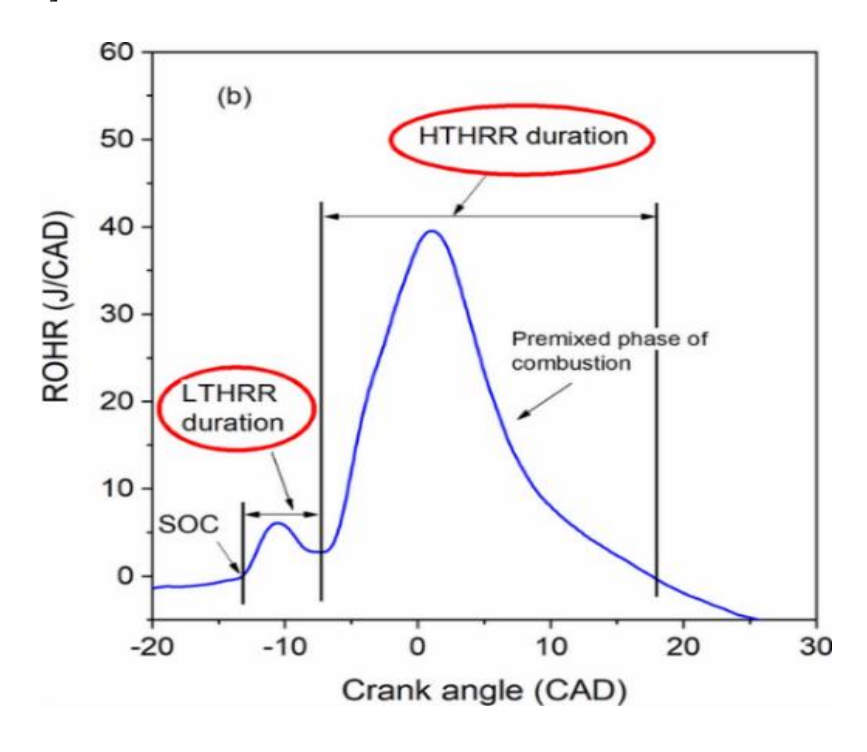


Figure 1.3 Heat release rate curve of RCCI combustion [1.58]

Advantage and challenges of RCCI engines

Merits of RCCI engines [1.28, 1.31]

- RCCI combustion achieves high thermal efficiency across a wide range of engine operating conditions, reaching a peak gross indicated efficiency of 56% at a 9.3 bar IMEP operating point in heavy-duty engines [1.33].
- Compared to other low-temperature combustion (LTC) techniques like HCCI and PCCI, RCCI combustion offers better control over combustion duration and phasing [1.28].
- RCCI is a versatile and fuel-flexible technology, enabling the use of a wide range of low-reactivity and high-reactivity fuels. This enables the effective and strategic use of renewable low carbon fuels [1.33].
- RCCI is a promising combustion strategy that can meet current emission regulations, such as Euro VI, without the need for costly NOx and soot aftertreatment systems.
- RCCI combustion demonstrates a significant reduction in NOx emissions by nearly three
 orders of magnitude and lowers soot emissions by a factor of six compared to conventional
 diesel combustion [1.33].

Challenges in RCCI engines

- Higher CO and HC emissions as compared to conventional diesel engines [1.33].
- Higher organic hydrocarbon emission compared to conventional diesel engines.
- Higher cyclic variability at lower engine load operations [1.28].
- Higher pressure rise rate at higher engine load and speed operations.

1.3 Automotive Fuels

Fuel is the chemical compound that serves as the primary source of energy for an internal combustion engine. Fuel chemically bound energy is released in form of heat after combustion which then converted into mechanical work through the engine's components such as pistons and crankshaft. Fuels are classified into liquid and gaseous phases according to their physical state. Liquid fuels, such as gasoline and diesel, are preferred over gaseous fuels like natural gas due to their higher energy density per unit volume, which allows for more efficient energy storage, transportation, and handling [1.34]. Furthermore, fuels are categorized based on their production

source as either fossil fuels, derived from non-renewable resources like crude oil and natural gas, or renewable fuels, which are generated from sustainable sources such as biomass, solar, or wind power. An example of renewable fuel production is the electrolysis of water using electricity from renewable sources to produce hydrogen. This process has gained significant attention due to its carbon-neutral attributes and potential for reducing greenhouse gas emissions in various sectors [1.35].

Different types of fuels, including gasoline, diesel, hydrogen, and methanol, have varying chemical compositions and combustion characteristics, impacting engine performance, efficiency, and emissions [1.36]. The selection of fuel types are important considerations in engine design and operation to achieve desired performance along with meeting regulatory emissions standards.

1.2.1 Diesel Fuel

Conventional diesel oil is produced through the process of petroleum cracking. It represents a specific fraction that boils initially at around 433 K (between 565 K and 635 K for 90% of its range) [1.37]. It consists primarily of saturated hydrocarbons such as paraffins (including normal and isoparaffins) and cycloparaffins, along with aromatic hydrocarbons like naphthalene and alkylbenzenes [1.37]. Physically, diesel fuel is liquid fuel that ranges in color from light yellow to amber, depending on its sulfur content and refining methods. Historically, diesel fuels contained higher levels of sulfur, leading to emissions of sulfur dioxide and particulate matter. However, modern diesel fuels, following regulatory standards, have significantly reduced sulfur content to mitigate environmental impacts [1.38]. The detailed fuel properties of diesel fuel and presence of chemical compounds is presented in Table 1.2.

Table 1.2: Diesel fuel properties [1.39].

Test	ASTM test method	ASTM limits
Distillation range (K)	D86	555-661
Flash point (K)	D93	325
Viscosity (m ² /sec)	D445	$1.9 - 4.1 \times 10^{-6}$
Density (g/m ³)		0.820-0.860
Aromatic content (vol %)	D5186	15 – 37

Water and sediment (vol %)	D1796	0.05 % max
Ash by weight (%)	D482	0.35 % max
Carbon residue by weight (%)	D524	0.01 Max
Sulphur by weight (%)	D129	0.5 % max
Cetane number	D613	40 min
Lower heating value (MJ/kg)		42.8 – 44

The ignition quality of diesel fuel is commonly assessed using ASTM D613, which measures and reports the cetane number (CN). This metric is determined by the ignition delay time of the fuel in an engine. Hexadecane (C₁₆H₃₄), also known as cetane, serves as the reference compound with a cetane number of 100 due to its short ignition delay [1.37]. The cetane number scale provides insights into the composition and molecular structure of diesel fuel compounds. Specifically, long-chain, straight-chain, saturated hydrocarbons (alkanes) exhibit higher cetane numbers and superior ignition quality, whereas branched hydrocarbons typically display lower cetane numbers and poorer ignition characteristics [1.37].

Reaction kinetics and emission formation mechanisms

Diesel fuel includes hundreds, often thousands, of distinct chemical compounds. To manage this complexity, these species are grouped into structural classes to understand their combustion properties and create surrogate mixtures [1.40]. Surrogates for practical fuels are commonly defined in terms of several basic structural classes of compounds, usually including n-alkanes, branched or iso-alkanes, aromatics, polycyclic alkanes, olefins, naphthene, and oxygenated hydrocarbons for gasoline [1.40]. Several researchers have investigated the combustion chemistry of diesel fuel using n-heptane as a diesel surrogate. Studies show that at both low and high temperature n-heptane undergoes H atom abstraction, leading to formation of four possible structurally distinct alkyl radicals. At high temperatures this radical decomposes via beta scission to yield smaller olefins and other radical species. At low temperatures these four radicals undergo the addition of O₂ leading to the formation of heptylperoxy radicals. A comprehensive modelling of n-heptane oxidation reported that the full oxidation of n-heptane can be classified into 25 major classes of elementary reactions [1.40]. In summary these reactions include unimolecular fuel decomposition, H- atom abstraction from fuel surrogate molecule, alkyl radical decomposition,

addition of oxygen molecule to alkyl radical to form the olefin and HO₂ radical directly, alkyl radical isomerization, olefin abstraction reaction by OH, H, O and CH₃, olefin addition reaction, alkyl radical decomposition, olefin decomposition, addition of alkyl radical to O₂, \dot{R} + R \dot{O}_2 = R \dot{O} + R \dot{O} , Alkyl peroxy radical isomerization (R $\dot{O}_2 \rightleftharpoons \dot{Q}OOH$), R \dot{O}_2 + H \dot{O}_2 = RO₂H + O₂, R \dot{O}_2 + CH₃ \dot{O}_2 = R \dot{O} + CH₃ \dot{O} + O₂, R \dot{O}_2 + R' \dot{O}_2 = R \dot{O} + R' \dot{O} + O₂, RO₂H = R \dot{O} + \dot{O} H, R \dot{O} decomposition, $\dot{Q}OOH$ = QO + \dot{O} H (cyclic ether formation via cyclization of diradical), $\dot{Q}OOH$ = olefin + H \dot{O}_2 (radical site β to OOH group), $\dot{Q}OOH$ = olefin + carbonyl + \dot{O} H (radical site γ to OOH group), Addition of $\dot{Q}OOH$ to O₂, Isomerization of \dot{O} 2QOOH and formation of ketohydroperoxide and \dot{O} H, Decomposition of ketohydroperoxide to form oxygenated radical species and \dot{O} H, Cyclic ether reactions with \dot{O} H and H \dot{O}_2 , e naming conventions used here include \dot{R} and R', which denote alkyl radicals or structures, and Q, which denotes CnH2n species or structures [1.40]. The understanding of fuel combustion chemistry and reaction mechanisms helps in explaining the numerical results.

1.2.2 Gasoline Fuel

Gasoline is a complex mixture of volatile hydrocarbons with distinct chemical and physical properties, derived from the fractional distillation of crude oil. Gasoline undergoes additional treatments to improve its octane rating, which enhances its resistance to engine knocking and allows for better performance. The fuel comprises hundreds of individual hydrocarbons, typically ranging from C₄ to C₁₁ [1.41]. These hydrocarbons include a mix of branched chain alkanes, cycloalkanes, and aromatic compounds, each contributing to gasoline's overall volatility, energy content, and combustion characteristics. The detailed properties of gasoline as fuel are presented in Table 1.3. Isooctane is identified as a surrogate to gasoline fuel, and detailed oxidation has been studied by several research. The complete oxidation of octane also follows a similar series of reactions as n -heptane [1.42].

Table 1.3 Gasoline fuel properties and test method [1.43]

Test	Method	Limit
Research octane no. (RON)	EN ISO 5164	97.5
Motor octane no. (MON)	EN ISO 5164	86.6
Density (g/m ³)	EN ISO 12185	0.743-0.756

Aromatic (% vol)	ASTM D1319	29-35
Olefins (% vol)	ASTM D1319	3-13
Saturates (% vol)	ASTM D1319	59
Benzene (% vol)	ASTM D6730	0-1
Carbon (% MASS)	ASTM D5291	85.6
Hydrogen (% mass)	ASTM D5291	12.6
Oxygen (% mass)	ASTM D5291	1.73
Lead (mg/L)	EN 237	<2.5
Sulfur (mg/kg)	EN ISO 20886	0-5
Net calorific value	IP12	42.42

1.2.3 Methanol Fuel

Methanol (CH₃OH), also known as wood alcohol, is recognized as an alternative fuel under the Energy Policy Act of 1992 [1.44]. As a fuel for engines, methanol has similar chemical and physical properties to ethanol. Methanol has a single carbon atom, which during combustion results in lower formation and emission of carbon-related pollutants [1.44]. Additionally, the presence of oxygen in methanol improves its combustion quality by promoting more complete combustion, thereby reducing emissions of carbon monoxide and unburned hydrocarbons. This combination of properties makes methanol a cleaner-burning fuel compared to conventional hydrocarbons [1.45]. Methanol is generally produced through the steam-reforming of natural gas, which creates synthesis gas (a mixture of hydrogen, carbon monoxide, and carbon dioxide). This synthesis gas is then fed into a reactor containing a catalyst, which facilitates the production of methanol and water vapor. While various feedstocks can be used to produce methanol, natural gas is currently the most economical source [1.45]. Methanol presents itself as a viable alternative to conventional transportation fuels, offering notable advantages. Firstly, it stands out for its lower production costs relative to other alternative fuels, making it economically attractive. Additionally, methanol boasts improved safety characteristics compared to gasoline, with a lower risk of flammability [1.46]. Moreover, methanol enhances energy security by being produced from a variety of domestic carbon-based sources such as biomass, natural gas, and coal. This versatility in feedstocks not only supports energy independence but also offers flexibility in production methods, aligning with sustainable energy practices and reducing reliance on imported fuels. As

global interest in cleaner energy solutions grows, methanol's attributes make it a compelling option for reducing both costs and environmental impacts associated with traditional transportation fuels [1.46]. There are several ways to use methanol as fuel in internal combustion engines. Principally, methanol is considered SI engine fuel for its high-octane number and higher heat of vaporization. The use of methanol in SI engine doesn't require much modification [1.47]. Methanol has also been used in diesel applications using dual fuel combustion strategy which requires a port fuel injection system to introduce methanol and use of diesel as ignition source due to high autoignition resistance of methanol [1.46]. Recently, dual fueling has been adopted in large ship engines, such as the Stena Germanica, where methanol is introduced separately from diesel, diesel serves as the ignition source. The port-fuel injection of methanol is being explored in these dual-fuel engines as a method to improve emissions in heavy duty engines used in ship industries [1.45].

Physical and chemical properties of methanol

Physical and chemical properties of methanol play an important role in its selection as alternative fuels to engines. Table 1.4 shows the physical and chemical properties of methanol compared to other alcohol fuels and gasoline.

Table 1.4: Physical and chemical properties of methanol [1.45].

Property	Gasoline	Methanol	Ethanol	Butanol
Chemical formula		CH ₃ OH	C ₂ H ₅ OH	C ₄ H ₉ OH
RON	95	109	109	94
MON	85	92	98	81
Cetane number	8-14	3	9	25
Flash point (^o C)	-45	11	14	37
LHV (MJ/kg)	42.5	19	24-26	33

First, examining the elemental composition (Table 1.3), it is evident that the hydrogen-to-carbon ratio of methanol is higher than that of gasoline. Consequently, carbon dioxide (CO₂) emissions on an energy-specific basis (g CO₂ / MJ), of methanol results in 7% lower specific CO₂ emissions compared to gasoline [1.45]. Assuming the same brake thermal efficiency, several studies reported that methanol also increases thermal efficiency. The oxygen content, which constitutes half of

methanol's molecular mass, significantly influences its properties as an engine fuel. The high oxygen content results in a low mass-based stoichiometric air requirement (air/fuel ratio, AFR), the lowest among the fuels listed in the table [1.45]. This also implies that the fraction of methanol in a stoichiometric mixture is high.

Reaction kinetics and emission formation mechanism

The reaction kinetics of the methanol-air system are reasonably well understood due to methanol's simple molecular structure. Its oxidation process serves as a foundation for understanding the oxidation of longer-chain alcohols. A study reviewed alcohol combustion chemistry, including methanol, listing the most important comprehensive kinetic mechanisms and detailing the primary reaction pathways. They pointed out that the most important reaction for the ignition delay in methanol air-system is $CH_3OH + HO_2 \leftrightarrow CH_2OH + H_2O_2$ reaction [1.48]. Burke et al. reported in their study proposing a comprehensive reaction mechanism for methanol oxidation validated against the available experimental data obtained from shock tubes, rapid compression machines, jet-stirred reactors, concluding that additional data at high pressure and low temperature are needed to explain the complete oxidation of methanol fuel [1.49]. A study conducted stochastic reactor simulations employing detailed chemistry, incorporating a soot model, to compare the emission formation pathways between methanol and diesel (represented by a blend of n-heptane and toluene) [1.50]. They generated maps depicting various emission species as functions of equivalence ratio (ϕ) and temperature (T), and subsequently analyzed the trajectories in ϕ -T coordinates expected during engine operation. The results clearly demonstrated that methanol combustion does not lead to soot formation for two main reasons. First, the region where soot is formed (defined by 0.01 ppm of soot) is much smaller compared to diesel combustion, limited to equivalence ratios (\$\phi\$) greater than 2.6 and temperatures (T) above 1950 K. Second, due to methanol's prolonged autoignition delay and high heat of vaporization, the mixing times are extended, and ignition occurs only after the methanol fuel has thoroughly mixed with air to equivalence ratios leaner than stoichiometric conditions [1.50]. A study reported that the linear breakdown of methanol molecules (CH₃OH → CH₂OH → CH₂O → HCO → CO) can result in the formation of formaldehyde, which is a major concern due to the carcinogenic nature of formaldehyde [1.51].

1.2.4 Hydrogen Fuel:

Hydrogen is classified as an alternative fuel according to the Energy Policy Act of 1992 [1.52]. The growing interest in hydrogen as a transportation fuel arises from its capability to power engines with zero carbon emissions. Hydrogen is widely abundant in our surrounding, existing in water (H₂O), hydrocarbons like methane (CH₄), and various organic materials [1.53]. One significant challenge in utilizing hydrogen as a fuel lies in efficiently extracting it from these compounds. Presently, the predominant method for hydrogen production is steam reforming, which involves combining high-temperature steam with natural gas to extract hydrogen. Alternatively, hydrogen can be generated from water through electrolysis [1.54]. Although more energy-intensive, electrolysis can utilize renewable energy sources such as wind or solar power, thereby avoiding the harmful emissions associated with conventional energy production methods [1.54]. The primary reasons for using hydrogen in diesel engines are to increase the hydrogen-tocarbon (H/C) ratio of the fuel mixture and to enhance the homogeneity of the air-fuel mixture. This improvement in homogeneity is due to hydrogen's high diffusivity, which allows the combustible mixture to be well-premixed with intake air [1.53, 1.55, 1.56,]. As a result, this leads to the complete combustion process. Compared to conventional hydrocarbon fuels, hydrogen has a significantly higher laminar flame speed (1.85-2.9 m/s) at least five times greater than that of typical hydrocarbon fuels like gasoline or diesel, which have a laminar flame speed of approximately 0.4 m/s [1.57]. Although a higher flame speed can result in faster and more complete combustion of the fuel, it does not necessarily translate into higher thermal efficiency [1.53, 1.56]. This is because some of the heat produced during the combustion process may be lost before it can be converted into useful work. Therefore, it should be noted that a higher flame speed does not always equate to higher thermal efficiency in a hydrogen-fueled diesel engine [1.53, 1.56, 1.55]. However, hydrogen-fueled diesel engines tend to emit more NOx due to the higher incylinder temperatures.

Physical and chemical properties of hydrogen

The physical and chemical properties of hydrogen as compared to other hydrocarbon fuels makes it a good alternative for a net zero emission vehicle [1.58]. The physical properties of hydrogen in presented in Table 1.5.

Table 1.5: Properties of hydrogen fuel [1.58].

Property	Hydrogen
Molecular weight (g)	2.016
Density (kg/m ³)	0.08
Diffusivity in air (cm ² /sec)	0.61
Minimum ignition energy (mJ)	0.02
Minimum quenching distance (mm)	0.64
Flammability limit in air (vol%)	4-75
Flammability limit	10-0.14
Lower heating value (MJ/kg)	120
Stoichiometric air-fuel ratio (kg/kg)	34.2

The wide range of flammability limits, with flammable mixtures from as lean as $\lambda = 10$ to as rich as $\lambda = 0.14$ (0.1 < ϕ < 7.1), allows for a broad range of engine power output by adjusting the mixture equivalence ratio. The minimum ignition energy of a hydrogen-air mixture at atmospheric conditions is an order of magnitude lower than that of methane-air and iso-octane-air mixtures [1.58].

Reaction kinetics and emission formation mechanisms

Hydrogen as a fuel is unique due to its simple oxidation kinetics, very fast mass diffusivity, and low molecular weight [1.59]. Interestingly, all chemical reactions that consume molecular hydrogen in the H_2 - O_2 system produce atomic hydrogen, which is an extremely reactive and diffusive species. The hydrogen atom is the most important radical needed for flame propagation and ignition in virtually all combustion systems [1.59]. As the H_2 -air stoichiometry shifts from rich to lean (Diesel engine type condition), the laminar flame speed becomes more sensitive to the reaction $OH + O = O_2 + H$ and reactions involving the HO_2 radical. The forward reaction in $H + O_2 = OH + O$ is endothermic, making its chemical kinetic rate particularly sensitive to temperature changes as hydrogen mixtures become leaner. The HO_2 radical, primarily produced by the reaction $H + O_2 + M = HO_2 + M$ (where M is any third body), competes with the $H + O_2 = O + OH$ reaction for the H-atom. Under ultra-lean conditions (less than $\phi = 0.5$), reactions involving the HO_2 radical become very significant. For instance, the $H + O_2 + M = HO_2 + M$ reaction competes with $H + O_2 = OH + O$ for the H-atom, thereby strongly influencing the OH radical pool for the main H_2

consumption reaction, OH + H_2 = H_2O + H. Additionally, the H + HO_2 = OH + OH reaction can convert an unreactive HO_2 radical into a reactive OH radical, thereby promoting the chain-propagating reaction OH + H_2 = H_2O + H [1.59].

1.4 Engine emission

Engine emissions refer to the combustion products released into the atmosphere as byproducts of the combustion process within internal combustion engines [1.60]. Engine emissions are classified into gas-phase and solid particulate-phase emissions depending on the physical state of the combustion products. Government regulations categorize engine emissions into regulated and unregulated emissions. Regulated emissions refer to those for which specific limits are imposed by governmental authorities to control their release into the atmosphere. In contrast, unregulated emissions are those for which direct emission standards have not been established by regulatory bodies.

1.4.1 Regulated emissions

Regulated emissions are those which are subject to governmental standards. Presently, these emissions include total hydrocarbons (THC), carbon monoxide (CO), nitrogen oxides (NOx), and particulate matter (PM). Among these emissions, total hydrocarbons (THC), carbon monoxide (CO), and nitrogen oxides (NOx) are regulated based on their mass concentrations. Particulate matter (PM) emissions, on the other hand, are subject to regulations that consider both their mass and number concentrations. This dual regulation approach aims to control both the overall quantity and the size distribution of particulate emissions, which are crucial for managing air quality and human health impacts.

1.4.1.1 Total hydrocarbon (THC) emission

Hydrocarbon emissions from engines primarily result from the incomplete combustion of fuel molecules or the incomplete oxidation of reaction intermediates formed during the breakdown of large fuel molecules. The hydrocarbon emissions from CI engines are one-fifth of those from SI engines. The main source of hydrocarbon emissions from CI engines is excessively lean regions inside the combustion chamber, where the charge is outside the flammability limit of the mixture [1.60, 1.27]. Additionally, locally rich regions (inside the fuel spray), where incomplete combustion occurs due to a lack of oxygen, also contribute to HC emission. Hydrocarbon

emissions are a significant concern in reactivity-controlled compression ignition (RCCI) engines [1.33]. The premixed charge increases the likelihood of low-reactivity fuel entering crevices and becoming trapped. When the combustion eventually reaches these areas, the heat transfer from the walls causes the temperature to be insufficient for igniting the charge [1.33]. Han et al., reported in their study that the main reason of HC emission in dual-fuel engine is that during the compression stroke, some of the air-fuel mixture is compressed into gaps in the combustion chamber, leading to incomplete combustion of the mixture [1.61]. Numerical studies on engine combustion have reported that the combustion reactions of large chain molecules can be categorized into elementary reactions, namely chain initiation, chain propagation, chain branching, and chain termination. Inside the combustion chamber, these reactions occur based on the local temperature, pressure, and concentration of fuel vapor. As these reactions proceed, reaction intermediates are formed and oxidized. Later, depending on combustion phasing and duration of combustion, available time at time temperature the formed HC appears in the engine exhaust [1.62]. Yadav et al. found that increasing the mass of low-reactivity fuel inside the combustion chamber delays the combustion phasing, resulting in higher total hydrocarbon (THC) emissions from both gasoline-diesel and methanol-diesel RCCI engines. This occurs because as the combustion phasing shifts towards the expansion stroke, the oxidation reactions freeze due to lower temperatures, causing the formed products to appear in the exhaust [1.63].

1.4.1.2 CO emissions

Carbon monoxide is recognized as one of the criterion pollutants by US-EPA. CO is a colorless, odorless but toxic gas [1.4]. CO emits when the oxidation of CO to CO₂ doesn't get complete during combustion reaction [1.27]. CO emissions are primarily influenced by the air/fuel ratio during combustion. In rich mixtures or regions where fuel concentration is high, carbon monoxide forms due to insufficient oxygen for complete oxidation [1.27]. Spark-ignition (SI) engines typically operate at a stoichiometric air/fuel ratio, resulting in higher CO emissions compared to diesel engines. Diesel engines always run on an overall lean mixture, leading to very low CO emissions. This means that at an air-to-fuel ratio of 20:1 and higher, up to 100:1, there is an excess of air available for combustion [1.27]. At a 20:1 air/fuel ratio, there is 30% more air than what is chemically necessary for complete combustion. Consequently, diesel exhaust gases contain a significant amount of oxygen. The spatial distribution of the air/fuel mixture within the combustion

chamber significantly affects CO emissions. In RCCI engines the emission of CO is higher than conventional diesel engines. A well-established formation pathway of CO is given in reaction R1 and R2.

$$RH \rightarrow R \rightarrow R + O2 \rightarrow RCHO \rightarrow RCO \rightarrow CO \dots (R1)$$

 $CO + OH \leftrightarrow CO2 + H \dots (R2)$

R1 reactions occur in regions with oxygen deficiency, such as fuel-rich zones. R2 reactions take place when sufficient oxygen is available and proceed rapidly at high temperatures, continuously maintaining equilibrium. During the combustion and expansion strokes, the C-O-H system remains approximately in chemical equilibrium until the temperature decreases below 1800 K. Only in the latter part of the expansion stroke does the conversion of CO to CO2 become kinetically controlled, occurring at a slower rate [1.27]. Furthermore, partial oxidation of hydrocarbons trapped in crevices also contributes to CO emissions in RCCI engine combustion [1.63].

1.4.1.3 NOx emissions

Formation and emission of oxides of nitrogen (NOx) strongly depends on in-cylinder combustion temperature, availability of air and residence time. The higher combustion temperature breaks down the N₂ molecule in N radicals which further reacts with oxygen to form oxides of nitrogen. NOx formation in compression ignition (CI) engines is higher than in spark ignition (SI) engines due to the elevated temperatures and pressures caused by the high compression ratio [1.27]. As the compression ratio increases, the temperature at the end of compression increases, leading to greater NOx production during the early stages of the power stroke. In CI engines, NOx formation is also higher due to the abundant availability of air. The primary factors driving NOx formation are high temperatures, sufficient oxygen content, and the flame's residence time. Moreover, the slower combustion in CI engines allows more time for nitrogen-oxygen reactions, further facilitating NOx formation. At low temperatures, atmospheric nitrogen remains as a stable diatomic molecule (N2). It only dissociates into highly reactive monoatomic nitrogen (N) at very high temperatures [1.27].

$$N_2 \rightarrow 2N \dots (R3)$$

The equilibrium constant for reaction (R3) is heavily influenced by temperature. Significant quantities of monoatomic nitrogen are produced within the temperature range of 2500-3000 K.

In the literature, various mechanisms have been proposed to explain NO formation during the combustion process in internal combustion (IC) engines. The Zeldovich mechanism, for instance, describes NO formation based on the temperature of the reaction zone. The nitrous oxide mechanism, on the other hand, details how NO is formed from intermediate species. For rich flames, the Fenimore mechanism accounts for NO formation, although it contributes the least. Lastly, the NNH mechanism illustrates the formation of NO in fuels with a high carbon-to-hydrogen ratio. These different mechanisms collectively provide a comprehensive understanding of NO formation in IC engine combustion [1.64].

In 1946, the Russian scientist Zeldovich introduced a pair of reactions (R4) and (R5) to explain how NO forms at high temperatures. These reactions mainly govern the thermal production of NO from molecular nitrogen [1.65, 1.66]. Subsequently, a third reaction (R6) was added to this mechanism to account for the influence of OH radicals during combustion [1.67].

$$O + N_2 \leftrightarrow NO + N \dots \dots (R4)$$

 $N + O_2 \leftrightarrow NO + O \dots \dots (R5)$
 $N + OH \leftrightarrow NO + H \dots \dots (R6)$

In RCCI engines, NO_x emissions are significantly lower in comparison to conventional engines primarily due to several factors related to combustion characteristics. NOx formation is intricately linked to in-cylinder temperature and oxygen availability. In RCCI combustion, the in-cylinder temperatures are generally lower, which limits the breakdown of N_2 molecules into nitrogen radicals essential for NO_x formation. Moreover, reactions responsible for NOx production are highly temperature-sensitive, and the inherently lower combustion temperatures in RCCI engines suppress these reactions effectively [1.64]. Furthermore, the unique combustion strategy of RCCI, which involves a combination of low-reactivity and high-reactivity fuels, contributes to the reduced NO_x emissions. The controlled blending of fuels allows for a more gradual and controlled combustion process, minimizing peak temperatures and hence reducing the formation of thermal NO_x . Additionally, the stratified nature of RCCI combustion can lead to locally lean conditions in certain regions of the combustion chamber, further inhibiting NO_x formation where fuel-rich zones

are typically prevalent in conventional combustion [1.64]. Overall, the combination of lower incylinder temperatures, reduced peak temperatures, and controlled combustion characteristics in RCCI engines results in significantly lower NO_x emissions compared to traditional combustion technologies [1.64].

1.4.1.4 PM emission

The mechanism behind PM formation during combustion is not yet fully understood due to the complex nature of the physical and chemical processes involved. Soot formation in flames occurs across three distinct zones: the oxidation zone (blue), the pyrolysis zone (yellow and luminous), and the combustion product zone. In the oxidation zone, side chain PAH molecules form, leading to the creation of the first soot particles once the concentration of PAHs reaches its peak. Currently, PAHs and polyacetylene are the well-established precursors to soot [1.68, 1.69]. In the pyrolysis zone, three theories are accepted for soot formation: chemical nucleation, physical nucleation, and homogeneous physical nucleation. Chemical nucleation mechanisms propose that a progressive series of chemical reactions leads to the formation of polynuclear molecules. As these transformations proceed, the concentration of these molecules increases until soot particles eventually appear [1.68,1.69]. However, this mechanism fails to explain the discontinuity of carbon particles in the soot. Despite the presence of a large amount of polyacetylene, no new soot nuclei form under certain conditions. Physical nucleation theory proposes that the formation of soot nuclei occurs on positive ions formed during combustion. However, experimental studies have shown that only 30% of particles in a flame are charged [1.69]. Therefore, the remaining 70% of particles must originate from other sources, meaning this theory provides only a partial explanation for soot formation. The homogeneous physical nucleation theory states that an increase in the concentration of polyaromatic species leads to supersaturation, resulting in the appearance of soot particles. When the species reach a high enough concentration or become supersaturated, nucleation occurs through condensation, forming intermediate droplets. These droplets then grow and undergo chemical transformations, leading to the formation of larger soot particles [1.70].

In engine combustion, the well-accepted mechanism involves a series of chemical reactions during combustion. Depending on the in-cylinder combustion temperature, pressure, and local equivalence ratio, reaction intermediates form, eventually leading to the formation of the first aromatic ring. This ring further grows into polycyclic aromatic hydrocarbons, forming the initial

nuclei in a process known as nucleation [1.70]. After nucleation, surface reactions contribute to the growth of these nuclei into particles. Subsequently, coagulation and oxidation processes occur, resulting in the formation of soot particles [1.70]. This soot particle once reaches expansion strokes the gas phase hydrocarbons absorb over their surface and the new particle is called particulate matter (PM). The heterogeneous nature of combustion in diesel engines is one of the reasons for higher PM emissions [1.27].

Particulate matter emitted from the heavy-duty CI engines is sometimes visible as black smoke coming out of the tailpipe [1.27]. The typical schematic of the PM is shown in figure 1.4.

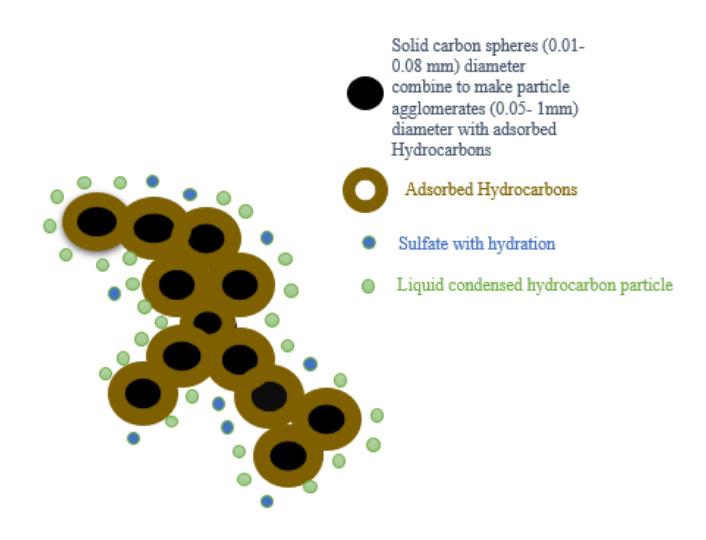


Figure 1.4: Schematic representation of particulate matter

The black spherical ball-like shape shown in the schematic is dry soot or solid carbon material. Other compounds such as soluble organic fractions (SOF), sulfates, and nitrogen dioxide are condensed over soot's surface. The SOF mainly consists of hydrocarbons from the fuel and lubricants, partially oxidized products, and PAHs [1.27]. The combined structure of soot and condensed volatiles on its surface is typically known as PM. Typically, when the temperature is high in the combustion chamber, only soot is formed, whereas, at a lower temperature, organic compounds condensed over soot are the major reason for PM formation [1.72].

The formation of PM in CI-engine does occur in two parts. One is in the tailpipe during condensation of VOCs over the surface of soot, and the other is during combustion. The exhaust emission particulate consists of visible, partially oxidized fuel like polycyclic aromatic hydrocarbon (PAHs), components of lubricating oil (heavy metals), and sulfates [1.73]. During the

combustion process, initially, soot is formed. During the expansion, the organic compounds major pollutant compounds absorbed over the surface of the soot lead to the formation of PM [1.72]. The composition of the PM formation depends on the in-cylinder operating conditions, which mainly include local fuel-air ratio, in-cylinder temperature, availability of oxygen, and the collection system used to measure the particulate matter. The temperature and the local equivalence ratio are the governing factors for the formation of particulates. The general trend for diesel engine particulate emission is that at higher load, the smoke emission increases due to local rich fuel-air mixture and long diffusion combustion duration.

1.4.2 Unregulated Emissions

Unregulated emissions refer to emissions categories not controlled by existing regulatory standards. For instance, current regulations govern hydrocarbon (HC) emissions by mass but do not specify individual chemical compounds. HC emissions encompass a variety of hydrocarbons, including alkanes, alkenes, alkynes, aromatics, and carbonyl compounds, which are collectively categorized as HC emissions. Similarly, particulate matter (PM) emissions are regulated by mass and number concentration, but the regulatory standards do not address the chemical composition of the PM particles, such as the organic fraction, particulate-phase PAHs, and trace heavy metals. The unregulated emissions from conventional diesel combustion are negligible. However, in the case of RCCI engines, the higher emission of THC makes unregulated emissions a major concern due to their diverse physical, chemical, and toxicological properties. For example, even if the total HC emissions are reduced to regulated levels, the chemical compounds present may be more harmful than those in diesel engine HC emissions. This section discusses the categories of unregulated emissions, their formation, and their emission during combustion. Unregulated emissions are typically categorized as saturated hydrocarbons (HC), unsaturated hydrocarbons (HC), carbonyl compounds, and aromatic emissions.

1.4.2.1 Saturated HC emissions

Saturated hydrocarbons are characterized by carbon atoms bonded to four other atoms, typically hydrogen, with each carbon forming single bonds only [1.73]. This structural configuration indicates that these compounds lack carbon-carbon double or triple bonds, distinguishing them as fully saturated hydrocarbons. In the present work the detected saturated HC are methane (CH₄), ethane (C₂H₆), pentane (C₅H₁₂). The formation of saturated HC during combustion is a very

complex phenomenon. As combustion of fuel molecules begins a series of complex reactions takes place and depending on the in-cylinder thermodynamic conditions the different reaction intermediates forms. Later during combustion these radicals form stable compounds to achieve the lower energy state or depending on the condition the formed intermediates get emitted as it is due to incomplete combustion. The typical path observed in chemical kinetics (engine like condition) for formation of saturated HCs mainly involves the reaction between methyl radical (CH₃) and other compounds such as methanol (CH₃OH), HCHO, CH₃CHO, C₂H₆ and others. A few of them are, addition of methyl radical to methanol (CH₃OH + CH₃ = CH₂OH + CH₄ and CH₃OH + CH₃ = CH₃O + CH₄), addition of methyl radical to ethane (C₂H₆ + CH₃ = C₂H₅ + CH₄), addition of methyl radical to CH₃CHO + CH₃ = CH₃CO + CH₄) [1.40, 1.42, 1.51]. Depending on the activation energy and rate of the reaction the net saturated HC emitted. However, the formation of methane also involves the reaction between phenyl radical (C₆H₅) and other oxygenated, unsaturated hydrocarbons [1.51].

1.4.2.2 Unsaturated HC emissions

Hydrocarbon compounds which are linked with each other by double and triple bond are known as unsaturated (alkene and alkyne) hydrocarbons. In the present investigation the detected unsaturated hydrocarbons are C₂H₂ (acetylene), C₂H₄ (ethylene) and C₃H₆ (propylene). The formation of C₂H₂, C₂H₄ and C₃H₆ in combustion happens through the thermal cracking of long chain compounds. In diesel engines, during combustion of spray due to locally rich fuel-air mixture and high temperature the thermal cracking of long chain compounds happens. This cracking leads to formation of reactive intermediates which includes C₂H₂, C₂H₄ and C₃H₆ [1.40, 1.42, 1.51]. However, later in combustion these get oxidized by O₂, OH and form stable compounds given that favorable conditions are available [1.51]. The rate of oxidation depends on temperature and at high temperature these species get completely consumed.

1.4.2.3 Carbonyl compound emission

The compounds which contain carbonyl group (C = O), are known as carbonyl compounds. The carbonyl compounds measured in the emission are formaldehyde (HCHO) and acetaldehyde (CH₃CHO). The formation of HCHO and CH₃CHO in engine combustion depends on low temperature combustion reaction path and the fuel type. Typically, at low temperature the radicals (R) undergo addition of R02 and form alkyl-peroxyl radicals (R02) through the R1 + R2 = R102

reaction. Later, internal H abstraction happens and a second O_2 addition and these subsequent decomposition yield to reactive hydroxyl radical and a carbonyl radical and compounds. The formation of carbonyl compounds also happens through direct abstraction of hydrogen atoms from methanol compound such as $CH_3OH \rightarrow CH_2OH \rightarrow CH_2O \rightarrow HCO \rightarrow CO$ [1.51].

1.4.2.4 Aromatic emission

Aromatic compounds are those chemical compounds that consist of conjugated planar ring (such as benzene) supplemented by delocalized pi-electron clouds. For example, the simplest aromatic compounds are benzene and toluene. The engine emitted aromatic compounds are majorly polycyclic aromatic hydrocarbons (PAHs) [1.73, 1.74]. Based on the number of rings present in PAHs and molecular weight they appear in the engine exhaust either as gas phase or particulate phase. The engine emits aromatic compounds in both gas and particulate phase [1.74]. These PAHs are identified as the precursor to particulate formation in engine during combustion. The formation of PAHs and their growth in diesel engine combustion is difficult to characterize due to the parallel progression of complex physical and chemical processes [1.75]. However, there is considerable agreement between the following steps of PAHs formation, which are - formation of PAHs precursor, addition of C₂-C₃ species with phenyl radical, formation of the stable aromatic ring through addition and recombination of species and radicals (such as benzene), and abstraction of hydrogen and addition of acetylene (HACA) to form new PAHs, and the growth through both the pathways HACA and dimerization of two large PAHs [1.76]. PAHs formation involves the pyrolysis of large chain hydrocarbon fuels (such as diesel) and the formation of carbon-containing unstable species (C₂H₂, C₃H₄ etc.) and radicals (CH₃) [1.76]. Diesel engines emit anthropogenic polycyclic aromatic hydrocarbons (PAHs) in higher concentrations [1.21]. PAHs are organic compounds having two or more fused aromatic rings. Many PAHs compounds are considerably toxic (mutagenic and carcinogenic) in nature [1.21, 1.77]. The toxicity potential of PAHs has been identified by several organizations such as IARC (International Association for Research on Cancer), US-EPA (Environmental Protection Agency), and WHO (World Health Organization). Based on their toxicity potential, IARC has classified the 17 PAH compounds into several categories (carcinogenic, probable carcinogenic, and possibly carcinogenic) (IARC 2021) [1.21].

1.5 Physico-chemical and toxicological properties of engine emissions

The physical and chemical properties of engine exhaust pollutants play a crucial role as they dictate their state, distribution, chemical composition, and toxicity. Particulate matter (PM) particles produced during combustion exhibit varied physical and chemical characteristics that affect their residence time in the environment and their reactivity [1.78]. Figure 1.5 shows the typical PM particle constituents from different sources such as lube oil, metal parts, combustion generated. It is imperative to comprehensively understand the physical, chemical, and toxicological properties of both PM and gas-phase emissions [1.78]. This understanding is essential for accurately assessing their detrimental impacts on human health and the environment, as well as for developing effective aftertreatment systems for RCCI engine exhaust emissions. The present section discusses the physico-chemical and toxicological characteristics of exhaust emission.

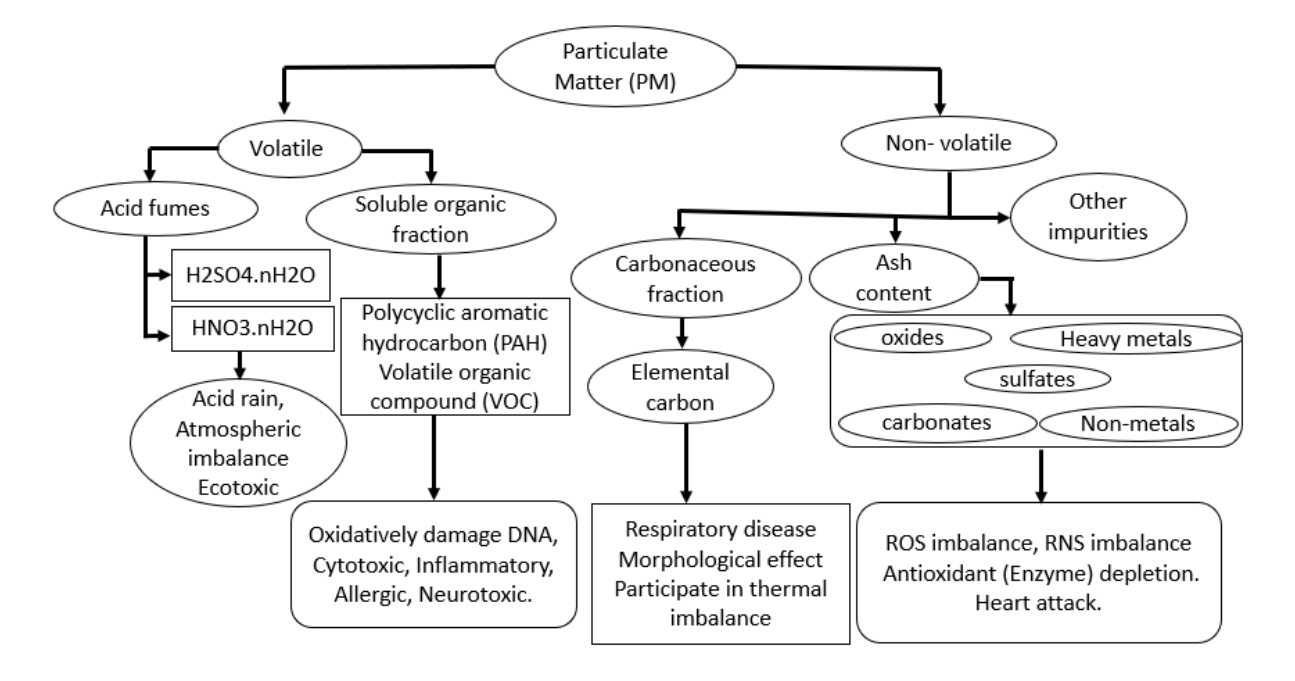


Figure 1.5: PM particle constituents and their impact on environment and human health [1.78].

1.5.1 Physico-chemical properties

Physico-chemical properties of PM and gas phase emissions include the particle number and size distribution, its morphology, soluble organic fraction present in PM particles and heavy metal elements present in PM particles [1.79].

1.5.1.1 Particle size and number emission

Particulates emitted from diesel and advanced dual-fuel combustion appear in the form of nanoparticles with a wide range of sizes and concentrations [1.80]. Particle emissions are indicative of incomplete combustion, as they primarily consist of carbon particles originating from the fuel [1.78]. The presence of these particles signifies that the combustion process is not fully efficient, leading to the formation of particulate matter. Therefore, particle emissions serve as a marker for improper combustion. Particles with diameters less than 50 nm are classified as nucleation mode particles (NMP), while those with diameters between 50 nm and 500 nm are classified as accumulation mode particles (AMP) [1.81]. NMPs generally form directly from gasto-particle conversion processes and mostly are volatile in nature, while AMPs result from the agglomeration of smaller particles or from the condensation of vapor-phase materials [1.81]. Typically, the PM number distribution follows a bimodal pattern with two peaks: the first peak corresponds to NMPs, and the second peak corresponds to AMPs. NMPs account for more than 90% of the number concentration, while AMPs account for more than 90% of the mass emissions. Nucleation mode particles (NMPs) are particularly harmful due to their small size and high number concentration [1.81]. The greater the number of particles, the larger the total surface area available for the adsorption of volatile organic compounds (VOCs), making NMPs effective carriers for these harmful substances. Additionally, smaller particles have a longer retention time in the atmosphere, increasing the likelihood of being inhaled by humans. Due to their small size, these particles have a higher deposition efficiency in the respiratory tract and can penetrate deeper into the respiratory system, posing significant health risks.

Moreover, the prolonged atmospheric lifetime of NMPs contributes to their widespread distribution, potentially affecting large populations. The interaction of these particles with other atmospheric components can also lead to secondary pollutant formation, further complicating their impact on air quality and health. Understanding these factors is crucial for developing targeted mitigation strategies to reduce the harmful effects of NMPs. Accumulation mode particles (AMPs) have adverse effects on particulate filters [1.78]. Their larger size increases the likelihood of clogging the filter, leading to more frequent regeneration cycles. This increased regeneration rate negatively impacts fuel economy, as the process consumes additional fuel. Consequently, managing AMP emissions is essential to maintain filter efficiency and optimize fuel consumption [1.78].

1.5.1.2 Particulate mass and morphology

Particulate mass and morphology directly influence engine performance, after-treatment system effectiveness, and their potential adverse effects [1.78]. Characterizing particulate mass is crucial because the inhalation and lung retention of particles are directly proportional to the inhaled mass of particulate matter. Additionally, the morphology of particulates plays a critical role in the design of particulate filters and their oxidation reactivity. Understanding the size, shape, and surface characteristics of particulates helps in optimizing filter designs to effectively capture and oxidize these particles, thereby improving engine performance, reducing emissions, and minimizing health risks [1.78, 1.21].

1.5.1.3 Soluble organic fraction

Soluble organic fractions (SOFs) are the organic constituents in particulate matter (PM) that can be extracted using an organic solvent. These fractions primarily include volatile organic compounds (VOCs) and polycyclic aromatic hydrocarbons (PAHs) [1.79]. PAHs in the particulate phase are particularly concerning due to their high toxicity and carcinogenic potential. Diesel engine emissions contain significantly lower levels of organic fractions compared to those from Reactivity Controlled Compression Ignition (RCCI) combustion modes. At lower engine loads, RCCI combustion using alternative fuels can emit more than 40% SOFs. Notably, a study by Storey indicated that the organic fraction in PM from RCCI combustion could be more than 90%, highlighting the need for careful consideration of emission profiles in different combustion modes [1.82].

1.5.1.4 Heavy metal emission

The sources of heavy metals in engines are multifaceted and can be traced to several key areas. Firstly, certain heavy metals are found fossil fuels and may get directly inside the combustion chamber during fuel injection. Secondly, engine components such as valves, piston rings, and cylinder liners are manufactured using alloys containing heavy metals like chromium and nickel [1.83]. Additionally, engine lubricants and additives introduce heavy metals into the combustion chamber, further contributing to emissions. The emission of heavy metals from engines depends on operating condition, fuel type and combustion modes.

1.5.2 Toxicological properties

The toxicological properties of regulated and unregulated emissions generally refer to their harmful effects on human health and the environment [1.21]. Once emitted, these exhaust substances enter the human body primarily through three routes: ingestion, inhalation, and dermal exposure. Among these, inhalation is the most likely route for pollutants emitted by engines. Upon inhalation, these pollutants, depending on their physical and chemical properties, mass concentration, and exposure duration, can engage in metabolic processes, diffuse into the bloodstream, and induce significant adverse health effects [1.21]. Table 1.6 - 1.8 presents the effects of NOx, CO, and HC emissions on various human organs, the associated symptoms, and their underlying causes.

Table 1.6. Effect of NO_x emission on human health [1.84-1.89].

Organ	Effect of NOx (NO and NO ₂)	Core reason
Skin	Aging, atopic sensitization, melanogenesis, Erythema.	NO ₂ (or its breakdown products due to photolysis develop the hydroxyl radicals) damages the cheek skin more effectively than any other anatomic site.
Lungs	Respiratory irritation, asthma symptoms, shortness of breathing, pulmonary inflammation.	Inhalation of NO_2 after a certain limit leads to hypersecretion of mucus and further gives birth to asthma and respiratory disease.
Eyes	Eyes irritation, mucous membrane damage	Nitric oxide in sun radiation forms ozone, which leads to irritation and lacrimation.
Respiratory tract	Irritation in nose and throat, difficulty in respiration.	Traffic-related air pollution develops oxidative stress in air pathways, which further worsens respiration.
Heart	Increased risk of heart attack, heart disease.	PM and gaseous NOx alters the automatic control of the heart and leads to cardiovascular effect.

Table 1.7 Effect of CO emission on human health [1.90-1.93].

Organ	Effect of CO on Health	Core reason
Eyes	Impaired vision. Diameter increase in the retinal blood vessel.	COHb reduces the oxygen-carrying capacity of the blood, which leads to dysfunction of visual ability.
Brain	Hypoxia, memory disorder, brain cell damage.	The brain required more oxygen to function, and CO has 200 times affinity to hemoglobin that reduces the oxygen supply to the brain.

Cardiovascular system	Pathogenesis of heart disease, cardiac arrest.	CO forms COHb, which depresses the myocardial function of the heart with coronary heart disease.
Respiratory tract	Difficulty in the breath, decrease in work capacity	An increase in COHb % leads to low oxygen supply which leads to breath fast to maintain the oxygen.

Table 1.8. Effect of hydrocarbon species emission on human health [1.94].

HC species	Effect on human health	
1,3-butadiene	Effects the bone marrow and leads to leukemia, a probable carcinogen,	
Benzene	Liver and immune system, carcinogenic to human.	
Toluene	Affects the central nervous system, physiological disorder.	
m-xylene	Toxic to human reproduction or development, damage central nervous system.	
o-xylene	Hearing damage and central nervous system.	

1.5.2.1 Toxicity mechanism of PM

The toxicity of combustion emitted aerosol is higher than the non-combustion aerosol (dust, the debris of tires). Diesel engine exhaust particles are the most toxic for the environmental and biological systems. Diesel engine emitted PM are mutagenic and carcinogenic in nature [1.21]. Mutagenicity typically depicts the carcinogenic nature of a chemical species. Mutagenicity is mainly due to organic compounds like PAHs. Several PAHs develop the Reactive oxygen species (ROS), which breaks the deoxyribonucleic acid (DNA) strands. A study reported that traffic particles are the most toxic than any other particles [1.95]. PM penetrates the skin through hair follicles and exerts its detrimental effect through inducing oxidative stress [1.96]. The most harmful particles in air pollutants are the nano-size particles from traffic sources. These small particles can serve as carriers to organic chemical species and heavy metals that can localize to mitochondria and generate oxidative stress [1.97]. The primary concern of particulate matter related to particle pollution is PM10 (PM size is equal to 10µm in diameter), and PM2.5 (PM size is equal to or less than 2.5 µm in diameter) [1.98]. The size of particulate matter affects human health severally as the smaller particulates reach the air pathways and may damage the respiratory system. The setting time of smaller particles is higher than the large size particles. The particulate matter toxicity also depends upon the time of exposure and route.

The major components which show a very toxic effect on human health and the environment are VOC (aldehyde, ketones, hydrocarbons, benzene, fluorocarbon, methane), heavy metal (lead, chromium, arsenic, cadmium, nickel), and PAHs [1.99]. Volatile organic carbons are the precursors of pollutants, which cause oxidative stress [1.99]. Additionally, heavy metals and particulates are toxic and develop oxidative stress in the human organ. Figure 1.6 depicts the hypothetical pathway of the toxicity of PM particles.

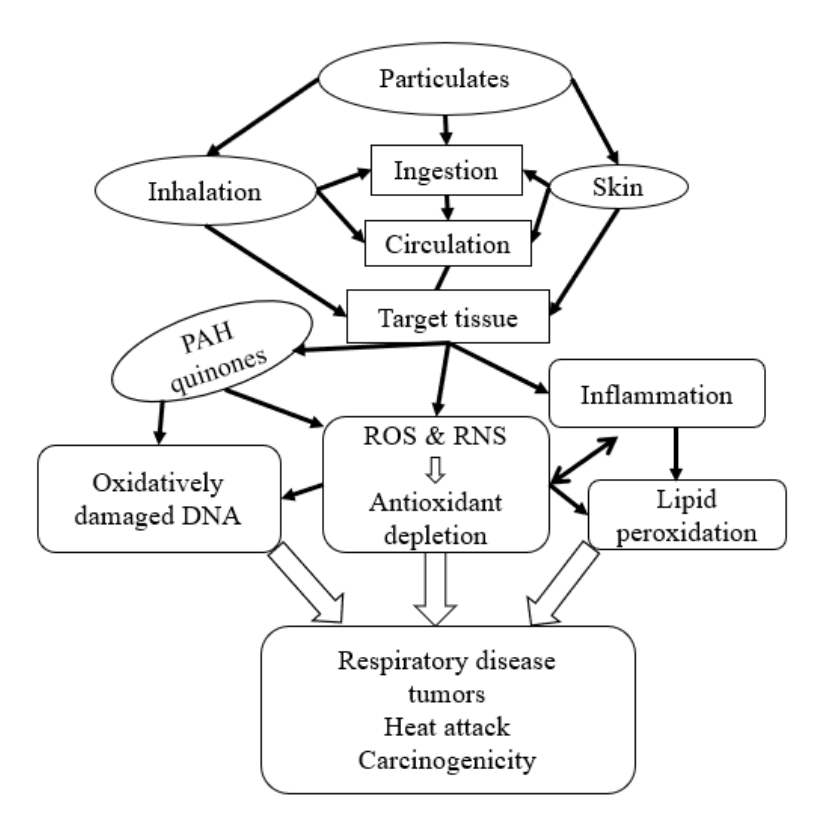


Figure 1.6 Hypothetical pathway for particle-induced oxidative stress and death or hospitalization of cancer and cardiovascular disease [1.99].

1.5.2.2 Mutagenicity and cytotoxicity of PM

Mutagenicity typically indicates the carcinogenic nature of a chemical species, primarily caused by organic compounds such as polycyclic aromatic hydrocarbons (PAHs). Many PAHs generate reactive oxygen species (ROS), which can break DNA strands. Cytotoxicity refers to the effect of particulate matter (PM) on cell toxicity. When PM is exposed to human cells, it can reduce their metabolic activity and, in severe cases, cause cell death [1.99]. The cytotoxicity of pollutants is assessed using the cell viability test, also known as the MTT assay. To assess mutagenicity and

carcinogenic potential, both experimental and analytical methods are available. The USEPA has prescribed guidelines based on the concentration and duration of pollutant exposure. The Integrated Risk Information System (IRIS) provides reference values for risk assessment of various pollutants and categories of exposure. The inhalation unit risk (IUR) is used in these calculations and is assigned to each pollutant based on its toxicity by international organizations such as the USEPA and IRIS. For example, formaldehyde IUR is 1.3×10–5 per μg/m³. This means that for every microgram per cubic meter (µg/m³) of formaldehyde in the air, there is an estimated additional cancer risk of 1.3 in 100,000 over a lifetime of exposure. This value quantifies the incremental risk of developing cancer due to continuous inhalation exposure to a specified concentration of formaldehyde. AMES test is one of the tests that investigate the mutagenicity of a particulate emitted chemical from the engine. The AMES test is discovered by Bruce N. Ames in 1970 to determine the chemical mutagen [1.100]. It is a biological assay to assess the mutagenicity potential of a chemical (pollutant). In AMES test, bacteria are used to test the chemical mutagenicity. The AMES test uses several strains of bacteria (salmonella, E. coli) that carry a mutation. Figure 1.7 shows the typical AMES test procedure, which is normally used in the laboratory to check whether the pollutant is mutagen or not. The mutagenicity of the chemical is proportional to the number of observed colonies. Comparisons for both plates can be made to know whether the chemical is mutagen or not. Very few colonies can be observed at the control plate also; this may be due to spontaneous change because of histidine.

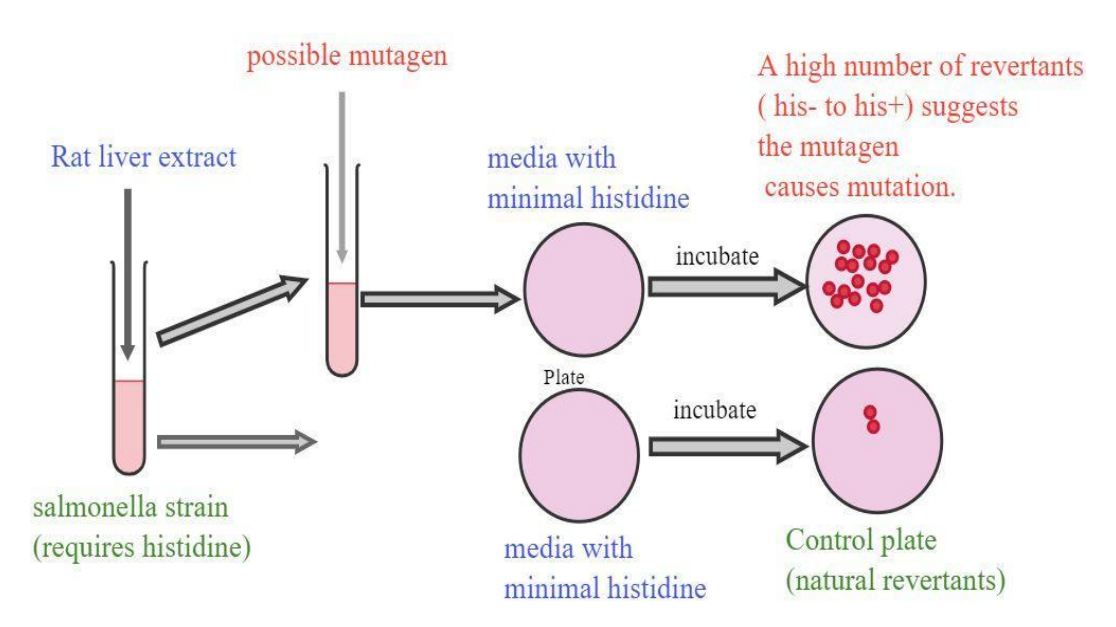


Figure 1.7. The procedure of AMES Test [1.100].

1.5.2.3 Lung retention of PM particles

The main health concern associated with PM particles is their ability to remain in the human respiratory system after being inhaled in. Because of their nanometer scale size, PM particles remain suspended in the air and follow the pathways of airflow in our respiratory system. Once inhaled, some of these particles settle in different parts of the respiratory tract, while others are exhaled during the expiration process [1.101]. This retention of particles can lead to various health problems, especially when exposure is prolonged or to high concentrations. PM particles exert toxic effects primarily through two mechanisms [1.102]. Firstly, chemical compounds within PM particles dissolve in the fluids lining the respiratory tract upon inhalation. Secondly, these particles occupy space within the respiratory tract, reducing the effective tidal volume and necessitating an increase in respiratory rate [1.103]. Additionally, the accumulation of PM particles in the respiratory system adds to the overall mass of the tract, a condition known as lung loading. The size of the PM particles determines their retention destination in the human respiratory tract. This retention is defined as regional deposition of PM nanoparticle. When particles are inhaled, they can deposit in various regions of the respiratory system, categorically defined as the nasopharyngeal, tracheobronchial, alveolar, and pulmonary regions [1.102]. Larger particles tend to settle in the nasopharyngeal region, including the nose and upper throat, where they may be trapped by mucous membranes or expelled through coughing or sneezing. Smaller particles penetrate deeper into the trachea and bronchi, known as the tracheobronchial region, where they can still be cleared by the mucociliary escalator, a mechanism that moves mucus and trapped particles out of the respiratory tract. Fine particles, including nanoparticles, reach the alveolar region, the deepest part of the lungs, where they may accumulate and potentially enter the bloodstream. Beyond the alveoli, particles can affect the pulmonary region, causing inflammation and impacting lung function [1.102].

1.5.3 Environmental risk factors

As engine exhaust pollutants enter the atmosphere, certain reactive pollutants contribute to the formation of secondary organic aerosols during their transport through the atmosphere. These organic aerosols serve as precursors to several detrimental atmospheric phenomena, including the generation of acid rain and the formation of tropospheric ozone, both of which can significantly harm the environment [1.104]. Additionally, these aerosols have the potential to disrupt natural cycles, such as those of nitrogen and oxygen, further complicating atmospheric chemistry and

ecosystem processes. Environmental risk factors associated with pollutants can be broadly classified into four categories: global warming potential (GWP), acidification potential (ACP), eutrophication potential (EUP), and ozone forming potential (OFP) [1.105]. GWP measures a pollutant's ability to trap heat in the atmosphere over time, contributing to climate change and its associated impacts on weather patterns and ecosystems. ACP assesses pollutants' capacity to form acids in the atmosphere, leading to acid rain that harms soil, water bodies, and aquatic life. EUP evaluates how pollutants contribute to nutrient enrichment in water bodies, triggering excessive algae growth and oxygen depletion, which disrupts aquatic ecosystems. OFP refers to pollutants that participate in chemical reactions leading to the formation of ground-level ozone, a harmful pollutant affecting human health and vegetation. Recognizing and addressing these environmental markers are critical for mitigating pollutant impacts and safeguarding both environmental quality and public health [1.105].

1.5.3.1 Global warming potential (GWP)

The "Climate Change 2023: Synthesis Report" states that humans are responsible for all global warming over the past 200 years, resulting in a current temperature increase of 1.1°C above preindustrial levels. This rise has led to more frequent and hazardous weather events, causing increasing destruction to both people and the planet [1.106]. Additionally, the report highlights the significant global warming potential of greenhouse gases, emphasizing the urgent need to reduce emissions to mitigate further climate impacts. According to the U.S. Environmental Protection Agency (USEPA), transportation is the largest contributor to U.S. greenhouse gas emissions, accounting for approximately 28% of the total. From 1990 to 2022, the transportation sector saw a greater absolute increase in GHG emissions than any other sector [1.107]. The concept of GWP was introduced in the First Assessment Report of the Intergovernmental Panel on Climate Change (IPCC-AR1) [1.108]. GWP is used to compare the greenhouse effects of different gases relative to a reference gas, typically carbon dioxide (CO₂). Under this definition, CO₂ is assigned a GWP value of 1. GWP is defined as:

$$GWP = \frac{\int_{0}^{a} a_{i}c_{i}dt}{\int_{0}^{a} a_{co_{2}}c_{co_{2}}dt}......(1)$$

Where a_i represents the instantaneous radiative forcing (RF) from the increased concentration of gas i, c_i denotes the remaining concentration of the gas after time t, for a particular duration in years over which the calculation is conducted [1.109]. The values for the reference gas, carbon dioxide (CO₂), are used in the denominator for comparison [1.109]. It is assumed that the gas is instantaneously released into the atmosphere, and its concentration diminishes over time while it continues to contribute to greenhouse warming during this period. Global Warming Potential (GWP) is a way to compare how much energy different greenhouse gases add to the Earth's atmosphere compared to carbon dioxide (CO₂). It's like a score that shows how much a gas contributes to global warming relative to CO₂.

1.5.3.2 Acidification potential (ACP)

By the late 1970s, acidification had become widely acknowledged as a significant environmental threat. Atmospheric emissions of acidifying substances like sulfur dioxide (SO₂) and nitrogen oxides (NO_x), primarily from burning fossil fuels, can linger in the air for several days and travel thousands of kilometers before undergoing chemical conversion into acids (sulphuric and nitric) [1.110]. These primary pollutants, along with ammonia (NH₃) and their reaction products, alter the chemical composition of soil and surface water upon deposition. This process disrupts ecosystems, leading to what is known as 'acidification'. Examples of its impact include forest decline in Central and Eastern Europe and the prevalence of 'dead' lakes in Scandinavia and Canada, largely attributable to acidification.

1.5.3.3 Eutrophication potential (EUP)

Term 'eutrophic' comes from the Greek word 'eutrophos', meaning well-nurtured. Eutrophication describes the state of an aquatic system with elevated levels of nutrients, particularly nitrogen and phosphorus, which lead to algal blooms and degrade water quality in aquatic ecosystems. The overabundance of nutrients reduces oxygen levels in water bodies, harming aquatic life and creating an undesirable imbalance. Eutrophication causes water to become cloudy with a greenish hue, reducing sunlight penetration and lowering the rate of photosynthesis in submerged aquatic plants. Furthermore, as algae die and decompose, oxygen levels decrease, which is essential for aquatic life. This depletion leads to the death of species that inhabit the depths of water bodies [1.111]. Algae synthesize through photosynthesis using sunlight and inorganic compounds. The process of eutrophication is as follows:

$$106CO_2 + 16NO_3^- + HPO_4^{2-} + 112H_2O + 18H^+ + energy + trace element$$

 $\rightarrow (CH_2O)_{106}(NH_3)_{16}(H_3PO_4) + 138O_2$ (2)

Here (CH₂O)₁₀₆(NH₃)₁₆(H₃PO₄) is chemical formula of algae.

1.5.3.4 Ozone forming potential (OFP)

Ozone is a gas consisting of three oxygen atoms. It exists in two main regions: the Earth's upper atmosphere and at ground level. Its effects vary depending on where it is found. In the upper atmosphere, known as stratospheric ozone, it is beneficial. This natural ozone layer acts as a protective shield, absorbing and filtering out the sun's harmful ultraviolet (UV) radiation before it reaches the Earth's surface. Ground-level ozone is regarded as a harmful air pollutant due to its detrimental effects on both people and the environment. It is a major constituent of "smog." Tropospheric or ground-level ozone is not directly emitted into the air; rather, it forms through chemical reactions involving nitrogen oxides (NO_x) and volatile organic compounds (VOCs). These reactions occur when pollutants from vehicles, power plants, industrial facilities, refineries, chemical plants, and similar sources interact in the presence of sunlight [1.112].

Within the lower atmosphere, ozone forms through chemical reactions involving these species in the presence of sunlight, typically following the path given as [1.113],

$$VOC + NOx + sunlight = Ozone + oxidized products$$

1.6 Motivation for the present research

The ongoing debate surrounding the electrification of the transport sector, climate change, and air pollution, coupled with the rapidly evolving user preferences, the fuel versus food dilemma, and the fast-growing industry, motivates researchers to explore innovative methods for enhancing the fuel conversion efficiency of internal combustion engines along with minimizing harmful emissions. As the world progresses towards decarbonization and zero-emission technologies, the adoption of renewable alternative fuels and advanced combustion engines has become essential. Regulatory bodies are setting ambitious targets for reducing greenhouse gas emissions. The International Maritime Organization aims for international shipping to achieve net-zero GHG emissions by around 2050. Similarly, the US Environmental Protection Agency has set a net-zero target for 2050. Additionally, India announced at the 26th session of the United Nations Framework Convention on Climate Change (COP 26) in November 2021 that it aims to achieve net-zero

emissions by 2070. In the pursuit of net-zero emissions, low-carbon and zero-carbon fuels such as methanol and hydrogen are capturing widespread attention. These innovative fuels stand out due to their exceptional properties, well-established supply chains, cost-effectiveness (especially for methanol), and the potential to produce methanol from waste, making them a compelling choice for a sustainable future. Utilizing these fuels in advanced dual-fuel combustion engines has the potential to significantly enhance efficiency and achieve ultra-low soot and NOx emissions, as reported by several studies. Before accepting these fuels with advanced combustion technology, it's essential to thoroughly assess their regulated and unregulated emissions to understand their impact on human health and the environment. Current engines are optimized for conventional fossil fuels and conventional combustion strategies and dedicated aftertreatment systems tailored to conventional engine technology. Shifting to new fuels or combustion modes alters the dynamics within the combustion chamber, resulting in different reaction products. As combustion mode shifts towards advanced combustion mode, low-temperature combustion reactions become increasingly significant, leading to the formation of reaction intermediates with different chemical structures. For example, the combustion of methanol in a low-temperature environment results in the formation of formaldehyde, which the International Agency for Research on Cancer (IARC) has identified as carcinogenic. Additionally, the combustion of diesel surrogates in advanced combustion modes leads to the formation of alkylperoxy radicals, which subsequently produce aldehyde compounds. Once combustion reaches the expansion stroke, local thermodynamic conditions determine the fate of the combustion products in the exhaust. Depending on their vapor pressure and saturation temperature, these products may either condense on the surface of soot particles or be emitted in the gas phase into the atmosphere. During atmospheric transport, these emissions can participate in the formation of secondary organic aerosols. Additionally, the methods employed to achieve advanced dual-fuel combustion, such as early injection timing, are susceptible to lube oil dilution. This can lead to the lube oil entering the combustion chamber, where it gets consumed and contributes to the emission of various organic compounds and metals. Due to the diverse nature of exhaust products, the physico-chemical and toxicological characterization of both regulated and unregulated emissions is essential. Additionally, the US-EPA charter mandates that any new technology introduced to the market should not emit more toxic species than existing technologies. This guideline underscores the urgency of this research, highlighting the critical need for thorough evaluation and validation of advanced combustion modes with alternative fuels. This thorough evaluation is crucial for accurately assessing the impacts of advanced combustion modes using alternative fuels.

1.7 Main goal and objective of thesis

The primary goal of the present work is to conduct a comprehensive comparative analysis of the physical, chemical and toxicological characteristics of both regulated and unregulated emissions emitted by conventional and advanced dual-fuel combustion engines. These engines utilize gasoline, methanol, and hydrogen as low-reactivity fuels and diesel as a high-reactivity fuel. The physical characterization aspect focuses on examining particle emission characteristics, including particle number, size, mass, and morphology. For chemical characterization, the research delves into the chemical speciation of emissions, assessing chemical compounds such as saturated and unsaturated hydrocarbons, carbonyls, aromatics, soluble organic fraction and heavy metal traces. The toxicological characterization encompasses both experimental and analytical assessments. The study aims to perform the in-vitro cytotoxicity and oxidative stress in human lung epithelial cell lines exposed to particulate aggregates to assess the toxicity. The study aims to predict the lung retention of nanoparticles and their chemical composition across different lung regions, such as the head, tracheobronchial, and alveolar regions. Furthermore, the thesis includes a cancer risk assessment following USEPA guidelines for a trespasser subject using carbonyl and metal emissions inhalation unit risk. Through these detailed investigations, this research aims to provide a detailed understanding of the environmental and health impacts of various dual-fuel combustion systems, offering valuable insights for future regulatory and technological advancements.

To achieve the main goal the following specific objectives are defined:

- Developing an advanced dual-fuel combustion method by integrating a port fuel injection system into a conventional diesel engine, utilizing advanced injection timing and fuel premixing ratio
- Conduct a comparative investigation on the effects of engine load and fuel premixing ratio on nanoparticle emissions (particle number, mass, and size distribution), as well as regulated and unregulated emissions, between conventional diesel combustion and advanced dual-fuel combustion modes (gasoline-diesel and methanol-diesel).

- Perform particulate sampling using a partial flow dilution tunnel to characterize PM aggregates
 physical (mass, morphology), chemical (soluble organic fraction, metal emission), and
 toxicological properties (cytotoxicity, reactive oxygen species, cancer risk potential, lung
 retention) from both combustion modes
- For heavy duty application purpose, a numerical investigation is conducted to predict the
 regulated and unregulated from conventional diesel and hydrogen-diesel dual fuel combustion
 mode. Additionally, the aim is to assess the mutagenicity and carcinogenicity potential of the
 predicted unregulated emissions.

1.8 Thesis organization

Chapter 1: Introduction: This chapter presents a comprehensive overview of conventional and advanced dual fuel combustion engines, describing the characteristics of conventional diesel engines and advanced dual fuel engines. It discusses automotive fuels, including diesel, gasoline, methanol, and hydrogen. The formation mechanism of emissions is examined, with a particularity between regulated (CO, NOx, HC, PM) and unregulated emissions (saturated and unsaturated hydrocarbons, carbonyl compounds, aromatic compounds, heavy trace metals). Additionally, the physico-chemical and toxicological characteristics of emissions are investigated, alongside their environmental risk factors such as global warming potential, acidification potential, eutrophication potential, and ozone forming potential. The chapter concludes by stating goals and outline of the thesis, and the research objectives.

Chapter 2: Literature Review: This chapter reviews existing research on the emission characteristics of diesel and dual-fuel engines, including both regulated and unregulated emissions. It discusses the physico-chemical characteristics, such as particle number and mass distribution, soluble organic fraction, and inorganic fractions. The toxicological characteristics, including cytotoxicity, carcinogenicity, mutagenicity, and lung retention, are also examined. Environmental risk factors, including global warming, acidification, eutrophication, and ozone forming potential, are reviewed. The chapter identifies gaps in the current literature, highlighting areas where further research is needed.

Chapter 3: Methodology: This chapter outlines the experimental setup and instrumentation used in the present thesis work. This chapter discusses the modification made in existing system to

operate it in RCCI mode. It also describes the sampling methodology and the approaches for physico-chemical and toxicological evaluations. This includes physical characterization, chemical characterization, cytotoxicity and reactive oxygen species (ROS) tests, carcinogenicity and mutagenicity calculations, and lung retention modeling. The chapter also covers the numerical methodologies for hydrogen-diesel dual fuel mode and quantification methods for environmental risk assessments, including global warming, acidification, eutrophication, and ozone forming potentials.

Chapter 4: Results and Discussion: This chapter presents and analyzes the results obtained during experimentation and numerical simulation. It discusses combustion characteristics, including in-cylinder pressure, heat release rate, start of combustion, and combustion phasing. Emission characteristics are analyzed, incorporating separate sections for regulated emissions (THC, CO, NOx, particulate emissions) and unregulated emissions (saturated and unsaturated hydrocarbons, carbonyls, aromatics, inorganics). The physico-chemical characterization includes particle number, size and mass distribution, SEM analysis, soluble organic fraction, and heavy trace metal identification and analysis. Toxicological analysis covers cytotoxicity, ROS imbalance, carcinogenicity, mutagenicity, and lung retention of nanoparticles. The chapter also discusses environmental risk factors, such as global warming, acidification, eutrophication, and ozone forming potentials and their analysis.

Chapter 5: Conclusion and Future Scope: This chapter summarizes the key findings of the research. It provides recommendations for future research, suggesting areas where further investigation could enhance the understanding of dual-fuel combustion systems and their emissions. The chapter discusses the societal implications of the present work.

Chapter 6: References: This chapter outlines the references cited in the present thesis work.

Chapter 2

Literature Review

This chapter presents a literature survey of combustion, emission and their effect on human health and environment from conventional diesel and advanced dual fuel engines. It provides a detailed review of existing research on the combustion and emission characteristics of diesel and dual-fuel engines. It covers both regulated emissions (such as carbon monoxide (CO), oxides of nitrogen (NOx), unburned hydrocarbons (HC), and particulate matter (PM)) and unregulated emissions (including saturated and unsaturated hydrocarbons, carbonyl compounds, aromatic compounds, and heavy metals). The review also delves into the physico-chemical characteristics of PM emissions, focusing on aspects such as particle number distribution, particle mass distribution, soluble organic fraction, and metal emission. The chapter critically examines the toxicological characteristics of these PM and gaseous emissions, including their cytotoxicity, carcinogenicity, mutagenicity, and the lung retention of PM nanoparticles. Additionally, the chapter addresses environmental risk factors associated with these emissions, such as their global warming potential, acidification potential, eutrophication potential, and ozone-forming potential of diesel and dual-fuel engines. Lastly, the chapter presents the research gap identified from the literature survey that needs to be addressed.

2.1 Combustion and emission characteristics of conventional and dual fuel engines

The present section discusses the combustion and emission characteristics of diesel and advanced dual-fuel engines. It covers how operating parameters influence ignition delay, combustion phasing, and combustion duration. Understanding these combustion characteristics is crucial, as the formation and emission of exhaust products are mainly dependent on the combustion process. Combustion occurs through a series of elementary reactions, and the products formed in these reactions can sometimes appear alongside the final exhaust products, depending on the local incylinder thermodynamic conditions [2.1].

2.1.1 Combustion characteristics of diesel and dual fuel engines

The engine combustion phenomena can be categorized into two types: premixed (or homogeneous) combustion and diffusion (or mixing-controlled) combustion. Diffusion or mixing-controlled combustion is typically observed in diesel engines due to the heterogeneous nature of the combustion process, which involves direct injection of fuel into the combustion chamber at the end of the compression stroke [2.2]. The evolution of in-cylinder pressure and the heat release rate are paramount combustion parameters from which secondary combustion characteristics are derived [2.3]. These secondary characteristics are discussed subsequently in detail.

To qualitatively understand the combustion several parameters are defined such as ignition delay, combustion phasing and combustion duration. Ignition delay is defined as the time difference (sometimes expressed in terms of crank angle) between the start of fuel injection and the onset of combustion. It is a crucial parameter because it influences the quality of combustion, the rate of premixed heat release, and subsequently, the overall heat release rate. This, in turn, affects combustion noise, NOx formation, and high-temperature reactions [2.2]. Combustion phasing, also known as CA50, quantitatively indicates the crank angle position at which 50% of the total heat release occurs during the combustion process. CA₅₀ serves as a critical indicator that governs several combustion characteristics: it influences combustion quality, the indicated work done, the oxidation rate of formed pollutants, and the temperature of exhaust gases [2.3]. Combustion duration, often expressed as CA₁₀₋₉₀, represents the total time taken for combustion from 10% to 90% of the heat release. This duration plays a critical role in influencing NOx formation as it signifies the duration of high-temperature reactions and affects the residence time, which directly impacts NOx emissions [2.3]. Additionally, combustion duration affects the rate of heat transfer and the amount of work produced during the combustion process. Understanding and controlling combustion duration is essential for optimizing engine performance and reducing emissions. Changes in operating conditions, fuel types, and combustion modes significantly influence combustion characteristics [2.3]. This section specifically explores the impact of low-reactive fuels such as methanol and hydrogen on the combustion characteristics of reactivity-controlled compression ignition (RCCI) engine.

Studies have found that increasing the fuel injection quantity results in higher in-cylinder peak pressure. Advancing the start of injection (SOI) leads to longer ignition delay, promoting premixed

combustion and resulting in higher maximum cylinder pressure and peaks in the rate of heat release (ROHR) [2.4], [2.5], [2.6], [2.7], [2.8], [2.9]. Conversely, retarding the injection timing closer to top dead center (TDC) during the compression stroke shortens ignition delay, leading to a higher amount of fuel consumed in diffusion-controlled combustion and thereby reducing maximum cylinder pressure. Increasing fuel injection pressure enhances peak cylinder gas pressure due to better fuel-air mixing, which promotes improved fuel oxidation and higher rates of heat release with rapid burning and a shorter combustion duration [2.10], [2.11], [2.12], [2.13]. An increase in engine load in conventional diesel engines extends the combustion duration due to the prolonged diffusion phase of combustion. However, it shortens the CA₁₀ because the higher in-cylinder mean gas temperature at higher loads enhances the rate of autoignition reactions [2.14]. In RCCI combustion due to only premixed combustion phase the combustion duration is less than the conventional diesel engines (CDC). Several studies have reported that methanol/gasoline-diesel RCCI combustion exhibits a shorter combustion duration compared to conventional diesel combustion (CDC) [2.15, 2.16]. However, due to the lower reactivity of methanol, at lower engine load conditions, both CA10 (crank angle at which 10% of the fuel has consumed) and CA50 (crank angle at which 50% of the fuel has consumed) are delayed compared to CDC. Additionally, as the methanol energy share in the combustion chamber increases, further retardation in these parameters is observed. Another reason mentioned by several researchers is that the higher latent heat of vaporization of methanol cools the in-cylinder charge, which also contributes to the retardation of CA10 [2.15, 2.16, 2.17].

2.1.2 Regulated emission characteristics

Regulated emissions include total hydrocarbon (THC), carbon monoxide (CO), oxides of nitrogen (NOx) and particulate matter (PM) emissions. The present section discusses this emission separately. The effect of operating parameters, combustion mode and fuel type are discussed in this section.

THC emission

The primary source of unburned hydrocarbon emissions in diesel engines is the incomplete combustion of fuel. Several factors contribute to these emissions, including the retention of unburned fuel in cylinder crevices, engine configuration, fuel structure, combustion temperature, oxygen concentration, and residence time [2.18]. Research has shown that using methanol-diesel

blended fuel results in significantly lower unburned hydrocarbon (uHC) emissions compared to using pure diesel [2.18, 2.19, 2.20, 2.21, 2.22]. The potential reasons for the decrease in unburned hydrocarbons include the presence of oxygen molecules in the fuel, which enhances combustion quality. Additionally, the methanol in the blend introduces oxygen into fuel-rich regions, increasing the oxidation of fuel molecules and subsequently reducing HC emissions. Additionally, Methanol's higher flame propagation speed compared to diesel enhances the rate of diffusive combustion when blended with diesel. This leads to a shorter combustion duration, increased peak heat release rate, and higher in-cylinder temperatures, finally reducing unburned hydrocarbon (HC) emissions. However, some studies [2.23, 2.24, 2.25, 2.26, 2.27] have reported slightly higher unburned hydrocarbon emissions at low loads for methanol-diesel blended fuel compared to pure diesel. At low loads, the injection of a less amount of fuel into the cylinder decreases the chances of fuel impingement on the cylinder walls. However, the substantial excess air at low loads causes poor fuel distribution within the combustion chamber and a lower average gas temperature due to the reduced fuel combustion. This, in turn, lowers the exhaust gas temperature. As a result, regions with a lean fuel-air mixture may not fully combust and can escape into the exhaust, leading to higher unburned hydrocarbon emissions. Additionally, Methanol's higher latent heat of evaporation potentially lowers the temperature of the charge at the end of the compression stroke. This longer ignition delay can retard combustion phasing. When combustion is delayed, it decreases the mean gas temperature. A reduced combustion temperature can make it more challenging to oxidize hydrocarbon fuel. Several studies investigated the dual-fuel combustion mode, injecting methanol in port during the intake stroke and diesel during the compression stroke. The studies reported that with an increase in methanol energy share the HC emission increases from dual fuel combustion mode. Higher HC emissions can be attributed to the formation mechanism of HC in the crevice. When the mixture has more methanol as the energy share increases, more HC tends to be trapped in the crevice volume. The lower combustion temperatures observed in methanol-diesel dual-fuel operations have been linked to increased HC emissions due to the greater mass of incompletely combusted fuel [2.28]. The study by [2.29] noted that hydrocarbon (HC) emissions decrease with advanced pilot injection timing. Increasing diesel injection pressure reduces HC emissions. Higher injection pressure improves spray atomization and enhances the mixing process, leading to better combustion of the premixed charge and increased combustion temperatures, thereby reducing HC emissions. Additionally, higher intake

air temperatures result in decreased total hydrocarbon emissions, with a more pronounced effect at higher fuel premixing ratios. Elevated intake air temperatures shorten ignition delays and reduce the lean mixture zone near the combustion limit [2.28]. However, higher intake air temperatures also raise the in-cylinder mean gas temperature, which can increase unburnt HC emissions while reducing quenching effects [2.28]. The advanced premixed dual-fuel combustion strategy RCCI shows notably higher hydrocarbon emissions than conventional diesel combustion. Additionally, in RCCI mode, increasing the methanol/diesel premixing ratio has been observed to further elevate HC emissions, as highlighted by [2.30]. The factors contributing to the increased HC emissions in RCCI engines compared to conventional diesel combustion are analogous to those observed in conventional dual-fuel operations. [2.31] conducted a comparative study between methanol-diesel RCCI and conventional diesel combustion modes. They found that as engine load increases, total hydrocarbon (THC) emissions decrease significantly in both combustion modes. However, at lower engine loads and with an increased proportion of methanol energy share, THC emissions were reported to increase specifically in the methanol-diesel RCCI combustion mode [2.31].

Several studies have documented that the addition of hydrogen in hydrogen-diesel dual fuel systems reduces hydrocarbon (HC) emissions due to the absence of carbon in hydrogen fuel [76]. Additionally, incorporating hydrogen into the intake air prolongs the ignition delay, leading to a more homogeneous mixture [2.32]. Furthermore, the high burning velocity of hydrogen enhances diesel combustion, thereby reducing unburned HC emissions [2.33]. Contrarily, some researchers have reported that adding hydrogen to diesel fuel can increase unburned hydrocarbon (UHC) emissions [2.34, 2.35]. This increase could be due to the inadequacy of the injected pilot fuel, which causes poor ignition of the gaseous fuel [2.36]. Moreover, hydrogen addition can lower the oxygen concentration in the air-fuel mixture, leading to incomplete combustion of the diesel fuel [2.37]. The rapid consumption of oxygen due to the instantaneous combustion of hydrogen might result in incomplete combustion of the diesel fuel injected at the end of the injection period [2.38]. The increased ignition delay in fuel-lean conditions, resulting from hydrogen addition, could also lead to incomplete combustion [2.39].

CO emission

Carbon monoxide (CO) is a toxic gas that poses environmental and health risks. It is among the primary regulated emissions, arising from insufficient oxygen during combustion which results in

incomplete oxidation of fuel. CO forms when there isn't enough oxygen available to fully convert fuel into CO2. Studies have consistently shown that increasing the methanol fraction in blended fuel leads to decreased carbon monoxide (CO) emissions across a wide range of load and speed conditions (Fig. 28). This trend has been documented by numerous researchers [2.19, 2.20, 2.40, 2.24, 2.21, 2.41, 2.42, 2.43]. Methanol-diesel blends consistently show lower CO emissions compared to neat diesel operation. These findings suggest that blending methanol into diesel fuel could be pivotal in reducing CO levels. The oxygen content present in methanol enhances combustion quality, leading to reduced CO emissions. Specifically, the presence of oxygencontaining methanol in locally rich spray regions improves post-flame oxidation, thereby decreasing CO formation. Conversely, certain studies have observed a slight increase in carbon monoxide (CO) emissions at low loads compared to neat diesel [2.23, 2.44, 2.27]. This observation can be attributed to the higher latent heat of evaporation of methanol, which introduces a quenching effect. This effect exacerbates CO formation at low loads because the lower temperature rise makes it more challenging to oxidize CO due to cooling inside the cylinder chamber. According to Singh et al. [2.30], a study on RCCI combustion reveals significantly higher carbon monoxide (CO) emissions compared to conventional diesel combustion. This difference is attributed to the lower in-cylinder mean gas temperature in RCCI combustion, which hinders the complete oxidation of CO to CO2. Furthermore, in operations with lower methanol premixing, an increase in diesel injection pressure has been observed to slightly reduce CO emissions. This reduction is credited to improved combustion efficiency at higher diesel injection pressures, where the oxygen molecules from methanol aid in CO oxidation to CO2 at optimal in-cylinder temperatures [2.30]. However, at higher methanol/diesel premixing ratios, the presence of a larger quantity of methanol can lower the in-cylinder mean gas temperature due to its higher heat of vaporization. This effect is exacerbated by higher diesel injection pressures. A comparatively lower in-cylinder mean gas temperature resulting from lower overall reactivity inside the combustion chamber, due to a more homogeneous distribution of diesel at higher injection pressures, could potentially contribute to higher CO emissions [2.30].

Adding hydrogen to the intake air can decelerate the formation rate of CO [2.35, 2.45] due to the decrease in the C/H ratio of the fuel [2.45]. Furthermore, the high diffusivity of hydrogen in the air helps form a well-homogenized combustible mixture, enhancing the combustion process and lowering CO emissions [2.37, 2.34]. The high flame speed of hydrogen can improve the

combustion process and raise the in-cylinder temperature, which reduces CO emissions [2.34]. Additionally, hydrogen can operate on a lean equivalence ratio, contributing to the reduction in CO emissions [2.46, 2.45]. However, some studies have indicated that incorporating hydrogen into diesel fuel can potentially increase CO emissions. This increase occurs because hydrogen addition can dilute the oxygen concentration in the air, leading to higher CO emissions [2.35]. Moreover, increasing the hydrogen content in diesel fuel can raise the in-cylinder temperature, causing the dissociation of CO2 into CO and O [2.36]. The high reaction rate of hydrogen can consume the available oxygen in the combustion chamber, leaving less oxygen for CO oxidation. Oxygen consumption in hydrogen oxidation and radical formation also contributes to this effect [2.45]. Additionally, the water produced by hydrogen oxidation can react with diesel hydrocarbons (steam reforming), further increasing CO emissions [2.45].

NO_x emission

Studies by Datta and Mandal [2.47], Yasin et al. [2.48], and Yilmaz [2.49] have demonstrated that the exhaust gas temperature increases when engines are fueled with methanol-diesel blends. This phenomenon is primarily due to the combustion of a greater amount of fuel per engine cycle under higher load conditions. The influence of methanol-diesel premixing ratios on NOx emissions in dual-fuel operations indicates that methanol-diesel dual-fuel operation generally results in lower NOx emissions compared to conventional diesel. Increasing the methanol-diesel premixing ratio correlates with a decrease in NOx and NO emissions [2.47]. The formation of NOx emissions is heavily influenced by factors such as mean gas temperature, combustion duration, and oxygen concentration [2.50, 2.51]. The higher heat of vaporization and lower reactivity of methanol tend to delay ignition timing and retard combustion phasing, leading to more charge burning during the expansion stroke and subsequently lowering the mean in-cylinder gas temperature. This decrease in temperature reduces NO formation (2.52, 2.39]. When the methanol-diesel premixing ratio increases from 0% to 40%, the local equivalence ratio of methanol in the premixed charge rises, enhancing HO2 formation and increasing NO2 emissions [2.52]. However, this increase in NO2 emissions is constrained by reduced NO emissions and increased heat release rates, which impact HO2 conservation negatively [2.52]. As the premixing ratio moves from 40% to 60%, NO2 emissions start to decline due to methanol's degraded post-combustion effects further reducing NO emissions, as reflected in the rising NO2/NO ratio [2.52]. Increasing exhaust gas recirculation (EGR) has been shown to decrease total NOx and NO2 emissions, with NO emissions initially decreasing until reaching a plateau after a certain EGR increase [2.52, 2.53]. EGR reduces the oxygen content in the intake air and enhances the charge's heat capacity, thereby reducing NO formation. A shorter combustion duration with increased EGR further reduces NO emissions but may impact HO2 conservation negatively, leading to decreased NO2 emissions [2.52]. In contrast, the reduction of HO2, which inhibits the conversion from NO to NO2, can promote NO conversion, explaining why NO emissions remain nearly unchanged with EGR increasing from 10% to 30%. In advanced dual-fuel RCCI (Reactivity Controlled Compression Ignition) combustion modes, NOx emissions are significantly lower compared to conventional diesel combustion. Increasing the methanol/diesel premixing ratio further decreases NOx emissions in RCCI combustion, as observed in the study by [2.30]. The reduced NOx emissions in RCCI mode can be attributed to the lower in-cylinder mean gas temperature. Additionally, higher diesel injection pressures have been shown to reduce NOx emissions in RCCI combustion, as highlighted by [2.30]. Moreover, advancing diesel injection timing in RCCI combustion also contributes to lower NOx emissions.

Various studies have shown that adding hydrogen to diesel fuel could increase NOx emissions [2.35, 2.54]. The high calorific value of hydrogen can increase the peak in-cylinder pressure and temperature, thus elevating NOx emissions [2.55]. Additionally, the high flame speed of hydrogen can lead to a more complete combustion process, further increasing in-cylinder pressure and temperature [2.46]. Hydrogen addition may also result in higher local temperatures earlier in the expansion stage, accelerating NOx generation [2.38]. The long ignition delay caused by adding hydrogen to diesel fuel can lead to the formation of a well-mixed air-fuel mixture before ignition, raising in-cylinder temperatures and increasing NOx emissions [2.56]. It has also been reported that NOx emissions from the hydrogen port injection method might be higher than those from the hydrogen induction technique [2.57]. This could be because the hydrogen port injection method improves combustion and volumetric efficiency, increasing the combustion temperature [270]. In contrast, other studies have reported that hydrogen addition to diesel fuel could reduce NOx emissions due to engine operation with a leaner mixture [2.58]. A very lean equivalence ratio can lower the peak combustion temperature, thereby decreasing NOx emissions [2.59]. Hydrogen can make the air-fuel mixture more homogeneous while eliminating fuel-rich zones, leading to a steady increase in in-cylinder temperature that suppresses NOx formation [2.60]. NOx emissions could

also be reduced at higher hydrogen supplement rates because prolonged combustion can lower the heat release rate [2.61]. The water produced from hydrogen oxidation can lower the in-cylinder temperature, further suppressing NOx emissions [2.62]. Additionally, adding hydrogen to diesel fuel can decrease the quantity of diesel fuel burned in the diffusion combustion phase. This reduction can lower NOx emissions since a significant portion of NOx is generated in the diffusive combustion phase [2.62].

PM emissions

Soot, recognized as the primary component responsible for smoke formation, is a major source of particulate matter. Smoke forms in fuel-rich regions where oxygen is severely deficient under high temperatures and pressures. As the air-fuel ratio increases, the oxygen deficiency in the combustion chamber decreases. Smoke formation primarily occurs through the thermal cracking of long-chain molecules in an oxygen-deficient environment [2.63, 2.64, 2.65]. The possible reasons for the reduction in PM with methanol-diesel blend is due to the lower carbon content, additional oxygen content and higher flame speed of methanol fuel. In dual-fuel operation, the smoke number increases with an increase in engine load. However, an increase in methanol premixing leads to a decrease in smoke emission. This reduction is primarily attributed to the lower amount of diesel that is injected when more methanol is used [2.50]. The formation of smoke in a compressionignition (CI) engine is generated from carbon particles formed by the thermal cracking of large hydrocarbon molecules in a fuel-rich core [2.50]. In methanol-diesel dual-fuel operation, a large fraction of the charge burns in the premixed combustion phase, significantly reducing smoke emission. Additionally, methanol has a higher oxygen content, and the premixing of methanol in dual-fuel combustion mode also contributes to lower smoke emission. According to several studies, soot emissions can be suppressed by adding hydrogen to diesel fuel [2.66, 2.60]. Hydrogen can create a more homogeneous air-fuel mixture, improving combustion efficiency and reducing soot emissions [2.67]. The addition of hydrogen to diesel fuel can decrease the carbon content or increase the hydrogen-to-carbon (H/C) ratio of the fuel, thus mitigating soot emissions [2.68]. By reducing the amount of diesel fuel in the mixture, hydrogen promotes the oxidation of soot while decreasing its initial formation [2.69]. Several studies have reported that adding hydrogen to diesel fuel can reduce smoke emissions due to the carbon-free nature of gaseous hydrogen and the high hydrogen-to-carbon (H/C) ratio of the air-fuel mixture [2.59]. In other words, hydrogen

combustion produces water and does not lead to smoke emissions. The high diffusivity of hydrogen can also improve the homogeneity of the air-fuel mixture and the availability of oxygen, thereby reducing smoke emissions [2.55]. Additionally, the turbulent flame generated during hydrogen combustion can oxidize the carbon particles formed from diesel combustion [2.70]. The formation of a premixed charge (hydrogen-air) in the dual-fuel operation mode can eliminate the primary cause of smoke emissions from diesel engines [2.70]. However, excessive hydrogen induction can increase smoke emissions by forming a rich air-fuel mixture [2.71].

2.1.3 Unregulated Emissions

Among these HC emissions such as carbonyl compounds, PAHs, few unsaturated HCs are not subject to direct regulations and are therefore referred to as unregulated emissions. Numerous studies have indicated that the unregulated gaseous emissions from alcohol-diesel dual fuel engines exhibit considerably higher levels of harmful effect on environment and human health [2.72, 2.73, 2.74, 2.75, 2.76, 2.77, 2.78, 2.79]. Oyama and Kakegawa conducted extensive testing on both low and heavy-duty vehicles' unregulated emissions. They found that the concentration of aromatic compounds and sulfur content in the fuel has a significant impact on particulate matter (PM) and other unregulated emissions. The study also indicated that implementing a diesel oxidation catalyst (DOC) can lead to a considerable reduction in unregulated emissions [2.73]. Takada et al., conducted a study on a heavy-duty diesel engine to examine the emission levels of formaldehyde, benzene, 1-3 butadiene, and benzo[a]pyrene. The study reported that under all the tested conditions, at lower engine load the emission of these species was significantly higher [2.74]. Natti et al. investigated diesel engines operating under the low temperature combustion (LTC) regime to analyze both regulated and unregulated emissions. The study revealed that the LTC regime resulted in increased emissions of unregulated hydrocarbons as the swirl ratio and injection pressure were raised. The study concluded that the LTC regime emitted significantly higher levels of unregulated emissions compared to conventional diesel combustion [2.77]. Ogawa and Taga study found that transitioning the engine to the LTC regime resulted in the emission of ultra-low levels of NOx and particulate matter PM. However, this shift also led to a significant increase in emissions of benzene, formaldehyde, 1-3 butadiene, and aldehydes [2.78]. Liu et al., reported in their study that with an increase in intake charge temperature the unregulated emission decreases from MD-RCCI engine [2.80]. Aries et al., investigated the effect of pentanol/diesel

blend on diesel engine carbonyl emission. The study revealed that the use of pentanol increases the carbonyl emission which further led to an increase in cancer risk potential of the exhaust emission [2.81]. Saxena and Maurya explored unregulated emissions from methanol and gasoline as low reactive fuel fueled RCCI engines. They demonstrated in their study that, with an increase LRF energy share and advanced injection timing the unregulated emission increase from RCCI engines. The highest increase was observed in carbonyl emissions (HCHO, CH3CHO) [2.82].

2.2 Physico-chemical characteristics of diesel and dual-fuel engines

The physical and chemical characteristics of particulate matter (PM) samples include particle size, number concentration, mass distribution, polycyclic aromatic hydrocarbons (PAHs) associated with PM samples, soluble organic fractions present in samples, and trace metals present in PM samples. The physico-chemical properties of PM samples are influenced by engine operating parameters, fuel type, and combustion mode. The present section discusses the particle emission characteristics, PAH emissions, soluble organic fraction, and trace metal emissions from diesel and methanol/ hydrogen diesel dual-fuel engines.

2.2.1 Particle emission characteristics

Along with gaseous emissions, diesel engines emit significant concentrations of nanoparticles. Particulates, or soot, are produced in the combustion chamber during both diffusion and premixed combustion of locally rich fuel-air mixtures. Soot particles are formed through thermal cracking, dehydrogenation, or pyrolysis of long-chain fuel molecules in oxygen-deficient conditions. Pyrolysis of long-chain fuels typically produces unsaturated hydrocarbons like acetylene and polyaromatic hydrocarbons (PAHs), known as precursors. These precursors condense to form soot nuclei through a nucleation process. During nucleation, a large number of small particles (1–2 nm) are generated. These small particles increase in size during the surface growth process, where intermediate combustion products are deposited on the surface of soot nuclei. The spherical particles then collide and combine to form larger particles in a process called coagulation. Coagulation begins with the surface growth of nano-sized particles (<10 nm), leading to the formation of larger particles. The surface growth and oxidation of soot particles occur simultaneously during the agglomeration process. The concentration of these particles decreases

due to coagulation and aggregation at the beginning of the expansion stroke, with agglomeration concluding at the end of the expansion stroke in the engine cycle [2.83, 2.84].

The particle size and number distribution indicate that neat diesel operation produces higher particle emissions across the entire size range compared to methanol-diesel blended fuel [2.85]. Blending methanol with diesel leads to a longer ignition delay, resulting in a greater fraction of the charge burning during the premixed combustion phase. This leads to lower particle formation compared to neat diesel operation [2.85]. As previously discussed, methanol has a higher oxygen content, which reduces the formation of soot precursors in locally rich fuel-air areas due to a higher fraction of O and OH radicals. These radicals enhance the oxidation of precursors to CO and CO2 and also limit the formation of aromatic rings and soot nucleation [2.85, 2.86, 2.87]. Additionally, the lower carbon content of the methanol-diesel blend further reduces particle formation. This effect is particularly significant for particles with diameters less than 30 nm in methanol-diesel blended fuel [2.85]. The particle size and number distribution for methanol-diesel dual-fuel CI engines follows a bimodal lognormal distribution curve [2.88, 2.89]. Methanol-diesel dual-fuel CI engines reduce particle number and mass concentration at lower and medium engine loads, but they exhibit an increase in particulate matter emissions at higher loads [2.88]. The study suggested that using a diesel oxidation catalyst is an effective method to reduce particle number and mass concentration for both neat diesel and methanol-diesel dual-fuel CI engines [2.88]. The influence of the methanol premixing ratio on particle size and number distribution, as well as particle number concentration, is a crucial aspect of optimizing emissions in these dual-fuel engines. The study observed that for neat diesel operation, at lower load, the peak of nucleation mode particles increases. As the load increases, the peak of accumulation mode particles rises. Higher engine loads result in higher combustion chamber temperatures, which enhance the agglomeration rate and reduce the formation of nucleation mode particles [2.89]. Additionally, higher combustion temperatures shorten the ignition delay, causing more of the charge to combust in the mixingcontrolled combustion phase, resulting in the formation of larger particles [2.89]. At lower loads, the combustion temperature is lower, leading to a longer ignition delay. This results in a higher fraction of the charge burning in the premixed combustion phase, creating a higher concentration of small particles. Similarly, methanol premixing leads to a higher peak of nucleation mode particles and fewer larger particles compared to neat diesel operation [2.89]. The study investigated the total particle concentration emission for methanol-diesel dual-fuel operation, indicating that total particle emissions increase with engine load. At higher loads, the air-fuel ratio is lower, leading to locally rich fuel zones in the combustion chamber. Combustion of these locally rich charges increases particle formation due to lower oxygen availability. An increase in methanol premixing results in a higher concentration of total particles, primarily due to a higher concentration of smaller-sized particles compared to larger/accumulation mode particles [2.89]. The higher concentration of smaller/nucleation particles is attributed to nucleation, condensation, and coagulation of unburnt hydrocarbon emissions formed due to lower mean gas temperatures. These unburnt hydrocarbons can generate particle emissions [2.89].

2.2.2 Soluble organic fraction and PAHs emission

The soluble organic fraction (SOF) of particulate matter (PM) refers to components that dissolve in organic solvents like dichloromethane and benzene. This fraction includes polycyclic aromatic hydrocarbons (PAHs), aldehydes, and volatile organic compounds. Studies indicate that in conventional diesel engines, the SOF emissions are primarily composed of PAHs. PAHs are also emitted in the gas phase, which has a lower molecular weight. The IARC has classified 17 PAHs as carcinogenic, and diesel engines are one of the anthropogenic sources of these PAHs. In contrast to conventional diesel engines, advanced dual fuel engines exhibit higher emissions of the soluble organic fraction (SOF) in PM. This fraction in dual fuel engines mainly consists of unburned fuel components, partially oxidized organic content from lubricating oil, and carbonyl compounds [2.90]. This phenomenon primarily arises from the operational strategy employed to achieve advanced dual fuel combustion modes, such as early diesel injection and a high exhaust gas recirculation (EGR) rate. Souza and Correa investigated the PAHs source in engine exhaust from a heavy-duty engine at idle condition. The results shows that the five PAHs (naphthalene (NAP), acenaphthylene (ACY), fluorine (FLU), phenanthrene (PHE), pyrene (PYE)) were identified in diesel, seven PAHs (NAP, ACY, FLU, PHE, FLT, PYR) identified in exhaust, and two PAHs (PYR, NAP) were identified in unused lubricating oil [2.91]. Lim et al., studies the PAHs emission from a bus engine and reported that at higher engine loads, while maintaining the same cruising speed, led to increased PAH emission factors, regardless of the fuel type used [2.92]. Mi et al. investigated the effect of engine load on PAH emissions and found that PAH concentrations were influenced by both cruising speed and load. At a constant speed of 1600 RPM, the PAH concentrations were as follows: $508 \mu g/m^3$ at 25% load, $563 \mu g/m^3$ at 75% load, and $1120 \mu g/m^3$ at 100% load. The

study also indicated that higher cruising speeds at the same engine load resulted in lower PAH emissions. Additionally, using monoaromatic fuels instead of polyaromatic fuels can help reduce PAH emissions [2.93]. Alkurdi et al. studied PAH emissions from three buses and three cars and reported that the total PAH concentration ($\mu g/m^3$) emitted from the MAN bus (2169.41 $\mu g/m^3$) was significantly higher compared to other vehicles. The MAN bus emissions were almost four times higher than the King Long bus (508.58 µg/m³), and three times higher than the Mazda minibus $(671.36 \mu g/m^3)$. The emissions were sixteen times higher than the DACIA vehicle (133.12 $\mu g/m^3$), six times higher than the Elantra vehicle (361.06 µg/m³), and thirty-one times higher than the Avante vehicle (69.28 µg/m³). Additionally, the MAN bus emissions were three times higher than the Mitsubishi vehicle (802 µg/m³) and ranged from six to twenty times higher than the Mazda E5 vehicle (106-314 µg/m³) [2.94]. Alves et al. investigated metal and PAH emissions from lightduty engines during cold start conditions for both spark-ignition (SI) and compression-ignition (CI) engines. They found that element emissions from diesel engine vehicles were 3 to 5 times higher than those from petrol engines. Additionally, PAH emissions were significantly higher during the cold start test conditions [2.95]. Kweon et al. investigated PAH and carbon-containing compound emissions from a Cummins N-series engine. They found that at light load and idling, carbon compounds with 20 to 30 carbon atoms were present in significant amounts. At high load, compounds with fewer than 30 carbon atoms were more prevalent, while compounds with more than 30 carbon atoms remained unchanged. Organic fraction emissions were higher at idle, light, and mid-load conditions. Most PAHs were produced under idle, light, and medium load conditions [2.96]. Hu et al. investigated the emission of PAHs from heavy-duty engines and discovered that After Treatment devices like DPF and SCR can effectively reduce particle-phase PAHs by up to 90%. However, some residual PAHs, such as Nap and NPAHs, still exit in the exhaust in small quantities [2.97]. Zang et al. studied the soluble organic fraction (SOF) absorbed on particulate matter (PM) samples from methanol-diesel dual fuel engines. Their findings indicate that SOF levels decrease as engine load increases, mainly due to increased exhaust temperatures that promote oxidation of the SOF absorbed on PM samples. Conversely, increasing methanol fumigation leads to higher SOF levels in the emissions [2.98]. Despite achieving near-zero smoke number in Reactivity Controlled Compression Ignition (RCCI) exhaust emissions, previous research by Storey et al. demonstrated that a substantial mass of particulate matter (PM) can still be collected on filter media used for certification measurements. The study indicated that a notable

proportion of the particulate matter (PM) consisted of semi-volatile organic compounds, with an average particle diameter ranging from 30 to 60 nm. Analysis of the PM composition revealed that organic carbon accounted for over 90% of the total PM mass, underscoring the predominance of organic components in the emissions studied [2.90].

2.2.3 Heavy metal emission

Transition metals have been documented to penetrate deeply into the airways of the human body and can even infiltrate human cells. This infiltration of trace metals is known to elevate the activity of reactive oxygen species (ROS) within cellular structures, leading to increased oxidative stress. Sources of trace metal emissions from vehicles, as outlined in the literature, include tailpipe emissions, metals released from tire wear, metals emanating from brake liner wear, metal contributing from the aftertreatment devices and the resuspension of road dust in the ambient environment [2.99]. These sources collectively contribute to the presence of trace metals in urban environments, impacting air quality and potentially posing health risks to exposed populations. Cheung et al. conducted a study investigating particulate bound trace metals and organic species emitted from diesel, gasoline, and biodiesel fueled vehicles, focusing on their oxidative potential [2.100]. They observed that a DPF-equipped Honda Accord achieved a substantial 98% reduction in oxidative potential compared to its original configuration, attributed to the effective trapping of major particulates within the DPF [2.100]. Verma et al. explored the oxidative stress activity of PM extracts from four heavy-duty vehicles retrofitted with various configurations (V-SCRT, Z-SCRT, DPX, hybrid, and school bus), using in vitro exposure to rat alveolar macrophages [64]. Despite an inherent increase in PM's intrinsic ROS with most control technologies, retrofitted engines showed reductions compared to baseline, with iron (Fe), chromium (Cr), and copper (Cu) explaining up to 90% of the ROS level variation, with Fe alone accounting for 84% [2.101]. Wang et al. investigated metal emissions from a non-catalyst turbo-charged diesel engine (Mitsubishi-6D14-2AT, manufactured in 1990) [2.102]. Their findings indicated that crustal elements (such as Al, Ca, Fe, Mg, and Si) comprised a larger proportion of emissions compared to anthropogenic elements (including Ag, Ba, Cd, Co, Cr, Cu, Mn, Mo, Ni, Pb, Sb, Sr, Ti, V, and Zn) under transient operating conditions. The main sources of these metals were attributed to their presence in fuel, lubricating oil, cylinder wear, and ambient dust. Emissions of particulate matter from the engines were inversely proportional to engine speed, with higher speeds correlating with increased metal

content due to elevated frictional losses [2.102]. Maurya et al. investigated the metal emission from alcohol-fueled HCCI using ethanol, methanol, and butanol [2.103]. They found higher concentrations of metal traces such as boron (B), calcium (Ca), iron (Fe), and copper (Cu) compared to chromium (Cr) and manganese (Mn) across all test conditions. Engine lubricating oil was identified as the primary source of boron. Metal trace concentrations were lower at higher loads due to increased thermal efficiency and reduced specific fuel consumption. Morphological analysis indicated higher particulate formation at high loads for all test fuels, with butanol showing lower carbon deposition compared to other fuels [2.103]. The study highlighted the potential toxicity of HCCI engine emissions, particularly through increased levels of boron-associated particulate matter.

2.3 Toxicological characteristics of diesel and dual fuel engines

The toxicity of combustion emitted aerosol is higher than the non-combustion aerosol (dust, the debris of tires). Diesel engine exhaust particles are the most toxic for the environmental and biological systems. Genotoxicity (mutagenicity) is the highest for the diesel engine particulate compared to other combustion sources. Mutagenicity typically depicts the carcinogenic nature of a chemical species. Mutagenicity is mainly due to organic compounds like PAHs. Several PAHs develop the Reactive oxygen species (ROS), which breaks the deoxyribonucleic acid (DNA) strands. Overall, the highest toxicity score is given to diesel engine exhaust (DEE) particles followed by gasoline engine exhaust (GEE) particles, biomass burning particles, coal combustion particles, road dust, desert dust, and ammonium sulfate [2.104]. A study reported that traffic particles are the most toxic than any other particles [2.105]. PM penetrates the skin through hair follicles and exerts its detrimental effect through inducing oxidative stress [2.106]. The most harmful particles in air pollutants are the nano-size particles from traffic sources. These small particles can serve as carriers to organic chemical species and heavy metals that can localize to mitochondria and generate oxidative stress [2.107]. The primary concern of particulate matter related to particle pollution is PM₁₀ (PM size is equal to 10µm in diameter), and PM_{2.5} (PM size is equal to or less than 2.5 µm in diameter) [2.108]. The size of particulate matter affects human health severally as the smaller particulates reach the air pathways and may damage the respiratory system [2.108]. The setting time of smaller particles is higher than the large size particles. The particulate matter toxicity also depends upon the time of exposure and route. The major

components which show a very toxic effect on human health and the environment are VOC (aldehyde, ketones, hydrocarbons, benzene, fluorocarbon, methane), heavy metal (lead, chromium, arsenic, cadmium, nickel), and PAHs [2.109]. Volatile organic carbons are the precursors of pollutants, which cause oxidative stress [2.109]. Additionally, heavy metals and particulates are toxic and develop oxidative stress in the human organ. Oxidative stress is a situation of imbalance between the ROS or RNS (Reactive nitrogen species) and the antioxidant defense. There is no direct measurement of ROS and RNS in multicellular organisms, so the biomarkers are used for the analysis. The biomarkers for oxidative stress in humans and animals are lipid peroxidation and oxidatively generated DNA lesions. These are biomarkers because it is difficult to measure the production of ROS and RNS in multicellular organisms [2.110]. A study on the toxicity of various metal content concentration and their effect on the human health showed that the metal content activates the estimated glomerular functional rate (EGFR) and increase the level of guanosine-triphosphate-bound Ras in lung cell [2.111]. Heavy metal content from the engine also leads to the generation of hydroxyl radicals, which can cause several damages to human physiology [2.112]. A laboratory investigating the effect of diesel particulate on mice and canines showed that the particulate with a substantial dose increases bladder cancer chances [2.113, 2.114]. Studies done on diesel particulate for short-time exposure showed that it could cause irritation in bronchial, eye affections, cough, nausea, headache, and other acute symptoms [2.114]. Recent investigation on diesel particulates shows that particulate SOF contents are the precursors for tumor formation [2.114]. The PM reacts with ozone and damages the lungs of rats [2.114]. The PM damages the respiratory system by enhancing inflammatory and allergic problems [2.114]. Moller et al. studied the role of oxidative damage in the toxicity of particulate [46]. However, for combustion exhaust and other particles, the study revealed that particles surface reactivity depends on the particulate's chemical composition, shape, size, solubility, and surface area. Surface area is a better characterization for carbon black elements [2.110]. Similar findings were reported by the [2.115, 2.116]. The particulate pathway for health effect is shown in figure 4. The PAHs metabolized with cytochrome P450 (CYPs) and formed quinones generate ROS, further damaging the DNA and cause mutation.

2.3.1 Cytotoxicity and mutagenicity of PM and gaseous emissions

This section discusses the mutagenicity of PM and gaseous products emitted from conventional engines. Investigating the mutagenicity and cytotoxicity of particulates is a key aspect of studying particulate toxicity. Cytotoxicity tests are performed on cultured cells (in vitro) or in living organisms (in vivo) to assess the effects of chemicals. Toxicity refers to a substance's potential to cause harmful changes in human health. Mutagenicity refers to a chemical's potential to cause DNA alterations, which can lead to cancer in animals and humans. Seagrave et al. investigated the mutagenicity and in-vivo toxicity of combined particulate and semi-volatile organic compounds (SVOCs) from gasoline and diesel emissions [2.117]. The investigation focused on PM samples taken from SUVs and pickup trucks manufactured between 1971 and 2000. They used TA98 and TA100 assays, both with and without S9 metabolic activation, to observe different effects. The study provided a toxicity ranking (bacterial mutagenicity, cytotoxicity, inflammation, parenchymal response) for a specific set of engine samples [2.117]. The bacterial mutagenicity results showed that diesel particulates in cold conditions exhibited the highest mutagenicity across all test cases. However, with metabolic activation (S9), gasoline emission samples demonstrated higher mutagenicity than diesel samples, potentially due to the presence of PAHs. Cytotoxicity was highest in white smoke-emitting gasoline engines, followed by heavy-duty diesel engines, mainly due to the release of protein in bronchoalveolar lavage fluid (BALF), indicating epithelial cell death or damage. Inflammatory responses were similar across all samples, but the parenchymal response was highest for white smoke gasoline engines and lowest for diesel engines in cold conditions. Acute PM exposure increased oxidant production in macrophages, with the highest production observed in white smoke gasoline emission engines [2.117]. A subsequent study by Seagrave et al. examined the in vitro toxicity of the same PM samples previously analyzed in vivo [2.118]. The study found that in vitro analysis did not always correlate with in vivo results, likely due to changes in the physical state of the samples when directly inhaled by living organisms in in vivo studies. In vitro cytotoxicity analysis showed the highest LDH levels for gasoline samples, indicating higher toxicity [2.119]. Most samples showed an increasing trend in macrophage peroxide production, with cytotoxic effects observed at lower sample concentrations due to high local concentration within cells. Interestingly, white smoke gasoline was the least cytotoxic in vitro, contrary to in vivo findings. Another study by Seagrave et al. reported that diesel particulate matter (DPM) binds a proinflammatory cytokine, leading to neutrophil migration. Neutrophils, a type of white blood cell, respond to immune changes [2.119]. The study found that even low doses of DPM increased interleukin-8 (IL-8) levels, causing changes in cell orientation and neutrophil migration. Interleukin-8 is produced by lung airspace cells in response to stress or injury. The study concluded that even in a cell-free system, IL-8 responded to DPM exposure, resulting in a loss of immunoreactivity. Further details on neutrophilic migration can be found in the original article [2.119].

McDonald et al. conducted a comparative toxicity study of diesel engine exhaust (DEE) with and without exhaust reduction (ER) techniques [2.120]. They investigated the effects of low sulfur fuel and a catalyzed particle trap on the composition and toxicity of diesel emissions. The study involved exposing mice to inhalation of DEE for 6 hours per day over 7 days, with a PM concentration of 200 µg/m³. Without ER, an increase in cytokines indicated cytotoxicity. The results showed that using a catalyzed trap and low sulfur fuel either reduced or eliminated the toxic effects, as ER significantly reduced particulate numbers and removed gas-phase organic compounds that generally cause cytotoxicity [2.120]. McDonald et al. used principal component analysis (PCA) and partial least squares (PLS) techniques to investigate the statistical relationship between toxicity and chemical composition [2.121]. They found that nitro-PAHs were major contributors to bacterial mutagenicity. The study extended conclusions from previous research, noting that inflammatory effects from high-emitting vehicles were due to partially burned crankcase-derived lubricating oil. The chemical components causing pulmonary damage differed from those causing bacterial mutagenicity [2.121]. Seagrave et al. performed a comparative study of in vitro and in vivo analyses of gasoline and diesel PM and SVOC samples [2.122]. They examined PM samples from various vehicles, including normal emitters and high emitters, under different conditions. In vivo cytotoxicity rankings showed that white smoke gasoline engines (WG) were the most potent, followed by blue smoke gasoline (BG), high-emitting diesel (HD), normal diesel (D), normal diesel at -10°C (D30), normal gasoline at -10°C (G30), and normal gasoline (G). In vitro cytotoxicity rankings differed significantly, likely due to differences in the depth of the epithelial lining fluid between in vivo and in vitro conditions [2.122]. Another study by Seagrave et al. investigated the responses of primary human epithelial cells to diesel exhaust (DE) exposure. They found significant acute toxicity, increased LDH levels, and loss of mitochondrial function in epithelial lung cells from three donors. DE exposure also led to substantial increases in oxidative stress. The study concluded that toxicity effects varied depending

on the donor and specific pollutants [2.123]. McDonald et al. studied the effects of gasoline emission inhalation on rodents, exposing them to high (60 µg/m³) and low (5 µg/m³) concentrations of gasoline emissions with an average particle size of 15 nm [2.124]. The results showed increased proinflammatory cytokine MIP-2 in BALF of rats after 6 months of exposure, as well as enhanced vascular abnormalities and allergies. High oxidative stress persisted even after particulate filtration, indicating that non-PM emissions also contributed to oxidative stress and health effects [2.124]. Agrawal et al. investigated the mutagenicity and cytotoxicity of biodiesel in three compliance (Euro II, Euro III, Euro IV) engines, comparing mineral diesel and B20 fuel. They performed chemical and biological analyses of particulates, finding metals (Cr, As, Ni) that are probable carcinogens. Asphaltenes were observed in emissions from both diesel and biodiesel engines, with higher molecular weight asphaltenes in biodiesel emissions. Naphthalene and fluoranthene emissions were highest in all tests except for the biodiesel-fueled Euro IV engine [2.125]. Biological characterization of PM samples using HEK 293T cells for cytotoxicity showed toxic effects at 50% load from Euro II and Euro IV vehicles at concentrations below 100 μg/mL. Reactive oxygen species (ROS) potential was highest in Euro II vehicles fueled with both mineral diesel and biodiesel at 50% and 100% load. Mutagenicity tests on Salmonella strains TA98 and TA100 revealed mutagenic effects in four samples, including those from mineral diesel and biodiesel-fueled Euro II engines at 50% load, and diesel-fueled Euro IV engines at 100% load. Detailed effects on TA98 strains with and without S9 can be found in the reference [2.125].

2.3.2 Nanoparticle inhalation toxicity

Ultrafine emitted particles are significantly smaller in diameter; they penetrate the respiratory tract and sometimes reach the bloodstream. Several studies show that the particle emitted from diesel engines, having a diameter of about 20nm, reaches the lungs and deposits in the alveolar region [2.126, 2.114]. The ultrafine particle tends to go in a deeper part of the lung and can damage the brain cells, which leads to a brain disorder [2.114]. The lung disorder and the higher mortality rate are also associated with diesel particulate and gases [2.114]. The deposition and retention of diesel particles in the lungs depend on several factors: particle characteristics such as diameter, concentration, and chemical composition; respiratory characteristics including respiration rate, frequency, and pause time; and lung characteristics such as tidal volume, lung volume, age, and health condition [2.127]. Smaller particle sizes exhibit higher deposition efficiency in lung regions.

As particle size decreases, they can penetrate deeper into the respiratory tract, reaching smaller airways and potentially depositing in the alveoli [2.127]. This enhances their retention within the lungs. Carbonyl emissions, which increase with diesel combustion, contribute significantly to the toxicity of gaseous emissions. Carbonyl compounds can attach to particle surfaces, particularly nucleation mode particles. These smaller particles have a greater surface area relative to their mass, making them effective carriers for carbonyl compounds. This increases the potential toxicity of emitted particles, as the combination of particle-bound carbonyls and other toxic components can exacerbate respiratory and systemic health effects upon inhalation. Studies [2.127, 2.128] focus on predicting DEP deposition, highlighting that smaller particle diameters increase deposition fractions in lung regions. Additionally, higher tidal volumes and respiratory frequencies independently increase deposition, demonstrating their significant roles in particle retention. A study investigates DEP retention, noting that higher particle concentrations and tidal volumes enhance total and regional lung particle loading. Respiratory frequency also impacts retention rates, with higher frequencies correlating with increased lung particle loading [2.129]. A kinetic model discussed in [2.130] underscores that particle clearance from lung regions follows exponential decay over time, heavily influenced by particle toxicity potential. A study [2.131] compares particle retention in humans and rats, finding humans exhibit greater inflammatory responses at comparable particle concentrations, emphasizing the need for accurate aerosol size and distribution data in cross-species comparisons. The study [2.132], perform an experiment on diesel engine with high cetane fuel to investigate the lung retention and suggests diesel fuels with higher cetane numbers increase particle retention in the respiratory tract, though no clear trend emerges with varying fuel types. Increased breathing rates are also linked to higher particle retention. Studies examining DEP deposition during engine testing, such as [2.133], reveal that particles emitted during idling tests deposit more efficiently than those from transient tests, with size variations influencing deposition across human subjects. Modeling studies, like [2.134], illustrate that diesel particulate filters reduce particle emissions and alter chemical composition, potentially affecting toxicity. A study [2.135] found that larger particle sizes decrease deposition in lung regions, though deposition remains significant in areas prone to cancer development. An investigation was done on the impact of DEP exposure on reactive oxygen species (ROS) and reactive nitrogen species (RNS), noting increased microphage infiltration and heightened ROS/RNS generation under high-fat diet conditions. These findings collectively underscore the

complex interplay between particle characteristics, respiratory dynamics, and lung health in understanding DEP deposition and toxicity [2.136].

2.4 Environmental risk assessment of emissions

The atmospheric transport of engine pollutants involves the dispersion and distribution of emissions into the air. These pollutants, such as particulate matter (PM), nitrogen oxides (NOx), sulfur oxides (SOx), volatile organic compounds (VOCs), and polycyclic aromatic hydrocarbons (PAHs), are released during the operation of engines in various sectors including transportation, industrial activities, and power generation. Once emitted, these pollutants can undergo complex atmospheric processes such as dispersion, transformation, and deposition, influencing air quality and posing potential health and environmental impacts over local to global scales. Additionally, engine emissions can contribute to the formation of secondary pollutants such as ozone (O₃), secondary organic aerosols (SOAs), and nitrogen dioxide (NO₂). These secondary pollutants can exacerbate air quality issues by contributing to smog formation, respiratory problems, and ecosystem damage. They also pose challenges for regulatory efforts aimed at controlling air pollution, requiring comprehensive strategies to mitigate both primary emissions and their secondary products. Ahlvik and Brandberg conducted a study to assess the ozone-forming potential (OFP), acidification potential (AP), eutrophication potential (EP), and cancer risk potential (CPMR) resulting from ethanol and methane as fuels in both CI and SI engines. The findings revealed that using ethanol led to a noteworthy increase in aldehyde emissions for both types of engines. Additionally, the SI engine emitted higher levels of HC (hydrocarbons) with greater OFP compared to the diesel engine. Jia and Debrett investigated the RCCI combustion strategy using methanol as low reactive fuel (LRF). The study reported that under all the tested condition the GHGs potential of the MD-RCCI emission is significantly lower than conventional diesel [2.79].

2.5 Gaps in the literature

The literature review highlights significant research conducted on the combustion, regulated and particle emission characteristics of conventional diesel engines and advanced dual fuel engines. Furthermore, the literature survey summarizes toxicological investigations conducted on diesel engine particulate matter (PM) emissions. However, there is a scarcity of studies concerning the chemical and toxicological assessment of PM and unregulated emissions from advanced dual-fuel

engines like RCCI. The present study aims to address this research gap by conducting a comprehensive comparative assessment of both physical and chemical characteristics of gasoline-diesel RCCI, methanol-diesel RCCI, and conventional diesel combustion. Additionally, the study will include a numerical analysis for heavy-duty applications in diesel and hydrogen-diesel dual-fuel modes to predict PAHs emissions and perform thorough chemical and toxicological investigations. This research intends to contribute significantly to understanding the environmental and health impacts of these engine technologies.

Chapter 3

Methodology

This chapter presents the methodologies adopted to conduct the present thesis work. The study is conducted for both light duty and heavy-duty application. The experimental study is performed for light duty application and numerical study is performed for heavy duty engine. The light duty engine setup is modified to operate on dual-fuel combustion mode utilizing gasoline and methanol as low reactive fuel. The experimental investigation includes the measurement of in-cylinder pressure, regulated (THC, CO, NOx, PM) and unregulated (saturated HC, unsaturated HC, carbonyl compounds and aromatic) emissions. The measured in-cylinder pressure, along with the crank angle position, is used to calculate derived combustion parameters. PM sampling is conducted on a preconditioned filter paper in a partial flow dilution tunnel. The collected PM samples are then analyzed for their physico-chemical and toxicological characteristics. The physical characteristics evaluated in this study included PM mass emission measurements and SEM image analysis. Additionally, physical characterization using a particle sizer was performed to assess particle number emissions, mass distribution, and size distribution. The toxicological characterization methods involved a comprehensive toxicity assessment, utilizing both measured regulated and unregulated emissions, as well as collected PM samples. Particle emission measurements are used to estimate lung retention due to inhalation using the lung compartment model. An in-vitro cytotoxicity test is performed to analyze the cytotoxicity and reactive oxygen species (ROS) imbalance caused by PM samples. Measured carbonyl emissions are used to calculate cancer risk potential following US-EPA and IRIS guidelines. The numerical investigation is conducted to predict PAH formation and emissions from heavy-duty diesel and hydrogen-diesel dual-fuel engines. The predicted PAHs are further used to quantify the mutagenicity and carcinogenicity potential of the emitted PAHs. The details about the separate methods are presented in detail in this chapter.

3.1 Test setup and instrumentation

This section presents the details about the engine setup to conduct the present thesis work. The study is conducted for both light-duty and heavy-duty application. The experimental study is

performed for light duty application and numerical study is performed for heavy duty engine. The light duty engine setup is modified to operate on dual-fuel combustion mode utilizing gasoline and methanol as low reactive fuel. The heavy-duty engine is used to operate on conventional diesel and hydrogen-diesel dual fuel mode. This section describes both the engines separately along with involved methods in the analysis.

3.1.1 Light-duty engine setup

The engine used for the experimental investigation is a Mahindra Jeeto (Manufacturer: Mahindra), a single-cylinder diesel engine. This engine is classified as a light-duty commercial vehicle, commonly used as a mini truck in India.

3.1.1.1 Experimental Methodology

Experiments are conducted on a single-cylinder, water-cooled, 625 cc, four-stroke, naturally aspirated automotive engine, with technical specifications listed in Table 3.1. The actual image of the experimental setup is shown in Figures 3.1 (a-d). Figure 3.1 (a) shows the actual image of the singlecylinder engine. Figure 3.1(b) displays the dynamometer and load cell used to control and apply the load on engine. Figure 3.1 (c) represents the port fuel injection line and injector, which injects the low-reactivity fuel (methanol/gasoline) into the combustion chamber. Figure 3.1(d) depicts the common rail direct injection (CRDI) system that injects the high-reactivity fuel into the combustion chamber. This engine is coupled with an eddy current dynamometer (Manufacturer: TECHNOMEC, Model: TMEC 20) for power absorption. Rotational torque is measured using a strain gauge load cell (Manufacturer: Load Master, Model: DB 100). Figure 3.1 (b) shows the engine coupled with an eddy current dynamometer. An eddy current dynamometer operates on the principle of electromagnetic induction to absorb torque and dissipate power. It consists of a rotating disc (also called the rotor) and magnetic poles (also called the stator). In this setup, the rotor is driven by a prime mover, such as an engine. A coil is wound around the stators in the circumferential direction, and this entire assembly is enclosed within a casing. When electric current is supplied to these coils, a magnetic flux is generated in the casing across the air gap on either side of the rotor. As the rotor turns in the magnetic field, eddy currents are induced in the stator. These currents create a braking effect between the rotor and the casing by tending to rotate the stator. The rotational torque exerted on the casing is measured by a strain gauge load cell. To prevent overheating, the dynamometer uses a water-cooling system for the casing.

Table 3.1: Specifications of the automotive diesel engine

Displacement Volume (cm ³)	625
Bore*Stroke (mm)	92.5 X 93
Connecting rod length (mm)	156
Compression ratio	18:1
Number of cylinders	1
Rated Power	11 BHP @ 3000 rpm
Rated Torque	38 Nm @ 1100-2000 rpm



Figure 3.1 (a-d): Actual images of (a) single cylinder engine, (b) dynamometer, (c) port-fuel injection system and (d) CRDI system.



Figure 3.2: Modified intake manifold of the engine for conducting RCCI experiments.

To achieve advanced dual fuel combustion or RCCI (Reactivity Controlled Compression Ignition) operating mode, the intake manifold is modified to accommodate a port fuel injector, which is independently operated by a low-pressure fuel pump. The modified intake manifold is depicted in Figure 3.2. The port fuel injector is positioned to inject fuel close to the intake valve. The major components of the port fuel injection system include fuel filter, fuel pump, fuel line, fuel injector, and fuel tank. A 12 V battery supplies power to the fuel pump and injector. The quantity and timing of the injected fuel are varied using a developmental ECU (Manufacturer: NIRA, Sweden, Model: Nira i7r). Low-reactivity fuels like methanol and gasoline are supplied into the intake manifold during the suction stroke of the engine cycle via the port fuel injector. A centrally mounted common rail injector in the cylinder head delivers direct-injected (DI) fuel. Diesel is injected into the cylinder using a common rail direct injection (CRDI) system with an adjustable fuel rail pressure ranging from 200 to 800 bar, variable injection timings, and durations. The developmental ECU controls the amount of diesel injected, the timing of the injections, and the number of injections.

A differential pressure transmitter (Manufacturer: SENSOCON; Model: 211-D010i-2) was used to measure the air flow rate and fuel transmitter (Manufacturer: Wika Model SL1) in the engine test setup by detecting the pressure difference across an orifice plate installed in the air intake line. As air passed through the restriction, a pressure drop occurred between the upstream and downstream sides, which the transmitter measured and shows the pressure drop value on the panel. This differential pressure, proportional to the square of the flow velocity, was then converted into a flow rate using Bernoulli's principle. The fuel flow was also measured using gravimetric method. During the experiment, the fuel supply was directed from the tank to the engine for a fixed period, and the readings were recorded from the burette. Based on these readings, the amount of fuel consumption was calculated. The actual picture of the differential pressure transmitter is shown in Figure 3.3.

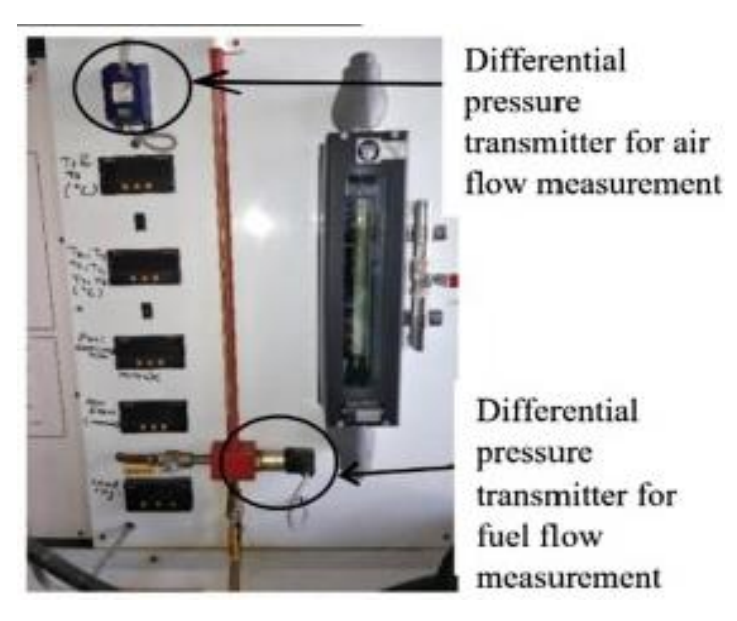


Figure 3.3: Differential pressure transmitter for fuel and air flow measurements.

In the engine setup, engine demand and fuel injection events are controlled and determined by a developmental engine ECU. The ECU processes data from various sensors and sends output signals to the actuators. It reads signals from the manifold absolute pressure sensor, manifold air temperature sensor, crankshaft position sensor, accelerator pedal position sensor, cam position sensor, engine coolant sensor, fuel temperature sensor, fuel pressure sensor, and oil pressure sensor. The developmental ECU manages actuators such as fuel injectors, EGR valve, fuel pressure control, fuel pump relay, and main relay by processing input signals from sensors and controlling the output signals. The schematic representation of complete experimental setup with all the instruments and emission analyzers is presented in Figure 3.4. The experimental setup includes all the systems used in the experimentation. The yellow line indicates the fuel line, carrying both low and high reactive fuels. The blue line shows the airflow inside the combustion chamber. The black line traces the engine exhaust path and the connection to emission measurement devices such as FTIR and particle sizer. The magenta line represents the signal and its processing network.

Engine operating condition

Engine testing is conducted under low and moderate load conditions by varying the energy share of methanol and gasoline in advanced dual fuel combustion or RCCI mode. The gross IMEP for low load (1.5 bar BMEP) was 4 bars, while for moderate load (2.2 bar BMEP), it was 5 bars. The

primary motivation for this testing is to compare the effects of conventional and advanced dual fuel combustion on combustion, emissions, and the physical, chemical, and toxicological characteristics of regulated and unregulated emissions. Testing is performed at a constant engine speed of 1500 rpm across three combustion modes: conventional diesel combustion (CDC), methanol-diesel RCCI (MD-RCCI), and gasoline-diesel RCCI (GD-RCCI). The engine speed was kept constant at 1500 rpm during testing, as it represents the maximum torque value for the automotive engine under study. Additionally, this speed was maintained across all three combustion modes to ensure the combustion frequency remained consistent, allowing for a valid comparison of combustion and emission characteristics across RCCI and CDC combustion strategies. The port fuel injection pressure is maintained at a constant 3 bar, which is typical for port fuel ensuring consistent fuel delivery and atomization. Diesel injection pressure is kept constant at 350 bar to maintain RCCI combustion strategy. Injection timings are set to -12° SOI (start of injection) for CDC, -22° SOI for MD-RCCI, and -35° SOI for GD-RCCI. These timings are selected through an iterative process to achieve a stable combustion regime in RCCI mode. The energy share of methanol (fuel premixing ratio) varies from 15% to 25% at both low and moderate loads for MD-RCCI. For GD-RCCI, the energy share of gasoline varies from 35% to 45%. The limits for fuel premixing ratios are determined based on achieving stable combustion and successfully operating in RCCI mode. The details about the respective characteristics and measurement methods are presented in the upcoming sections.

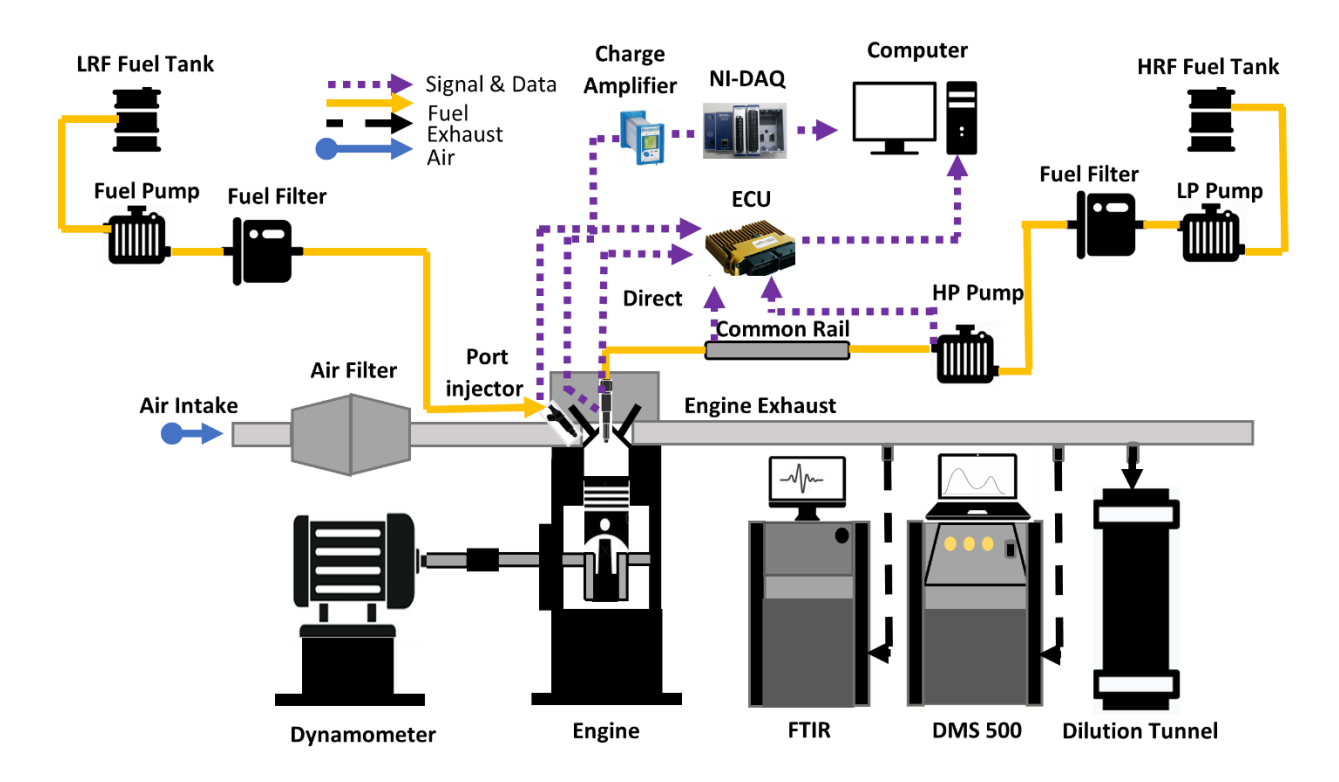


Figure 3.4: Experimental set up schematic

3.1.1.2 In-cylinder pressure measurement

To measure combustion pressure, a piezoelectric pressure transducer (Manufacturer: KISTLER; Model: 211B2) is mounted on the cylinder head. This transducer converts combustion pressure into an electric charge proportional to the force acting on its piezoelectric crystal. This electric charge is then converted into a corresponding voltage using a charge amplifier (Manufacturer: Kistler; Model: Type 5018). The actual image of the pressure sensor, the slot for installation in the engine head, and the installed pressure sensor are presented in Figures 3.5 (a-c). For measuring the crankshaft position, a crank angle encoder with a resolution of 0.1 CAD is installed on the crankshaft.

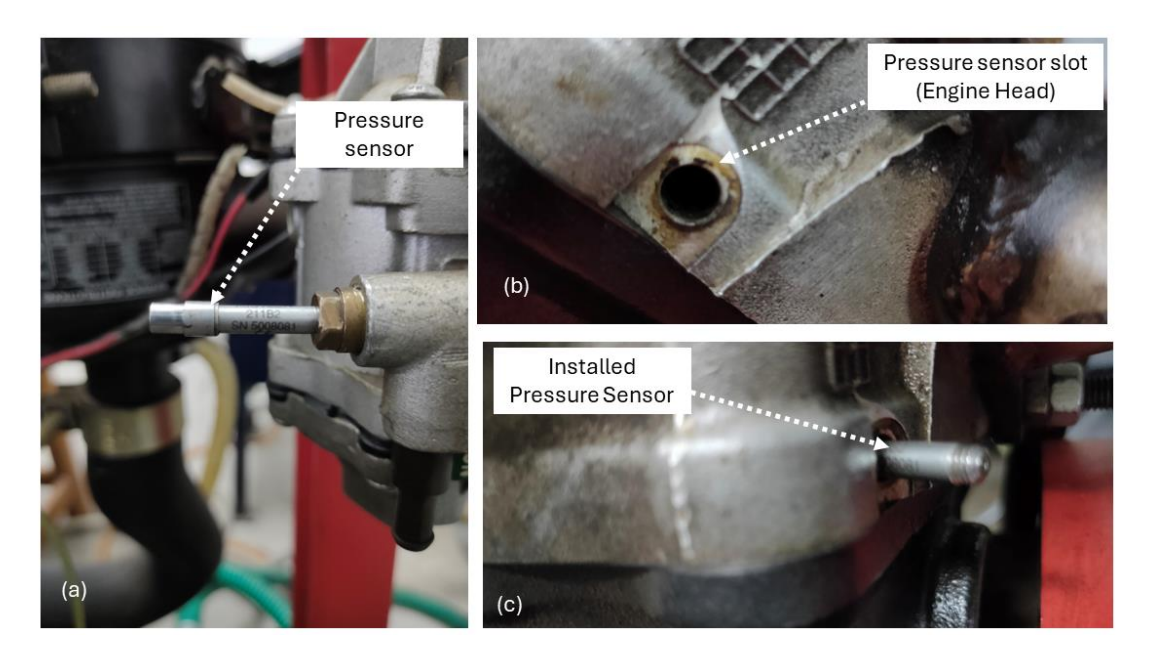


Figure 3.5: (a) Pressure sensor, (b) Pressure sensor slot in engine head and (c) Installed pressure sensor.

The pressure data, once converted to voltage, is logged into a computer using high-speed data acquisition hardware and a LabVIEW-based program. The data processing involves four steps: absolute pressure correction, phasing with respect to the crank angle, filtering high-frequency noise using a digital Butterworth filter, and cycle averaging to obtain mean cylinder pressure and heat release rate. In this study, a CDAQ system (Manufacturer: National Instruments; Model: NI CDAQ-9718) is used to acquire both analog (cylinder pressure) and digital (angle encoder) signals through two separate NI modules (NI-9222 and NI-9411). The averaged in-cylinder pressure data, used to calculate combustion parameters, is obtained by averaging the results of multiple successive engine cycles to ensure consistent combustion. For the engine testing and combustion analysis of the RCCI engine, a crank angle encoder with 0.1-degree resolution (Manufacturer: Kubler - Germany) is employed. A separate 5 to 24 VDC power supply is used to operate the encoder. This encoder is crucial for determining the engine crank angle corresponding to the measured pressure data, which is essential for combustion analysis.

3.1.1.3 Combustion characteristics calculations

Online in-cylinder pressure data is recorded for 1000 consecutive cycles. The combustion characteristics are analyzed based on the in-cylinder pressure data recorded for these cycles using the equations below. The rate of heat-release (J/deg.) is calculated using a zero-dimension heat-release model given in Equation (3.1) [3.1],

$$\frac{dQ}{d\theta} = \frac{\gamma}{\gamma - 1} P \frac{dV}{d\theta} + \frac{1}{\gamma - 1} V \frac{dP}{d\theta} + \frac{dQ_{\text{wall}}}{d\theta} \dots \dots (3.1)$$

where P and V are the in-cylinder pressure and volume of cylinder as a function of crank angle position (θ) respectively. $\frac{dQ}{d\theta}$, γ , and $\frac{dQ_{\text{wall}}}{d\theta}$ are heat release rate (HRR), ratio of specific heat and heat transfer loss from the cylinder wall respectively. γ is calculated using the following expression as in Equation (3.2) [3.2],

$$\gamma = \gamma_0 - \frac{k}{100} \frac{T}{1000} \dots \dots (3.2)$$

where γ_0 is the γ value at a reference temperature, typically 300 K, γ_0 is a function of gas composition. The value of γ_0 for air is 1.4 and for lean air fuel mixture is 1.38. The value of constant k is 8. T is the in-cylinder mean gas temperature. Rate of heat transfer loss (J/deg.) from the cylinder wall is calculated using the convention heat transfer relation given as in Equation (3.3),

$$\frac{dQ_{\text{wall}}}{d\theta} = \frac{h(T - T_w)A}{360N} (3.3)$$

where h, T_w , A and N are heat transfer coefficient, cylinder wall temperature, surface area of cylinder and engine speed respectively. The average cylinder wall temperature (400 K) is assumed to be constant over the entire cycle operation. In this study Hohenberg correlation is used to determine the h value and given as in equation (3.4) [3.3],

$$h = \alpha_s V^{-0.06} P^{0.8} T^{-0.4} (S_p + 1.4)^{0.8} \dots (3.4)$$

Here, S_P is the mean piston speed, α_S is the scaling factor, P, V and T are the pressure, volume, and temperature of the combustion chamber respectively. The start of combustion (SOC), CA₅₀ (Combustion phasing), duration of combustion is calculated by finding the crank angle position

corresponding to 10%, 50% and duration of 10% - 90% (CA $_{10-90}$) heat release of total heat release value.

3.1.1.4. Emission Measurements

The present section discusses the details about the particle and gaseous emission measurement instruments.

Particle emission measurement

Engine exhaust particle size and number distribution is measured by differential mobility spectrometer (Manufacturer: Cambustion, UK, Model: DMS 500) [3.4]. Measurement of PM emissions is done using a differential mobility spectrometer (Manufacturer: Cambustion, UK, Model: DMS 500). For measurement of PM emission exhaust line of the engine is modified and separate probes have been fabricated for exhaust sampling. Particles of 38 different sizes in the range 5 nm to 1000 nm can be measured by the instrument. It is real time instrument and measures particle size and number characteristics based on electrical mobility diameter. Exhaust gas sample from the engine exhaust tail pipe. The DMS500 uses electrical mobility measurements to produce particle size distributions between 5 nanometres and 2.5 microns [3.4]. Since the classification of particles according to their differing electrical mobility takes place in parallel (rather than in series as in a scanning instrument) the DMS can offer the fastest measurement of its type. The user interface processes the size distribution data in real-time to output particle mass, surface area and number. A DMS 500 system for engine sampling incorporates two stage dilution system. The 1st dilution stage uses metered compressed air to provide low dilution factor up to 5: 1. The second dilution stage uses a rotating disc to provide a high dilution factor which may be varied to maintain good signal to noise ratio. The DMS uses a classifier column operating at 0.25 bar absolute with an external vacuum pump. A cyclone separator removes particles above measurement range to reduce need for cleaning. Two optional stages of software-controlled dilution are applied before the sample gas passes through a corona charger and into classifier column. The charged particles flow within a particle free sheath which is uniform cylindrical laminar column designed to carry charged particles in a predictable manner. The particles are then deflected toward ground electrometers rings by repulsion from high central voltage electrode. When high voltage is applied to the central electrode, the charged particles are deflected toward electrometer rings. Particles with a higher charge/ lower drag will be deflected more and will land on electrometer ring closer

to sample inlet. Their landing position is uniform function of their charge and their aerodynamic drag. The particles yield their charge to the electrometer amplifier and the resulting current are translated by user interface into particle size and number data. The working principle of DMS 500 is depicted in Figure 3.6.

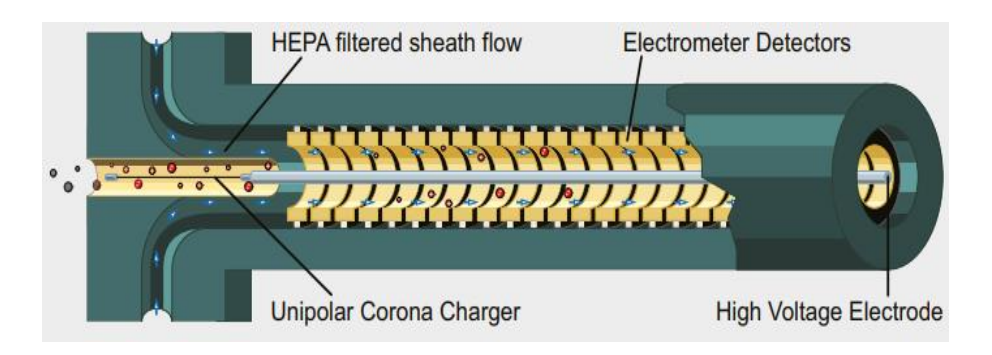


Figure 3.6: Working principle of DMS 500 [3.12]

Gaseous emission measurement

Both regulated and unregulated gaseous emissions were measured using FTIR (Fourier transform infrared spectroscopy) based emission analyzer (Manufacturer: AVL) model (SESAM). The gaseous emission measurement is performed using AVL manufactured FTIR-SESAM analyzer [3.5]. The FTIR analyzer is based on the FTIR spectrometer which measures real time concentration of exhaust gas species. The FTIR detects gas molecules in the sample by measuring their absorption of infrared radiation due to their molecular rotation and oscillations. The heteroatomic gases exhibit distinct infrared absorption at various wavelengths, resulting to characteristic spectra. Basic principle of the Device (SESAM i60 FT) is, it records the exhaust samples information in the form of interferogram (intensity/time) over wild range of spectra and analysed through Fourier transform technique and hence it terms as Fourier Transform Infrared Spectroscopy. The instrument stores the spectra of all measured gases in its memory. These stored spectra serve as reference data, and when an exhaust gas sample is taken, the detected spectra are compared with the reference spectra to determine the corresponding values. The FTIR instruments comprise four key components: an infrared radiation source for emitting infrared radiation, an interferometer to generate constructive and destructive interference patterns, a sample cell for taking samples, and a detector to detect the signal [3.6]. Figure 3.6 shows the working principle of the instrument. The IR source produce radiation range between 4000-400 cm⁻¹ and beamed into

the interferometer optic via deflection mirror. In the interferometer, by the adjustment of the mirror an optical interference pattern is produced which contain all the spectral information with time domain, frequency signal is converted into time signal (interferogram). The outgoing signal from interferometer is then transmitted to sample gas measuring cell and this information is acquired by the highly sensitive MCT detector. Molecule in the sample gas chamber absorbs the energy from the incoming known signal (interference pattern) and the receiving signal at detector gives the indirect information about the number of particles presented in the gas chamber (Figure 3.7). Then this information is calibrated in the form of PPM (Parts per million). For maintain the high accuracy the MCT must be cooled by liquid nitrogen bellow -196^o C. The following set of regulated and unregulated gaseous measurements is done in the present study. For regulated gases: CO, CO₂, NOx, and THC. For unregulated exhaust gases: CH₄ (methane), C₂H₂ (acetylene), C₂H₄ (ethylene), C₂H₆ (ethane), C₃H₆ (propylene), HCHO (formaldehyde), CH₃CHO (acetaldehyde), methanol (CH₃OH), toluene (C₇H₈), sulfur dioxide (SO₂), ammonia (NH₃).

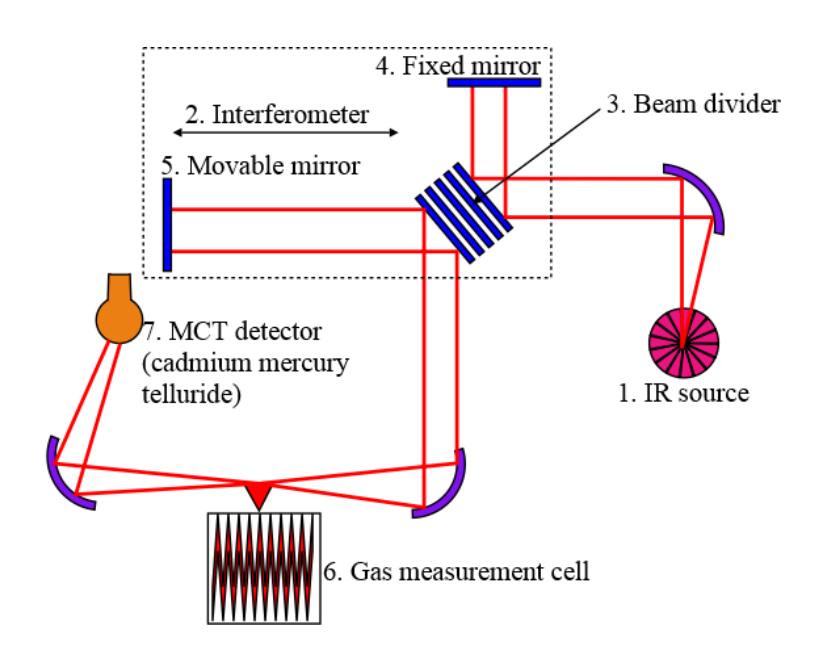


Figure 3.7: Working principal of FTIR

3.1.1.5 Particulate Sampling Methodology

This section discusses the method used for particulate matter (PM) sampling. PM sampling is conducted to investigate the different physical, chemical, and toxicological characteristics of PM.

The main requirement for sampling is to ensure that enough samples are collected on a preconditioned filter paper to analyze the desired characteristics. Two types of sampling are performed in the present study: raw sampling, which is done through emission analyzers such as a particle sizer, and diluted sampling, which is done through a partial flow dilution tunnel.

3.1.1.5.1 Partial flow dilution tunnel

A partial flow dilution tunnel is utilized for particulate matter sampling to assess the overall physical chemical and toxicological characteristics of the aggregate PM. The exhaust line is connected to the dilution tunnel through a stainless-steel tube to prevent any chemical reactions between the particulate matter-associated species and the sampling line. Glass wool insulation was applied to the tube to prevent particle condensation on its surface. Sampling is performed under stable conditions at a constant temperature ($50 \pm 5^{\circ}$ C). The sample was collected for a duration of 30 minutes with a constant dilution ratio (10:1). The sampling time was determined to ensure enough sample collection for further analysis. The dilution ratio is calculated using expression (). The actual image of the sampling process is presented in Figure 3.8. The dilution ratio was checked both before and after the sample collection on the filter paper.

Dilution ratio (DR) =
$$\frac{[\text{Undiluted exhaust CO}_2]}{[\text{Diluted exhaust CO}_2 - \text{Ambient air CO}_2]} \dots \dots (3.5)$$

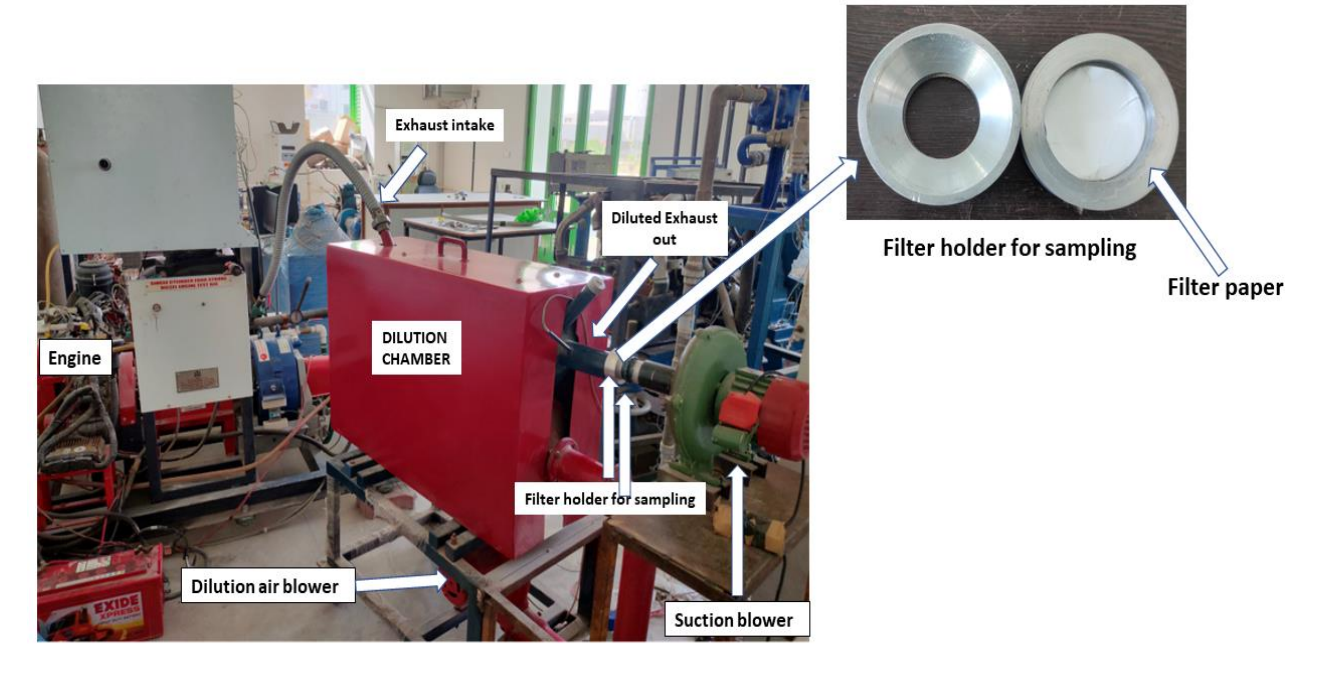


Figure 3.8. Actual image of dilution tunnel and sampling process.

3.1.1.5.2: Filter paper preparation

The particulate samples are collected on the 47mm diameter quartz filter paper (Pallflex membrane filter). Before and after the sampling the filter is kept in a desiccator for 12 hours to remove the moisture content. The filter is weighted before and after the sampling to calculate the mass of PM collected, which is further used to determine the PM mass, SOF, and toxicity. The real image of desiccator is shown in Figure 3.9.

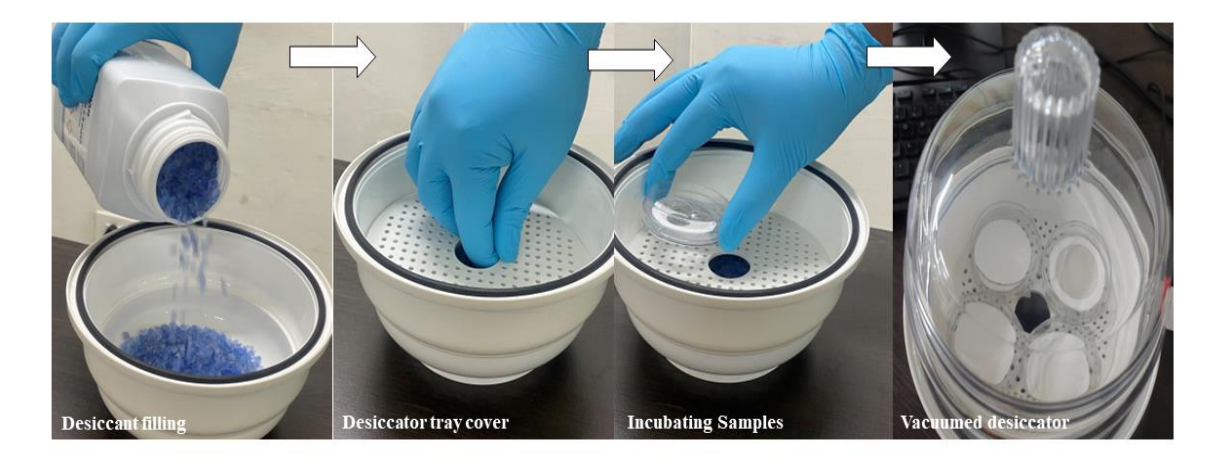


Figure 3.9: Moisture removal before and after the sampling of PM on filter paper.

3.1.1.6 Physico-chemical characterization method

The physico-chemical characterization of particulate matter (PM) is conducted to investigate its various properties. Physical characterization includes the particle number concentration, mass, and morphology. Chemical characterization involves determining the chemical compounds present in the PM samples and engine exhaust. The schematic of the physical characterization process is presented in Figure 3.10.

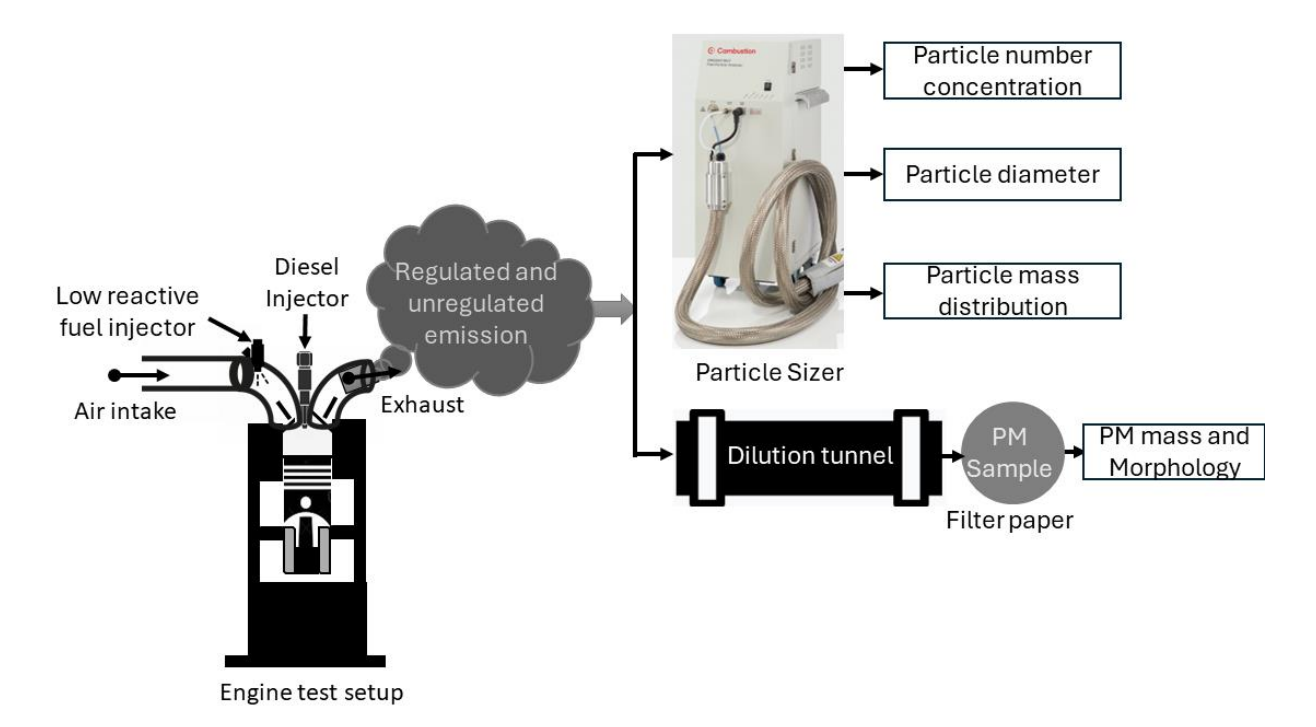


Figure 3.10: Physical characterization method

The engine exhaust is partially sampled using two devices. The first device is a particle sizer, which samples the exhaust to measure the particle number concentration and particle size. The second device is a partial flow dilution tunnel, which collects a sample for 30 minutes on preconditioned filter paper. Before and after sampling, the filter paper is weighed to determine the PM mass. A portion of the filter paper is then cut using a plastic cutter and analyzed with scanning electron microscopy to examine the morphology of the PM.

The chemical characterization of engine exhaust is performed for both the gaseous components and the particulate matter (PM) associated organic fraction. For gaseous exhaust emissions, the chemical characterization is based on chemical bonds and functional groups. Fourier Transform Infrared Spectroscopy (FTIR) is used for gaseous measurements and has the potential to measure saturated hydrocarbons, unsaturated hydrocarbons, carbonyl compounds, inorganic emissions, and aromatic compound emissions. Figure 3.11 shows the chemical characterization of PM and gaseous samples.

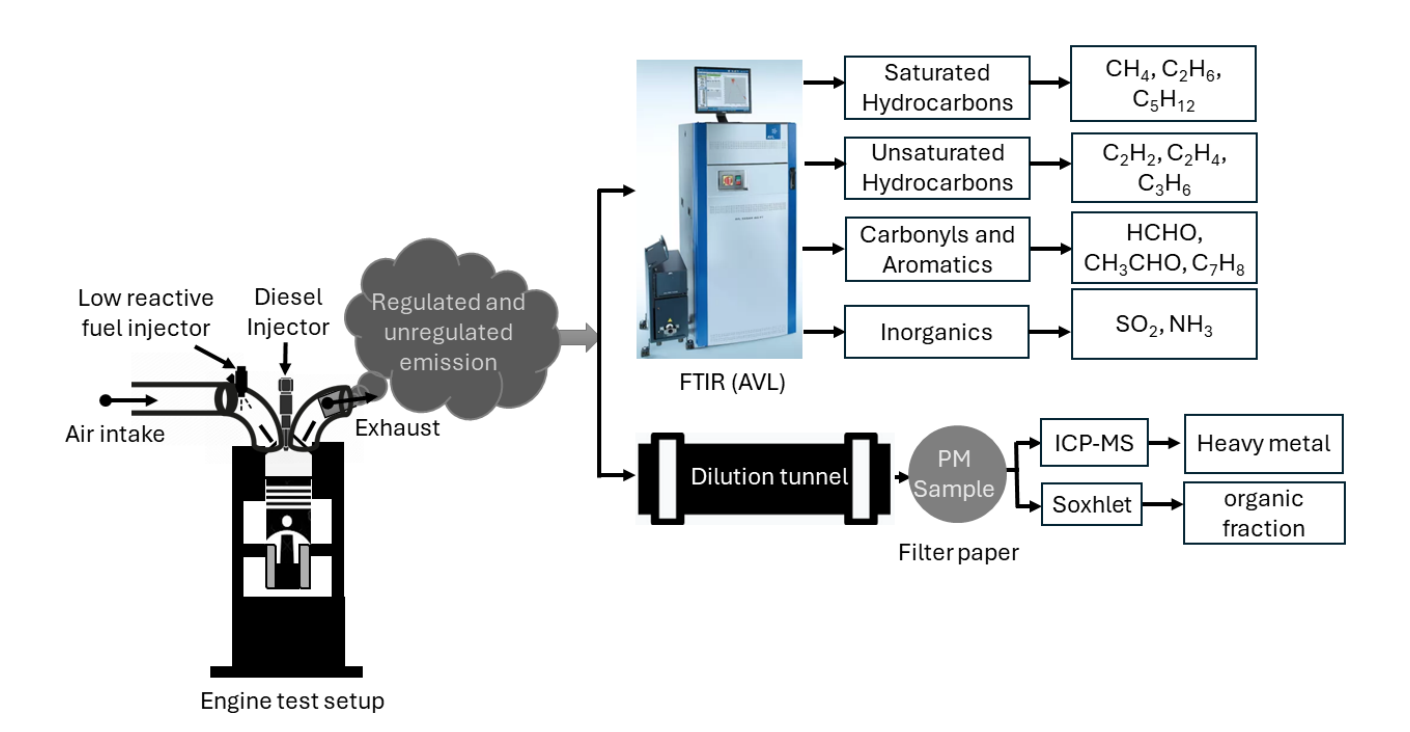


Figure 3.11: Chemical characterization method

For PM associated chemical characterization the soluble organic fraction and metal trace emission is determined. The soluble organic fraction (SOF) of collected PM samples was extracted using a

Soxhlet extractor [3.7]. A Soxhlet extractor is a laboratory instrument typically used to extract chemical compounds from solid samples. It consists of an extraction flask, a siphon tube, a condenser, and an extractor housing. The process involves heating the solvent in the flask, causing it to vaporize, rise through the siphon, and condense in the condenser. The condensed solvent drips back into the flask, continually cycling through the solid sample. As it cycles, it dissolves the target compounds from the sample [3.7]. When the solvent level in the flask reaches a certain point, a siphon action occurs, transferring the solvent and dissolved compounds to a separate receiving flask. The SOF is calculated using the following expression given in Equation (3.6),

$$SOF = \frac{M_{LF} - M_{EF}}{M_{LF} - M_{BF}} \dots \dots (3.6)$$

Here M_{LF} is the mass of loaded PM filter, M_{EF} is the mass of filter paper after extraction and M_{BF} represents the mass of blank filter paper. The real image of Soxhlet extractor is presented in figure 3.12.

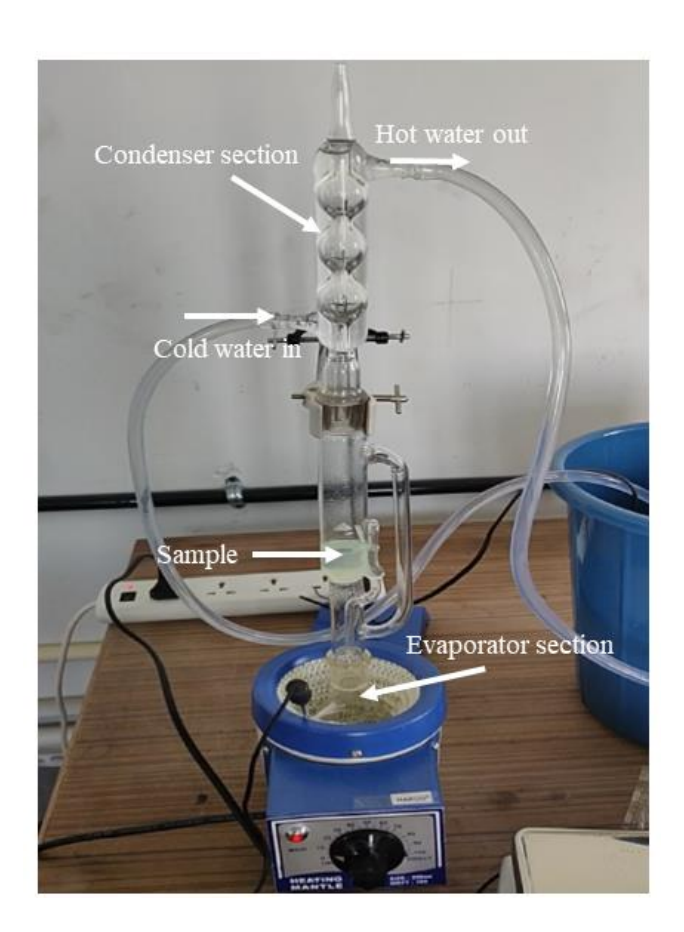


Figure 3.12: Actual Soxhlet Extractor image

A pre-conditioned and pre-weighed portion of the PM-collected filter paper is placed in the extractor section. In the evaporator section, a premeasured amount of solvent (Dichloromethane) is filled for the extraction process. The extraction is conducted for 7 cycles per hour for a total duration of 24 hours [3.7]. The step-by-step procedure for SOF extraction is presented in the form of a flow chart, depicted in Figure 3.13.

The metal trace analysis is done using an ICP-MS. The collected samples were digested according to instrument requirements, and the digested sample is used for the characterization. ICP-MS comprises plasma, a high-temperature ion source, and a mass spectrometer, typically featuring a quadrupole mass filter and a detector. A liquid sample undergoes pumping through a nebulizer, generating an aerosol transported in a gas stream to the plasma. Plasma, an electrical discharge of high temperature, vaporizes the sample material, atomizing and ionizing the elements. These ions traverse through an interface into a vacuum chamber, where they undergo separation from photons, neutral particles, and interfering ions using an ion lens and a collision/reaction cell (CRC). Subsequently, the analyte ions are sorted by the quadrupole mass filter, with each mass directed to the detector for counting [3.8]. This analysis is performed at IIT Delhi central research facility.

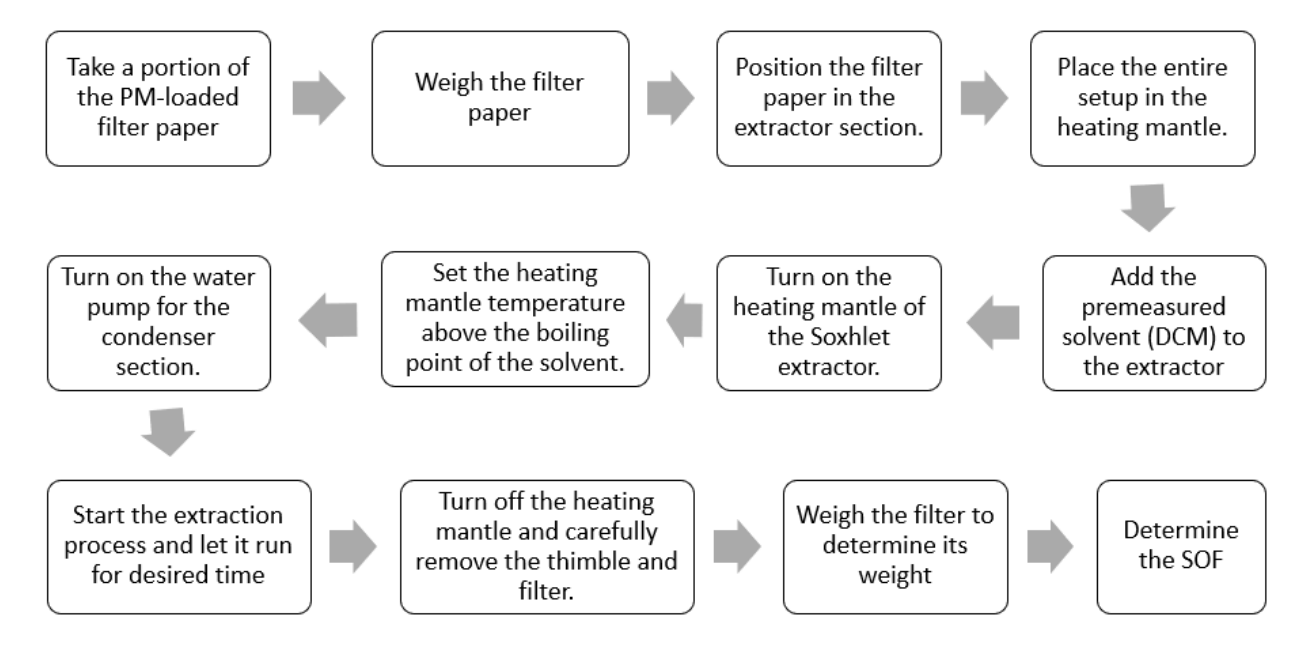


Figure 3.13: Step by step procedure to determine the soluble organic fraction.

3.1.1.7 Toxicological characteristics

The toxicological study examines toxicity related to both unregulated and PM emissions. For unregulated emissions, the cancer risk potential is assessed for emitted carbonyl and aromatic emissions from CDC, MD-RCCI, GD-RCCI, and hydrogen-diesel dual fuel combustion modes. For PM toxicity, the study includes assessing cytotoxicity and reactive oxygen species (ROS) through direct in-vitro exposure to cells, calculating analytical lung retention resulting from particle inhalation based on size, mass, and chemical composition, and evaluating cancer risk potential associated with metal trace emissions using the method prescribed by the US-EPA. Figure 3.14 presents methods used to characterize the toxicity potential of engine emissions.

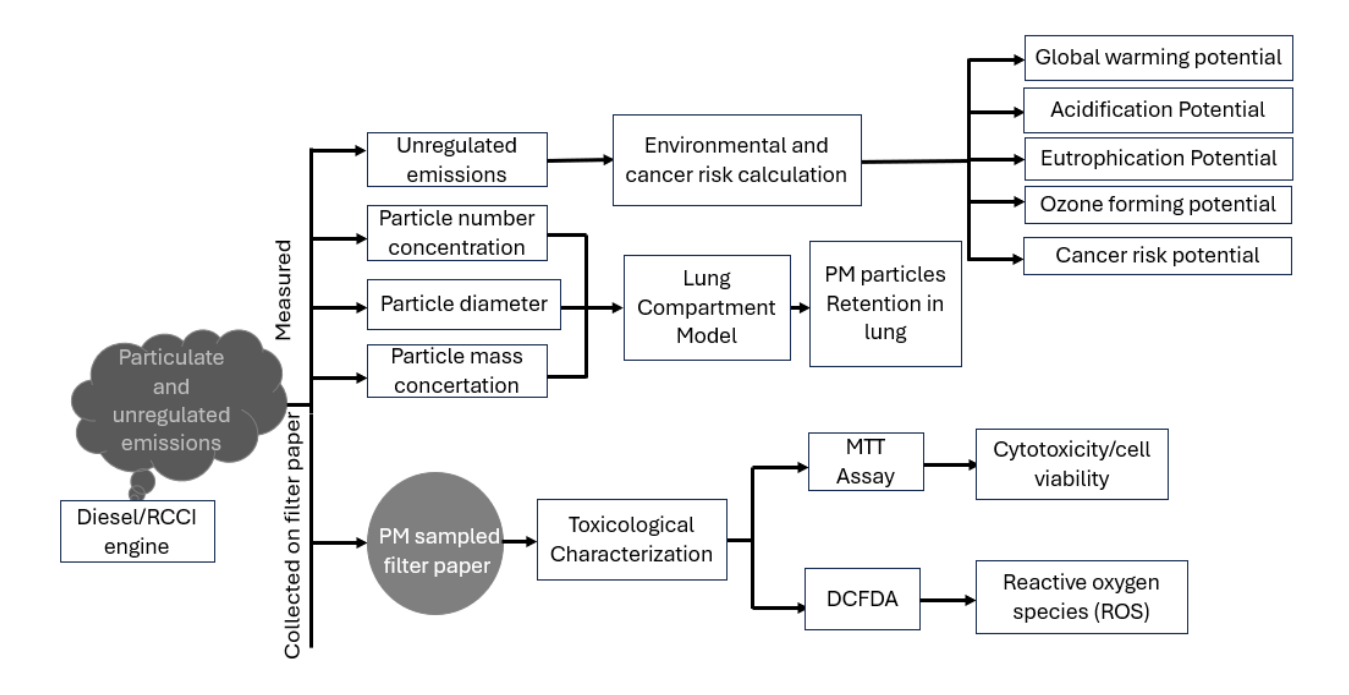


Figure: 3.14: Toxicological characterization of emissions

3.1.1.7.1 Cytotoxicity and ROS assessment of PM

The MTT assay was used to determine the cytotoxicity of PM-laden filters on the BEAS 2B cell line. The cells were grown in DMEM medium with 10% fetal bovine serum, and 1% antibiotic in a Nunc coated T-25 flask. The cells were kept at 37°C in a humid environment containing 5% CO₂ until the confluency of 80-90% was reached. Upon reaching the confluency, the cells were then detached for analysis using a trypsin-EDTA solution. In a cell culture treated 96-well plate, the cells were seeded with a cell density of 10,000 cells/well. The samples were kept in 1 mL of incomplete media and incubated at 37°C to collect the samples extracts after 24 h. A 0.2 µm syringe

filter was used to collect the extract. The cells cultured in 96 well plate was treated with the sample extracts at a concentration of 100 μ L/well. However, the cells treated with complete media only were taken as positive control. The treated cells were incubated for further 24 h for the cytotoxicity analysis of the PM-laden filters. After the mentioned time, a 20 μ L of the MTT solution (5 mg/mL) was added in each well. The 96-well plate was kept in dark at 37 °C for 3.5 h incubation. Following the incubation, MTT solution was removed from each well and DMSO was added to dissolve the formed formazan crystals. The absorbance of the formed solution was taken at 570 nm (n = 3) using a plate reader [3.9]. The absorbance ratio of the cells treated with samples to the cells treated with the media gives the cell viability.

The ability of samples to induce intracellular reactive oxygen species (ROS) stress in BEAS-2B cells was evaluated using the oxidant-sensitive DCFDA fluorescent assay. Cells with a density of 1×10⁴ were cultured in DMEM at 37 °C in a humidified environment with 5% CO₂ in a Nunccoated 96-well black plates. After 24 h, the media in the wells was replaced by the 100 μL of the syringe filtered sample extracts and again incubated for another 24 h. the cells treated with 0.5mM H₂O₂ were taken as control as H₂O₂ stimulates the production of ROS. After 24 h, the media was removed, and cells were washed with PBS. The cells were then treated with 25 μM DCFDA solution and were kept in dark for 1 h. Following 1 h exposure in dark, the DCFDA-containing incomplete medium was removed, PBS was added, and the fluorescence intensity was measured at 485 and 530 nm for excitation and emission using a plate reader [3.9].

The cytotoxicity and ROS tests are repeated three times to ensure the repeatability of the results. The same mass of extracted samples from all tested conditions is used for each time testing. The average data from the three test conditions are collected and analyzed for further investigation.

3.1.1.7.2 Carcinogenicity and mutagenicity calculations

Carcinogenicity denotes the capability of a substance to induce cancer in living organisms, encompassing the initiation, promotion, or advancement of cancerous cells within the body. Mutagenicity, conversely, signifies the capacity of a substance to provoke mutations or alterations in the genetic material (DNA) of an organism, which can disrupt normal cellular functions and potentially elevate the risk of cancer or other genetic disorders [3.10]. The US-EPA has prescribed methods to calculate the cancer risk potential of the substances based on their chemical composition [3.11]. The IRIS database documents the toxicity data for different chemical

compounds, providing their reference values along with inhalation unit risk numerical values. The data for the identified carbonyl compounds is used from the IRIS database in the present study [3.11].

Carbonyl and metal associated cancer risk assessment

Formaldehyde (HCHO) and acetaldehyde (CH₃CHO) are classified as carcinogenic (group 1) to humans and possibly carcinogenic to humans (group 2B) by the International Agency for Research on Cancer (IARC) [3.12]. Cr, Co, Ni, As, Cd, Pb are carcinogenic metals as per US-EPA. The present study calculates the cancer risk potential for a specific exposure scenario: a person commuting 2 hours a day for 30 years, which USEPA identifies as a recreational receptor [3.13]. Quantifying cancer risk potential requires the exposure concentration (EC) and the inhalation unit risk (IUR) value. The pollutant concentration (CA) represents the amount of pollutant present in the air, which is the primary input for calculating the exposure concentration (EC). This concentration can either be raw engine exhaust for near tailpipe risk estimation or diluted exhaust for traffic-related situations. The present study assumes that the exhaust dilution before inhalation is the same as it is at the dilution tunnel outlet. The emission analyzer is connected to the dilution tunnel outlet to measure the diluted concentration of PM-associated metal content and carbonyl emissions. EC ($\mu g/m3$) is calculated by the expression given in equation (3.7) as [3.13],

$$EC = \frac{CA^*ET^*EF^*ED}{AT} \dots \dots (3.7)$$

Here, *CA*, *ET*, *EF*, *ED* are carbonyl (HCHO and CH₃CHO) concentration (diluted), exposure time (hours/day), exposure frequency (days/year), exposure duration (years) respectively. *AT* is the averaging time and calculated as *ED* in years * 365 days/year * 24 hour/day. The cancer risk potential of the inhaled HCHO and CH₃CHO is evaluated by the expression given in equation (3.8) as,

$$CR = IUR_{carbonyl/metal} *EC \dots (3.8)$$

The equation (3.8) contains Inhalation unit risk (IUR) of carbonyl compounds and metals, which according to USEPA, physically signifies the maximum estimated risk of developing cancer over a lifetime due to continuous exposure to carbonyl compound (HCHO and CH₃CHO) at a concentration of 1µg/m3 in air. The numerical value of IUR is taken from the Integrated Risk

Information System (IRIS), and the values are $1.3E^{-5}(\frac{\mu g}{m^3})^{-1}$ for formaldehyde and $2.2E^{-6}(\frac{\mu g}{m^3})^{-1}$ for acetaldehyde [38]. The metal IUR values can be found in IRIS database [3.14].

PAHs carcinogenicity and mutagenicity assessment

The mutagenicity and carcinogenicity potential of PAHs is calculated on the basis of statistical method [3.15]. The physical meaning of MEQ and CEQ is, the equivalent mass of the total PAHs which participate in the mutagenicity and carcinogenicity potential of emitted PAHs. MEQ represents the mutagenicity potential of total PAHs. The TEF and MEF physically represent the factor by which a PAHs is toxic relative to B[a]P by giving the numerical value of 1 to B[a]P. The TEF for Acenp, Bep, B[g,h,i]P, Chry, Nap, Penath, Pyr are 0.001, 0.01, 0.01, 0.001, 0.001 respectively. The MEF equivalency containing PAHs emitted are only B[a]P, Bep, B[g,h,i]P, Chry and their MEF is 1, 0.19,0.19,0.017 respectively. The TEQ and MEQ is calculated as given in equation (3.9) and (3.10) [3.15],

$$TEQ = \sum_{i=1}^{N} (PAH)_i * TEF_i \dots \dots (3.9)$$

$$MEQ = \sum_{i=1}^{N} (PAH)_i * MEF_i \dots (3.10)$$

3.1.1.7.3 Particle lung retention calculation

To study the transport, retention (particle loading) and clearance of the inhaled nanoparticle in respiratory system, developed lung compartment model is used [3.16]. The compartment model comprises of four compartments: nasopharyngeal or head (H), tracheobronchial (T), alveolar (A), and lung associated lymph nodes (L) as given in Figure 3.15. The model also includes two additional compartments, which are blood (B) and gastrointestinal tract (G). All these compartments together give the complete description of lung retention and clearance.

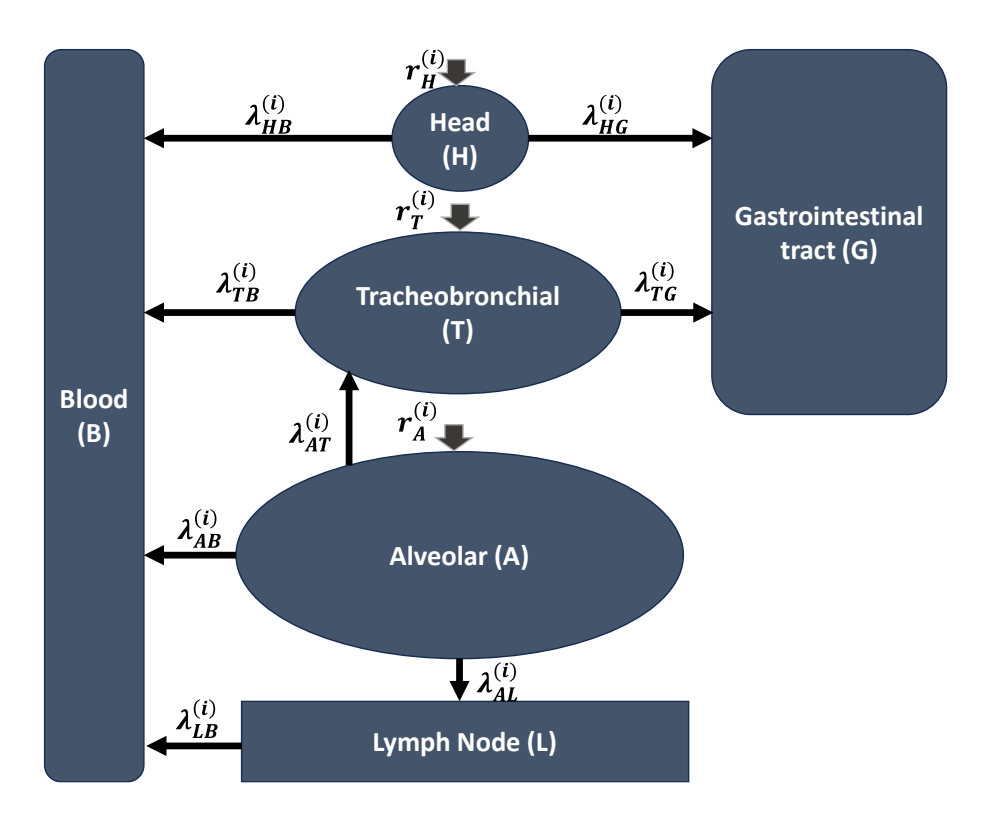


Figure 3.15: Lung compartment model for the diesel particle retention [3.16]

In figure 3.14, $r_H^{(i)}$, $r_T^{(i)}$, and $r_A^{(i)}$ are represents the mass deposition rates of PM component (i) in (H), (T) and (A) lung regions respectively. λ_{XY}^i is the rate of transport of (i) from X compartment to Y compartment. If, the mass fraction of a PM particle component (i) is f_i [3.16]. Then,

$$r_H^{(i)} = f_i r_H \dots (3.11)$$

 $r_T^{(i)} = f_i r_T \dots (3.12)$
 $r_A^{(i)} = f_i r_A \dots (3.13)$

Here, r_H , r_T and r_A are total mass deposition of PM particles in (H), (T) and (A) lung regions respectively. The r_H , r_T and r_A are determined using the expressions given as [3.16]

$$r_H = C(TV)(RF)(DF)_H \dots (3.14)$$

 $r_T = C(TV)(RF)(DF)_T \dots (3.15)$
 $r_A = C(TV)(RF)(DF)_A \dots (3.16)$

Here, C is the mass concentration of the PM particles in air, TV is the lung tidal volume, RF is the respiratory frequency, DF is the deposition efficiency in different lung regions. The DF is a function of particle diameter, lung volume, respiratory frequency, and respiration rate. The value

of DF for different lung regions is taken from [3.17]. The mass particle concentration (C) and particle diameter (dp) is measured using the DMS500 particle sizer. The Tidal volume of 500 cc (assuming adult human) and respiratory frequency of 14 min - 1 (assuming adult human) is used in the present study. After, calculation of r_H , r_T and r_A the fractional deposition is calculated using the equation 3.11, 3.12 and 3.13. In the present study the fraction of organics in the PM is determined using SOF analysis and the obtained fraction is used in the calculation of organic deposition. CP Yu and KJ Yoon [3.16] validated the model in their research, assessing both the deposition fraction and lung retention using experimental data. Their findings showed that the total lung retention predictions were within 7% of the experimental values, and the total deposition fraction was within 5% of the experimental values [3.17].

The governing differential equation for the mass of particulate particle components $(m_X^{(i)})$ as a function of exposure time for different compartments, which is presented in Table 3.2. The governing equations are first order time dependent differential equation and are solved using the MATLAB for PM particle regional loading with initial condition. The values of transport rates are used from the Ref. [3.16]. The complete description and details about the determination of transport rate are mentioned in the ref. [3.16]

Table 3.2: Governing differential equation:

Head Region (H)	$\frac{dm_H^{(i)}}{dt} = r_H^{(i)} - \lambda_{HG}^{(i)} m_H^{(i)} - \lambda_{HB}^{(i)} m_H^{(i)} \dots \dots (3.17)$
Tracheobronchial Region (T)	$\frac{dm_T^{(i)}}{dt} = r_T^{(i)} + \lambda_{AT}^{(i)} m_A^{(i)} - \lambda_{TG}^{(i)} m_T^{(i)} - \lambda_{TB}^{(i)} m_T^{(i)} \dots \dots (3.18)$
Alveolar Region (A)	$\frac{dm_A^{(i)}}{dt} = r_A^{(i)} - \lambda_{AT}^{(i)} m_A^{(i)} - \lambda_{AL}^{(i)} m_A^{(i)} - \lambda_{AB}^{(i)} m_A^{(i)} \dots \dots (3.19)$
Lung lymph node (L)	$\frac{dm_L^{(i)}}{dt} = \lambda_{AL}^{(i)} m_A^{(i)} - \lambda_{LB}^{(i)} m_L^{(i)} \dots \dots (3.20)$

3.1.1.7.4 Environmental risk assessment

The environmental risk factors used markers in the present work are global warming potential (GWP), ozone forming potential (OFP), acidification potential (ACP) and eutrophication potential (EP). The GWP quantifies the environmental impact of various gases by calculating the amount of heat energy an emitted gas will absorb over a specific period in comparison to the emission of an equivalent amount of CO₂ [3.18]. According to their molecular structure, the gases absorb the heat energy of different wavelengths. CO₂ is taken as reference to GWP calculation because it remains in the atmosphere for thousands of years. The GWP of CO₂ is 1. The GWP in the present study is calculated in CO₂ equivalent form as given in expression (3.21) [3.19],

Total GWP =
$$\sum_{i} C_i \times GWP_i$$
 (CO2 equivalent) (3.21)

Here, Ci is the concentration of the exhaust gas component i and the GWPi is the global warming potential of the gas component i.

The OFP quantifies the formation potential of ozone resulting from the release of volatile organic carbon (VOCs), CO, and NOx. Within the lower atmosphere, ozone forms through chemical reactions involving these species in the presence of sunlight, typically following the path given as in reaction (3.22) [3.20],

$$VOC + NOx + sunlight = Ozone + oxidized products (3.22)$$

The OFP is calculated using the maximum incremental reactivity (MIR) factor given by carter [3.21]. The MIR is a factor which is based on the photochemical reactivity of different gases. The expression given in equation 3.23 is used for the determination of total OFP [3.22],

$$OFP = \sum_{i} C_i \times MIR_i \dots \dots (3.23)$$

The ACP is the potential of a gas species which contributes to the acidification of the environment. It refers to the compounds, which are precursors to acid rain. The compounds include sulfur dioxide (SO₂), nitrogen oxides (NOx), nitrogen monoxide (NO), nitrogen dioxide (N₂O). The reference for the ACP is the SO₂, which has an ACP of 1. The ACP is presented as SO₂ equivalent, and the expression used in the calculation is given in equation 3.24 [3.19]

Total
$$ACP = \sum_{i} C_i \times AP_i$$
 (SO2 equivalent) (3.24)

EP is defined as the potential to cause overfertilization of water and soil, which can induce excessive nutrient enrichment in water and soil, leading to increased biomass growth. It is calculated as given in equation 3.25 [3.19],

Total EUP =
$$\sum_{i} C_i \times EP_i$$
 (PO4 equivalent) (3.25)

3.1.2 Heavy duty engine test setup

The engine used for the heavy-duty application investigation is a single-cylinder, direct injection (DI), 4-stroke diesel engine at the Sandia National Laboratory, based on a Cummins N-series production engine. It is a heavy-duty application modified for research purposes at Sandia National Laboratory. The engine is optically accessed to visualize the spray combustion and validate the numerical models developed for diesel combustion. It has laser access to observe the spatial distribution of OH radicals, providing better visualization of combustion and numerical model validation. The engine operates in both low-temperature combustion and high-temperature combustion across a wide range of conditions and is used to validate different reaction mechanisms involving single and multi-component fuel types. This engine is an ideal tool for developing and validating numerical models. The same engine is used for the numerical investigation in the present work, leveraging the availability of crank angle-based soot formation and emission data to validate the simulated results. The specification of the engine is presented in Table 3.3.

Table 3.3: Engine setup Sandia Cummins [3.23].

Base engine type	Cummins N-14 DI diesel
Number of cylinders	1
Bore × Stroke	$13.97 \times 15.24 \text{ cm}$
Connecting rod length	30.48 cm
Displacement	2.34 L
Simulated compression ratio	16:1
Bowl width	9.78 cm
Bowl depth	1.55 cm
Fuel injector type	Common rail
Cup type	Mini sac

Number of holes	8, equally spaced
Spray included angle	152°
Nozzle orifice diameter	0.196 mm
Nozzle orifice (L/D)	5

3.1.2.1 Numerical methodologies

The simulation is performed using the commercially available licensed ANSYS FORTE CFD solver of combustion reactive flows. The fluid flow in simulation is considered as turbulent, multiphase reactive and basic fluid dynamics is governed by Navier-stokes equation. The transport equations of mass, momentum and energy are formulated for compressible, gas phase flow and solved for the dependent variables in Forte CFD solver. Forte uses the exchange function spray liquid droplet and gas phase dynamics during the injection. The assumptions used in the development of the conservation equations are thermodynamic equation of state for gas phase, Fick's law of mass diffusion, Newtonian fluid, and Fourier law of conduction [3.24].

3.1.2.1.1 Governing equations and simulation setup

The gas phase working fluid of combustion engines in forte is modelled as mixture of individual species or gas component. The changes taken into account during the cycle are flow convection, molecular diffusion, turbulent transport, fuel spray interaction and combustion. The governing equations, which forte solves are given in Table 3.4.

Table 3.4: Governing equations

$\frac{\partial \bar{\rho}_k}{\partial t} + \nabla \cdot (\bar{\rho}_k \bar{u}) = \nabla \cdot [\bar{\rho} D \nabla \bar{y}_k] + \nabla \cdot \phi + \bar{\rho} \bar{g} + \bar{\rho}_k^c + \bar{\rho}_k^s$	Species Conservation	(3.26)
$\frac{\partial}{\partial t} + v \cdot (\rho_k u) = v \cdot [\rho D v y_k] + v \cdot \phi + \rho g + \rho_k^* + \rho_k^*$	Equation	
k = 1,, K		
$\frac{\partial \bar{\rho}\bar{u}}{\partial t} + \nabla \cdot (\bar{\rho}\bar{u}\bar{u}) = \nabla P + \nabla \cdot \bar{\sigma} - \nabla \cdot \Gamma + F^s + \bar{\rho}\bar{g}$	Turbulent Reactive	(3.27)
$\frac{\partial t}{\partial t} + v \cdot (\rho u u) = v P + v \cdot o - v \cdot I + F + \rho g$	Navier- Stokes with spray	
$\bar{\sigma} = \bar{\rho}v \left[\nabla \bar{u} + (\nabla \bar{u})^{\mathrm{T}} - \frac{2}{3} (\nabla \bar{u})I \right]$	Equation	
<u> </u>		
$\frac{\partial \bar{\rho}I}{\partial t} + \nabla \cdot (\bar{\rho}\bar{u}I) = -p\nabla \cdot \bar{u} - \nabla \cdot J - \nabla \cdot H + \bar{\rho}\epsilon + Q^c + Q^s$	Energy Equation	(3.28)
$J = -\lambda \nabla T - \bar{\rho} D \sum h_k \nabla y_k$		
$\bar{p} = R_u \tilde{T} \sum_k \left(\frac{\bar{\rho}_k}{W_*} \right)$	Mixture Gas phase	(3.29)
$V = W_u L_k (W_k)$	Equation of State	

$\dot{\omega}_{ki} = (v_{ki}^{\prime\prime} - v_{ki}^{\prime})q_i(k=1,\cdots,K)$	Production rate of K th species	(3.30)
$\dot{Q}_{c} = -\sum_{i=1}^{I} Q_{i} q_{i} = \sum_{i=1}^{I} \sum_{k=1}^{K} (v_{ki}^{"} - v_{ki}^{"}) (\Delta h_{f}^{0})_{k} q_{i}^{"}$ $Q_{i} = \sum_{k=1}^{K} (v_{ki}^{"} - v_{ki}^{"}) (\Delta h_{f}^{0})_{k}^{"}$	Chemical heat release rate,	(3.31)

The conservation equation for a species k is given in equation (1) where, $\bar{\rho}_k$ is the density of species k, \overline{u} is flow velocity vector, \overline{y}_k is mass fraction of species k, D is molecular diffusion coefficient, ϕ is account for the effect of ensemble averaging of convection term, $\bar{\rho}_k^c$ and $\bar{\rho}_k^s$ are the source term account for the chemical reaction and spray evaporation respectively. K is the total number of species. The summation of equation (1) over all species gives the continuity equation for total gas phase fluid. Effect of convection, pressure force, viscous stress, turbulent transport, impact from liquid spray and body force are taken in account in momentum conservation equation, can be seen in equation (2). Where, p is the pressure force, F^S is the rate of momentum gain due to spray, g is specific body force, v is the kinematic viscosity, $\bar{\sigma}$ is the viscous shear stress modeled as in equation (2). $\Gamma = \overline{u}\overline{u} - \overline{u}\overline{u}$ are the stress accounts for nonlinear convection term obtained during ensemble averaging of momentum equation (2). In the RANS approach it is the Reynolds stress and in the LES approach it is called SGS stress. The governing equation for internal energy is modelled for the flow problem relevant to internal combustion engines in such a way that it considered the effect of convection, turbulent transport, turbulent dissipation, sprays chemical reactions and enthalpy diffusion of multi-component. The internal energy transport equation is given in equation (3), where I is the specific internal energy, J is the heat flux vector accounting for the contribution due to heat conduction and enthalpy diffusion. \vec{Q}_C and \vec{Q}_S are the source terms due to chemical heat release and spray interactions. The H accounts for ensemble averaging or filtering of convection terms that $H = \bar{\rho} (u\tilde{i} - \tilde{u}\tilde{l})$ which is modelled using turbulence approach. The mixture gas phase equation of state is shown in equation (4). Forte uses ANSYS CHEMKIN pro chemistry solver to solve the rate of production of species (equation 5) and chemical heat release rate (equation 6) [3.24]. These governing equations are solved for the dependent variable at every time step till convergence. The flow chart of setting up the simulation cases is illustrated in Figure 3.16. In this study, the modified RNG $k - \epsilon$ turbulent model is used with validated initial

turbulent kinetic energy and turbulent length scale [3.24]. The details about the kinetic energy transport and turbulent dissipation can be found in the ANSYS theory manual [3.24]. For the spray model, the discharge coefficient spray model is used. Method of moments is used as soot model in this analysis. The details description of these methods is explained in detail in ANSYS CHEMKIN PRO theory manual [3.25].

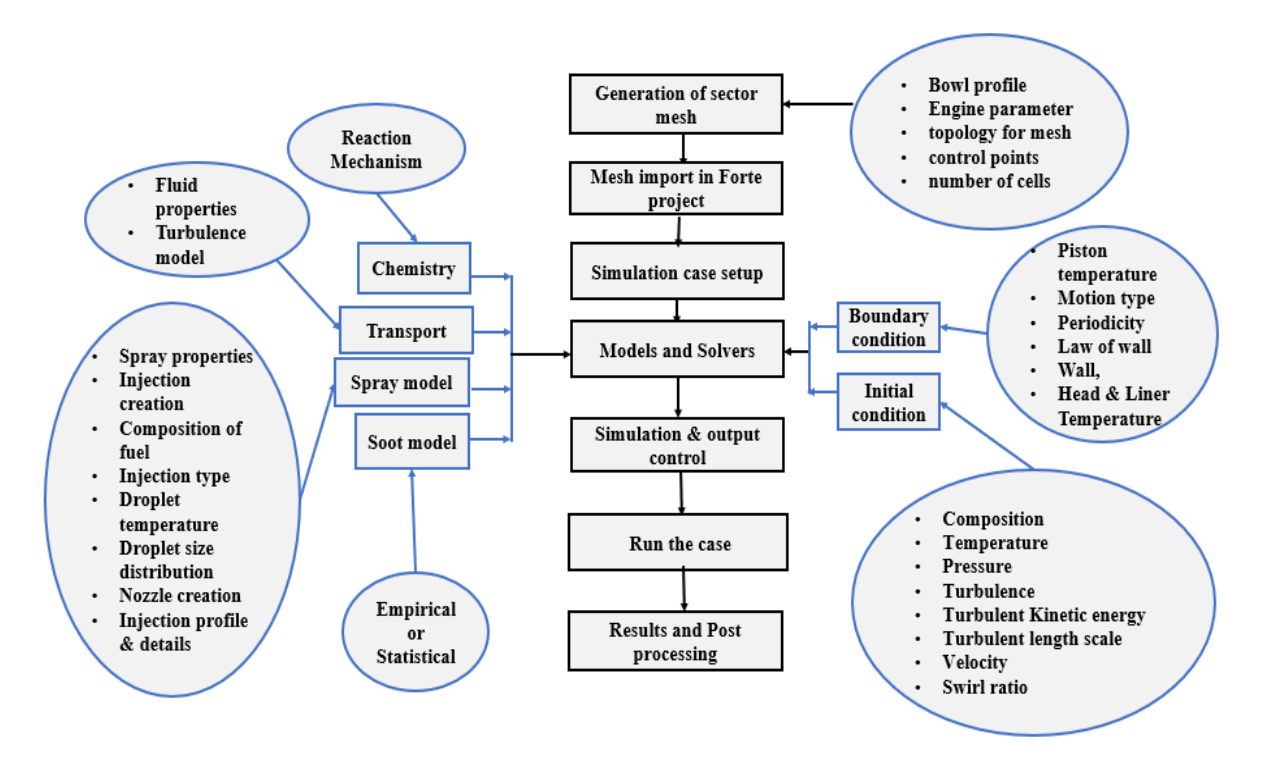


Figure 3.16: Simulation procedure to set-up the simulation case.

3.1.2.1.2 Computational domain, Sub models and operating matrix

For direct injection diesel engines, the combustion process is often simulated from the inlet valve closure (IVC) to exhaust valve open (EVO). The full modelling of intake and exhaust flow process involving valve motion is very rare in the case of diesel engine simulation study. This assumption is reasonably valid since the gas at IVC is a relatively homogeneous mixture of air and residual gas before the fuel injection timing. Furthermore, the fuel injection from nozzle hole gives rise to periodic symmetry, based on the number of holes present in the nozzle. The use of sector mesh takes advantage of this periodicity of fuel spray to simulate the diesel engine. A sector can represent the full geometry by using the periodicity of the cylinder and injector nozzle pattern.

Various physical and chemical sub-models available in the ANSYS FORTE CFD code are used in this study. Spray atomization and drop breakup are modeled using the Kelvin-Helmholtz (KH) -Rayleigh-Taylor (RT) hybrid model, which operates on the theory of the linear stability of liquid jets [3.26]. The KH model, based on the linear stability analysis of liquid jets, is employed to model the primary breakup region of the jet. Beyond the breakup length from the nozzle exit, the RT model is used together with the KH model to predict the secondary breakup of spray droplets [3.26]. Air entrainment is modeled using the gas jet model, which is based on the unsteady gas jet theory [3.27], [3.28]. Mesh dependency in coupling from the gas phase to the liquid phase primarily arises from gas velocity in the droplet momentum equation. ANSYS FORTE employs an unsteady gas jet model to eliminate this mesh dependency for liquid droplet ambient gas coupling. The gas jet model, based on unsteady gas jet theory, models the axial droplet gas relative velocity without discretizing the CFD mesh. An adaptive collision mesh model is used for modeling fuel droplet collisions [3.29]. This model uses a pseudo collision mesh to partition parcels into collision partners and adaptively refines the mesh according to local parcel number density, making it independent of the gas phase mesh. For fuel droplet evaporation, a discrete multi-component fuel vaporization model is employed [3.30]. This model tracks fuel droplets during evaporation and allows incorporation with the reaction kinetics of individual fuel molecules [3.30]. The multi-component fuel vaporization model predicts similar distributions of liquid droplets and fuel mass fractions for gasoline and diesel sprays compared to single-component fuel models. However, the local vapor fuel composition, not resolved by a single-component model, varies significantly depending on the mixture location and time after fuel injection [3.30]. Wall heat transfer is modeled using a temperature wall function model developed in this study [3.31]. In-cylinder turbulence is modeled using an advanced version of the k-\varepsilon model, derived from the Renormalization Group (RNG) theory proposed by Yakhot and Orszag [3.32, 3.33]. While the k equation in the RNG version of the model remains the same as in the standard version, the ϵ equation is derived from rigorous mathematical derivation rather than empirically derived constants. Studies have shown that the modified RNG k-\varepsilon model accurately simulates engine compression and expansion flows and that large-scale flow structures affected by spray and squish flows are consistent with endoscopic combustion images [3.33]. Moreover, there is good quantitative agreement between measured and predicted NOx and soot emission data using the modified RNG k-ε model [3.34]. This RNG k-ε model has since been widely adopted in various

CFD codes and applications, including this study. The chemical reaction mechanism used in the present work is specifically developed for a diesel surrogate consisting of 66.8% n-decane and 33.2% alpha-methyl naphthalene (AMN) by weight. This mechanism includes 189 species and 1392 reactions [3.25]. The mechanism includes both low and high-temperature reactions of hydrogen oxidation, making it suitable for simulating hydrogen-diesel dual fuel combustion. This comprehensive approach allows for accurate modeling of the complex interactions and combustion characteristics of dual fuel systems. It features reaction pathways necessary for predicting soot precursors required for the soot surface mechanism. Soot nucleation is modeled from pyrene, acenaphthylene, naphthalene, benzene, and acetylene. Soot surface growth occurs via the HACA (hydrogen abstraction and carbon addition) mechanism and PAH (polycyclic aromatic hydrocarbon) condensation routes. Soot oxidation is modeled through the interaction with oxygen molecules and hydroxyl radicals. The mechanism accounts for both active and inactive sites on the soot surface [3.25]. Singh et al. investigated the ignition, combustion and emission characteristics of a single cylinder, 4-stroke, direct injection optical diesel engine based on a Cummins N-14 production engine [3.35]. The detail about the engine is specified in Table 3.2. The same engine is used in the present study, the typical diesel engine case (short ignition delay) is validated from his work then the parametric simulation for conventional diesel and hydrogen-diesel dual fuel combustion is performed on the same. The sector mesh, computational grid and piston geometry are used in this study and is presented in Figure 3.17. The sector represents the one injector hole considering that the injector has 8 equally spaced nozzle holes. The sector computational grid is used to save computational time. The mesh is generated using the standard ANSYS FORTE preprocessor. The mesh size and number of elements was selected based on Singh et al. work [3.35]. The mesh is composed of about 80,000 cells at bottom dead center with size $1.2 \times 1.2 \times 1.2$ mm near the piston bowl wall.

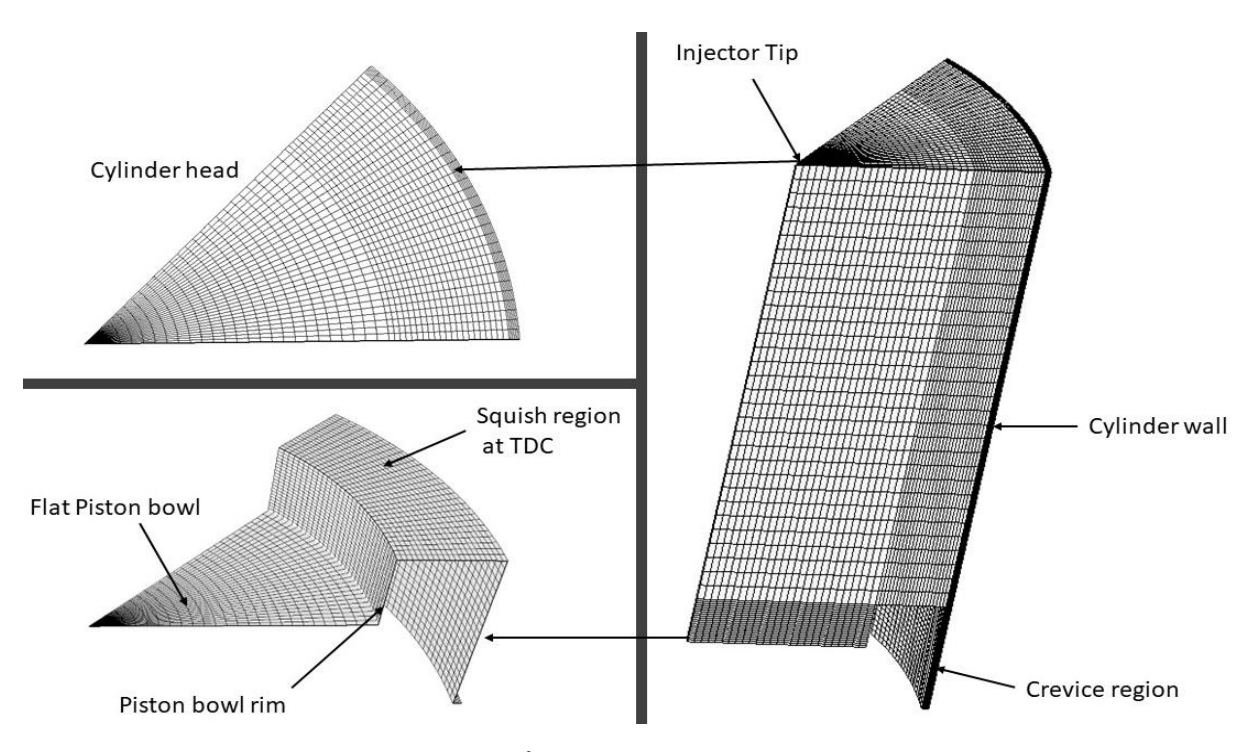


Figure 3.17: Detailed description of 45^o sector computational domain at BDC (with 80,000 cells)

The simulation includes low fuel loading (lower engine load), high fuel loading (medium engine load), hydrogen-diesel dual fuel case. The low fuel loading and high fuel loading is achieved through changing the average equivalence ratio inside the combustion chamber. The mass of diesel fuel is changed to achieve these two conditions [3.36]. According to the Φavg , the amount of diesel fuel required to maintain the is Φavg calculated and injected. The selected simulation of hydrogen diesel dual fuel case is performed for three different hydrogen additions on energy basis i.e., 10%, 20% and 30%. The description of test condition is presented in Figure 3.18.

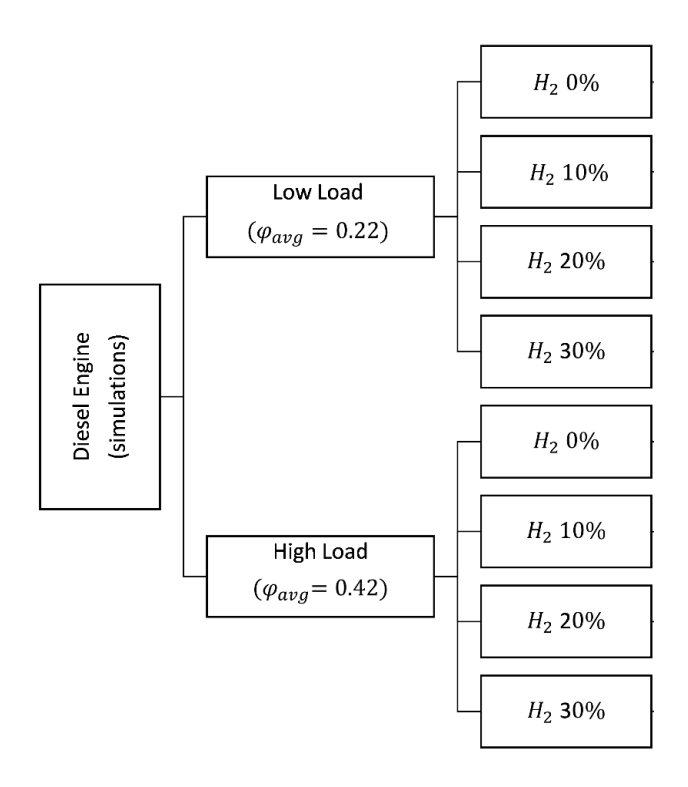


Figure 3.18: Detail description of test conditions.

The hydrogen-substitution is modeled on energy basis. A fraction of total energy supplied by the primary fuel (i.e., diesel surrogate) is replaced by hydrogen. The hydrogen energy share is calculated using the equation, H_2 (energy %) = $\frac{m_{\rm H_2} \cdot \rm LHV_{H_2}}{m_{\rm Diesel} \cdot \rm LHV_{Diesel} + m_{\rm H_2} \cdot \rm LHV_{H_2}}$

The simulation is initialized with homogeneous premixed charge of hydrogen-air. The global air fuel equivalence ratio of the premixed charge based on the hydrogen mass fraction alone is calculated and will be incorporated in the revised thesis in table format for both low and high load condition.

The $(\lambda)_{H_2-air}$ is calculated using the equation $(\lambda)_{H_2-air} = \frac{\dot{m}_{air}}{AFR_{H_2}^{st} \cdot \dot{m}_{H_2}}$.

Table 3.5: Global equivalence ratio inside the combustion chamber based on hydrogen mass.

Condition	$(\lambda)_{ m H_2-air\ (Low\ Load)}$	$(\lambda)_{ m H_2-air}$ (High Load)
D90 H10	65	31.28
D80 H20	32.49	15.6
D70 H30	21.6	10.5

3.1.1.2.3 Model validation

The numerically simulated in-cylinder combustion pressure, apparent heat release rate and normalized soot emission are validated with the experimental in-cylinder combustion pressure published in the previous study [3.35]. The validation of in-cylinder pressure, AHRR and soot is important because the in-cylinder pressure, temperature and AHRR manifests the quality of combustion, which governs the chemical reaction rates in the combustion chamber. These chemical reaction rates are responsible for the formation and decomposition of species, which are responsible for the formation of PAHs. The operating condition for which the validation is performed is presented in Table 3.5. The validation results of in-cylinder pressure, AHRR and soot are shown in Figure 3.19. The validation of simulated in-cylinder pressure and AHRR with experimental results are presented in Figure 3.19 (a). The simulated in-cylinder pressure shows good agreement with the experimental results. However, in the case of AHRR, a difference in peak AHRR is observed. It is because the experimental data published in the previous study is frequency filtered to remove the acoustic ringing before calculating the AHRR [3.35]. Consequently, the experimental peak AHRR is artificially reduced, and its width is increased. The other possible reason for this difference is due to the difference in the fuel properties. In this study, physical properties of tetradecane are used during performing the simulation whereas, in the experimental work the number 2 diesel was used. Due to the difference between the physical properties of these two fuels, the calculated atomization and evaporation process gets affected after the fuel injection event. This difference certainly leads to faster evaporation and atomization process, which increases the rate of premixed heat release in simulated cases. Figure 3.19 (b) presents the evaluation of normalized soot validation with the experimental results. The predicted and

experimental evaluation of soot shows the same trend for the formation and oxidation, which indicates a good agreement between the simulated and experimental result. The validation of soot also indicates that, the prediction of soot precursors (such as PAHs), surface growth species, oxidants (OH and O₂), and the in-cylinder conditions is accurately reproduced by the present model. However, at 11 CAD ATDC, a second peak is observed in the experimental result. A possible reason for this is due to a change in the temperature of soot particles, when they collide with the surface of the piston; another reason could be the migration of soot particles from squish to the piston bowl [3.35]. The grid independence test is also performed to choose the number of cells. The results of the grid independence test are presented in Figure 3.19 (c). The present number of cells is at TDC. The results show that the variation in cylinder pressure is very low for all the simulated cases. After validation, the simulations are performed for conventional diesel and hydrogen/diesel dual-fuel combustion for different premixing ratios at low and medium engine loads. The mass of fuel and composition of initial gas mixture is varied according to the simulated test cases. The detailed boundary and initial condition of the simulation is presented in Table 3.6.

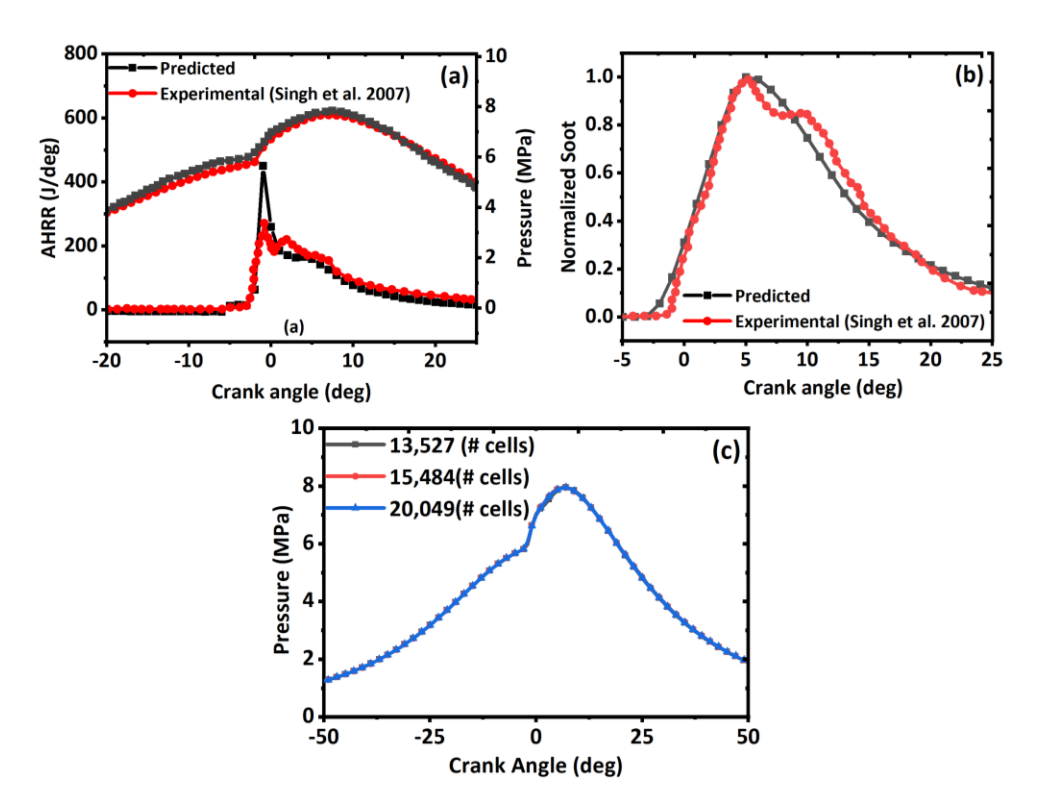


Figure 3.19: Validation of (a) in-cylinder pressure and AHRR, (b) normalized soot [3.35], and (c) grid independence test for varying the cell size (shown numbers are at TDC).

Table 3.5: Validated Operating condition of the Cummins N-14 engine.

Parameters	Values
Engine speed (rpm)	1200
Rail Pressure (MPa)	120
Injection timing (deg CA ATDC)	-7
Injection duration (deg)	10
Temperature of intake air (K)	384
Pressure of the intake air (MPa)	0.233
Fuel injection mass (mg)	61

Table 3.6: Initial and boundary conditions [3.35].

Parameter	Details
Diesel surrogate fuel composition	66.8 % n-decane and 33.2% α-methylnaphthalene
No. of gas phase species & reactions	189 species and 1392 reactions
Spray, nozzle and turbulent model	$KH-RT$ spray breakup, nozzle discharge coefficient model & RNG $k-\varepsilon$ model ($TKE-10000~cm2/s2, TLS-1~cm$)
Initial mixture composition	22.7% O ₂ & 77.3% N ₂ (mass basis) [depend on case]
Cylinder head temperature (<i>K</i>)	470
Piston temperature (<i>K</i>)	500
Cylinder wall (K)	420
Computation duration	-165 ATDC to 125 ATDC

3.1.3 Uncertainty and accuracy

Uncertainty analysis is important to quantifying the uncertainty in the measured data to build more confidence in experimental results [3.37, 3.38, 3.39]. Conducting uncertainty analysis for engine experiments displays distinctive challenges due to the multiple and varied parameters measured, the signal conditioning performed, and the large amount of data collected [3.37]. In this study, uncertainties due to both systematic and random errors in engine measurement are calculated. This section is divided into two subsections presenting uncertainty analysis of combustion parameters (in cylinder pressure, heat release rate, CA_{10} and CA_{50}), and particle emissions. Additionally, the section provides the accuracy details of the measuring instrument.

3.1.3.1 Uncertainty analysis of combustion parameters

In-cylinder pressure is a critical parameter that plays a crucial role in determining combustion parameters. Furthermore, these parameters demonstrate the combustion behavior, quality, and performance of the engines [3.38]. Therefore, recording the undistorted and unbiased cylinder pressure from the pressure transducer is critical. The primary sources of uncertainty in measuring in-cylinder pressure are linearity (systematic error) and cyclic temperature drift (systematic error) during most of the cycle. However, near the point of maximum pressure, random fluctuations (random error) become the predominant source of uncertainty [3.38]. Studies have derived the combined overall uncertainty of the in-cylinder pressure ($P_{cylinder}$) by using root mean square method as [3.38]:

$$u_c^2\left(P_{cylinder}\right) = u^2(linearity) + u^2(cylic temperature drift) + u^2(charge amplifer accuracy) + u^2(quantization) + u^2(random fluctuation) (3.32)$$

Uncertainties for the systematic errors (linearity, cyclic temperature drift, charge amplifier accuracy) in in cylinder pressure measurement is obtained from manufacturers data sheets. The main source of error due to quantization introduced by the analog to digital convertor is quantization error, which is computed as half of the resolution and is calculated using equation (3.33) [3.38].

Quantization error =
$$0.5 \times Resolution = 0.5 \times \left(\frac{V_D}{V_S.2^{(n-B)}} \times E\right) \dots \dots (3.33)$$

Where V_D is the full-scale output range of the convertor, V_s is the full-scale output range of the signal, E is the full-scale output of transducer, n is the bit resolution of the converted signal and B is the polarity factor (B=1 if the range is bipolar, = 0 if unipolar). The used module for acquiring analog in-cylinder signal in the present study is NI 9222, which is a 16-bit module with \pm 10 V range. Linearity and temperature drift uncertainties account for more than 90% of the overall uncertainty. Experimental fluctuation becomes predominant near the top dead centre and combustion event. The random component of the uncertainty for measurement of the in-cylinder pressure is estimated by calculating the standard deviation of peak pressure among 100 cycles at a stable engine operating point. The heat release is usually integrated from net heat release rate expression given by as:

$$\frac{dQ}{d\theta} = \frac{\gamma}{\gamma - 1} P \frac{dV}{d\theta} + \frac{1}{\gamma - 1} V \frac{dP}{d\theta} \dots \dots (3.34)$$

Uncertainty in equation (3.34) is mostly due to uncertainty in the $\frac{dP}{d\theta}$ estimates. The intervals chosen for the calculation of derivatives have to be carefully chosen since it has a significant impact on the estimation of uncertainty of value. Assuming linearity, the uncertainty for $\frac{dP}{d\theta}$ can be written as a function of the interval (j-i):

$$\frac{dP}{d\theta} = \frac{P_j - P_i}{\theta_j - \theta_i} \dots \dots (3.35)$$

Where i and j refer to i_{th} and j_{th} row of experimental data (here: pressure) recorded every 0.1 crank angle degrees with j-i > 0. P_j, P_i, θ_j , and θ_i each having an associated uncertainty, see Table 3.6. Therefore, $U(\theta_i) = U(\theta_j)$:

$$U\left(\frac{dP}{d\theta}\right) = \frac{\sqrt{U^{2}(P_{i}) + U^{2}(P_{j}) + 2\left(\frac{P_{j} - P_{i}}{0.1(j - i)}\right)U^{2}(\theta_{i})}}{0.1(j - i)} \dots \dots (3.36)$$

The uncertainty in pressure, volume, and ratio of specific heat plays an insignificant role and hence not considered in the analysis for uncertainty of equation 3.36 [3.38]. After performing the calculation, the uncertainty for pressure measurement comes out to be 5%. Also, uncertainty in $\left(\frac{dP}{d\theta}\right)$ comes out to be 5%. The uncertainty in heat release rate is directly related to uncertainty in $\left(\frac{dP}{d\theta}\right)$.

Table 3.7 Technical details of measured parameters

Variable measured	Instruments	Range	Accuracy	Linearity	Hysteresis	Resolution
Pressure	Piezoelectric sensor	5000 psi	± 1.2 bar	± 1%	1%	0.05 psi (rms)
Crank angle	Optical encoder		±0.1 CAD			0.1 CAD

3.1.3.2 Uncertainty Analysis of Particle Emission Measurements

Uncertainties in particle emission measurement can arise from the accuracy of the particle measurement instrument and random errors [3.40, 3.41, 3.42]. For particle emission measurement tests are carried out steady state engine operating conditions. Particle emissions are measured close to the engine exhaust valve, and the data have been collected for sampling frequency of 1HZ. For every engine operating condition, the data is logged at steady state and thermally stable condition. The mean of data of 60 sec is utilized for analyzing particle size and number distribution. Combined standard uncertainty u_N at 95% confidence level for total particle number concentration, nucleation mode particle concentration, and accumulation mode particle concentration was calculated using the root sum square method assuming normal distribution of errors [3.40].

$$u_N = \sqrt{u_r^2 + u_s^2} \dots \dots (3.37)$$

Where u_s represents the uncertainty due to systematic error and u_r represent uncertainty due to random error. The random error was calculated by taking the standard deviation of 64 measurements. Uncertainty (%) of particle emissions parameters is presented in Table 3.8. The accuracy of the particle sizer is presented in Table 3.9.

Table 3.8 Uncertainties of Particle Emissions Parameters

Particle emission parameter	Uncertainty (%)
Total Particle number	1.3
Nucleation mode particle number	1.5
Accumulation mode particle number	1

Table 3.9 Accuracy of particle sizer

Particle diameter (nm)	Accuracy (95% CI)
Upto 300 nm diameter	± 5% Standard deviation
Over 300 nm	±10% Standard deviation

3.1.3.3 Accuracy of the instruments

The instruments used in the study, including their manufacturers, models, and respective accuracies, are listed in Table 3.10. These details highlight the precision and reliability of the measurement tools employed, ensuring that the data collected can support comprehensive analysis.

Table 3.10: Accuracy and technical details of measured parameters in experiment [3.43]

Measured variable	Instrument	Manufacturer/Model	Accuracy
In-cylinder Pressure	Piezo-electric	KISTLER, Model: 603 CB	± 1.2 bar
	Pressure		
	transducer		
Crank Angle	Encoder	Kubler, Model:	± 0.1 CAD
		8.5000.8351.3600	
Particle Size	Particle Sizer	Cambustion, DMS 500	< 300 nm, ± 5% SD
			> 300 nm, ± 10% SD
Regulated and unregulated	FTIR	AVL, Model: SESAM i60 FT	<± 2% (linearity)
emission species			

Chapter 4

Result and discussion

This chapter presents the main findings and analysis derived from the observations. The section is divided into five subsections to elucidate and explain the results. These subsections are combustion analysis, emission analysis, physico-chemical characteristics, toxicological characteristics, and environmental risk assessment. The combustion analysis section delves into in-cylinder pressure, heat release rate (HRR), start of combustion (CA₁₀), combustion phasing (CA₅₀), and combustion duration (CA₁₀₋₉₀). In the emission analysis section regulated and unregulated emissions are discussed. The physico-chemical characteristics section examines the physical and chemical properties of emissions. The toxicological characteristics section explores the impact of unregulated and particulate emissions on human health, both experimentally (in-vitro cytotoxicity and ROS imbalance test) and analytically, using a lung compartment model and USEPA-prescribed methods. The environmental risk assessment section addresses the adverse effects of regulated and unregulated emissions on environmental risk indicators such as global warming potential, acidification potential, eutrophication potential and ozone forming potential.

4.1 Combustion analysis

Combustion is the fundamental process that generates both work and combustion by-products in conventional diesel and advanced dual-fuel (reactivity-controlled compression ignition (RCCI)) engines. The characteristics of combustion, including its nature (homogeneous or heterogeneous), in-cylinder pressure, temperature, heat release rate, start of combustion, combustion phasing, and duration, vary depending on factors such as operating conditions, fuel type, and combustion mode. This change in combustion related parameters changes the in-cylinder combustion kinetics, and various combustion reaction intermediate forms inside the combustion chamber depending on incylinder charge properties. Furthermore, during exhaust stroke these emissions are released into the environment. For these reasons, it is imperative to investigate and understand the combustion characteristics.

In-cylinder pressure, heat release rate and combustion characteristics

The present section discusses the effect of operating parameters on in-cylinder pressure, HRR, CA₁₀, CA₅₀ and CA₁₀₋₉₀ in conventional diesel combustion (CDC), methanol-diesel (MD) RCCI, gasoline diesel (GD) RCCI and hydrogen diesel dual-fuel engines. Figure 4.1 (a-d) shows the effect of combustion mode and engine load on combustion characteristics of conventional diesel, GD-RCCI and MD-RCCI. Figure 4.1 (a-d) depicts the in-cylinder pressure, HRR, CA₁₀, CA₅₀ and CA₁₀₋₉₀. The results shows that as at constant load as the combustion mode shifts from CDC to MD-RCCI, the in-cylinder peak pressure and HRR decrease along with retard CA₁₀ and CA₅₀ (Figure 4.1 (a-d). Methanol, characterized as a low-reactivity fuel, introduces a reactivity gradient within the combustion chamber. Consequently, combustion initiation occurs from the most reactive zones within the charge. The lower reactivity of methanol results in delayed CA₁₀ and CA₅₀ compared to CDC and GD-RCCI. Moreover, methanol has a higher latent heat of vaporization, leading to a decrease in in-cylinder charge temperature within the combustion chamber during the compression stroke [4.1]. The initiation and rates of combustion reactions are highly reliant on ambient temperature, decreasing as temperature decreases [4.2]. Subsequently, the transitions to MD-RCCI combustion mode result in delays in CA₁₀ and CA₅₀.

The in-cylinder peak pressure increases as the combustion mode shifts from CDC to GD-RCCI engine. The increase in peak pressure is due to the early CA₁₀ and premixed combustion of charge near TDC (Figure 4.1 (a, b)). The CA₅₀ is comparable in both CDC and GD-RCCI. In GD-RCCI combustion mode, the autoignition of charge happens earlier than in MD-RCCI engines due to the reactivity difference in both fuels. Gasoline is more reactive as compared to methanol due to its lower octane number compared to methanol [4.3]. The CA₁₀₋₉₀ duration is lower in RCCI combustion mode than in the CDC. RCCI combustion mode only exhibits premixed combustion, so the duration to consume the charge is small.

Figure 4.1 (c) indicates the moderate load condition results; the results demonstrate that as the engine load increases the in-cylinder peak pressure and HRR increases for all three combustion modes. This increase is attributed to the increase in energy input inside the combustion chamber. As the engine load increases, more fuel is burned inside the combustion chamber. This increase in

fuel increases the energy released inside the combustion chamber, which manifests as an increase in peak pressure and HRR [4.4]. Figure 4.1 (d) shows the moderate engine load condition on combustion parameters; the results show that at moderate load conditions, the CA₁₀₋₉₀ duration is larger than lower load for CDC, whereas it is smaller for RCCI combustion mode. As the engine load increases, the diffusion combustion duration increases in CDC mode, which results in a larger duration of CA₁₀₋₉₀. However, in the case of RCCI, the CA₁₀₋₉₀ decreases because of an increase in in-cylinder combustion temperature with an increase in engine load. The higher combustion temperature accelerates the combustion reactions, decreasing the combustion duration for premixed nature of combustion.

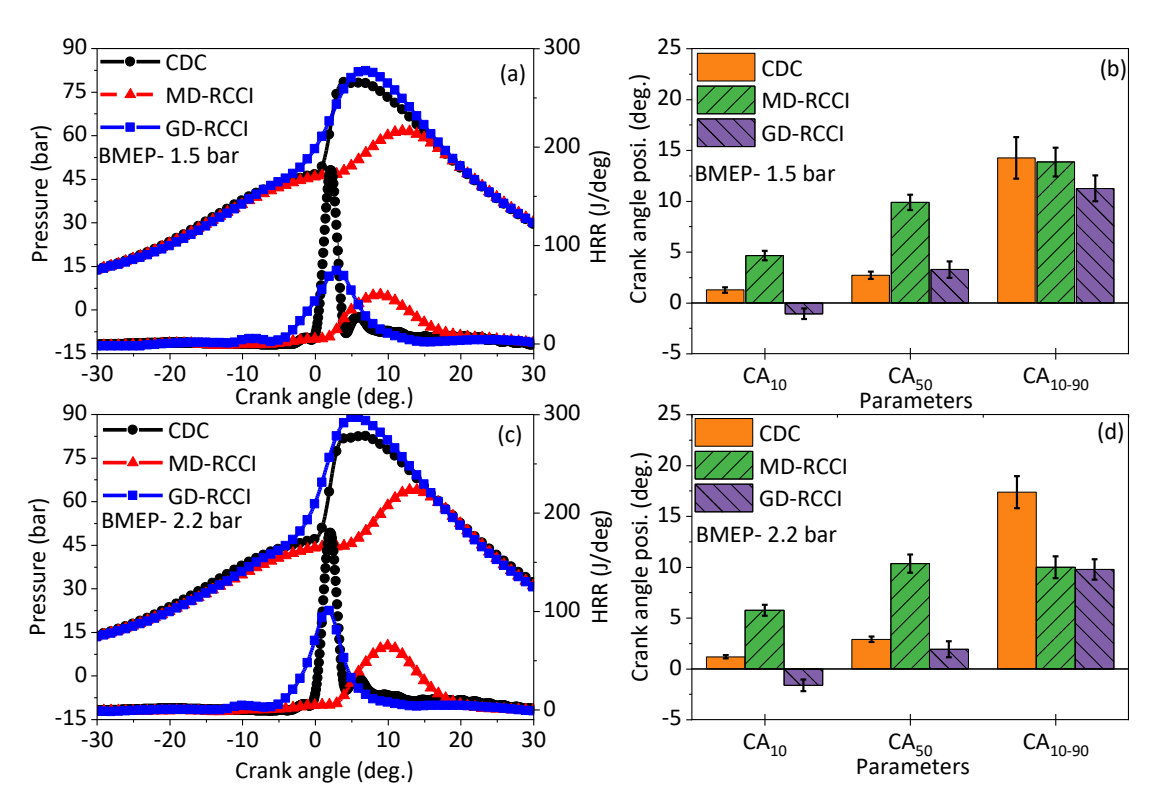


Figure: 4.1 (a-d) effect of combustion mode and engine load on in-cylinder pressure, HRR, CA₁₀, CA₅₀ and CA₁₀₋₉₀.

Figures 4.2 (a-d) depict the impact of fuel premixing ratio (RP), i.e., energy share of low-reactive fuel (methanol/gasoline), on the in-cylinder pressure and HRR parameters of RCCI combustion mode. The findings reveal that, under constant engine load, increasing RP in MD-RCCI engines leads to a decrease in peak pressure and HRR. As RP increases, the reactivity of the charge decreases, shifting combustion towards the expansion stroke (Figure 4.2 (a)). Moreover, higher RP

results in retardation of CA₁₀, CA₅₀, and CA₁₀₋₉₀, attributed to the lower reactivity and higher latent heat of vaporization of methanol (Figure 4.2 (b)).

Figures 4.2 (c, d) illustrate similar trends in GD-RCCI engines, with increasing RP leading to decreased charge reactivity and delayed CA₁₀ and CA₅₀. However, the CA₁₀₋₉₀ duration decreases as RP increases. As discussed, RCCI combustion initiates from the most reactive zone within the combustion chamber. In GD-RCCI engines, combustion begins with initial heat release, leading to a phenomenon known as local charge heating. This process heats the local charge, increasing the likelihood of combustion in neighboring mixtures. With increasing RP, the proportion of gasoline within the combustion chamber rises, increasing local heating due to greater heat release. Consequently, the charge consumption accelerates, resulting in a decrease in combustion duration.

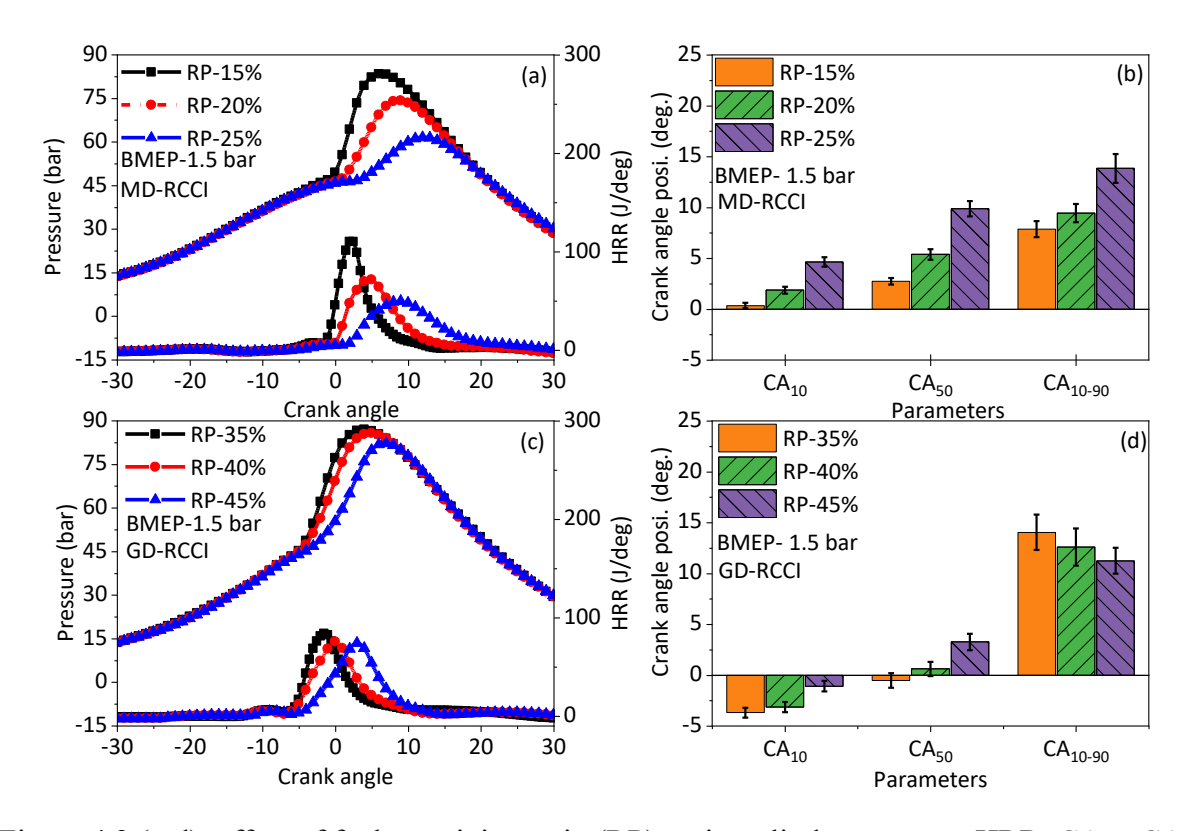


Figure 4.2 (a-d): effect of fuel premixing ratio (RP) on in-cylinder pressure, HRR, CA₁₀, CA₅₀ and CA₁₀₋₉₀ in methanol diesel and gasoline diesel RCCI engines.

The effect of hydrogen energy shares on in-cylinder pressure, average temperature, and AHRR is shown in Figure 4.3 (a-d). The effect of hydrogen can be categorized into three different and simultaneous phenomena happening inside the combustion chamber i.e., physical, chemical, and

mass effects. The physical effect is mainly associated with the properties of hydrogen fuel. The chemical effect of the hydrogen addition is associated with the impact of hydrogen on the reaction intermediates and in-cylinder radical distribution. The mass effect of hydrogen is contributing in two ways one is the reduction of mass of the diesel fuel, and the other is the lower molecular mass of the hydrogen leads to high diffusion of hydrogen in in-cylinder charge. The result shows that at a lower load with an increase in the hydrogen energy share, the in-cylinder peak pressure (P_{max}) and peak HRR decrease (Figure 4.3 (a, c)). The decrease in the peak pressure is mainly due to slower and poor combustion of hydrogen at a lower load. The slower rate of combustion retards the combustion, and the combustion of charge shifts towards the expansion stroke. The autoignition temperature of hydrogen is higher as compared to diesel fuel. The addition of hydrogen tends to increase the delay period. The autoignition reactions start from the most reactive zone in the combustion chamber. Initially, a fraction of diesel fuel initiates the combustion process and premixed diesel fuel burns in the premixed phase of combustion. Later, the premixed charge (hydrogen-air) burns during the diffusion phase of combustion. The evidence of this phenomenon can be observed in the HRR curve (Figure 4.3 (c)). At lower engine load, with an increase in hydrogen energy share the reactivity of the charge decreases due to high autoignition temperature of hydrogen. So, as the hydrogen share increases the reactivity of the charge decreases and hence more amount of unburned hydrogen appears at exhaust valve open condition.

To verify the combustion of hydrogen at a lower load, the consumption of hydrogen fuel and the evolution of OH radical for different hydrogen energy share is explored and presented in Figure 4.4 (a, b). The consumption of hydrogen fuel at lower load for the cases of D90 H10, D80 H20, and D70 H30 is 66%, 63%, and 60% respectively. It suggests that more than 34% of hydrogen is unutilized during combustion and comes out as unburned hydrogen emission. The slope of the hydrogen consumption curve represents the rate of combustion of hydrogen. It is observed that at lower load with an increase in hydrogen addition, there is no significant difference in the peak of OH radical concentration (Figure 4.4 (b)). The OH radical represents the chain branching reaction and the spread of it is a measure of high temperature reactions and combustion duration. The peak of OH radical represents the high-temperature combustion zones. No significant difference in OH radical peak and distribution represents the inefficient combustion of hydrogen at a lower load. The OH radicals play a key role in the oxidation of reaction intermediates (C₂H₂, C₆H₅) formed during combustion. However, the in-cylinder mean gas temperature increases for 10% hydrogen

energy share (D90 H10) while further increase in hydrogen energy share i.e., for 20% and 30% (D80 H20 and D70 H30), a decrease in mean gas temperature is observed as compared to the 10% case.

Figure 4.3 (b, d) represents the effect of hydrogen energy share on in-cylinder pressure, temperature, and AHRR at medium load condition. It is observed that at a higher load, an increase in the hydrogen energy share leads to an increase in the P_{max}, peak HRR and temperature. The increases in in-cylinder pressure and temperature are due to the efficient combustion of hydrogen. The combustion temperature is high at a higher load in comparison to a lower load and promotes the rate of combustion. A more fraction of hydrogen is consumed near the TDC position and hence the increase in-cylinder combustion pressure. The highest in-cylinder peak pressure (10.4 MPa) is observed for the D80 H20 case. However, the highest in-cylinder mean gas temperature (1710 K) is observed for the D70 H30 case. The HRR trend for higher load is presented in figure 4.3 (d). The qualitative comparison of AHRR trends shows good agreement with previous study [4.7]. Zhou et.al., demonstrated in their study, that at lower engine load (λH_2 -air = 22.09) condition the addition of hydrogen (30 % HES), the peak of heat release rate was decreased by 15% as compared to neat diesel case. However, at higher engine load (λH_2 -air = 8.51) with the addition of hydrogen (30% HES), the peak of HRR is increased by 33% [4.7]. In the present study at same hydrogen energy share i.e., at 30% hydrogen energy share (HES) and at lower engine load (λH_2 -air = 21.6) the peak of HRR is decreased by 18% and at higher engine load (λH_2 -air = 10.5) for 30 % hydrogen energy share the peak of HRR is increased by 30%. In conclusion it can be stated that the simulated results of hydrogen/diesel dual-fuel combustion are qualitatively comparable and well predictive in comparison to the previous experimental studies [4.7]. The figure depicts that with an increase in the hydrogen energy share, the more fraction of charge is burned in the premixed combustion phase and less amount of charge is burnt in the diffusion combustion phase. Hydrogen has higher auto-ignition temperature, high flame speed, high diffusivity, and high energy content per unit mass. As the hydrogen fraction increases, the rate of auto-ignition reactions decreases and leads to a slightly longer ignition delay. Because of the longer ignition delay, more fraction of premixed charge burns during the premixed phase of combustion and results in increased peak of HRR.

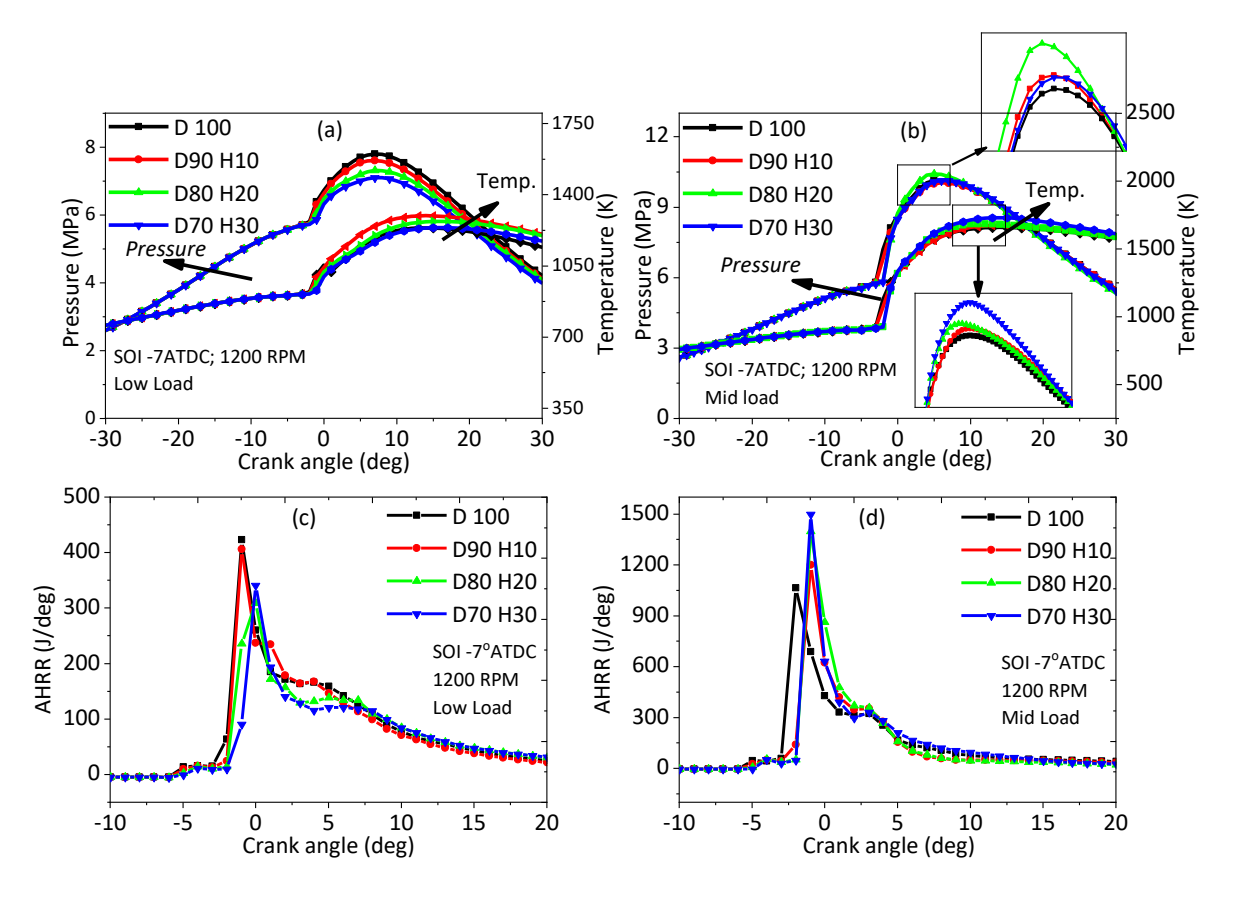


Figure 4.3 (a-d): Effect of hydrogen energy share and engine load on in-cylinder pressure, avg. temperature and HRR.

The evidence of the efficient combustion of hydrogen at a higher load can be seen in figure 4.4 (a, b). The consumption curve shows that at mid load the consumption of hydrogen for the cases of D90 H10, D80 H20, and D70 H30 is 85%, 88%, and 86% respectively. The slope of the curve is also steeper than the lower load and the rate of combustion is high (Figure 4.4 (a)). However, a small bump is observed in hydrogen consumption curve at lower load condition. The reason for the bump is due to the increase in concentration of H₂ before the consumption of hydrogen. The oxidation of diesel at both low and high temperature initiates by H abstraction leading to formation of alkyl radical. The H atom further participates in combustion and one of the possible events is leading H₂ molecule. This might be the reason for the observed small bump in the consumption curve. The concentration and spread of OH radical increased with an increase in hydrogen energy

share at a higher load (Figure 4.4 (b)). The increase in the concentration of OH radical is due to more consumption of hydrogen fuel molecules during combustion.

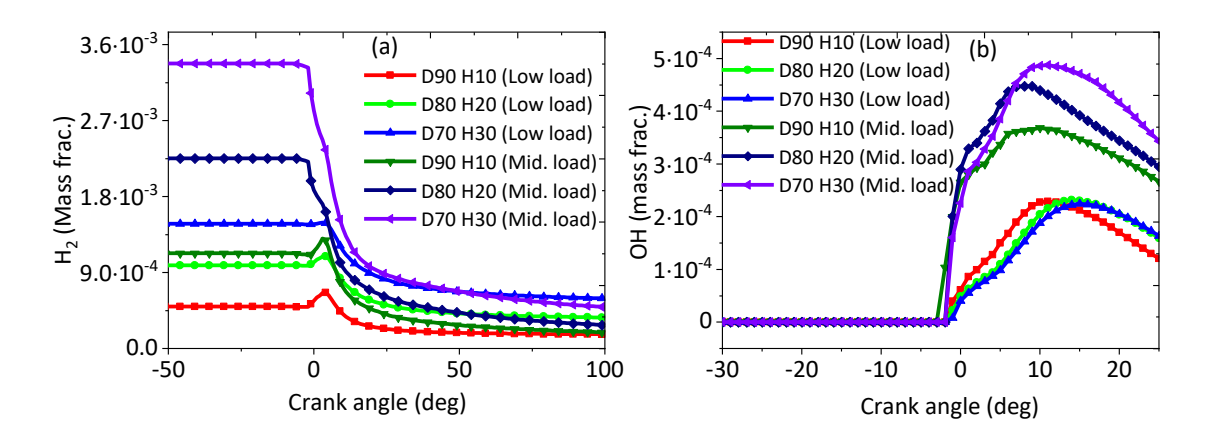


Figure 4.4 (a, b): effect of hydrogen energy shares on in-cylinder combustion of H2 fuel and evolution of OH radical at both low and medium load conditions.

4.2 Emission Analysis

The present section discusses the emission characteristics. This section is divided into two subsections named as regulated and unregulated emission characteristics. The regulated emissions are THC (total hydrocarbon), CO (carbon monoxide), NO_x (oxides of nitrogen) and PM (particulate matter) emission. The unregulated emissions include saturated HCs, unsaturated HCs, carbonyl compounds and aromatic emissions. The species includes CH₄ (methane), C₂H₂ (acetylene), C₂H₄ (ethylene), C₂H₆ (ethane), C₅H₁₂ (n-pentane), C₃H₆ (propylene), HCHO (formaldehyde), CH₃CHO (acetaldehyde), methanol (CH₃OH), toluene (C₇H₈), sulfur dioxide (SO₂) and ammonia (NH₃).

4.2.1 Regulated emissions

This section presents the effect of operating parameters on the emission of regulated species from conventional diesel, MD-RCCI, GD-RCCI and hydrogen diesel dual fuel engines. The regulated species includes THC, CO, NO_{x_1} and particulate matter (PM) or soot.

4.2.1.1 THC, CO and NO_x emission

Figure 4.5 (a-d) illustrates the effect of combustion mode, engine load and premixing ratio (RP) on regulated emissions. The results show that when the combustion mode is shifted from CDC to RCCI at both low and moderate engine load, the NO_x emission decreases significantly. The decrease in NO_x emission is attributed to the low-temperature combustion phenomenon in RCCI combustion mode. The highest decrease in NOx is observed for the GD-RCCI engine (Figure 4.5 (a)). However, THC and CO emissions increase significantly as the combustion mode shifts to RCCI from CDC mode. The highest CO and THC emissions are observed for the MD-RCCI engine (Figure 4.5 (a)). As discussed in the combustion section, when the combustion mode shifts to MD-RCCI, the CA_{50} retards, causing combustion to shift towards the expansion stroke. Consequently, the combustion reactions freeze, and the formed CO and THC appear in the exhaust.

Figure 4.5 (b) indicates the moderate engine load condition that as the engine load increases from low to moderate load conditions, the emission of NO_x increases in all three combustion modes compared to low load conditions. This increase is attributed to an increase in in-cylinder combustion temperature due to burning a larger amount of fuel. In the case of MD-RCCI operation the methanol oxygen content also supports the NOx emission at higher engine load. At higher temperature the fuel oxygen atom gets released due to bond breaking and participates in NOx formation. A decrease in THC and CO emissions is observed at moderate load condition. The decrease in THC and CO is due to the increase in in-cylinder mean gas temperature. The increase in mean gas temperature increases the rate of oxidation reaction and hence the formed CO gets converted into CO₂. Additionally, the partially reacted HC species also gets oxidized due to high temperature. Also, with an increase in engine load the cylinder wall and liner temperature increases, which increases the evaporation rate of the trapped low reactive fuel and that gets consumed (Figure 4.5 (b)).

Figure 4.5 (c, d) presents RP on emission of THC, CO, and NOx. In the case of GD-RCCI engines, an increase in RP leads to a decrease in NOx emissions, while CO and THC emissions increase. The reduction in NOx emissions is attributed to the lower in-cylinder mean gas temperature. The increase in CO and THC emissions is due to the decreased reactivity of the charge. Figure 4.5 (d) depicts the effect of RP for MD-RCCI combustion mode. The results depict that with an increase in RP in MD-RCCI operation the NOx emission decreases significantly. However, the CO and THC emission of MD-RCCI is significantly higher. The low in-cylinder combustion temperature

and lower reactivity of charge is one of the important reasons for increases CO and THC emission from MD-RCCI engines. Due to low in-cylinder combustion temperature the rate of oxidation of CO and HC is relatively low. Also, due to low reactivity of in-cylinder charge the combustion phasing is retarred in MD-RCCI. Another reason for the increase in the THC and CO emission with an increase in RP is due to the increase in ignition delay period. The increase in ignition delay period contributes to overmixing of the mixture and the in-cylinder charge becomes overly lean which is not favorable for the combustion and leads to the unburned HC emission.

The effect of hydrogen energy share on soot, NOx, and CO emissions from conventional diesel and hydrogen/diesel dual-fuel operations is presented in Figure 4.5 (e, f). The results indicate that with an increase in engine load, the emissions of soot, NOx, and CO increase compared to lower load operations for conventional diesel combustion. At high loads, the mass of the injected fuel is greater, and the air-fuel ratio is lower, leading to worse charge uniformity and higher soot emissions. The increase in NOx is primarily due to the significant rise in in-cylinder combustion temperature with increased engine load, as NOx formation is strongly dependent on combustion temperature. The results for hydrogen/diesel dual-fuel combustion are also shown in Figure 4.5 (e) for lower engine loads and (f) for higher engine loads. The data show that increasing the hydrogen energy share reduces the emissions of soot, CO, while NOx emissions increase. The increase in NOx emissions is due to the higher in-cylinder mean gas temperature. The reduction in soot, and CO, emissions is attributed to the replacement of neat diesel with hydrogen fuel. As the hydrogen energy share increases within the combustion chamber, the mass of injected diesel decreases, resulting in fewer carbon-containing radicals and thus lower emissions of carbon-containing products. The higher mass of hydrogen in the combustion chamber decreases the global C/H ratio, thus further decreasing the formation of soot. The effective use of oxygen is also enhanced. The evidence of this phenomenon can be related to an increase in the hydroxy radical concentration with the increase in hydrogen energy share as discussed in the combustion analysis section. A similar trend is observed at high engine loads; however, the emission concentrations are higher compared to lower load operations.

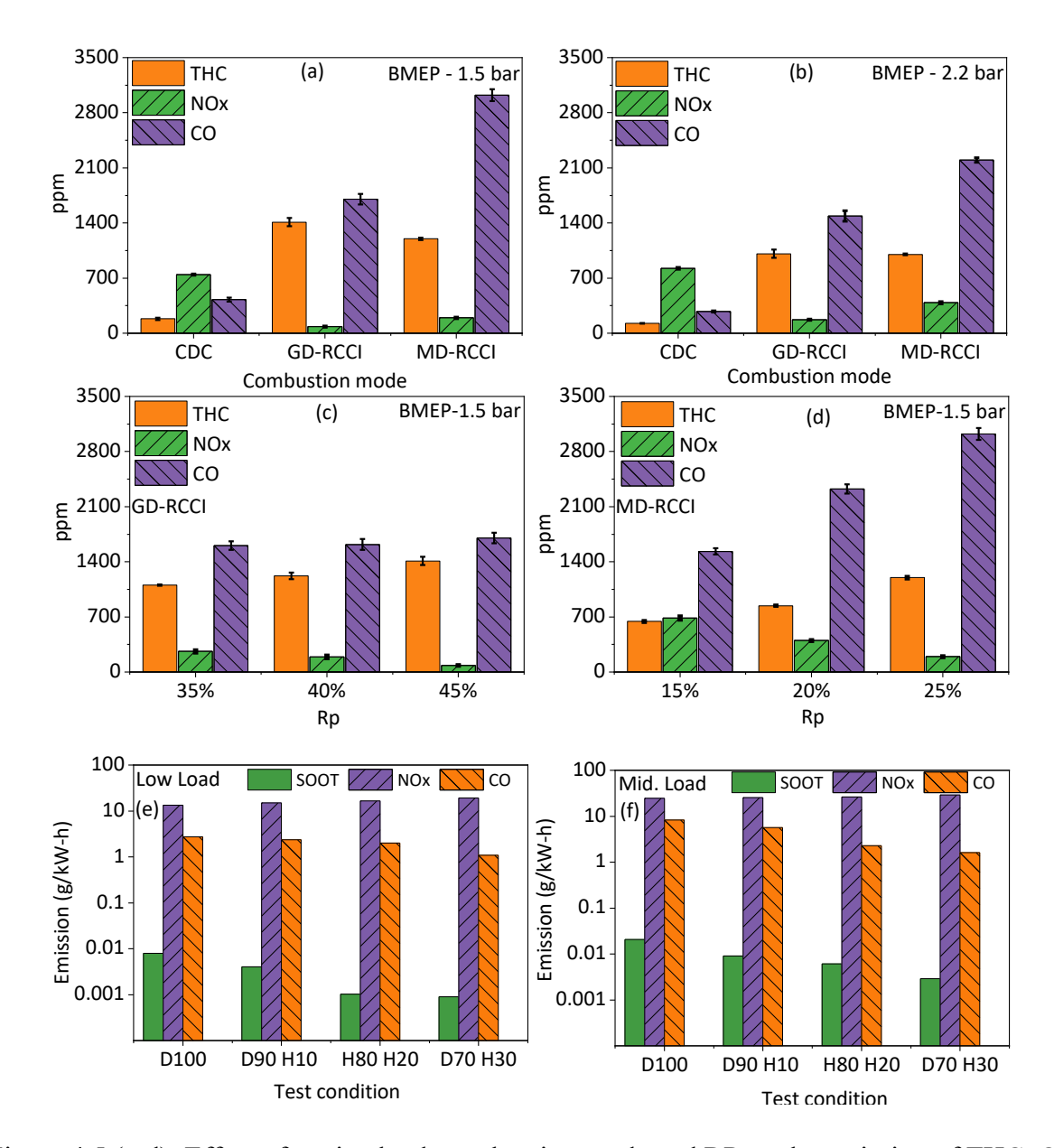


Figure 4.5 (a-d): Effect of engine load, combustion mode and RP on the emission of THC, CO and NOx from CDC and RCCI combustion engines, (e, f) Effect of engine load and hydrogen energy share on the emission of CO, NOx and soot emissions.

4.2.1.2 Particulate emissions

Particulate emissions (PM) from conventional diesel and MD/GD-RCCI engines are measured using filter paper. Figure 4.6 (a) depicts the effect of engine load and combustion mode on the emission of aggregate PM mass. The results indicate that under both low and moderate load

conditions, shifting the combustion mode from CDC to RCCI significantly reduces PM emissions. Among the three combustion modes, the greatest decrease is observed in MD-RCCI. In GD-RCCI, PM emissions decrease compared to CDC due to the absence of diffusion combustion and lower temperatures. MD-RCCI exhibits the lowest emissions due to its fuel properties; the low carbon content and additional oxygen content inhibit PM formation, resulting in lower emissions. However, as the engine load increases, PM emissions increase for all three combustion modes due to the higher fuel mass being burned inside the combustion chamber.

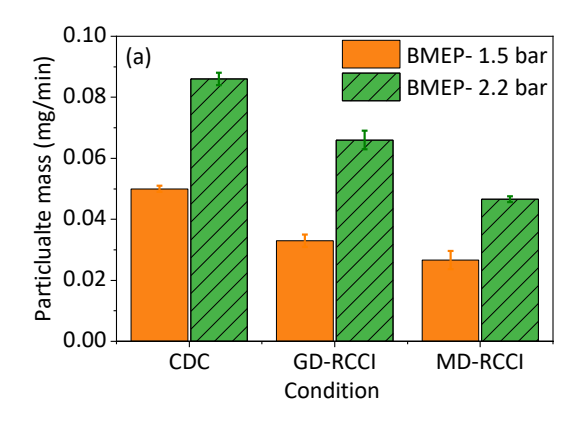


Figure 4.6 (a): Effect of engine load, combustion mode on PM mass emission from CDC, MD-RCCI and GD-RCCI engines.

4.2.2 Unregulated emission analysis

The present section discusses the unregulated species emissions from CDC, MD-RCCI, GD-RCCI and hydrogen diesel dual-fuel combustion engines. The section is divided into four subheadings which are saturated hydrocarbon emissions, unsaturated hydrocarbon emissions, carbonyl compound emissions and aromatic emissions.

4.2.2.1 Saturated hydrocarbon emissions

In saturated hydrocarbons, carbon and hydrogen are linked by single bonds. In the present investigation the measured saturated hydrocarbons are CH₄ (methane), C₂H₆ (ethane) and C₅H₁₂ (pentane). The formation of CH₄ and C₂H₆ in combustion happens through a series of complex reactions involving. The typical path observed in chemical kinetics (engine like condition) studies mainly involves the reaction between methyl radical (CH₃) and other compounds such as methanol (CH₃OH), HCHO, CH₃CHO, C₂H₆ and others. A few of them are, addition of methyl radical to

methanol (CH₃OH + CH₃ = CH₂OH + CH₄ and CH₃OH + CH₃ = CH₃O + CH₄), addition of methyl radical to ethane (C₂H₆ + CH₃ = C₂H₅ + CH₄), addition of methyl radical to CH₃CHO (CH₃CHO + CH₃ = CH₃CO + CH₄) [4.5]. Depending on the activation energy and rate of the reaction the net CH₄ is emitted. However, the formation of methane also involves the reaction between phenyl radical (C₆H₅) and other oxygenated, unsaturated hydrocarbons.

Figure 4.7 (a-b) shows the effect of engine load and combustion mode on the emission of saturated HCs. For CDC operation the observed emission of CH_4 is less than 5 ppm for all the tested load condition. The emission of C_2H_6 is also below the detection limit. Hence, these emissions are not presented for CDC.

The results demonstrate that among all three saturated HC emissions, the C₅H₁₂ has the highest emission from GD/MD-RCCI. The GD-RCCI exhibits a higher emission of C₅H₁₂ than MD-RCCI (Figure 4.7 (a)). This is because of the branched chain structure of gasoline fuel molecules. The consumption of fuel molecules in the engine takes place through a series of complex reactions which involve the formation of several saturated and unsaturated HCs. The larger branched chain alkane-like structured fuel molecules break down into small chain molecules during combustion. During the process of decomposition, depending on the in-cylinder temperature and mixture equivalence ratio, the saturated HCs formed. As combustion chemistry has a finite time in enginelike conditions, depending on the duration of combustion, these saturated HCs appear in the exhaust. As gasoline fuel molecules have higher chain lengths and higher carbon concentrations, the C₅H₁₂ formation is more in the GD-RCCI combustion engines than in the MD-RCCI engines. In MD-RCCI combustion engines, the primary source of C₅H₁₂ is diesel fuel decomposition. However, CH₄ and C₂H₆ emissions are higher in MD-RCCI than in GD-RCCI. The formation of CH₄ in engine-like conditions environment where methanol is present happens through reactions like addition of CH₃ to CH₃OH (CH₃OH + CH₃ = CH₂OH + CH₄ and CH₃OH + CH₃ = CH₃O + CH₄), addition of CH₃ to C_2H_6 ($C_2H_6 + CH_3 = C_2H_5 + CH_4$), addition of CH₃ to acetaldehyde $(CH_3CHO + CH_3 = CH_3CO + CH_4)$ [4.6]. The presence of methanol molecules in the combustion chamber promotes these paths, and because of that, the emission of CH₄, C₂H₆ is observed to be higher in MD-RCCI combustion engines than GD-RCCI combustion engines. As the engine load rises all three saturated HCs in both combustion modes decrease due to improved combustion (Figure 4.7 (b)).

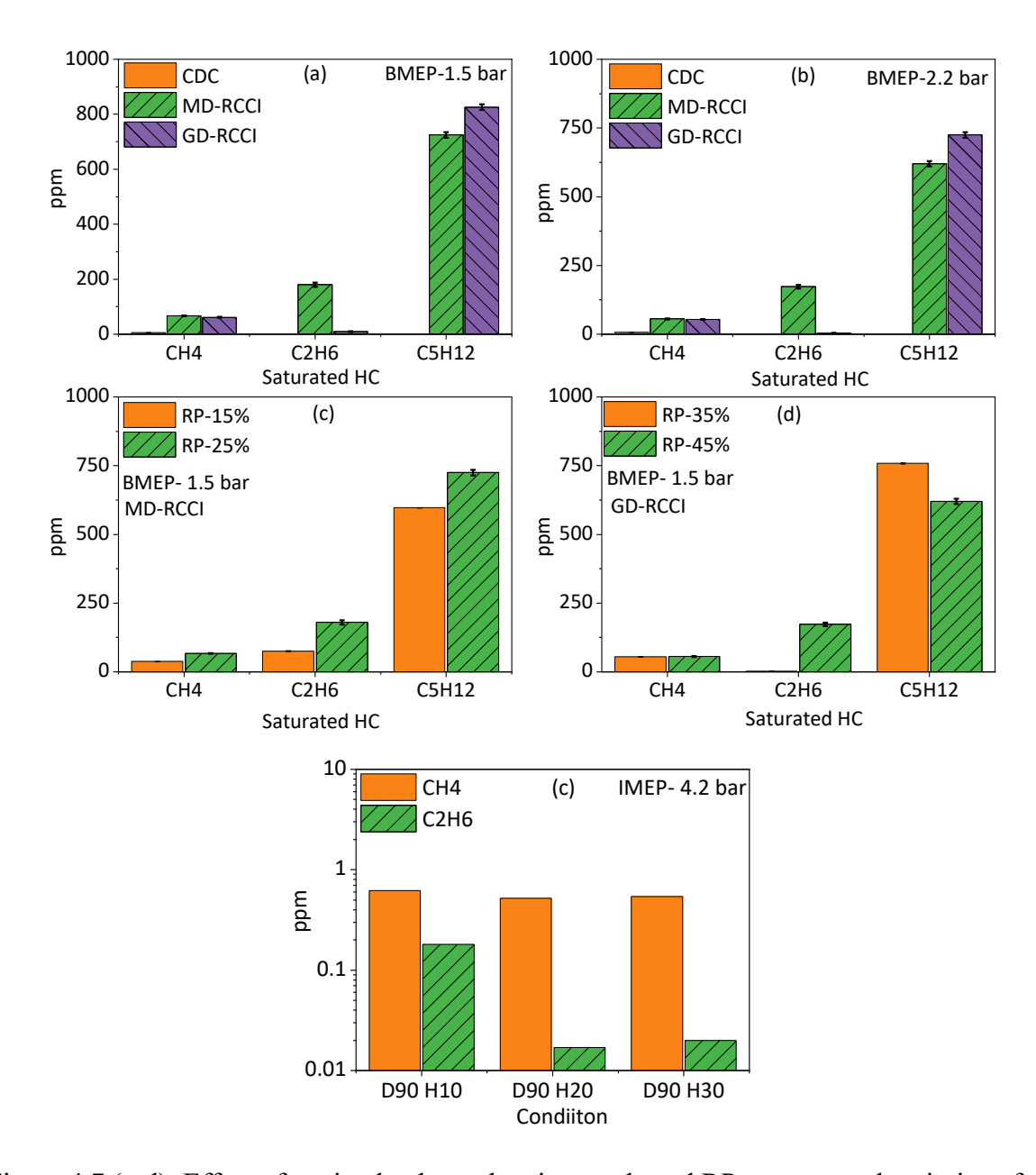


Figure 4.7 (a-d): Effect of engine load, combustion mode and RP on saturated emissions from MD-RCCI and GD-RCCI engines. (e) Effect of hydrogen energy share on the emission of saturated HCs from hydrogen-diesel dual fuel engine.

The influence of RP on saturated HC emissions for both combustion modes is demonstrated in Figure 4.7 (c, d). The results show that as RP rises the CH₄, C₂H₆ and C₅H₁₂ emission increases due to the decrease in reactivity of charge with a rise in RP. The lower reactivity reduces the rate of oxidation of the created CH₄, C₂H₆ and C₅H₁₂. The addition of CH₃OH as fuel raises the HCHO concentration along with CH₃CHO, which also leads to the formation of CH₄ and C₂H₆ in MD-

RCCI operation. Figure 4.7 (e) shows the effect of hydrogen energy share on the emission of saturated HCs in hydrogen-diesel dual fuel combustion engine. The results show that the emission of CH₄ and C₂H₆ is below 1 ppm under all the simulated conditions. This shows that hydrogen-diesel dual fuel combustion engines have insignificant emission of these species.

4.2.2.2 Unsaturated hydrocarbon emissions

Hydrocarbon compounds in which carbon and hydrogen are linked with each other by double and triple bond are known as unsaturated (alkene and alkyne) hydrocarbons. In the present investigation the detected unsaturated hydrocarbons are C₂H₂ (acetylene), C₂H₄ (ethylene) and C₃H₆ (propylene). The formation of C₂H₂, C₂H₄ and C₃H₆ in combustion happens through the thermal cracking of long chain compounds. In diesel engines, during combustion of spray due to locally rich fuel-air mixture and high temperature the thermal cracking of long chain compounds happens. This cracking leads to formation of reactive intermediates which includes C₂H₂, C₂H₄ and C₃H₆. However, later in combustion these get oxidized by O₂, OH and form stable compounds given that favorable conditions are available. The rate of oxidation depends on temperature and at high temperature these species get completely consumed.

Figure 4.8 (a-d) shows the effect of engine load and fuel premixing on the emission of C₂H₂, C₂H₄ and C₃H₆ from MD-RCCI and GD-RCCI operation. During, experiment the emitted concentration of C₂H₂, C₂H₄ and C₃H₆ for CDC operation was under the detection limit of the FTIR.

The results show that as the combustion mode transitions from GD-RCCI to MD-RCCI under both low and moderate engine load conditions, the emission of C₂H₄ increases, while the emission of C₃H₆ decreases compared to GD-RCCI (Figure 4.8 (a, b)). Additionally, at moderate load, the emission levels of these species are lower than at low load. The increase in engine loads the incylinder temperature increases and accelerates the rate of oxidation reaction. Hence, formed C₂H₄ and C₃H₆ get oxidized, and less concentration appears in the exhaust. The emission of C₂H₂ remains comparable across both engine load conditions (Figure 4.8(a, b)).

Figure 4.8 (c) presents the effect of RP on the emissions of C₂H₂, C₂H₄, and C₃H₆ for MD-RCCI engines. The results indicate that with an increase in RP, the emissions of C₂H₂, C₂H₄, and C₃H₆ increase. This rise in emissions is attributed to a lower in-cylinder combustion temperature, which slows the rate of oxidation reactions, allowing C₂H₂, C₂H₄, and C₃H₆ to escape oxidation and

appear in the exhaust. Figure 4.8 (d) shows the effect of RP on the emissions of C2H2, C2H4, and C3H6 from GD-RCCI engines. The results reveal that with an increase in RP, the emission of C2H4 increases while the emission of C3H6 decreases. Figure 4.8 (e) presents the effect of hydrogen energy share on these emissions. The results show that the emissions of these species are insignificant (less than 5 ppm) from hydrogen-diesel engines. Furthermore, as the hydrogen energy share increases, these emissions decrease even more.

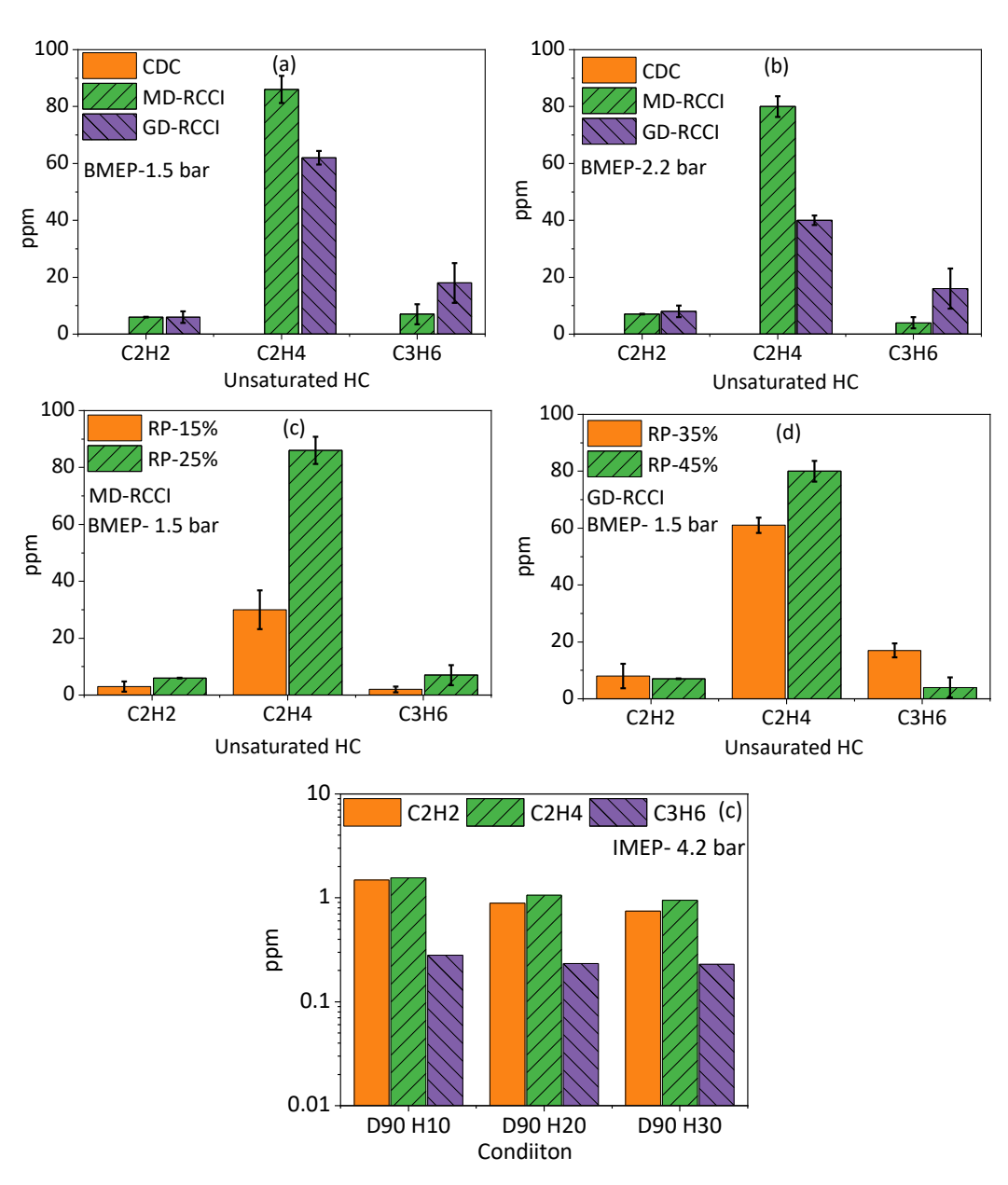


Figure 4.8 (a-d): Effect of engine load, combustion mode and RP on saturated emissions from MD-RCCI and GD-RCCI engines. (e) Effect of hydrogen energy share on the emission of saturated HCs from hydrogen-diesel dual fuel engine.

4.2.2.3 Carbonyl compound emissions

The compounds which contain carbonyl group (C = O), are known as carbonyl compounds. The carbonyl compounds measured in the emission are formaldehyde (HCHO) and acetaldehyde (CH₃CHO). The formation of HCHO and CH₃CHO in engine combustion depends on low temperature combustion reaction path and the fuel type. Typically, at low temperature the radicals (R) undergo addition of O_2 and form alkyl-peroxyl radicals RO_2 through the $R+O_2=RO_2$ reaction. Later, internal H abstraction happens and a second O_2 addition and these subsequent decomposition yield to reactive hydroxyl radical and a carbonyl radical and compounds. The formation of carbonyl compounds also happens through direct abstraction of hydrogen atoms from methanol compound such as $CH_3OH \rightarrow CH_2OH \rightarrow CH_2O \rightarrow HCO \rightarrow CO$ [4.5].

Figure 4.9 (a-d) shows the effect of combustion mode, engine load and RP on the emission HCHO and CH₃CHO. The results show that the emission of CH₃CHO and HCHO is very low in CDC operation as compared to RCCI operation. Figure 4.9 (a, b) shows that in CDC operation, the value of CH₃CHO and HCHO is lower than 20 ppm at both low and moderate engine loads. Also, as the engine load increases CH₃CHO and HCHO emission decreases. Higher in-cylinder combustion temperature leads to decrease the formation of CH₃CHO and HCHO. At higher engine load the low temperature path of formation of these species does not contribute to the emission. Additionally, the rate of oxidation reactions at high temperature suppresses the formation of these compounds.

As the combustion mode shifts from CDC to RCCI mode the emission of carbonyl compounds increases significantly. The highest HCHO emission is observed in the case of MD-RCCI engine at both engine load condition (Figure 4.9 (a, b)). The emitted concentration of HCHO is higher than CH_3CHO at all the loads. Methanol consumption during combustion happens through the $CH_3OH \rightarrow CH_2OH \rightarrow CH_2O \rightarrow HCO \rightarrow CO$. This linear reaction path forms the HCHO directly, and to form the CH_3CHO an additional methyl radical is required which comes from the breakdown

of diesel fuel. In MD-RCCI mode, with an increase in engine load the emission of HCHO and CH₃CHO decreases. The increase in engine load in MD-RCCI engine increases the in-cylinder charge reactivity (due to increase in diesel mass) which leads to improved combustion of methanol and results in lower HCHO and CH₃CHO emission. The emitted concentration of HCHO is higher than CH₃CHO at all the loads. In the case of GD-RCCI combustion mode the emission of both CH₃CHO and HCHO is comparable at both load conditions. However, as the combustion mode shifts to GD-RCCI from MD-RCCI the CH₃CHO emissions increase significantly.

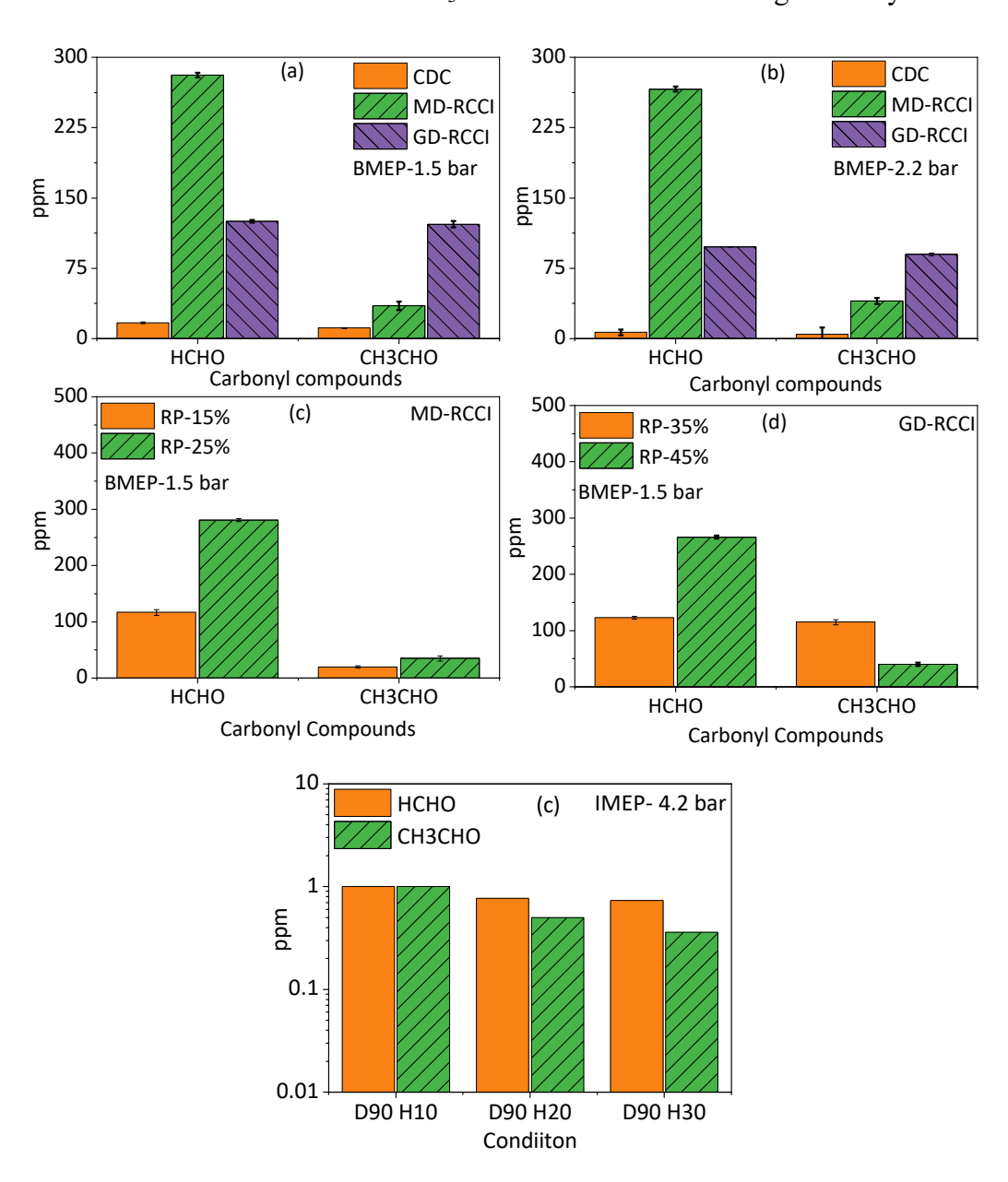


Figure 4.9 (a-d): Effect of engine load, combustion mode and RP on carbonyl emissions from CDC, MD-RCCI and GD-RCCI engines. (e) Effect of hydrogen energy share on the emission of carbonyl compounds from hydrogen-diesel dual fuel engine.

Figure 4.9 (c, d) illustrates that as the RP increases, the emissions of HCHO, CH₃CHO, and increases form both MD-RCCI and GD-RCCI combustion modes. In MD-RCCI, the increase in RP results in higher levels of methanol inside the combustion chamber, leading to a significant increase in HCHO emissions. Additionally, due to lower reactivity and low-temperature combustion, the formed C₇H₈ does not undergo oxidation in both combustion modes, resulting in increased emissions. Figure 4.9 (e) shows the effect of hydrogen energy share on the emission of HCHO and CH₃CHO. The results indicate that as the hydrogen energy share increases the emission of HCHO and CH₃CHO decreases. Also, the amount of these emissions is insignificant in the case of hydrogen-diesel dual fuel combustion.

4.2.2.4 Aromatic Emissions

The emissions of aromatic hydrocarbons (AHCs) are illustrated in Figure 4.9 (a-d). During the experimental tests, the detected gas-phase AHC was toluene (C7H8). The results indicate that as the combustion mode shifts from CDC to RCCI, the emission of C7H8 increases, with the highest increase observed in the MD-RCCI mode. The primary source of toluene in MD-RCCI exhaust is partially oxidized diesel fuel. Additionally, as the engine load increases to a moderate level, the emission of C7H8 decreases. At higher engine load the in-cylinder combustion temperature is higher and hence the rate of oxidation reaction is higher and a decrease in emission of C7H8 (Figure 4.9 (a)). Figure 4.9 (b) shows the effect of RP on the emission of C7H8 from the MD-RCCI and GD-RCCI operation. The results show that with an increase in RP, the toluene emission increases, this is due to lower combustion temperature and over lean charged, with an increase in RP the charges reactivity decreases significantly and hence the formed reaction intermediates do not get oxidized. The slow rate of oxidation reaction at higher RP leads to an increase in toluene emission.

Figure 4.9 (c, d) presents the effect of hydrogen energy share on the individual PAHs mass emission, total PAHs mass emission in hydrogen/diesel dual-fuel combustion for low and high engine load. For lower load, PAHs mass emission is presented in bar chart form and can be seen in Figure 4.9 (c). The result depicts that with an increase in hydrogen energy share, the PAHs mass

emission containing 2 – 4 rings (Nap, Acenp, Phenth, Chry, Pyr) increases. However, decrease in high ring containing PAHs (BaP, BeP, B[g,h,i]P) is observed for all the hydrogen energy share. The highest mass emission is observed for Nap. This is mainly due to the reaction between H radical and 1-methylnapthalene (C₁₀H₇CH₃). The addition of H to C₁₀H₇CH₃ leads to formation of C₁₀H₈ (naphthalene) and CH₃. The diesel fuel (diesel surrogate used in the simulation) also contains the 1- methylnaphthalene, which contributes to the formation of Nap. The increase in 2-4 ring PAHs mass emission is mainly associated with H atom involving PAHs growth reactions. However, the decrease in higher ring PAHs is due to delayed combustion. The delayed combustion decreases the available time for high temperature reactions inside the combustion chamber and suppress the formation higher ring PAHs. The effect of hydrogen energy share on individual PAHs mass emission for medium engine load (IMEP-10 bar) is presented in Figure 4.9 (d). Figure 4.10 shows that at higher load for neat diesel (D100) operation, the 2-4 ring containing PAHs (Nap, Acenp, Phenth, Chry, Pyr) mass emission decreased as compared to lower load with neat diesel operation. However, the higher ring containing PAHs mass increased. The decrease in 2-4 rings containing PAHs mass is due to the higher in-cylinder temperature, which promotes the formation of higher ring PAHs. The higher ring PAHs formation is happening through the involvement of lower ring PAHs in HACA reaction mechanism and results in higher PAHs mass emission containing high ring PAHs. Furthermore, Figure 4.10 (d) depicts that at high load, the increase in hydrogen energy share leads to a decrease in the emission of both high as well as low ring containing PAHs emission. The addition of hydrogen replaces the significant mass of carbon containing diesel; thus, less fraction of carbon is available in the combustion chamber to participate in growth of PAHs. Additionally, at higher engine load the hydrogen energy share increases the concentration of oxidation reactions involving radical OH which further oxidizes the formed PAHs.

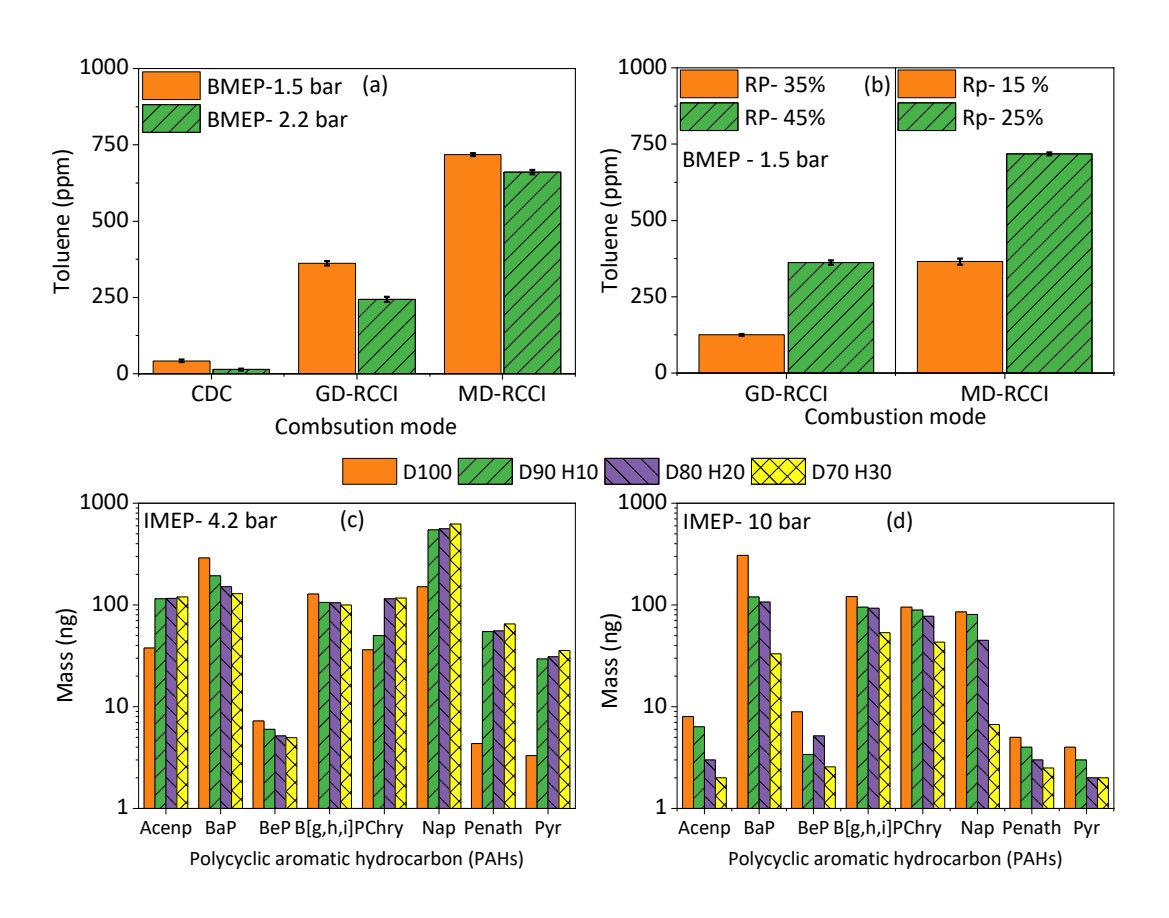


Figure 4.10 (a, b): Effect of engine load, combustion mode and RP on toluene emissions from CDC, MD-RCCI and GD-RCCI engines. (c, d) Effect of hydrogen energy share on the emission of PAHs from hydrogen-diesel dual fuel engine.

4.3 Physico-chemical characterization and analysis

This section explores the physical and chemical properties of particulate matter (PM) emissions. The particle size, concentration, and mass distribution of PM are analyzed to determine their physical characteristics. The size and concentration of these particles significantly influence their deposition in human lungs. The chemical properties of PM encompass soluble organic fractions and trace metals present in the particles.

4.3.1 Particle size distribution

The effect of engine load on particle number distribution (PSD) for CDC and MD-RCCI operations is presented in figure 4.11 (a, b). At lower engine load (1.5 bar BMEP), the smaller size particles dominate, while larger size particles dominate at moderate load (2.2 bar BMEP) in CDC. The increase in engine load tends to raise the in-cylinder combustion temperature along with

dominating diffusion combustion. The higher the charge burn in the diffusion combustion (at medium load) leads to the formation of larger size particles. The formation of particle strongly depends on local in-cylinder combustion temperature and nature of combustion. A similar trend is observed for the MD-RCCI and GD-RCCI combustion operation i.e., with an increase in engine load the larger size particle emission dominates (figure 4.11 (b, c)). The effect of fuel RP on particle emission in MD-RCCI combustion is presented in Figure 4.11 (d). The result shows that at constant engine load (1.5 bar BMEP), with an increase in RP the smaller size particle emission starts dominating. As, RP increases, the CA₅₀ retards significantly (as seen in combustion analysis section), and more fraction of charge burn during the expansion stroke. During the expansion stroke, the in-cylinder temperature decreases steeply, which leads to a decrease in the rate of agglomeration. Thus, results in the formation of smaller size particles. Additionally, the formed volatiles during the combustion doesn't get oxidized further and hence the smaller size particle appears in the particle emission. In other words, the RCCI regime is mainly dominated by premixed combustion. The combustion of charge during the premixed phase also leads to the formation of smaller size particles. Figure 4.11 (d) also indicates that within increase in the RP, the peak of larger size particles decreases. The effect of RP for GD-RCCI engine is presented in figure 4 (e). The results demonstrate a similar trend to that of MD-RCCI engine such as, when RP increases the smaller size particles distribution increases.

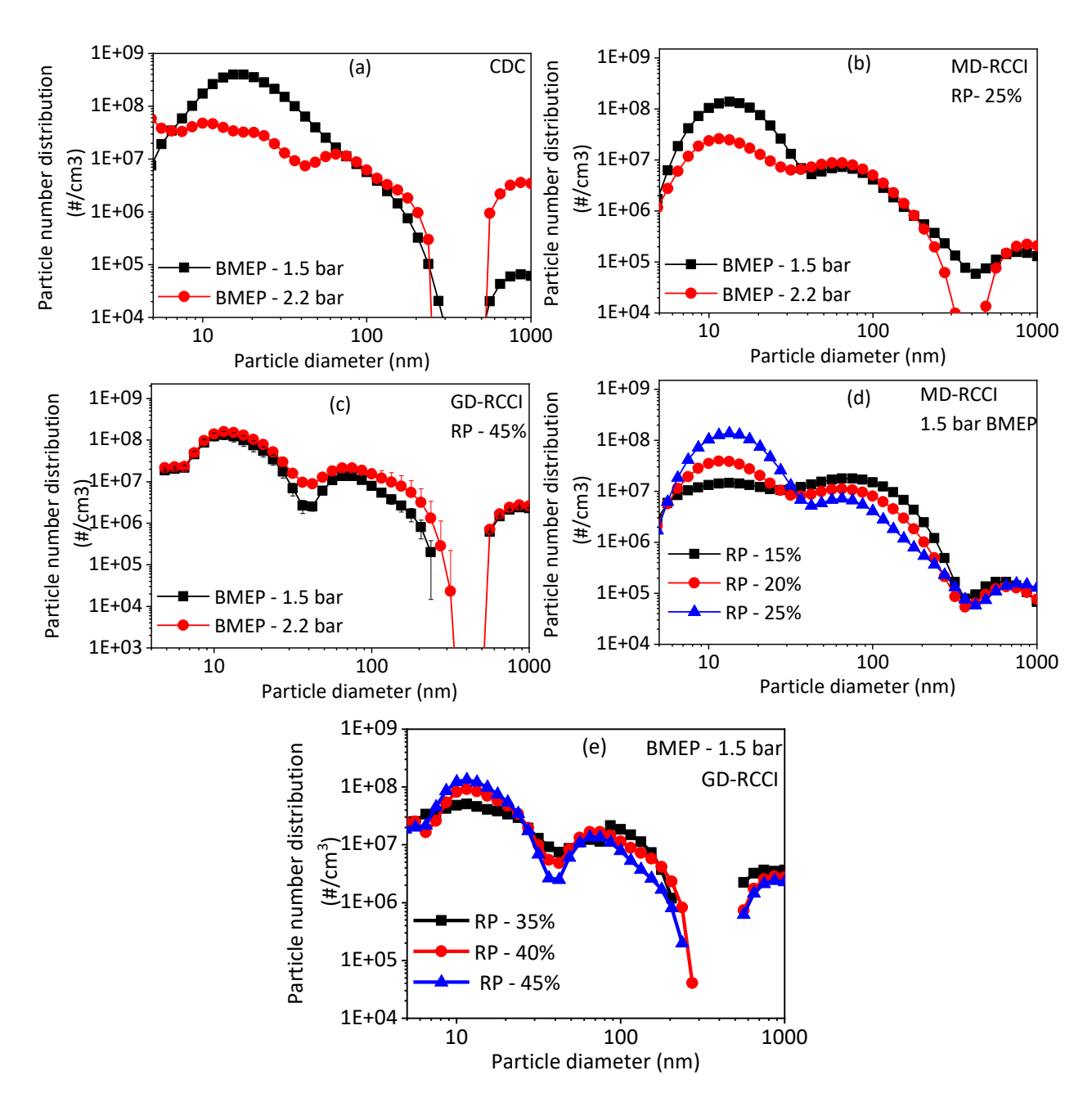


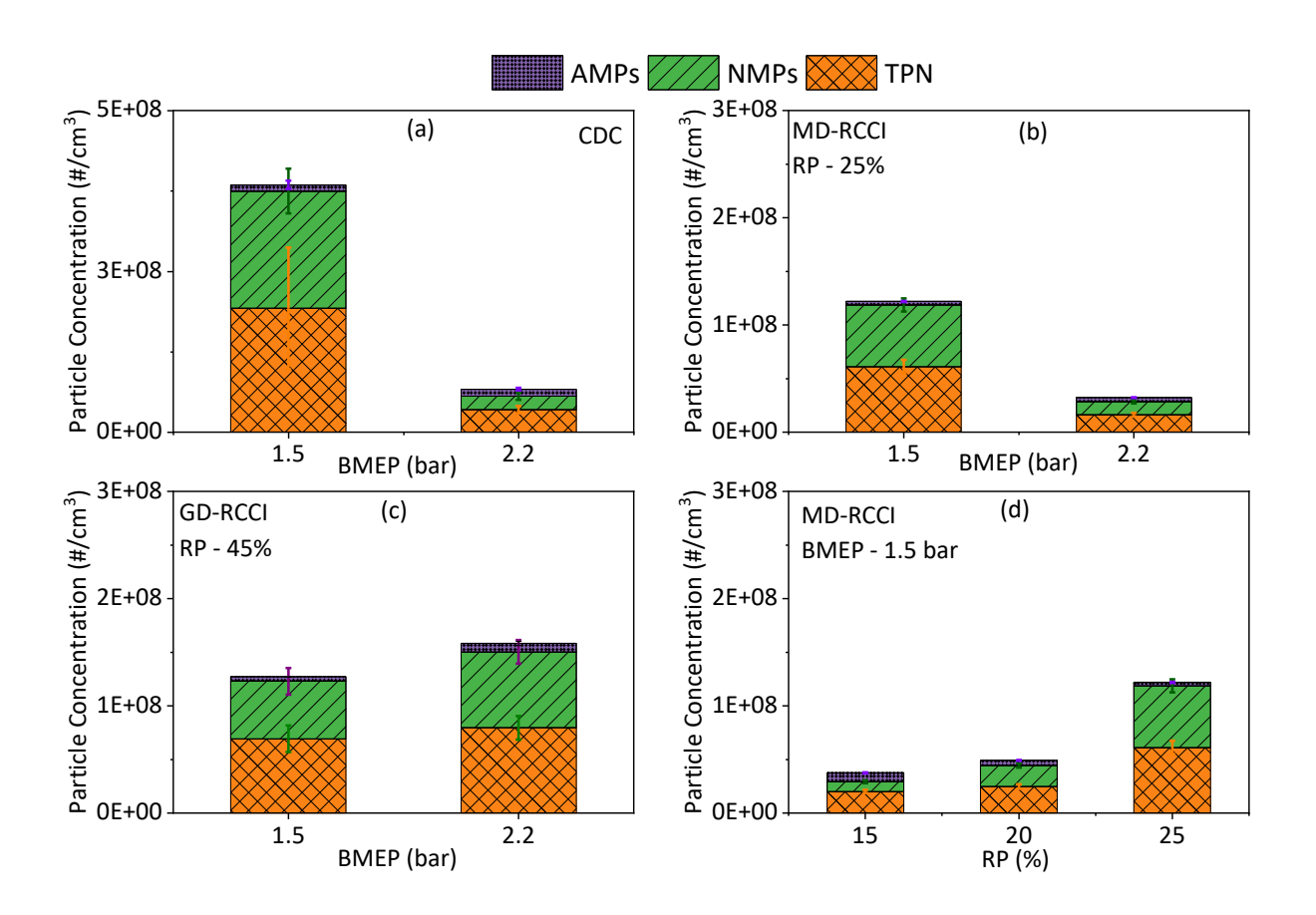
Figure 4.11: (a) Effect of engine load on particle size number distribution in CDC engine, (b)

Effect of engine load on particle size number distribution in MD-RCCI engine, (c) Effect of
engine load on particle size number distribution in GD-RCCI engine, (d) Effect of premixing
ratio (RP) on particle size number distribution in MD-RCCI engine, (e) Effect of premixing ratio

(RP) on particle size number distribution in GD-RCCI engine.

The total particle number (TPN), nucleation mode particle (NMPs) and accumulation mode particle (AMPs) concentration is presented in figure 4.12 for CDC, GD-RCCI and MD-RCCI

combustion operations. The results demonstrate that for CDC at lower engine load, the concentration of NMPs is significantly high as compared to medium load (Figure 4.12 (a)). A similar trend is observed for MD-RCCI and GD-RCCI operation also with respect to engine load (Figure 4.12 (b, c)). In CDC, as engine load increases the diffusion combustion dominates over the premixed combustion and hence causing formation of AMPs. The TPN emission at lower engine load operation is highest as compared to medium load operation for all three combustion modes. The increase in TPN is due to the increase in the NMP mode particle concentration. Figure 4.12 (d, e) shows the effect of RP on the emission of NMPs, AMPs and TPN emission for both GD-RCCI and MD-RCCI. The results show that at lower RP the TPN and NMPs are lower in concentration as compared to higher RP for both MD-RCCI and GD-RCCI.



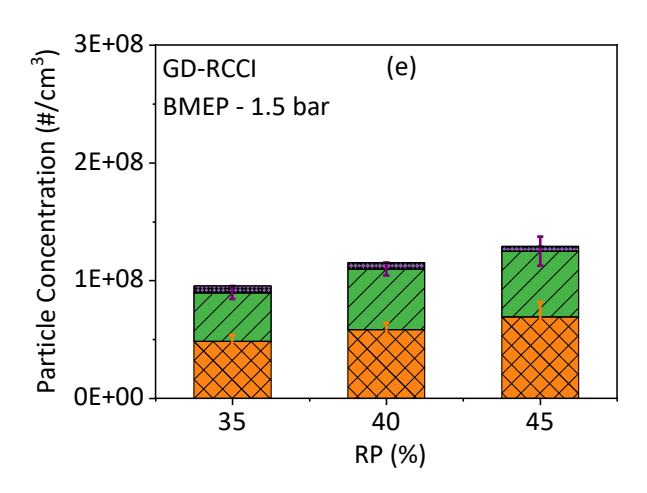


Figure 4.12: (a) Effect of engine load on TPN, NMPs and AMPs number concentration in CDC engine, (b) Effect of engine load on TPN, NMPs and AMPs number concentration in MD-RCCI engine and (c) Effect of engine load on TPN, NMPs and AMPs number concentration in GD-RCCI engine (d) Effect of premixing ratio (RP) on TPN, NMPs and AMPs number concentration in MD-RCCI engine and (e) Effect of premixing ratio RP on TPN, NMPs and AMPs number concentration in GD-RCCI engine

At higher RP the in-cylinder mass of low reactive fuel is higher that causes lower the in-cylinder combustion temperature. The NMPs increase due to the consequence of enhanced charge homogeneity within the combustion chamber. Enhanced homogeneity within the combustion chamber raises the likelihood of homogeneous particle nucleation at lower engine loads, and subsequently, these nucleated particles manifest as NMPs in the exhaust. As the RP increases, the in-cylinder mean gas temperature decreases due to retards combustion phasing for RCCI and hence the formed NMPs emitted in higher concentration.

4.3.2 Particle size and mass lobes

To understand the dominance of concentration and mass of emitted nanoparticles, the number concentration and mass correlation lobes are presented in Figure 4.13 (a-d). The mass distribution of nanoparticles plotted on x – axes and the number concentration is plotted on y – axes. The size of the lobe signifies the amount of PM, and the inclination of the lobe shows the dominance of mass/number over each other. Inclination of the lobe towards x – axes demonstrates the mass dominance and inclination of the lobe towards y – axes demonstrates the number dominance.

The results depict that as the engine load is increased from 1.5 bar BMEP to 2.2 BMEP bar in CDC, the lobe size decreased along with a greater inclination towards the x — axes (Figure 4.13 (a)). This signifies that at lower engine load the number concentration dominates over mass emission and with an increase in engine load the mass emission of particulate dominates over number concentration in CDC. The dominance of mass at medium load is because of the higher concentration of AMPs for medium load operation in CDC. In case of MD-RCCI and GD-RCCI combustion at constant RP when the load is increased from 1.5 bar BMEP to 2.2 bar BMEP, a similar finding is observed (Figure 4.13 (b, c)). This means the qualitative effect of engine load on particle emission is the same in MD-RCCI, GD-RCCI and CDC engine. Figure 4.13 (d) shows the effect of RP on particle number and mass correlation for MD-RCCI engine. The effect of RP is plotted only for the MD-RCCI engine as the GD-RCCI qualitatively follows a similar trend. The results depict that, when the RP is increased from 15% to 25 %, for MD-RCCI engine the number concentration of particles starts to dominate over the mass emission as inclination of the lobe is more towards the y – axes. It is mainly because of the formation of NMPs in higher concentration with an increase in the RP.

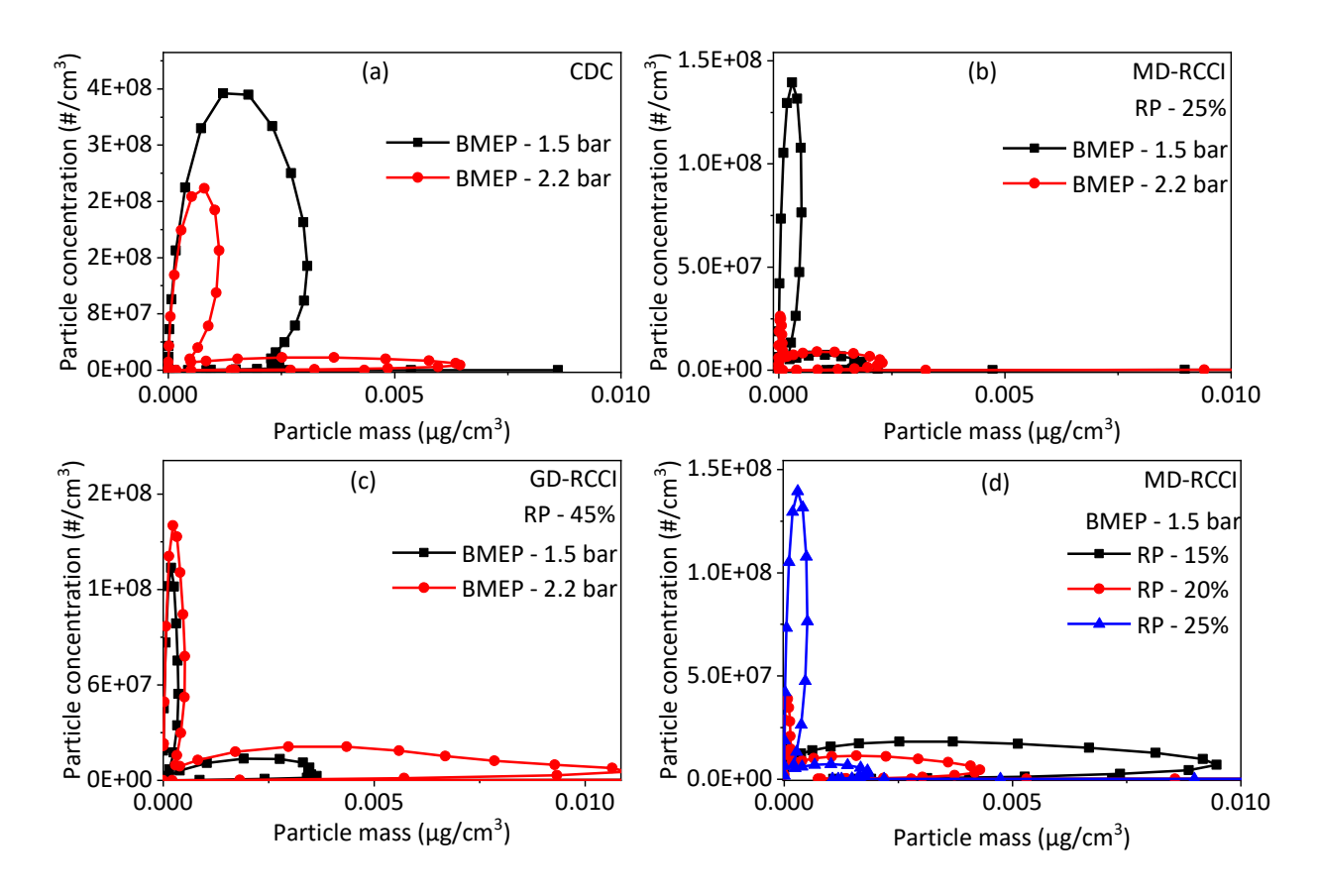


Figure 4.13: (a) Effect of engine load on Particle number and mass correlation in CDC, (b) Effect of engine load on Particle number and mass correlation in MD-RCCI (c) Effect of engine load on Particle number and mass correlation in GD-RCCI, and (d) Effect of premixing ratio (r_p) on Particle number and mass correlation in MD-RCCI.

4.3.3 Particulate visualization and morphology

The visual appearance of particulate matter (PM) provides an initial impression of engine exhaust emissions. An image of collected PM on sampled filter paper is presented in Figure 4.14. Scanning electron microscope (SEM) images were also taken to examine the morphology of aggregate PM samples (Figure 4.15). The results indicate that as the combustion mode shifts from CDC to MD-RCCI, the PM samples appear progressively whiter. This change is likely due to the reduced black carbon emissions from the RCCI engines. The low carbon content of methanol and the absence of diffusion combustion in RCCI combustion mode reduce the formation and emission of elemental or black carbon. As a result, the images appear whiter even at moderate engine load conditions.

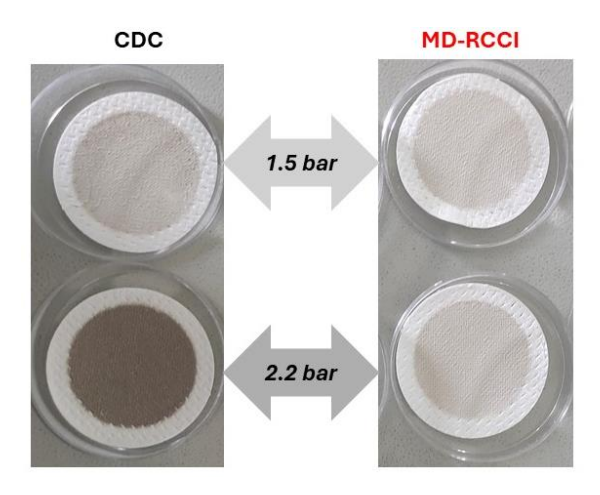


Figure 4.14: Images of sampled filter paper for CDC and MD-RCCI combustion mode.

The SEM images for all three combustion modes are presented in Figure 4.15. The results indicate that at a constant engine load, as the combustion mode shifts from CDC to RCCI, the particles attached to the filter fibers decrease in both size and number within a given area. The SEM images provide surface details but do not reveal information about the internal structure. It can be observed that in MD-RCCI mode, the emitted PM has the smallest size and a fluffier structure compared to GD-RCCI and CDC. This is primarily due to the higher organic fraction present in the PM samples, which results in a less defined and rigid structure of the PM particles emitted from RCCI combustion modes.

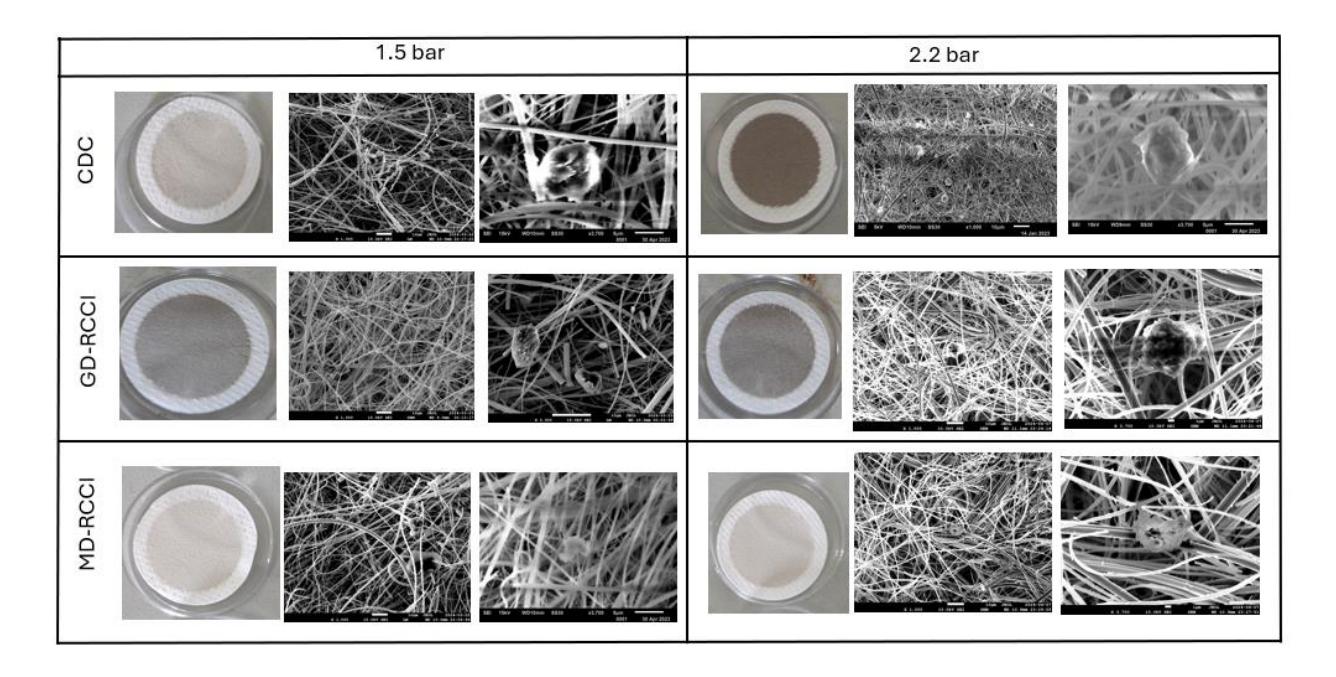


Figure 4.15: SEM images of PM samples from CDC,MD-RCCI and GD-RCCI at low and moderate engine loads

4.3.4 Heavy metal analysis

The sources of heavy metals in engines are multifaceted and can be traced to several key areas. Firstly, certain heavy metals are found in conventional fuels and may get directly inside the combustion chamber during fueling. Secondly, engine components such as valves, piston rings, and cylinder liners are manufactured using alloys containing heavy metals like chromium and nickel. Additionally, engine lubricants and additives introduce heavy metals into the combustion chamber, further contributing to emissions. The emission of heavy metals from engines depends on operating condition, fuel type and combustion modes. In the present study 16 metals have been detected. These metals are characterized as carcinogenic and non-carcinogenic metals emission based on their toxicity potential. The Na, Mg, Al, K, Ca, Mn, Fe, Cu, Zn, Ba are non-carcinogenic metals. Whereas, Cr, Co, Ni, As, Cd, Pb are carcinogenic metals.

The effect of combustion mode and engine load on the emission of trace metals is presented in figure 4.16 (a-d). The results demonstrate that at lower engine load, the emission of non-carcinogenic trace metals doesn't show a clear increasing or decreasing trend. Al and Zn emission is higher in CDC mode compared to RCCI combustion mode, whereas other trace metals are comparable (Figure 4.16 (a)). However, at medium engine load conditions, the trace metal emission decreases as the combustion mode shifts from CDC to RCCI combustion mode (Figure 4.16 (b)). This could be due to two main reasons: one is at a higher load, more fuel is injected, and dominating diffusion combustion leads to the emission of associated metals. On the other hand, the efficient combustion of RCCI leads to lower emissions of non-carcinogenic metals.

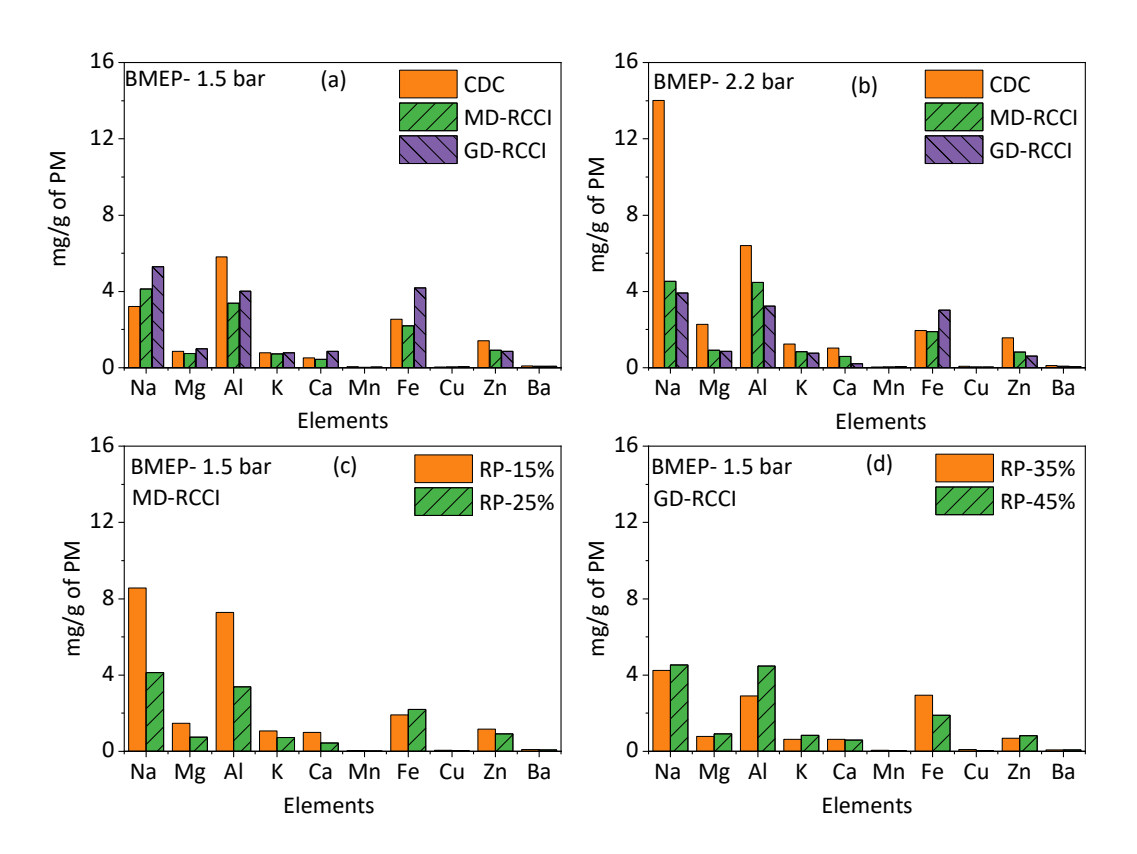


Figure 4.16 (a-d) Influence of combustion mode and engine load on the emission levels of noncarcinogenic trace metals

Figure 4.17 (a, b) shows the effect of combustion mode and engine load on carcinogenic metal trace emissions. The results show that as the combustion mode shifts from CDC to RCCI the emission of Ni, As and Cd emission decreases whereas Pb emission is comparable. As the engine load increases the Co emissions increase in MD-RCCI mode whereas other emissions are comparable in all combustion modes.

To further investigate the impact of RP on trace metal emission the results are presented in figure 4.16 (c, d) and 4.17 (c, d). The results demonstrate that for MD-RCCI combustion mode the Rp increases the metal trace emission of both carcinogenic and non-carcinogenic nature metals decreases. This decrease is due to the decrease in high reactivity fuel consumption. As the RP increases the injected mass of diesel decreases based on the energy input. Hence the metal emission associated with diesel fuel decreases. However, in the case of GD-RCCI engine it is observed that with an increase in RP the metal trace emission increases.

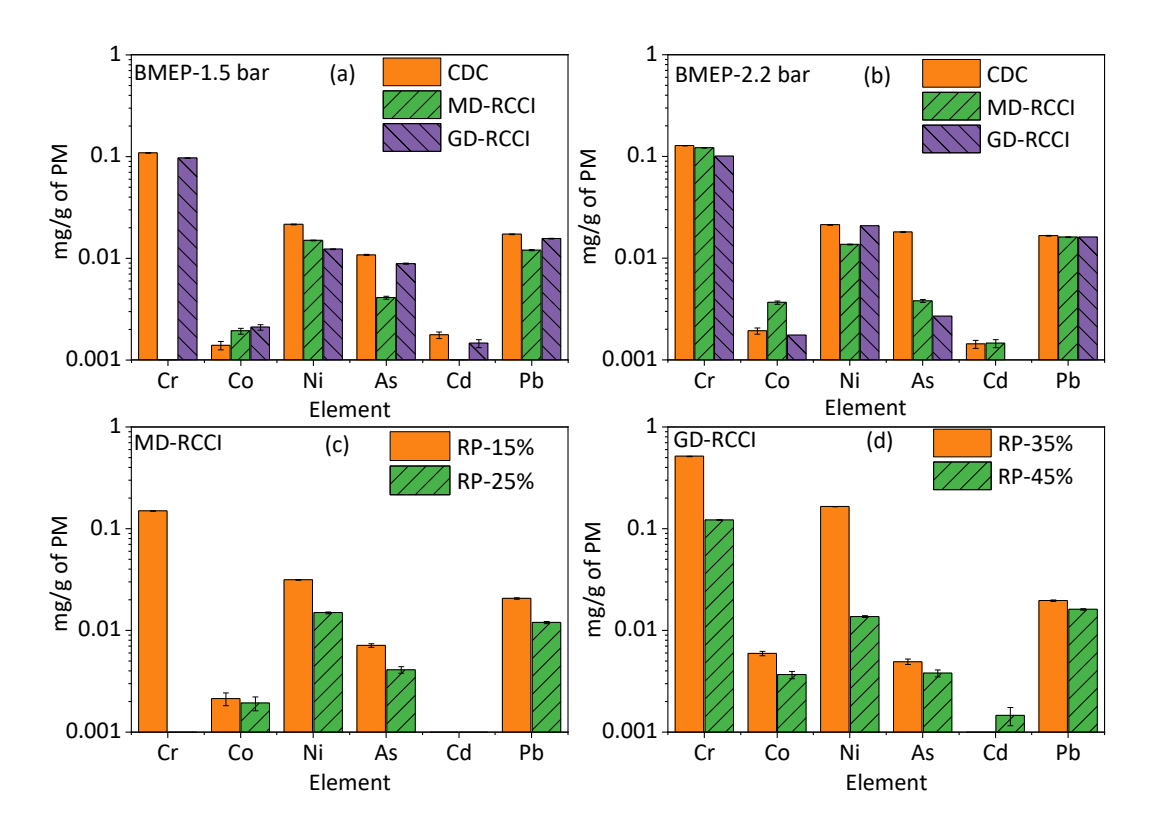


Figure: 4.17 (a-d) Influence of combustion mode and engine load on the emission levels of carcinogenic trace metals.

4.3.5 Soluble organic fraction analysis

The soluble organic fraction (SOF) of particulate matter (PM) samples was analyzed to determine their organic content, which was then used for lung loading calculations. Figure 4.18 (a) illustrates the impact of combustion mode and engine load on SOF. The results indicate that shifting from conventional diesel combustion (CDC) to reactivity-controlled compression ignition (RCCI) combustion mode leads to an increase in SOF. This rise in SOF is attributed to higher emissions of regulated and unregulated hydrocarbons (HCs). As discussed in the emissions section, the low-temperature combustion mode in RCCI engines results in increased HC emissions, and during the expansion stroke, some HCs may condense and be emitted as SOF. However, as engine load increases, SOF decreases. This is because higher engine loads increase the in-cylinder mean gas temperature, which promotes the oxidation of HCs, thereby reducing their emissions across all combustion modes. Figure 4.18 (b) demonstrates the effect of RP on SOF emissions. The results

show that increasing RP leads to higher SOF emissions from both GD-RCCI and MD-RCCI engines.

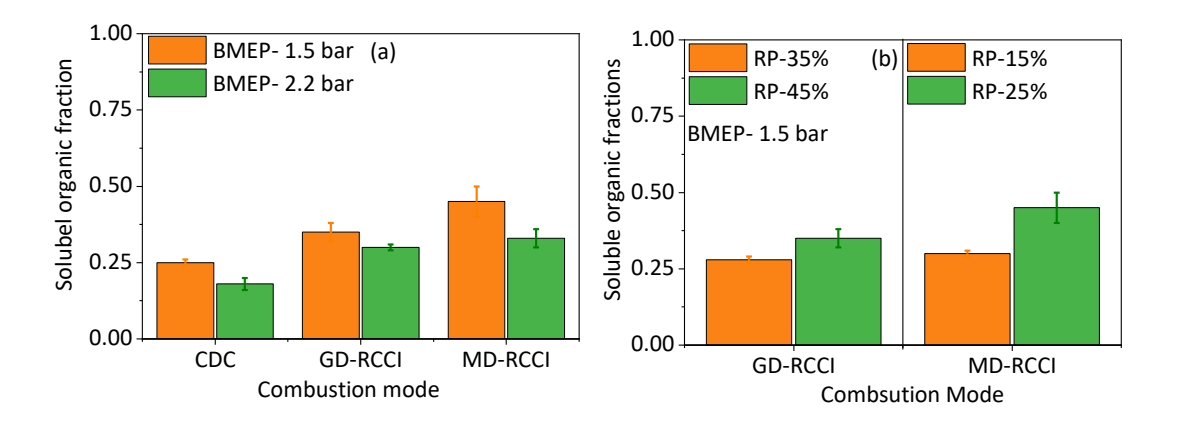


Figure: 4.18 (a, b) Influence of combustion mode, engine load and RP on the PM associated soluble organic fraction.

4.4 Toxicological characteristics and analysis

Exposure to particulate matter (PM) and gaseous emissions, both regulated and unregulated, can have negative effects on health. This section focuses on several specific aspects, including the cytotoxicity of PM, lung loading of PM particles due to inhalation and assessment of cancer risk associated with carbonyl and aromatic emissions.

4.4.1 Cytotoxicity and reactive oxygen species analysis

The primary purpose of cytotoxicity testing is to evaluate the potential harmful effects of substances on cellular health and viability. The cytotoxicity test is conducted on the human lung epithelial cell line (BEAS-2B). This cell line was chosen because the respiratory tract is lined with epithelial cells that form a barrier between the external environment and the internal tissues of the lungs and airways. These cells play a crucial role in gas exchange and mucociliary clearance. As exposure to PM happens through inhalation, the smaller particles take part in the gas exchange process, and hence, their chemical composition determines their toxicity.

The results depicting cell viability are illustrated in Figure 4.19 (a-d). Figure 4.19 (a) depicts the influence of load and combustion mode on PM cytotoxicity.

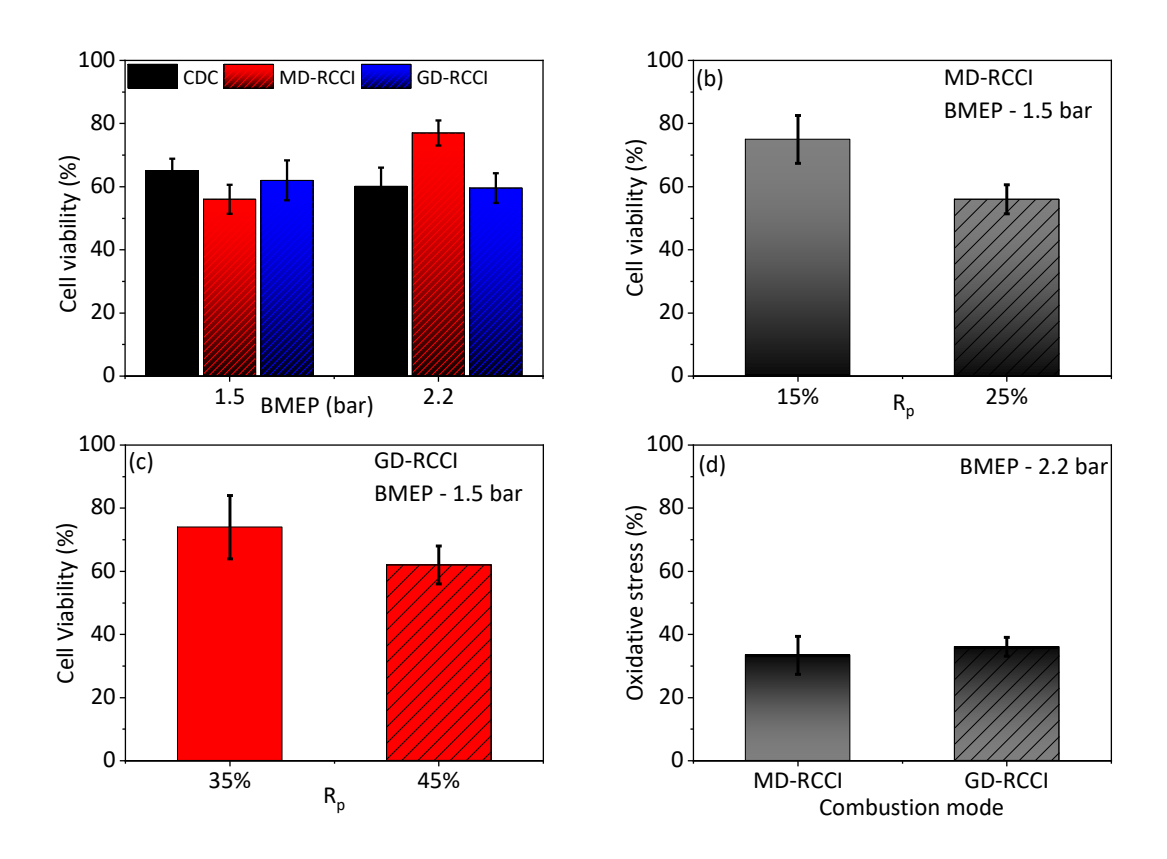


Figure 4.19: (a) Impact of load and combustion mode on cytotoxicity of PM emitted from RCCI engines, (b) Effect of Rp on cytotoxicity of PM emitted from MD-RCCI, (c) Influence of Rp on cytotoxicity of PM emitted from GD-RCCI and (d) Effect of combustion mode on oxidative stress induced by PM in cells.

The findings reveal that, at lower engine loads, PM emitted by MD-RCCI demonstrates a higher potential for cell toxicity compared to PM from the CDC and GD-RCCI engine. The elevated cell toxicity at lower engine loads may be attributed to aldehyde compounds formed during methanol combustion. However, with an increase in engine load from low to moderate conditions, the toxicity potential of PM from MD-RCCI significantly decreases. The decline in toxicity potential of PM from the MD-RCCI engine at moderate engine loads is ascribed to the more complete combustion process. This enhanced combustion, occurring at moderate engine loads, results in a reduced formation and emission of toxic components from the MD-RCCI engine. Conversely, at moderate engine loads, PM emitted by the CDC and GD-RCCI engine exhibits higher cytotoxicity potential compared to lower engine loads. To further investigate the impact of RP on the

cytotoxicity potential of emitted PM, samples are collected and tested for both GD-RCCI and MD-RCCI engines at two premixing ratios. As the engine load increases from low to moderate for CDC, the cytotoxicity potential increases significantly. This might be due to the increases in PAHs content in PM samples in the case of CDC. Several studies have shown that with an increase in engine load the PAHs emissions from diesel engine increases. The sources of PAHs in a diesel engine primarily stem from two pathways: fuel-bound PAHs and combustion-generated PAHs. As the engine load increases, the amount of fuel inside the combustion chamber also increases. Additionally, with the increase in diffusion combustion, more locally rich zones form. These rich zones lead to the formation of soot precursors due to pyrolysis, resulting in higher PAH formation at higher engine loads. Due to these combined phenomena the higher PAHs might be the reason for the increase in the cytotoxicity for CDC mode. Figure 4.19 (b, c) presents the effect of RP on cytotoxicity potential. The results demonstrate that, at a constant load, a rise in RP correlates with an increase in the cytotoxicity potential of PM. This increase may be attributed to the elevated emission of fuel-associated hydrocarbon (HC) compounds, as observed in the emission section, where an increase in RP led to a significant rise in total hydrocarbons (THC), carbonyl compounds, and aromatic hydrocarbons (AHC) emissions. Figure 4.19 (d) shows the oxidative stress induced in the cells due to the PM exposure from both combustion modes at medium engine load. The findings show that at medium engine load, the MD-RCCI-emitted PM shows lower oxidative stress development than GD-RCCI-emitted PM. As previously mentioned, at medium engine loads, the improved combustion of methanol takes place and hence leads to decreased formation of toxic compounds, resulting in reduced toxicity levels.

4.4.2 Cancer risk potential due to carbonyl and metal emissions

Figure 4.20 (a, b) shows the effect of combustion mode, engine load and RP on the cancer risk potential (CRP) associated with metal emissions. The results show that as the combustion mode shifts from CDC to RCCI mode, the CRP decreases at lower engine load for the RCCI combustion modes. However, as the engine load increased to moderate load conditions, the CRP increased for RCCI mode. This is because the carcinogenic metal emission increases for the RCCI mode as the engine load increases. The effect of RP on CRP of metal emission is presented in figure 4.20 (b); the results show that as the RP increases, the metal toxicity decreases for both combustion modes.

In MD-RCCI, as the RP increases, the mass of injected diesel decreases, and the metal emission decreases.

Figure 4.20 (c, d) presents the effect of combustion mode, engine load and RP on the cancer risk potential (CRP) associated with carbonyl emission (HCHO and CH₃CHO). The results show that as the combustion mode shifts from CDC to RCCI combustion, the CRP is higher for RCCI than for CDC. In CDC mode, the emission of carbonyl compounds is very low, and hence low CRP is observed. In the case of RCCI modes, the CRP decreases as the engine load increases; this decrease is due to a decrease in formaldehyde (HCHO) emissions. MD-RCCI shows the highest CRP compared to CDC and GD-RCCI combustion mode due to higher HCHO emissions. Figure 4.20 (d) demonstrates the effect of RP on the CRP; the result shows that for both RCCI combustion engines, with an increase in RP, the CRP increases due to the increases in carbonyl emissions, as discussed in the emission characteristics section.

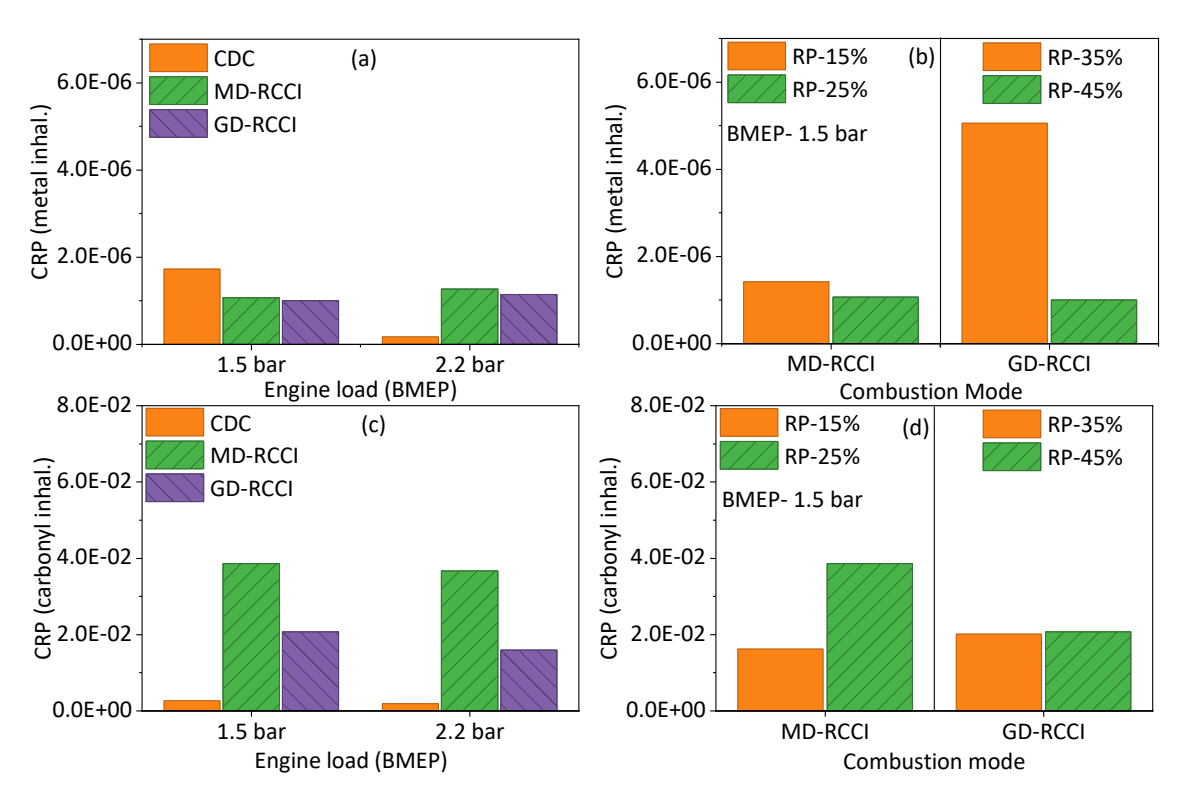


Figure: 4.20 (a-d) Influence of combustion mode, engine load and RP on the cancer risk potential associated with metal and carbonyl emission

4.4.3 Carcinogenic and mutagenic potential due to aromatic emission

Figure 4.21 (a, b) presents the total PAHs mass emission along with toxicity potential (TEQ and MEQ) for low and high engine load for hydrogen diesel dual fuel combustion engines. Figure 4.21 (a) depicts that at lower load an increase in the hydrogen energy share tends to increase the total PAHs mass emission. However, the decrease in carcinogenicity (TEQ) and mutagenicity (MEQ) potential is observed with an increase in the hydrogen energy share. The decrease in toxicity potential is due to the decrease in the PAHs mass emission containing high ring PAH such as B[a]P. As the hydrogen energy share increases, the B[a]P mass decreases. B[a]P has the highest toxicity equivalence factor and mutagenic equivalence factor which is 1.

The maximum decrease in toxicity potential is found for D90 H30. The mutagenicity potential (MEQ) is observed to be more than that of Carcinogenicity (TEQ) potential for all the cases. This is due to the difference in the calculation method of TEQ and MEQ. Figure 4.21 (b) indicates that with an increase in the load the toxicity potential increases for the neat diesel (D100) operation as compared to low load condition. The increase in toxicity potential at high loads is due to an increase in the emission of benzo[a]pyrene. However, with an increase in the hydrogen energy share for higher load, the emitted PAHs decreases along with decrease in toxicity potential. The MEQ and TEQ both are decreased along with mass of the emitted PAHs for higher engine load operation. At higher load, the complete combustion of hydrogen decreases the mass of PAHs emitted during combustion. It can be said that the replacement of carbon containing fuel (diesel) by hydrogen at higher engine load is a better way to decrease both the mass and the toxicity.

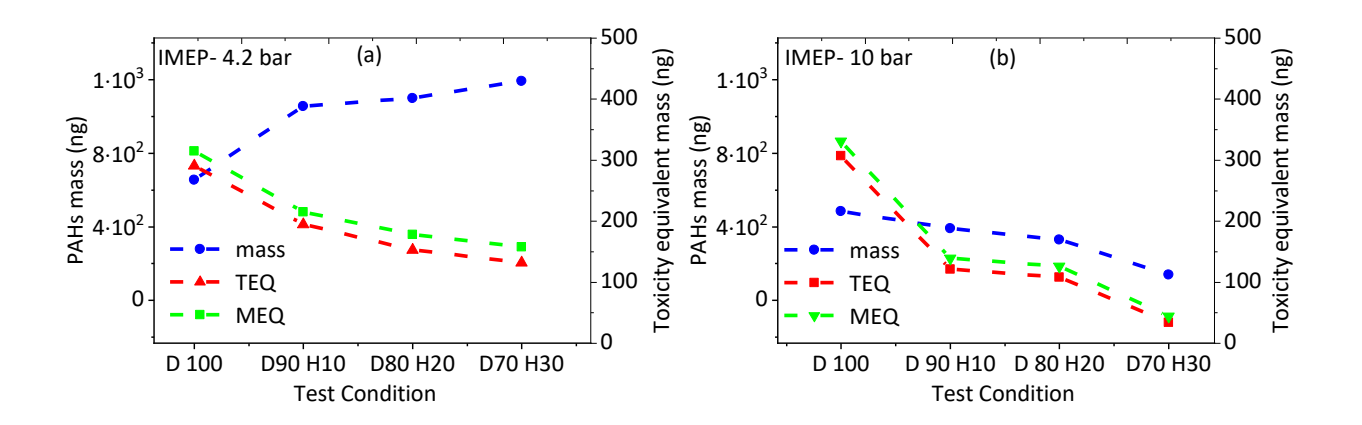


Figure: 4.21 (a, b) Influence of engine load and hydrogen energy share on the carcinogenicity and mutagenicity potential of PAHs emission.

4.4.5 PM particle lung retention analysis

The present section discusses the inhalation health risk of the emitted nanoparticles. In this section, the regional and overall lung retention for the nanoparticles emitted by CDC, GD-RCCI and MD-RCCI engines is discussed. The calculation is performed for the ultra-fine particle size range of 23 nm < dp < 500 nm.

Figure 4.22 (a-r) describes the lung retention load of nanoparticles emitted from CDC, GD-RCCI and MD-RCCI mode. In the plotted figures the x-axes represent the exposure time in years and y-axes represents lung loading. The results are presented separately for each, the carbonaceous fraction i.e., soot particles and the organic fraction such as absorbed SOF over the particulate. The fractional retention of the inhaled particles depends on the exposed concentration of the nanoparticle, chemical composition of the nanoparticles, tidal volume of the lung (TV), respiration frequency (RF) and deposition fraction (DF). However, the net lung loading of the inhaled particle is the difference between the rate of deposition and rate of clearance. Both deposition and clearance of the particle begin as soon as exposure to particles begins. The results shows that the lung load of the particles follows an exponential growth initially and then becomes stable. However, a difference is observed in the lung load for soot and SOF. The stable growth represents a condition when the rate of clearance becomes equal to the rate of deposition.

The impact of engine load on particle lung load is illustrated for the CDC mode in Figure 4.22 (a-f). The results show that as the engine load increases from 1.5 bar BMEP to 2.2 bar BMEP, the total lung load resulting from particle inhalation also increases (Figure 4.22 (a, b)). This increase is attributed to the increase in the mass of emitted particulate matter. As the engine load increases, a greater quantity of fuel is burned within the combustion chamber, leading to the formation of a larger amount of particulate matter. Furthermore, the diffusion combustion in CDC mode also contributes to the increase of particulate mass. To further investigate the deposition in individual lung compartments, the regional lung load resulting from the inhalation of particles is examined and illustrated in figure 4.22 (c-f). The regional lung compartment depicted includes the

tracheobronchial (Trac.) and alveolar (Alvo.) regions. As evident in Figure 4.22 (c-f), the particle loading in the tracheobronchial region is considerably lower when compared to the particle load in the alveolar region under both tested conditions. This can be attributed to the faster rate at which particles are cleared from the tracheobronchial region to other lung compartments compared to the clearance rate from the alveolar region to other compartments. This same reason also leads to the early saturation of soot mass in the tracheobronchial region with exposure time, occurring within a few months. Nevertheless, the highest retention is observed in the alveolar region at 2.2 bar BMEP. This is attributed to the slower rate of particle clearance from the alveolar region.

The influence of engine load on particle loading from GD-RCCI is illustrated in Figure 4.22 (g-1). The results exhibit a similar trend to engine load as observed in CDC mode. However, under all tested conditions, GD-RCCI particle inhalation shows lower total as well as regional lung loading compared to CDC mode (Figure 4.22 (g-l)). This is attributed to the lower particle emission concentration in GD-RCCI combustion mode as compared to CDC mode. The premixed combustion phase in GD-RCCI mode results in reduced particulate emissions, with the lowest lung load observed under low-load conditions. The lung load resulting from the inhalation of particles emitted by the MD-RCCI engine is depicted in Figure 4.22 (m-r). The results indicate that as engine load increases, both the regional and total lung load of particles decrease for the MD-RCCI engine. At a moderate engine load (2.2 bar BMEP), MD-RCCI exhibits superior combustion compared to the lower engine load (1.5 bar BMEP). At lower engine load, there is a higher emission of nanoparticles with smaller aerodynamic diameters (<100nm) compared to higher engine load. The deposition efficiency of smaller nanoparticles is higher than that of larger particles. Despite the increase in accumulation size range particles with higher engine load, the lung load decreases due to the increase in particle size. As the particle size increases, the deposition efficiency decreases. This result contrasts with CDC and GD-RCCI combustion modes. Additionally, the chemical properties of methanol significantly reduce particle formation compared to diesel and gasoline. The low carbon content and the presence of an additional oxygen atom in the methanol fuel molecule inhibit the formation of particulates inside the combustion chamber.

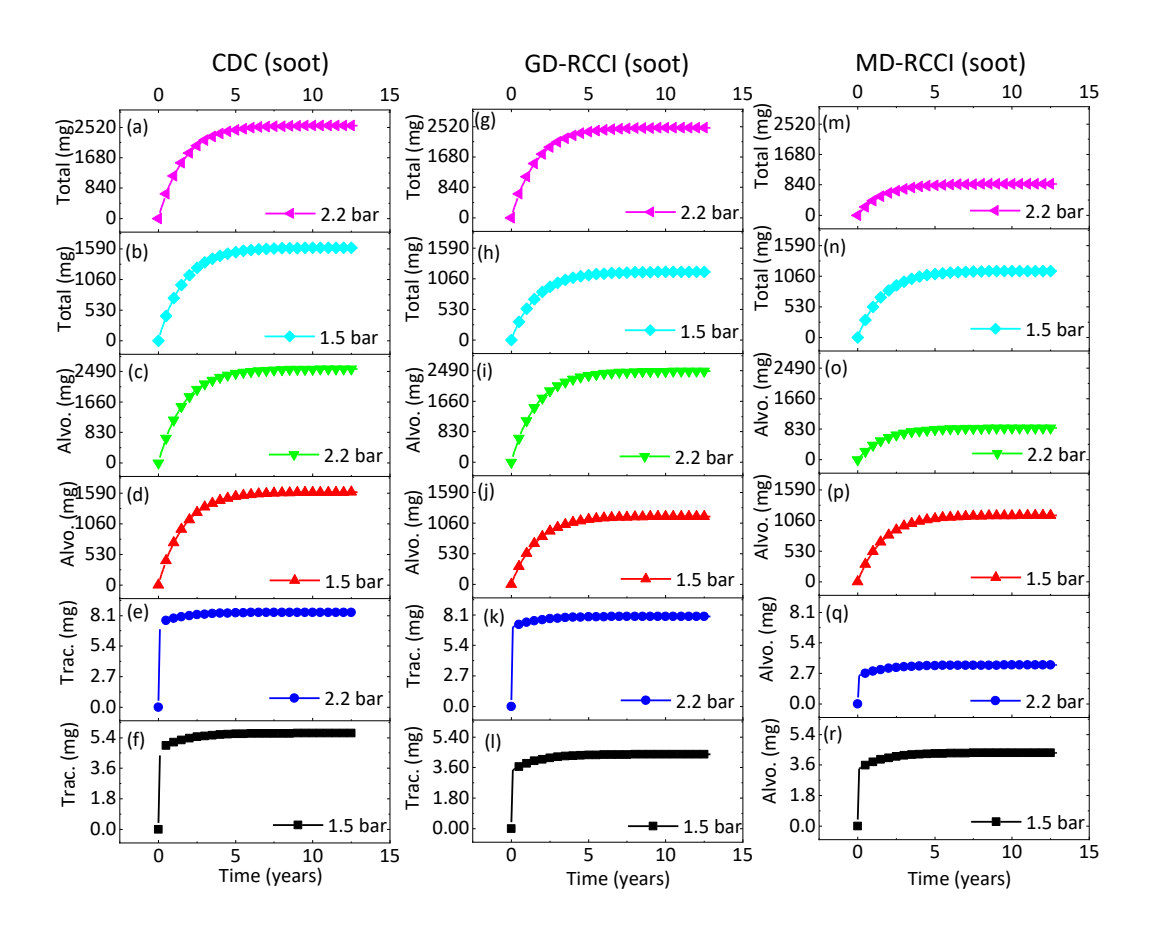


Figure 4.22: Effect of engine load on regional and total lung load due to the inhalation of soot nanoparticles emitted from CDC, GD-RCCI and MD-RCCI with respect to average concentration and an exposure time of 13 years.

The impact of engine load on the lung retention load of Soluble organic fraction (SOF) is illustrated for CDC mode in Figure 4.23 (a-f). The results demonstrate that as the engine load increases from 1.5 bar to 2.2 bar, the total lung load due to SOF particles increases (Figure 4.23 (a-b)). Even though the SOF fraction in the particulate decreases with increasing engine load, the lung loading due to SOF increases. This is because the total PM mass concentration increases. As the engine load increases, the net mass of particulate matter increases, resulting in an observed increase in SOF lung load. However, the saturation mass and saturation time are lower in the case of SOF. The lower saturation mass is attributed to the smaller fraction of organics absorbed over the surface of nanoparticles. The early saturation time is due to the high rate at which the organic fraction clears from the lung regions compared to the rate at which soot clears.

A similar trend is observed in SOF lung loading due to GD-RCCI engine-emitted particulates. However, in the case of MD-RCCI emissions, the SOF loading is comparable under all tested conditions. This is because the fraction of SOF is comparable in both tested conditions. In MD-RCCI mode the particle mass concentration with an increase in engine load decreased but the SOF loading is comparable since the fraction of SOF is higher at lower engine load that counterbalances the effect of particulate mass.

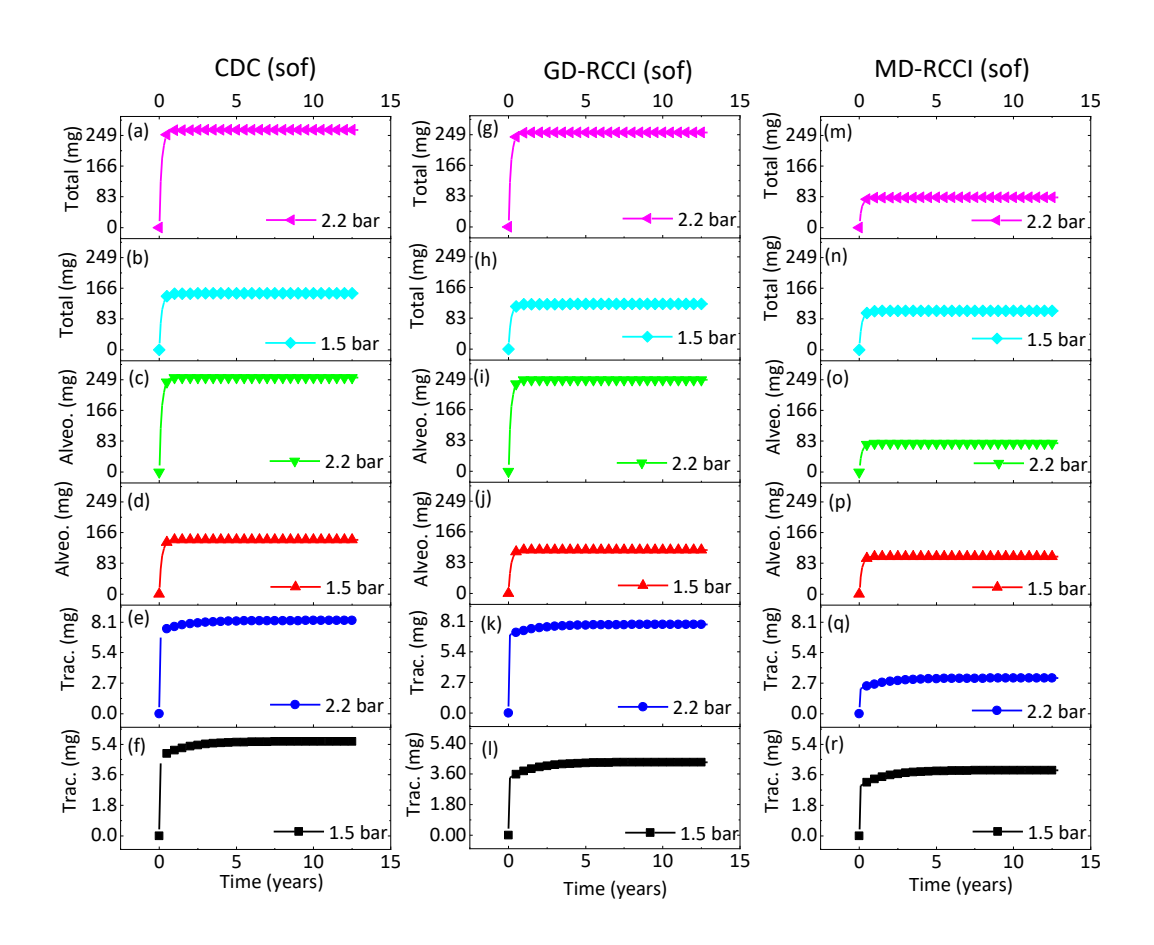


Figure 4.23: Effect of engine load on regional and total lung load due to the inhalation of soot nanoparticles emitted from CDC, GD-RCCI and MD-RCCI with respect to average concentration and an exposure time of 13 years.

To observe the impact of the fuel premixing ratio RP on lung loading resulting from GD-RCCI and MD-RCCI, identical calculations were executed, and the outcomes are illustrated in Figure 4.24 (a-l). The presented results correspond to a constant load of 1.5 bar BMEP. Two specifics r_p values were selected based on the conducted tests. The results show that with an increase in RP

the regional as well as total lung load decreases in both GD-RCCI and MD-RCCI engines. When, the RP is increased the TPN increases, however, the AMPs decreases. The decrease in the concentration of larger size particle decreases the overall mass concentration of the emitted particulates and hence the retention of particle mass decreases with an increase in RP. Figure 10 (a-f) presents the GD-RCCI emitted particle lung loading. At lower premixing ratios, the particle counts median diameter (CMD) decreases, but this reduction in CMD is significantly less pronounced than the decrease in mass concentration. Consequently, the influence of the lower particle diameter is suppressed by the impact of mass concentration. The growth rates of total lung load, alveolar lung load, and tracheobronchial lung load are depicted in Figure 4.24 (a, b), Figure 4.24 (c, d), and Figure 4.24 (e, f) respectively. Figure 4.24 (g-l) illustrates the impact of rp on particle lung load in MD-RCCI mode. The results exhibit a similar trend to that observed in GD-RCCI.

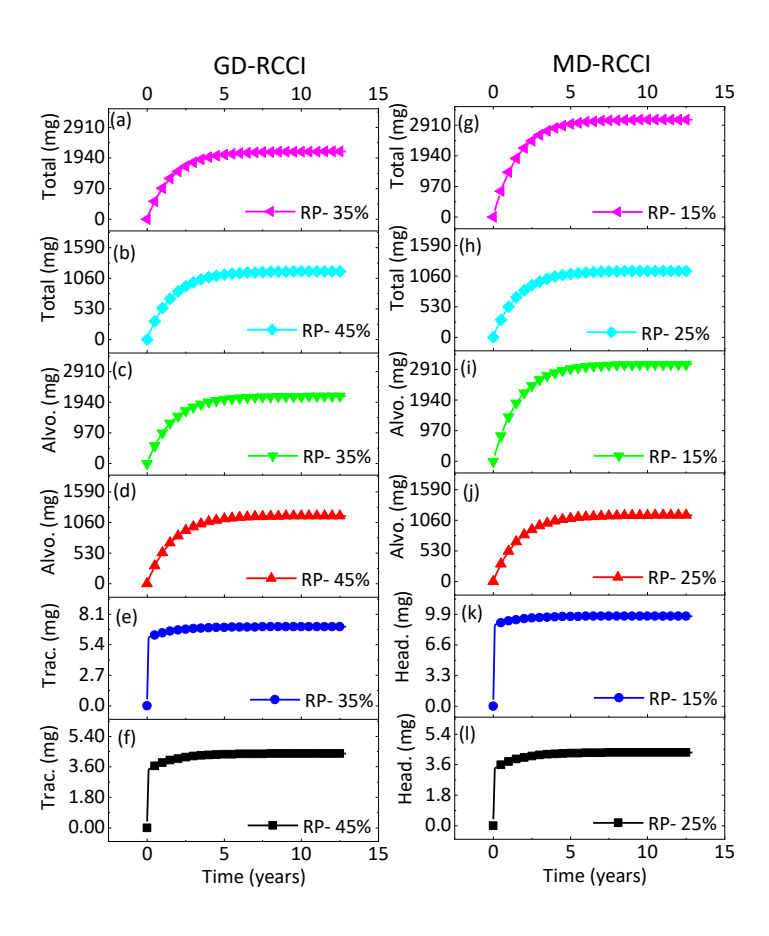


Figure 4.24: Effect of premixing ratio (RP) on regional and total lung load for GD/MD -RCCI engine

In order to comprehend the impact of particle diameter within each size range on regional lung loading, the relationship between regional lung loading and particle diameter is graphically represented in figure 4.25 (a-i). The x-axes display particle diameter, while the y-axes depict regional lung load. The results are presented for a constant load of 1.5 bar bmep. The tracheobronchial, alveolar and head region lung load for CDC with particle diameter is presented in the figure 4.25 (a-c). Figure 4.25 (c) presents the head region loading of particle. The deposition in head region only occurs when the diameter of particle is greater than 200 nm keeping respiratory frequency and tidal volume constant [9]. This is the reason of plotting the head region loading only beyond the 200 nm diameter particles. As it is already discussed that the regional lung loading depends on both particle diameter and concentration. The head region load doesn't show a clear increasing or decreasing trend because both the concentration and particle diameter are variables. The highest head region load is observed for a particle diameter of 200 nm for CDC mode. Among all the combustion modes the highest head load is observed for particle having diameter 500 nm for MD-RCCI mode (figure 4.25 (i)). The tracheobronchial and alveolar lung load with particle diameter for CDC is presented in the figure 4.25 (a & b). The findings reveal that the lung loading of particles across various lung compartments, based on their diameter, aligns with the particle distribution trend observed in CDC mode. As depicted in Figure 4.25 (a, b), it is evident that the regional lung loading attributed to smaller-sized particles surpasses that of larger-sized particles. This phenomenon is attributed to the increased concentration of smaller-sized particles. The smaller size particles also have higher deposition efficiency. A smaller particle size and elevated concentration, both factors contribute to increased regional lung loading of smaller particles. Across all lung compartments, the highest lung load for particles smaller than 100 nm is evident in CDC mode, in comparison to GD-RCCI and MD-RCCI modes. Nevertheless, as the particle diameter increases, the observed lung load for the GD-RCCI engine surpasses that of other combustion modes. This rise is attributed to the increased concentration of particles within that size range in the GD-RCCI engine. Conversely, the lung load for the MD-RCCI engine remains the lowest among all combustion modes.

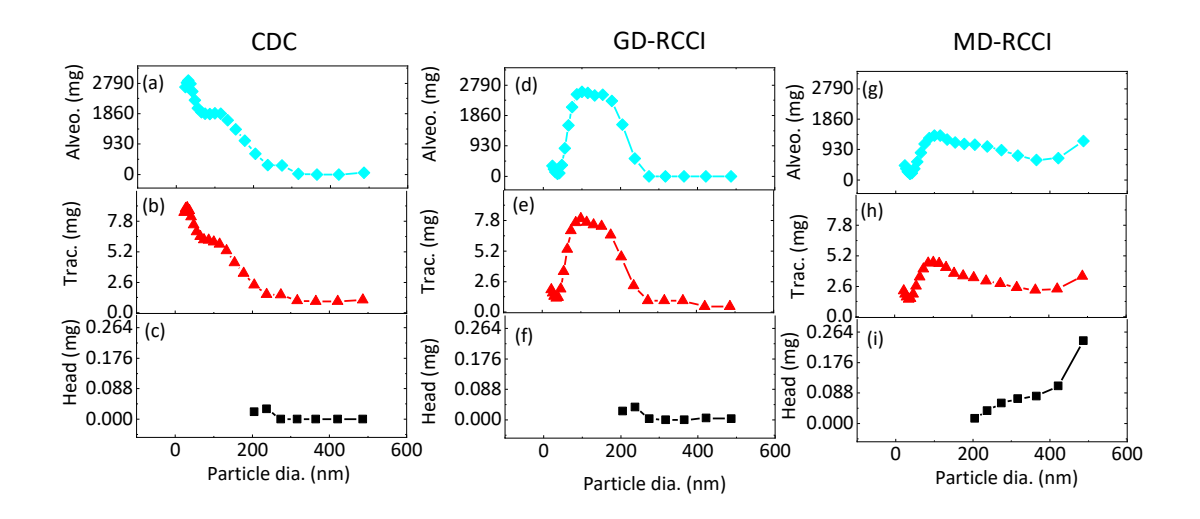


Figure 4.25: Regional lung loading with respect to particle diameter for CDC GD-RCCI and MD-RCCI engine.

To explore the effect of RP on regional lung loading with particle size, the regional loading at different RP is calculated and presented in figure 4.26 (a-l) for both GD-RCCI and MD-RCCI mode. The presented result is for the test conducted at constant engine load (1.5 bar) and varied RP. The results demonstrate that as the RP increases the overall regional lung load decreases for all diameter for both combustion modes. The highest regional lung load is onserved for lower premixing ratio for both combustion modes. As the premixing ratio increases the mass particle concentration decreases and hence the lung loading decreases. However, at lower RP the mass of diesel is more in the combustion chamber as compared to methanol and hence more rich zones are available in the combustion chamber which increases the mass concentration. The lowest regional lung load for tracheobronchial and alveoli is observed for MD-RCCI with RP -25%. The regional deposition if particles with particle diameter shows the similar trend that of particle mass distribution.

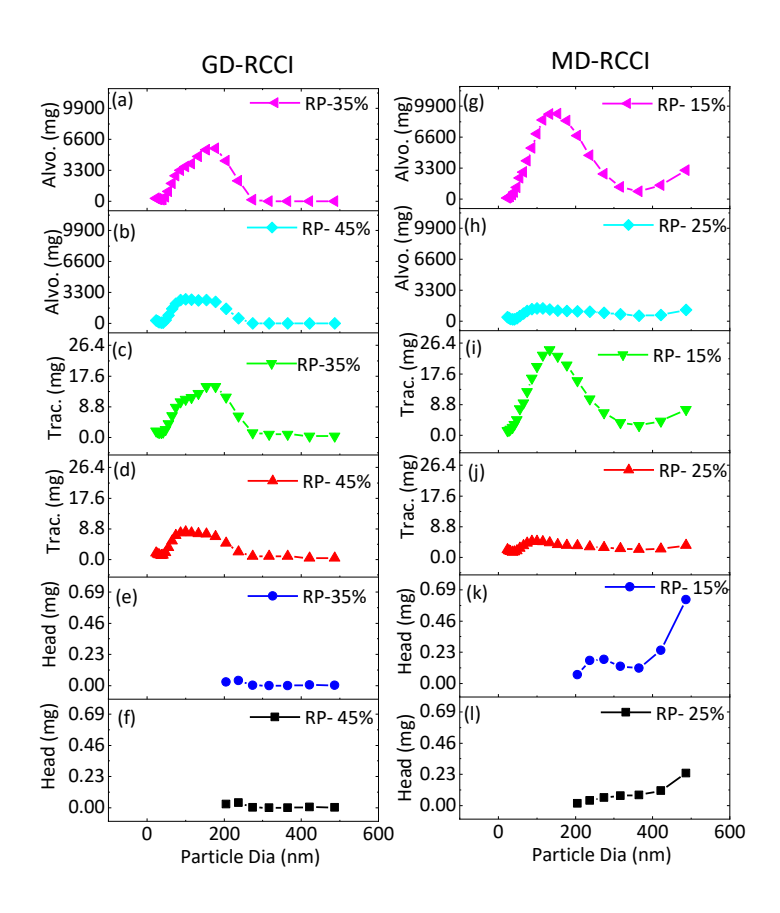


Figure 4.26: Regional lung loading with respect to particle diameter at different premixing ratio (RP) for MD-RCCI engine.

4.5 Environmental risk assessment

In this section, the influence of engine load and PMR on the potential environmental and health risks associated with regulated and unregulated emissions from CDC, GD-RCCI and MD-RCCI is discussed. To understand the impact on the environment of the emissions, global warming potential (GWP), acidification potential (ACP), Eutrophication potential (EP) and ozone forming potential (OFP) are calculated and presented. The effect of combustion mode and engine load on GWP, ACP, EP and OFP is presented in figure 4.26 (a-d).

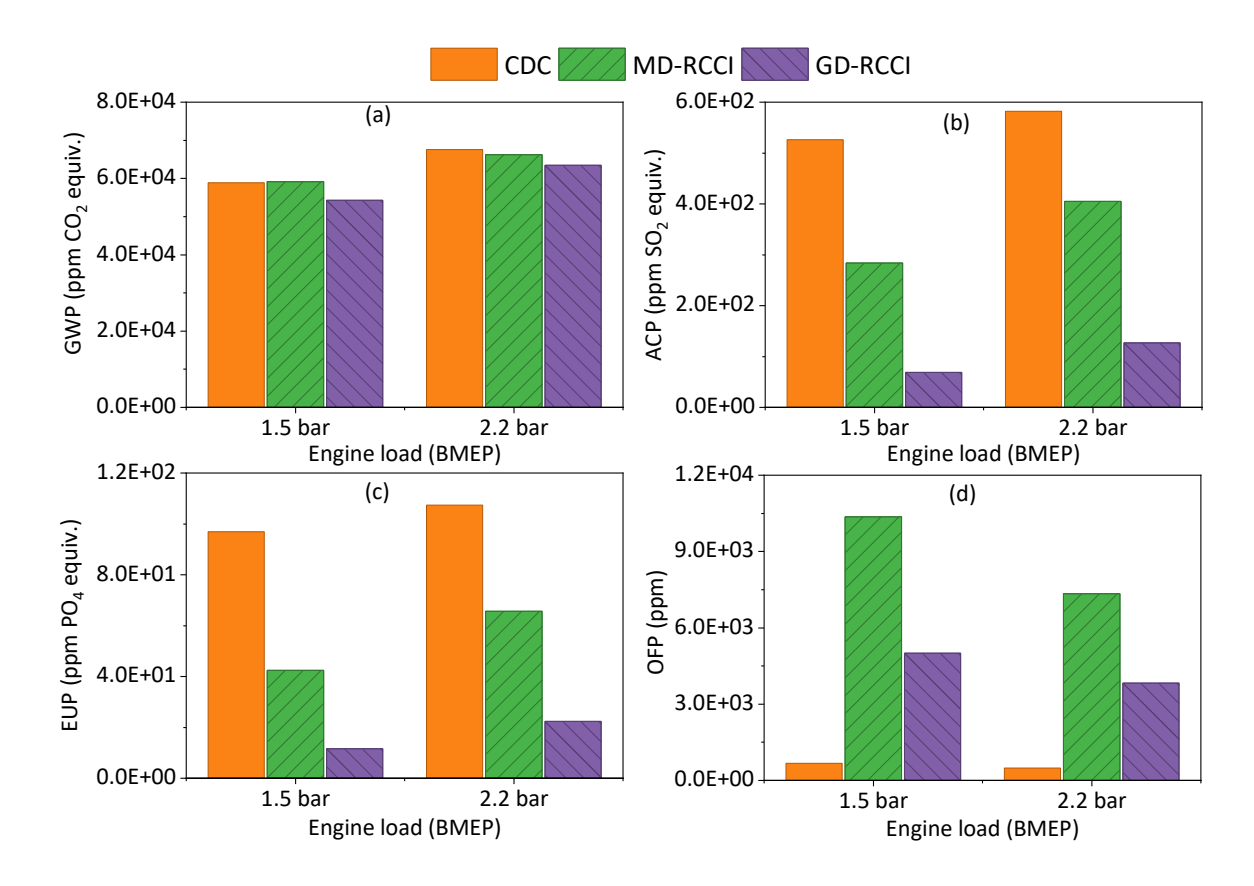


Figure 4.27 (a-d): Effect of combustion mode and engine load on environmental risk markers.

Figure 4.26 (a) presents the GWP of the emitted gaseous emission. The GWP is expressed in CO₂ equivalent, which represents the collective impact of emitted emissions in terms of CO₂. The GWP calculation in the present study includes gas components such as CO₂, CO, NOx, N₂O, and CH₄. Each gas's concentration is multiplied by its respective GWP relative to CO₂, as described in the methodology section. The numerical value of GWP indicates its environmental impact; larger values indicate more detrimental effects on the environment. The results depict that as the engine combustion mode shifts from CDC to RCCI the GWP potential decreases for GD-RCCI and slightly increases for MD-RCCI compared to CDC.

The GWP emission increases in all three combustion modes at moderate engine load. The increase in engine load increases the amount of diesel inside the combustion chamber which leads to an increase in GWP. At medium load condition the MD-RCCI shows lower GWP emission as compared to the CDC. This is due to the introduction of methanol and lower combustion temperature inside the combustion chamber. The addition of methanol decreases the carbon content of the fuel which decreases the CO₂ emission and the lower in cylinder combustion

temperature decreases the NO_x and N_2O formation. Among all the gas components the highest GWP is N_2O . However, at low load condition (1.5 bar BMEP), the MD-RCCI exhibits slightly higher GWP as compared to CDC, that is because of higher CO and CH₄ emission of MD-RCCI at lower load. The GD-RCCI combustion mode emits lower GWP emissions compared to both CDC and GD-RCCI. This is because the GD-RCCI has the lowest NOx emission.

Figure 4.26 (b) presents the effect of combustion mode and engine load on ACP emissions from the CDC, GD-RCCI and MD-RCCI. The ACP physically signifies the compounds that are precursors to acid rain. The larger value of ACP means the negative impact on environment. The gas components used in the ACP calculation in the present study are: SO₂, NH₃ and NO_x. The results demonstrate that as the combustion mode shifts from CDC to RCCI the ACP emissions decrease significantly at both engine load conditions.

As the engine load increases, the ACP increases for all three combustion modes. This increase in ACP is primarily due to higher NOx emissions. Although the RCCI emits higher unregulated emissions its ACP is lower than CDC. This is because the impact of NO_x, with its higher concentration, outweighs the effects of other gas components in CDC.

The effect of engine load on EP is presented in figure 4.26 (c). The EP physically signifies the potential of the compound to enrich the soil and water nutrients by increasing the nitrogen level. The EP is detrimental to the environment because the increase in EP increases the growth of algae and other aquatic plants, the rapid growth of algae in water bodies creates a dense mat like structure over the water body which block the direct sun light to lower levels of water. Furthermore, when these algae's dies and decompose, they use up the oxygen of the water and decrease the life span of aquatic organisms. The results depict that with an increase in engine load from low to medium load the EP increases. The increase in EP is due to the increase in NO_x emission. As compared to CDC the MD-RCCI and GD-RCCI show lower EP at both the tested load as NOx emission is very low in RCCI.

Figure 4.26 (d) presents the effect of engine load on OFP from CDC, MD-RCCI and GD-RCCI. The gas components used in OFP calculation are: CH₄, C₂H₆, C₃H₆, C₂H₂, C₇H₈, CH₃OH, HCHO, CH₃CHO, C₅H₁₂. The results show that with an increase in engine load the OFP decreases for all three combustion modes. The decrease in OFP is mainly because the emission of unregulated HCs decreases with engine load. The MD-RCCI shows higher OFP as compared to CDC and GD-RCCI

at both loads. The main reason for this observation is in MD-RCCI engine the emission of the above-mentioned gas components is significantly higher than CDC and GD-RCCI. The lower incylinder combustion temperature suppresses the rate of oxidation of these species and the unoxidized species emitted and increases the OFP.

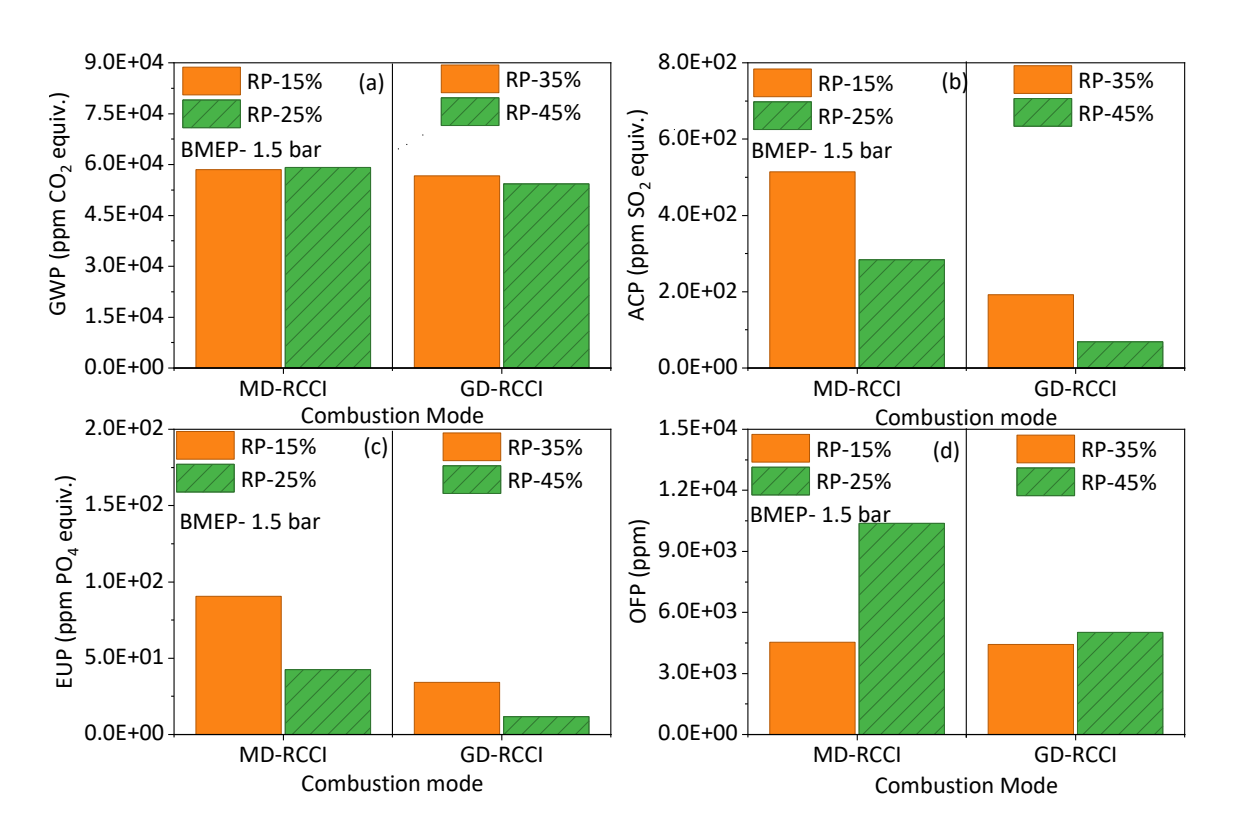


Figure 4.28: Effect of RP environmental risk markers from MD-RCCI and GD-RCCI engines.

To further explore the MD-RCCI related emission effect on GWP, ACP, EP and OFP. The effect of RP is plotted and presented in figure 4.27 (a-d). Figure 4.27 (a) presents the effect of RP on GWP, at a constant engine load 1.5 bar BMEP. The result indicates that with an increase in RP the GWP increases for MD-RCCI and decreases for GD-RCCI. As the RP increases the GWP increases because of increased emission of CO and higher GWP associated HCs in MD-RCCI. At higher RP, the delayed combustion phasing and lower in-cylinder combustion temperature led to increased emissions of GWP-contributing gas components. It's noteworthy that despite the replacement of injected diesel with methanol, the GWP rises due to the impact of other emissions on the overall

GWP value. In the case of GD-RCCI the GWP decreases with an increase in RP due to lower emission of NOx along with other HCs compared to MD-RCCI engines. Figure 4.27 (b) shows the effect of RP on ACP, and the findings reveal a significant decrease in ACP potential with an increase in RP for both MD-RCCI and GD-RCCI engines. The reason behind this trend is the substantial reduction in NOx emissions as RP increases. While there is an increase in unregulated emissions with an increase in RP, the lower concentration of NOx outweighs their effect, thereby suppressing the overall acidification potential as RP increases. The effect of RP on EP is presented in figure 4.27 (c), the result shows that with an increase in RP, the EP decreases significantly, the decrease in NOx emission led to significant decrease in EP. The effect of RP on the OFP is presented the figure 4.27 (d), with an increase in PMR increases the OFP. The increase in RP results increases in the emission of CH₄, C₂H₆, C₃H₆, C₂H₂, C₇H₈, CH₃OH, HCHO, CH₃CHO, C₅H₁₂ and hence OFP increases significantly.

Chapter 5

Conclusions and Future Scope

In the present thesis a detailed experimental study was conducted on three modes of engine operation: gasoline-diesel RCCI, methanol-diesel RCCI, and conventional diesel combustion (CDC). The investigation focused on combustion characteristics, regulated and unregulated emissions, physico-chemical properties of particulate matter, toxicological effects, and environmental risks associated with these methods. Additionally, a CFD model of a heavy-duty engine was developed to study hydrogen-diesel dual-fuel combustion, which was then compared with conventional diesel combustion. The present chapter summarizes the conclusions drawn from this thesis work. This chapter also discusses the implications of the present work for the industry, working professionals, and society, as well as future research directions. This chapter is divided into subsections namely regulated and unregulated emission characteristics, physicochemical characteristics of PM and toxicological characteristics of engine emissions to segregate and summarize the major findings.

5.1 Regulated and unregulated emission characteristics

This section summarizes the key findings on regulated and unregulated emissions. Regulated emissions include hydrocarbons (HC), carbon monoxide (CO), nitrogen oxides (NOx), and particulate matter (PM). Unregulated emissions encompass saturated and unsaturated hydrocarbons, carbonyl compounds, and aromatic (toluene) compounds. The main findings are as follows:

- The engine load and fuel premixing ratio (RP) greatly influences the combustion characteristics which further affects formation and emission of regulated and unregulated emission from CDC, MD-RCCI and GD-RCCI engines.
- As the combustion mode transitions from CDC to RCCI under all tested conditions, NOx
 emissions decrease significantly. Under certain conditions the decrease in NOx is up to
 90%. Furthermore, as the RP increases at a constant load, NOx emissions decrease even
 more.

- As the combustion mode transitions from CDC to RCCI, the emissions of THC and CO increase significantly. However, with an increase in engine load, these emissions decrease but remain higher than in the CDC mode.
- The emissions of saturated, unsaturated, carbonyl, and aromatic (toluene) compounds increase with an increase in RP in both RCCI modes. These emissions are significantly higher at lower engine load operations. However, as the engine load increases, a decrease in these emissions is observed.
- Among carbonyl emissions the formaldehyde emissions are highest in the MD-RCCI combustion mode among all three modes, suggesting that methanol addition leads to increased formaldehyde emissions.

5.2 Physicochemical characteristics of PM

This section summarizes the physicochemical characteristics of particulate matter (PM) emissions. The physical characteristics include PM nanoparticle size distribution, mass distribution, and number concentration. Additionally, the visual appearance of PM and findings from scanning electron microscopy (SEM) analysis are summarized. The chemical characterization includes the soluble organic fraction (SOF), and the traces of heavy metals present in the PM samples. The major findings are as follows,

- Under all tested conditions, the methanol-diesel reactivity-controlled compression ignition (MD-RCCI) combustion mode emits lower nanoparticles than the conventional diesel combustion (CDC) and gasoline diesel (GD) RCCI modes. MD-RCCI reduces total particle number (TPN) emissions by up to 60% compared to CDC.
- The emission of nucleation mode particles (NMPs) is more prominent at lower engine loads
 in all three combustion modes. The emission of NMPs from the MD/GD-RCCI engine
 increased with an increase in premixing ratio (RP) and decreased with an increase in engine
 load.
- The analysis of particle concentration and mass correlation suggests that the mass of particle emissions is mainly due to accumulation mode particles, whereas the particle

number concentration is related to nucleation mode particles. The mass-number correlation lobe for MD-RCCI is the smallest compared to GD-RCCI and CDC modes, indicating lower mass and number emissions.

- Under moderate load conditions, the PM samples collected on filter paper for MD-RCCI
 appear brighter and slightly yellowish, whereas in the case of CDC, they appear black in
 color.
- Under all tested conditions, the SEM images of PM samples collected on filters for MD-RCCI show the lowest particle attachment per area compared to CDC and GD-RCCI.
- The soluble organic fraction (SOF) in PM samples increases in the following order: lowest in CDC, followed by GD-RCCI, and highest in MD-RCCI. However, as engine load increases, the SOF content in PM samples decreases for all three combustion modes.
- As the combustion mode transition from CDC to RCCI, the metal traces CDC to RCCI the
 emission of Ni, As and Cd (carcinogenic metals) emissions decreases under all the tested
 conditions.
- Heavy metal trace emission from MD-RCCI engines is lower than GD-RCCI engines at lower engine load operation. Additionally, with an increase in RP the metal emission decreases significantly in MD-RCCI engine.

5.3 Toxicological characteristics of emissions

Toxicological characteristics are focused on analytical and experimental toxicity evaluation of PM and gas phase emissions. The analytical toxicity evaluation includes the lung retention of nanoparticles due to inhalation and calculation of cancer risk potential of carbonyl and metal compounds using USEPA guidelines. The experimental toxicity evaluations include the in-vitro cytotoxicity and reactive oxygen species (ROS) imbalance. The major finding of toxicological characteristics are as follows:

• The Methanol-diesel RCCI engine shows lower inhaled nanoparticle lung retention than GD-RCCI and CDC under all the test conditions. As engine load increases (medium) at the constant premixing ratio (RP), GD-RCCI exhibits increased lung retention, while methanol-diesel RCCI engines show decreased retention, which suggests reduced health risks associated with particle inhalation.

- Engine load and RP significantly influence the cytotoxicity of PM samples. At medium
 engine load, the methanol-diesel RCCI emitted PM has lower cytotoxicity potential than
 gasoline-diesel RCCI and CDC. Meanwhile, at lower engine load, with an increase in
 premixing ratio, the cytotoxicity of PM increases in both RCCI engines.
- Improved combustion of methanol at medium engine loads leads to reduced cytotoxicity, particle inhalation toxicity, and ozone-forming potential, emphasizing the importance of methanol combustion in mitigating emission toxicity.
- The highest cancer risk potential is observed for MD-RCCI engines at lower engine load compared to CDC and GD-RCCI engines due to the higher emission of formaldehyde emissions.
- In the case of simulation study, the predicted PAHs caused mutagenicity and carcinogenicity potential significantly decreases as the hydrogen energy share increases in diesel engine under all the simulated conditions.

5.4 Environmental risk assessment of emissions

This section summarizes the environmental risk assessment conducted to quantify the adverse effects on the environment. The environmental risk assessment markers include global warming potential (GWP), acidification potential (ACP), eutrophication potential (EP) and ozone forming potential (OFP) equivalent emissions. The major findings are as follows,

- As the combustion mode shifts from CDC to RCCI, the global warming potential, acidification potential, eutrophication potential decreases significantly under moderate load condition. However, an increase in ozone forming potential is observed.
- Increase in RP in RCCI combustion mode leads to increase in the ozone forming potential and global warming potential due to increase in carbonyl emissions along with the unsaturated hydrocarbon emissions.
- As the RP increases in RCCI combustion mode, the acidification and eutrophication potential decreases significantly due to lower emissions of nitrogen-containing compounds.

5.5 Societal implications of the present work

The present research outcome will impact public health and the environment by providing a detailed assessment of the cytotoxicity, cancer risk potential, lung retention due to inhalation of nanoparticles, global warming potential, acidification potential, eutrophication potential, and ozone-forming potential associated with engine emission pollutants based on their physical and chemical properties. The results of the present investigation can be used by government bodies and policymakers to establish emission norms for advanced combustion engines using methanol as an alternative fuel. This study can assist chemical industrialists in developing catalytic converters for advanced combustion engines to mitigate the toxicity of formaldehyde and acetaldehyde emissions. Practicing engineers in interdisciplinary field can understand the reasons of the formation of different pollutants and can take measures to avoid the formation by designing the appropriate combustion systems for advanced combustion engines. Furthermore, it can help public representatives make informed decisions in the best interests of the people.

5.6 Future directions for research

- Further research is needed to elucidate the underlying mechanisms driving toxicity variations with fuel composition and engine operation parameters, facilitating the development of effective strategies to minimize emission toxicity and mitigate associated environmental and health risks.
- The development of a dedicated exhaust after-treatment system for the RCCI combustion mode is necessary to reduce the adverse impact on human health and the environment due to higher emissions of unregulated pollutants.
- Future research can focus on integrating advanced combustion modes into hybrid vehicles
 and conducting a lifecycle analysis to minimize the overall impact of these new
 technologies on human health and the environment.
- Future research into methanol as a fuel could play a key role in decarbonizing hard-toelectrify systems, such as marine transportation, by providing a viable alternative to conventional fossil fuels in future marine engines.

Chapter 6: References

- [1.1] Acheampong, A. O., Dzator, J., Dzator, M., & Salim, R. (2022). Unveiling the effect of transport infrastructure and technological innovation on economic growth, energy consumption and CO2 emissions. *Technological Forecasting and Social Change*, 182, 121843. https://doi.org/10.1016/j.techfore.2022.121843
- [1.2] Colvile, R. N., Hutchinson, E. J., Mindell, J. S., & Warren, R. F. (2001). The transport sector as a source of air pollution. *Atmospheric environment*, 35(9), 1537-1565. https://doi.org/10.1016/S1352-2310(00)00551-3
- [1.3] Ferguson, C. R., & Kirkpatrick, A. T. (2015). *Internal combustion engines: applied thermosciences*. John Wiley & Sons.
- [1.4] https://www.epa.gov/criteria-air-pollutants

- [1.5] International Transport Forum / OECD 2024. https://www.itf-oecd.org/worldwide-transport-activity-double-emissions-rise-further
- [1.6] Kalghatgi, G. T. (2015). Developments in internal combustion engines and implications for combustion science and future transport fuels. Proceedings of the Combustion Institute, 35(1), 101-115.
- [1.7] Kalghatgi, G. (2018). Is it really the end of internal combustion engines and petroleum in transport? Applied energy, 225, 965-974.
- [1.8] Kalghatgi, G. (2013). Fuel/engine interactions. SAE international.
- [1.9] Schiffer, H. W., Kober, T., & Panos, E. (2018). World energy council's global energy scenarios to 2060. Zeitschrift für Energiewirtschaft, 42(2), 91-102.
- [1.10] Frei, C., & General, S. (2011). Global transport scenarios 2050. World Energy Council: London, UK.
- [1.11] Reitz, R. D., Ogawa, H., Payri, R., Fansler, T., Kokjohn, S., Moriyoshi, Y., ... & Zhao, H. (2020). IJER editorial: The future of the internal combustion engine. International Journal of Engine Research, 21(1), 3-10
- [1.12] Agarwal, A. K., Singh, A. P., García, A., & Monsalve-Serrano, J. (2022). Challenges and Opportunities for Application of Reactivity-Controlled Compression Ignition Combustion in Commercially Viable Transport Engines. Progress in Energy and Combustion Science, 93, 101028
- [1.13] Paykani, A., Garcia, A., Shahbakhti, M., Rahnama, P., & Reitz, R. D. (2021). Reactivity controlled compression ignition engine: Pathways towards commercial viability. Applied Energy, 282, 116174.
- [1.14] Sharma, I., & Chandel, M. K. (2020). Will electric vehicles (Evs) be less polluting than conventional automobiles under Indian city conditions? Case Studies on Transport Policy, 8(4), 1489-1503
- [1.15] Nimesh, V., Sharma, D., Reddy, V. M., & Goswami, A. K. (2020). Implication viability assessment of shift to electric vehicles for present power generation scenario of India. Energy, 195, 116976.
- [1.16] Senecal, P. K., & Leach, F. (2019). Diversity in transportation: Why a mix of propulsion technologies is the way forward for the future fleet. Results in Engineering, 4, 100060
- [1.17] Reitz, R. D. (2013). Directions in internal combustion engine research. Combustion and Flame, 160(1), 1-8.
- [1.18] https://www.who.int/news-room/fact-sheets/detail/ambient-(outdoor)-air-quality-and-health
- [1.19] https://www.who.int/publications/i/item/9789240034228
- [1.20] https://www.who.int/teams/environment-climate-change-and-health/air-quality-and-health/health-impacts/types-of-pollutants
- [1.21] Yadav, N. K., Saxena, M. R., & Maurya, R. K. (2021). A review of toxicity analysis of particulate emissions from conventional and low-temperature combustion engines.
- [1.22] Pundir, B. P. (2017). Engine emissions: fundamentals and advances in control (No. 8278). Alpha Science International.
- [1.23] https://www.epa.gov/sites/default/files/2014-12/documents/rfd-final.pdf

- [1.24] Ristovski, Z. D., Miljevic, B., Surawski, N. C., Morawska, L., Fong, K. M., Goh, F., & Yang, I. A. (2012). Respiratory health effects of diesel particulate matter. Respirology, 17(2), 201-212.
- [1.25] https://monographs.iarc.who.int/agents-classified-by-the-iarc/
- [1.26] Heywood, J. B. (2018). Internal combustion engine fundamentals. McGraw-Hill Education.
- [1.27] Pundir, B. P. (2010). IC engines: Combustion and emissions.
- [1.28] Maurya, R. K. (2019). Reciprocating engine combustion diagnostics: In-Cylinder pressure measurement and analysis. Springer.
- [1.29] Diesel, R., 1892. "A process for producing motive work from the combustion of fuel", British Patent,GB189207241http://worldwide.espacenet.com/publicationDetails/biblio?CC=GB&NR=18920724 1A&KC=A&FT=D&ND=3&date=18921008&DB=worldwide.espacenet.com&locale=en_EP
- [1.30] Flynn, P., 2000. "Diesels—Promises and Issues", US DOE, 6th Diesel Emissions Reduction Workshop (DEER), San Diego, CA, USA, August 2000, https://www.osti.gov/biblio/827487
- [1.31] Maurya, R. K (2018). *Characteristics and control of low temperature combustion engines* (pp. 31-133). Cham, Switzerland: Springer.
- [1.32] Agarwal, A. K., Singh, A. P., & Maurya, R. K. (2017). Evolution, challenges and path forward for low temperature combustion engines. *Progress in energy and combustion science*, 61, 1-56.
- [1.33] Reitz, R. D., & Duraisamy, G. (2015). Review of high efficiency and clean reactivity controlled compression ignition (RCCI) combustion in internal combustion engines. *Progress in Energy and Combustion Science*, 46, 12-71.
- [1.34] Bae, C., & Kim, J. (2017). Alternative fuels for internal combustion engines. *Proceedings of the Combustion Institute*, 36(3), 3389-3413.
- [1.35] Bhandari, R., Trudewind, C. A., & Zapp, P. (2014). Life cycle assessment of hydrogen production via electrolysis—a review. *Journal of cleaner production*, 85, 151-163.
- [1.36] Doğan, O., Çelik, M. B., & Özdalyan, B. (2012). The effect of tire derived fuel/diesel fuel blends utilization on diesel engine performance and emissions. *Fuel*, *95*, 340-346.
- [1.37] Demirbas, A. (2008). Distillation properties of various diesel oils. *Energy Sources, Part A*, 30(16), 1484-1490.
- [1.38] Singal, S. K., Singh, I. P., Pandey, D. C., Runda, M. K., Semwal, P. B., & Gandhi, K. K. (1999). Fuel quality requirements for reduction of Diesel emissions (No. 1999-01-3592). SAE Technical Paper.
- [1.39] https://www.chevron.com/-/media/chevron/operations/documents/diesel-fuel-tech-review.pdf
- [1.40] Curran, H. J., Gaffuri, P., Pitz, W. J., & Westbrook, C. K. (1998). A comprehensive modeling study of n-heptane oxidation. *Combustion and flame*, *114*(1-2), 149-177.
- [1.41] https://afdc.energy.gov/fuels/properties
- [1.42] Curran, H. J., Gaffuri, P., Pitz, W. J., & Westbrook, C. K. (2002). A comprehensive modeling study of iso-octane oxidation. *Combustion and flame*, 129(3), 253-280.

- [1.43] Sarathy, S. M., Farooq, A., & Kalghatgi, G. T. (2018). Recent progress in gasoline surrogate fuels. *Progress in Energy and Combustion Science*, 65, 67-108.
- [1.44] https://afdc.energy.gov/fuels/emerging-methanol
- [1.45] Verhelst, S., Turner, J. W., Sileghem, L., & Vancoillie, J. (2019). Methanol as a fuel for internal combustion engines. *Progress in Energy and Combustion Science*, 70, 43-88.
- [1.46] Valera, H., & Agarwal, A. K. (2019). Methanol as an alternative fuel for diesel engines. *Methanol and the alternate fuel economy*, 9-33.
- [1.47] Wouters, C., Burkardt, P., Steeger, F., Fleischmann, M., & Pischinger, S. (2023). Comprehensive assessment of methanol as an alternative fuel for spark-ignition engines. *Fuel*, *340*, 127627.
- [1.48] Sarathy, S. M., Oßwald, P., Hansen, N., & Kohse-Höinghaus, K. (2014). Alcohol combustion chemistry. *Progress in energy and Combustion Science*, 44, 40-102.
- [1.49] Burke, U., Metcalfe, W. K., Burke, S. M., Heufer, K. A., Dagaut, P., & Curran, H. J. (2016). A detailed chemical kinetic modeling, ignition delay time and jet-stirred reactor study of methanol oxidation. *Combustion and Flame*, 165, 125-136.
- [1.50] Svensson, E., Li, C., Shamun, S., Johansson, B., Tuner, M., Perlman, C., ... & Mauss, F. (2016). *Potential levels of soot, NO x, HC and CO for methanol combustion* (No. 2016-01-0887). SAE Technical Paper.
- [1.51] Westbrook, C. K., & Dryer, F. L. (1979). Comprehensive mechanism for methanol oxidation. *Combustion Science and Technology*, 20(3-4), 125-140.
- [1.52] https://afdc.energy.gov/fuels/hydrogen
- [1.53] Hosseini, S. H., Tsolakis, A., Alagumalai, A., Mahian, O., Lam, S. S., Pan, J., ... & Aghbashlo, M. (2023). Use of hydrogen in dual-fuel diesel engines. *Progress in Energy and Combustion Science*, 98, 101100.
- [1.54] Nikolaidis, P., & Poullikkas, A. (2017). A comparative overview of hydrogen production processes. *Renewable and sustainable energy reviews*, 67, 597-611.
- [1.55] Shadidi, B., Najafi, G., & Yusaf, T. (2021). A review of hydrogen as a fuel in internal combustion engines. *Energies*, 14(19), 6209.
- [1.56] Stępień, Z. (2021). A comprehensive overview of hydrogen-fueled internal combustion engines: Achievements and future challenges. *Energies*, *14*(20), 6504.
- [1.57] Dong, C., Zhou, Q., Zhang, X., Zhao, Q., Xu, T., & Hui, S. E. (2010). Experimental study on the laminar flame speed of hydrogen/natural gas/air mixtures. *Frontiers of Chemical Engineering in China*, 4, 417-422.
- [1.58] Verhelst, S., & Wallner, T. (2009). Hydrogen-fueled internal combustion engines. *Progress in energy and combustion science*, *35*(6), 490-527.
- [1.59] Marinov, N. M., Westbrook, C. K., & Pitz, W. J. (1996). Detailed and global chemical kinetics model for hydrogen. *Transport phenomena in combustion*, *I*(118-129), 80.
- [1.60] Khair, M. K., & Majewsky, W. A. (2006). Diesel emissions and their control. SAE International.

- [1.61] Han, D., Ickes, A. M., Bohac, S. V., Huang, Z., & Assanis, D. N. (2012). HC and CO emissions of premixed low-temperature combustion fueled by blends of diesel and gasoline. *Fuel*, *99*, 13-19.
- [1.62] Liu, J., Zhang, X., Wang, T., Zhang, J., & Wang, H. (2015). Experimental and numerical study of the pollution formation in a diesel/CNG dual fuel engine. *Fuel*, *159*, 418-429.
- [1.63] Yadav, N. K., Saxena, M. R., & Maurya, R. K. (2024). Inhalation toxicity characterization of nanoparticle and carbonyl emission from conventional diesel and methanol/gasoline-diesel RCCI engine. *Fuel*, *366*, 131353.
- [1.64] Ashok, B. (Ed.). (2021). NOx Emission Control Technologies in Stationary and Automotive Internal Combustion Engines: Approaches Toward NOx Free Automobiles. Elsevier.
- [1.65] Zeldvich, Y. B. (1946). The oxidation of nitrogen in combustion and explosions. *J. Acta Physicochimica*, 21, 577.
- [1.66] Zel'dovich, I., Barenblatt, G. I., Librovich, V. B., & Makhviladze, G. M. (1985). Mathematical theory of combustion and explosions.
- [1.67] Bozzelli, J. W., & Dean, A. M. (1995). O+ NNH: A possible new route for NOx formation in flames. *International journal of chemical kinetics*, 27(11), 1097-1109.
- [1.68] Prado, G., Lahaye, J., & Haynes, B. S. (1983). Soot particle nucleation and agglomeration. In *Soot in combustion systems and its toxic properties* (pp. 145-161). Boston, MA: Springer US.
- [1.69] Lahaye, J., & Prado, G. (1974). Formation of carbon particles from a gas phase: Nucleation phenomenon. *Water, Air, and Soil Pollution*, *3*, 473-481.
- [1.70] Bockhorn, H. (Ed.). (2013). Soot formation in combustion: mechanisms and models (Vol. 59). Springer Science & Business Media.
- [1.71] Mohankumar, S., & Senthilkumar, P. (2017). Particulate matter formation and its control methodologies for diesel engine: A comprehensive review. *Renewable and Sustainable Energy Reviews*, 80, 1227-1238.
- [1.72] Williams, P. T., Andrews, G. E., & Bartle, K. D. (1987). The role of lubricating oil in diesel particulate and particulate PAH emissions. *SAE transactions*, 457-465.
- [1.73] Yilmaz, N., & Davis, S. M. (2016). Polycyclic aromatic hydrocarbon (PAH) formation in a diesel engine fueled with diesel, biodiesel and biodiesel/n-butanol blends. *Fuel*, 181, 729-740.
- [1.74] Rhead, M. M., & Hardy, S. A. (2003). The sources of polycyclic aromatic compounds in diesel engine emissions \(\precent \). Fuel, 82(4), 385-393.
- [1.75] Dong, X., Chang, Y., Niu, B., & Jia, M. (2020). Development of a practical reaction model of polycyclic aromatic hydrocarbon (PAH) formation and oxidation for diesel surrogate fuel. *Fuel*, 267, 117159.
- [1.76] Richter, H., & Howard, J. B. (2000). Formation of polycyclic aromatic hydrocarbons and their growth to soot—a review of chemical reaction pathways. *Progress in Energy and Combustion science*, 26(4-6), 565-608.

- [1.77] Rana, S., Saxena, M. R., & Maurya, R. K. (2022). A review on morphology, nanostructure, chemical composition, and number concentration of diesel particulate emissions. *Environmental Science and Pollution Research*, 29(11), 15432-15489.
- [1.78] Agarwal, A. K., & Krishnamoorthi, M. (2023). Review of morphological and chemical characteristics of particulates from compression ignition engines. *International Journal of Engine Research*, 24(7), 2807-2865.
- [1.79] Maricq, M. M. (2007). Chemical characterization of particulate emissions from diesel engines: A review. *Journal of Aerosol Science*, 38(11), 1079-1118.
- [1.80] Burtscher, H. (2005). Physical characterization of particulate emissions from diesel engines: a review. *Journal of Aerosol Science*, 36(7), 896-932.
- [1.81] Kittelson, D. B. (1998). Engines and nanoparticles: a review. *Journal of aerosol science*, 29(5-6), 575-588.
- [1.82] Dempsey, A., Curran, S., Storey, J., Eibl, M., Pihl, J., Prikhodko, V., ... & Parks, J. (2014). *Particulate matter characterization of reactivity controlled compression ignition (RCCI) on a light duty engine* (No. 2014-01-1596). SAE Technical Paper.
- [1.83] Shukla, P. C., Gupta, T., Labhsetwar, N. K., & Agarwal, A. K. (2017). Trace metals and ions in particulates emitted by biodiesel fuelled engine. *Fuel*, *188*, 603-609.
- [1.84] Trebs, I., Bohn, B., Ammann, C., Rummel, U., Blumthaler, M., Königstedt, R., ... & Andreae, M. O. (2009). Relationship between the NO 2 photolysis frequency and the solar global irradiance. *Atmospheric Measurement Techniques Discussions*, 2(4), 1537-1573.
- [1.85] Ji, X., Han, M., Yun, Y., Li, G., & Sang, N. (2015). Acute nitrogen dioxide (NO2) exposure enhances airway inflammation via modulating Th1/Th2 differentiation and activating JAK-STAT pathway. *Chemosphere*, 120, 722-728.
- [1.86] Depayras, S., Kondakova, T., Heipieper, H. J., Feuilloley, M. G., Orange, N., & Duclairoir-Poc, C. (2018). The hidden face of nitrogen oxides species: from toxic effects to potential cure. In *Emerging Pollutants-Some Strategies for the Quality Preservation of Our Environment*. IntechOpen.
- [1.87] Krzeszowiak, J., Stefanow, D., & Pawlas, K. (2016). The impact of particulate matter (PM) and nitric oxides (NOx) on human health and an analysis of selected sources accounting for their emission in Poland. *Medycyna Środowiskowa-Environmental Medicine*, 19(3), 7-15.
- [1.89] Laumbach, R. J., & Kipen, H. M. (2012). Respiratory health effects of air pollution: update on biomass smoke and traffic pollution. *Journal of allergy and clinical immunology*, 129(1), 3-11.
- [1.90] Resch, H., Zawinka, C., Weigert, G., Schmetterer, L., & Garhofer, G. (2005). Inhaled carbon monoxide increases retinal and choroidal blood flow in healthy humans. *Investigative ophthalmology & visual science*, 46(11), 4275-4280.
- [1.91] McFarland, R. A. (1970). The effects of exposure to small quantities of carbon monoxide on vision. *Annals of the New York Academy of Sciences*, 174(Art 1).
- [1.92] Schulte, J. H. (1963). Effects of mild carbon monoxide intoxication. *Archives of Environmental Health: An International Journal*, 7(5), 524-530.

- [1.93] Aronow, W. S. (1979). Effect of carbon monoxide on cardiovascular disease. *Preventive medicine*, 8(3), 271-278.
- [1.94] Haupt, D., Nord, K., Egebäck, K. E., & Ahlvik, P. (2004). *Hydrocarbons and aldehydes from a diesel engine running on ethanol and equipped with EGR, catalyst and DPF* (No. 2004-01-1882). SAE Technical Paper.
- [1.95] Park, M., Joo, H. S., Lee, K., Jang, M., Kim, S. D., Kim, I., ... & Park, K. (2018). Differential toxicities of fine particulate matters from various sources. *Scientific reports*, 8(1), 17007.
- [1.96] Lademann, J., Schaefer, H., Otberg, N., Teichmann, A., Blume-Peytavi, U., & Sterry, W. (2004). Penetration of microparticles into human skin. *Der Hautarzt*, 55, 1117-1119.
- [1.97] Vierkötter, A., & Krutmann, J. (2012). Environmental influences on skin aging and ethnic-specific manifestations. *Dermato-endocrinology*, 4(3), 227-231.
- [1.98] https://www.epa.gov/pm-pollution/particulate-matter-pm-basics.
- [1.99] Møller, P., Jacobsen, N. R., Folkmann, J. K., Danielsen, P. H., Mikkelsen, L., Hemmingsen, J. G., ... & Loft, S. (2010). Role of oxidative damage in toxicity of particulates. *Free radical research*, 44(1), 1-46.
- [1.100] https://microbiologyinfo.com/ames-test/
- [1.101] Ristovski, Z. D., Miljevic, B., Surawski, N. C., Morawska, L., Fong, K. M., Goh, F., & Yang, I. A. (2012). Respiratory health effects of diesel particulate matter. *Respirology*, *17*(2), 201-212.
- [1.102] Yu, C. P., Yoon, K. J., & Chen, Y. K. (1991). Retention modeling of diesel exhaust particles in rats and humans. *Journal of aerosol medicine*, 4(2), 79-115.
- [1.103] Nagar, J. K., Akolkar, A. B., & Kumar, R. (2014). A review on airborne particulate matter and its sources, chemical composition and impact on human respiratory system. *International Journal of Environmental Sciences*, 5(2), 447-463.
- [1.104] Alam, M. S., & Khan, A. (2020). The impact study of vehicular pollution on environment. *International Journal for Science and Advance Research in Technology*, 6(12), 30-37.
- [1.105] Yadav, N. K., Saxena, M. R., & Maurya, R. K. (2024). *Environmental and Cancer Risk Potential Assessment of Unregulated Emissions from Methanol-Diesel Dual Fuel RCCI Engine* (No. 2024-26-0152). SAE Technical Paper.
- [1.106] Lee, H., Calvin, K., Dasgupta, D., Krinner, G., Mukherji, A., Thorne, P., ... & Park, Y. (2023). IPCC, 2023: Climate Change 2023: Synthesis Report, Summary for Policymakers. Contribution of Working Groups I, II and III to the Sixth Assessment Report of the Intergovernmental Panel on Climate Change [Core Writing Team, H. Lee and J. Romero (eds.)]. IPCC, Geneva, Switzerland.
- [1.107] https://www.epa.gov/ghgemissions/sources-greenhouse-gas-emissions#:~:text=When%20considering%20only%20direct%20emissions,decreased%20by%20less%20than%201%25.
- [1.108] https://www.ipcc.ch/site/assets/uploads/2018/03/ipcc far wg I full report.pdf
- [1.109] Lightfoot, H. D., & Mamer, O. A. (2014). Calculation of atmospheric radiative forcing (warming effect) of carbon dioxide at any concentration. *Energy & environment*, 25(8), 1439-1454.

- [1.110] https://www.eea.europa.eu/publications/92-826-5409-5/page031new.html
- [1.111] Akinnawo, S. O. (2023). Eutrophication: Causes, consequences, physical, chemical and biological techniques for mitigation strategies. *Environmental Challenges*, *12*, 100733.
- [1.112] Bufalini, J. J., Walter, T. A., & Bufalini, M. M. (1976). Ozone formation potential of organic compounds. *Environmental Science & Technology*, 10(9), 908-912.
- [1.113] Verma, S., Yadava, P. K., Lal, D. M., Mall, R. K., Kumar, H., & Payra, S. (2021). Role of lightning NOx in ozone formation: A review. *Pure and Applied Geophysics*, *178*, 1425-1443.
- [1.114] https://www2.arb.ca.gov/resources/overview-diesel-exhaust-and-health#:~:text=Diesel%20Particulate%20Matter%20and%20Health&text=In%201998%2C%20CARB%20identified%20DPM,and%20other%20adverse%20health%20effects.
- [2.1] Curran, H. J., Gaffuri, P., Pitz, W. J., & Westbrook, C. K. (1998). A comprehensive modeling study of n-heptane oxidation. *Combustion and flame*, *114*(1-2), 149-177. https://doi.org/10.1016/S0010-2180(97)00282-4
- [2.2] Ferguson, C. R., & Kirkpatrick, A. T. (2015). *Internal combustion engines: applied thermosciences*. John Wiley & Sons.
- [2.3] Maurya, R. K., Maurya, L., & Luby. (2019). *Reciprocating engine combustion diagnostics*. Cham, Switzerland: Springer International Publishing.
- [2.4] Agarwal, A. K., Srivastava, D. K., Dhar, A., Maurya, R. K., Shukla, P. C., & Singh, A. P. (2013). Effect of fuel injection timing and pressure on combustion, emissions and performance characteristics of a single cylinder diesel engine. Fuel, 111, 374-383.
- [2.5] Panneerselvam, N., Murugesan, A., Vijayakumar, C., Kumaravel, A., Subramaniam, D., & Avinash, A. (2015). Effects of injection timing on bio-diesel fuelled engine characteristics—An overview. Renewable and Sustainable Energy Reviews, 50, 17-31.
- [2.6] Kook, S., Bae, C., Miles, P. C., Choi, D., & Pickett, L. M. (2005). The influence of charge dilution and injection timing on low-temperature diesel combustion and emissions. SAE transactions, 1575-1595.
- [2.7] Kook, S., Park, S., & Bae, C. (2008). Influence of early fuel injection timings on premixing and combustion in a diesel engine. Energy & Fuels, 22(1), 331-337.
- [2.8] Sharma, A., & Murugan, S. (2015). Combustion, performance and emission characteristics of a DI diesel engine fuelled with non-petroleum fuel: a study on the role of fuel injection timing. Journal of the Energy Institute, 88(4), 364-375.
- [2.9] Sazhina, E. M., Sazhin, S. S., Heikal, M. R., Babushok, V. I., & Johns, R. J. R. (2000). A detailed modelling of the spray ignition process in diesel engines. Combustion Science and Technology, 160(1), 317-344.
- [2.10] Cao, D. N., Hoang, A. T., Luu, H. Q., Bui, V. G., & Tran, T. T. H. (2020). Effects of injection pressure on the NOx and PM emission control of diesel engine: A review under the aspect of PCCI combustion condition. Energy Sources, Part A: Recovery, Utilization, and Environmental Effects, 1-18.

- [2.11] Dodge, L. G., Simescu, S., Neely, G. D., Maymar, M. J., Dickey, D. W., & Savonen, C. L. (2002). Effect of small holes and high injection pressures on diesel engine combustion (No. 2002-01-0494). SAE Technical Paper.
- [2.12] Roy, M. M. (2009). Effect of fuel injection timing and injection pressure on combustion and odorous emissions in DI diesel engines. Journal of Energy Resources Technology, 131(3).
- [2.13] Agarwal, A. K., Dhar, A., Gupta, J. G., Kim, W. I., Choi, K., Lee, C. S., & Park, S. (2015). Effect of fuel injection pressure and injection timing of Karanja biodiesel blends on fuel spray, engine performance, emissions and combustion characteristics. Energy Conversion and Management, 91, 302-314.
- [2.14] Agarwal, A. K., Srivastava, D. K., Dhar, A., Maurya, R. K., Shukla, P. C., & Singh, A. P. (2013). Effect of fuel injection timing and pressure on combustion, emissions and performance characteristics of a single cylinder diesel engine. *Fuel*, *111*, 374-383.
- [2.15] Saxena, M. R., Maurya, R. K., & Mishra, P. (2021). Assessment of performance, combustion and emissions characteristics of methanol-diesel dual-fuel compression ignition engine: A review. *Journal of Traffic and Transportation Engineering (English Edition)*, 8(5), 638-680.
- [2.16] Wang, L. J., Song, R. Z., Zou, H. B., Liu, S. H., & Zhou, L. B. (2008). Study on combustion characteristics of a methanol—diesel dual-fuel compression ignition engine. *Proceedings of the institution of mechanical engineers, Part D: Journal of automobile engineering, 222*(4), 619-627.
- [2.17] Ning, L., Duan, Q., Chen, Z., Kou, H., Liu, B., Yang, B., & Zeng, K. (2020). A comparative study on the combustion and emissions of a non-road common rail diesel engine fueled with primary alcohol fuels (methanol, ethanol, and n-butanol)/diesel dual fuel. *Fuel*, 266, 117034.
- [2.18] Sayin, C., Ozsezen, A. N., & Canakci, M. (2010). The influence of operating parameters on the performance and emissions of a DI diesel engine using methanol-blended-diesel fuel. *Fuel*, 89(7), 1407-1414.
- [2.19] Canakci, M., Sayin, C., & Gumus, M. (2008). Exhaust emissions and combustion characteristics of a direct injection (DI) diesel engine fueled with methanol— diesel fuel blends at different injection timings. *Energy & Fuels*, 22(6), 3709-3723.
- [2.20] Canakci, M., Sayin, C., Ozsezen, A. N., & Turkcan, A. (2009). Effect of injection pressure on the combustion, performance, and emission characteristics of a diesel engine fueled with methanol-blended diesel fuel. *Energy & Fuels*, 23(6), 2908-2920.
- [2.21] Ciniviz, M., Köse, H., Canli, E., & Solmaz, O. (2011). An experimental investigation on effects of methanol blended diesel fuels to engine performance and emissions of a diesel engine. *Scientific Research and Essays*, 6(15), 3189-3199.
- [2.22] Sayin, C., Ilhan, M., Canakci, M., & Gumus, M. (2009). Effect of injection timing on the exhaust emissions of a diesel engine using diesel–methanol blends. *Renewable energy*, 34(5), 1261-1269.
- [2.23] Chao, M. R., Lin, T. C., Chao, H. R., Chang, F. H., & Chen, C. B. (2001). Effects of methanol-containing additive on emission characteristics from a heavy-duty diesel engine. *Science of the Total Environment*, 279(1-3), 167-179.

- [2.24] Chu, W. (2008, August). The experimental study about the influence of methanol/diesel fuel mixture on diesel engine performance. In 2008 Workshop on Power Electronics and Intelligent Transportation System (pp. 324-327). IEEE.
- [2.25] Karabektas, M., Ergen, G., & Hosoz, M. (2013). Effects of the blends containing low ratios of alternative fuels on the performance and emission characteristics of a diesel engine. *Fuel*, *112*, 537-541.
- [2.26] Yazhe, L., Jian, W., Bin, X., & Zhihao, M. (2011, April). The influence of fuel supply angle on the combustion and emissions of methanol/diesel engine. In 2011 International Conference on Electric Information and Control Engineering (pp. 5510-5512). IEEE.
- [2.27] Xu, B., Liu, Y., Wu, J., Li, C., Shang, W., & Ma, Z. (2015, August). Performance and exhaust emissions of a turbocharged common rail DI diesel engine fueled with alcohol. In 2015 International Conference on Advanced Mechatronic Systems (ICAMechS) (pp. 5-9). IEEE.
- [2.28] Pan, W., Yao, C., Han, G., Wei, H., & Wang, Q. (2015). The impact of intake air temperature on performance and exhaust emissions of a diesel methanol dual fuel engine. *Fuel*, *162*, 101-110.
- [2.29] Wei, H., Yao, C., Pan, W., Han, G., Dou, Z., Wu, T., ... & Shi, J. (2017). Experimental investigations of the effects of pilot injection on combustion and gaseous emission characteristics of diesel/methanol dual fuel engine. *Fuel*, 188, 427-441.
- [2.30] Singh, A. P., Sharma, N., Satsangi, D. P., & Agarwal, A. K. (2020). Effect of fuel injection pressure and premixed ratio on mineral diesel-methanol fueled reactivity-controlled compression ignition mode combustion engine. *Journal of Energy Resources Technology*, 142(12), 122301.
- [2.31] Yadav, N. K., Saxena, M. R., & Maurya, R. K. (2024). *Environmental and Cancer Risk Potential Assessment of Unregulated Emissions from Methanol-Diesel Dual Fuel RCCI Engine* (No. 2024-26-0152). SAE Technical Paper.
- [2.32] McWilliam, L., & Megaritis, A. (2009). Experimental investigation of the effect of combined hydrogen and diesel combustion on the particulate size distribution from a high speed direct injection diesel engine. *International journal of vehicle design*, 50(1-4), 107-123.
- [2.33] Koten, H. (2018). Hydrogen effects on the diesel engine performance and emissions. *International journal of hydrogen energy*, 43(22), 10511-10519.
- [2.34] Karagöz, Y., Güler, İ., Sandalcı, T., Yüksek, L., & Dalkılıç, A. S. (2016). Effect of hydrogen enrichment on combustion characteristics, emissions and performance of a diesel engine. *International journal of hydrogen energy*, 41(1), 656-665.
- [2.35] Deb, M., Sastry, G. R. K., Bose, P. K., & Banerjee, R. (2015). An experimental study on combustion, performance and emission analysis of a single cylinder, 4-stroke DI-diesel engine using hydrogen in dual fuel mode of operation. *International journal of hydrogen energy*, 40(27), 8586-8598.
- [2.36] Dhole, A. E., Yarasu, R. B., Lata, D. B., & Baraskar, S. S. (2014). Mathematical modeling for the performance and emission parameters of dual fuel diesel engine using hydrogen as secondary fuel. *International Journal of Hydrogen Energy*, 39(24), 12991-13001.
- [2.37] Karagöz, Y., Sandalcı, T., Yüksek, L., & Dalkılıç, A. S. (2015). Engine performance and emission effects of diesel burns enriched by hydrogen on different engine loads. *International Journal of Hydrogen Energy*, 40(20), 6702-6713.

- [2.38] Varde, K. S., & Frame, G. A. (1983). Hydrogen aspiration in a direct injection type diesel engine-its effects on smoke and other engine performance parameters. *International Journal of Hydrogen Energy*, 8(7), 549-555.
- [2.39] Zhou, J. H., Cheung, C. S., Zhao, W. Z., & Leung, C. W. (2016). Diesel-hydrogen dual-fuel combustion and its impact on unregulated gaseous emissions and particulate emissions under different engine loads and engine speeds. *Energy*, *94*, 110-123.
- [2.40] Chinmaya, M., Anuj, P., Singh, T. V., & Naveen, K. (2013). Combustion, emission and performance characteristics of a light duty diesel engine fuelled with methanol diesel blends. *International Journal of Mechanical and Mechatronics Engineering*, 7(5), 791-801.
- [2.41] Guo, Z., Li, T., Dong, J., Chen, R., Xue, P., & Wei, X. (2011). Combustion and emission characteristics of blends of diesel fuel and methanol-to-diesel. *Fuel*, 90(3), 1305-1308.
- [2.42] Huang, Z. H., Lu, H. B., Jiang, D. M., Zeng, K., Liu, B., Zhang, J. Q., & Wang, X. B. (2004). Engine performance and emissions of a compression ignition engine operating on the diesel-methanol blends. *Proceedings of the Institution of Mechanical Engineers*, *Part D: Journal of Automobile Engineering*, 218(4), 435-447.
- [2.43] Karabektas, M., Ergen, G., & Hosoz, M. (2013). Effects of the blends containing low ratios of alternative fuels on the performance and emission characteristics of a diesel engine. *Fuel*, *112*, 537-541.
- [2.44] Premkartikkumar, S. R. (2015). Reducing oxides of nitrogen (NOx) emission of DI diesel engine using refrigerated methanol blend as a fuel. *International Journal of ChemTech Research*, 7(5), 2469-2473.
- [2.45] Zhou, J. H., Cheung, C. S., & Leung, C. W. (2014). Combustion, performance, regulated and unregulated emissions of a diesel engine with hydrogen addition. *Applied energy*, 126, 1-12.
- [2.46] Saravanan, N., Nagarajan, G., Kalaiselvan, K. M., & Dhanasekaran, C. (2008). An experimental investigation on hydrogen as a dual fuel for diesel engine system with exhaust gas recirculation technique. *Renewable Energy*, 33(3), 422-427.
- [2.47] Datta, A., & Mandal, B. K. (2016). Impact of alcohol addition to diesel on the performance combustion and emissions of a compression ignition engine. *Applied thermal engineering*, 98, 670-682.
- [2.48] Yasin, M. H. M., Mamat, R., Yusop, A. F., Aziz, A., & Najafi, G. (2015). Comparative study on biodiesel-methanol-diesel low proportion blends operating with a diesel engine. *Energy Procedia*, 75, 10-16
- [2.49] Yilmaz, N. (2012). Comparative analysis of biodiesel–ethanol–diesel and biodiesel–methanol–diesel blends in a diesel engine. *Energy*, 40(1), 210-213.
- [2.50] Masimalai, S. K. (2014). *Influence of methanol induction on performance, emission and combustion behavior of a methanol-diesel dual fuel engine* (No. 2014-01-1315). SAE Technical Paper.
- [2.51] Saxena, M. R., & Maurya, R. K. (2018). Effect of fuel injection strategy on nano-particle emissions from RCCI engine (No. 2018-01-1709). SAE Technical Paper.
- [2.52] Lu, H., Yao, A., Yao, C., Chen, C., & Wang, B. (2019). An investigation on the characteristics of and influence factors for NO2 formation in diesel/methanol dual fuel engine. *Fuel*, 235, 617-626.

- [2.53] Maiboom, A., Tauzia, X., & Hétet, J. F. (2008). Experimental study of various effects of exhaust gas recirculation (EGR) on combustion and emissions of an automotive direct injection diesel engine. *Energy*, 33(1), 22-34.
- [2.54] Yang, Z., Chu, C., Wang, L., & Huang, Y. (2015). Effects of H2 addition on combustion and exhaust emissions in a diesel engine. *Fuel*, *139*, 190-197.
- [2.55] Sandalcı, T., & Karagöz, Y. (2014). Experimental investigation of the combustion characteristics, emissions and performance of hydrogen port fuel injection in a diesel engine. *International journal of hydrogen energy*, 39(32), 18480-18489.
- [2.56] McWilliam, L., & Megaritis, A. (2009). Experimental investigation of the effect of combined hydrogen and diesel combustion on the particulate size distribution from a high speed direct injection diesel engine. *International journal of vehicle design*, 50(1-4), 107-123.
- [2.57] Verma, S., Kumar, K., Das, L. M., Kaushik, S. C., & Tyagi, S. K. (2019). Experimental analysis on the effect of hydrogen supply systems in a diesel dual fuel engine. *J. Energy Environ. Sustain*, 7, 59-62.
- [2.58] Saravanan, N., Nagarajan, G., Dhanasekaran, C., & Kalaiselvan, K. M. (2007). *Experimental investigation of hydrogen fuel injection in DI dual fuel diesel engine* (No. 2007-01-1465). SAE Technical Paper.
- [2.59] Saravanan, N., & Nagarajan, G. (2007). An experimental investigation on optimized manifold injection in a direct-injection diesel engine with various hydrogen flowrates. *Proceedings of the Institution of Mechanical Engineers, Part D: Journal of Automobile Engineering*, 221(12), 1575-1584.
- [2.60] Ahmadi, R., & Hosseini, S. M. (2018). Numerical investigation on adding/substituting hydrogen in the CDC and RCCI combustion in a heavy-duty engine. *Applied Energy*, 213, 450-468.
- [2.61] Dimitriou, P., Tsujimura, T., & Suzuki, Y. (2019). Low-load hydrogen-diesel dual-fuel engine operation—A combustion efficiency improvement approach. *International Journal of Hydrogen Energy*, 44(31), 17048-17060.
- [2.62] Yilmaz, I. T., & Gumus, M. E. T. İ. N. (2018). Effects of hydrogen addition to the intake air on performance and emissions of common rail diesel engine. *Energy*, *142*, 1104-1113.
- [2.63] Lapuerta, M., Martos, F. J., & Cárdenas, M. D. (2005). Determination of light extinction efficiency of diesel soot from smoke opacity measurements. *Measurement Science and Technology*, 16(10), 2048.
- [2.64] Pickett, L. M., & Siebers, D. L. (2004). Soot in diesel fuel jets: effects of ambient temperature, ambient density, and injection pressure. *Combustion and Flame*, 138(1-2), 114-135.
- [2.65] Schobert, H. H. (2013). The chemistry of hydrocarbon fuels. Butterworth-Heinemann.
- [2.66] An, H., Yang, W. M., Maghbouli, A., Li, J., Chou, S. K., & Chua, K. J. (2013). A numerical study on a hydrogen assisted diesel engine. *International journal of hydrogen energy*, 38(6), 2919-2928.
- [2.67] Koten, H. (2018). Hydrogen effects on the diesel engine performance and emissions. *International journal of hydrogen energy*, 43(22), 10511-10519.
- [2.68] Monemian, E., Cairns, A., Gilmore, M., Newman, D., & Scott, K. (2018). Evaluation of intake charge hydrogen enrichment in a heavy-duty diesel engine. *Proceedings of the Institution of Mechanical Engineers, Part D: Journal of Automobile Engineering*, 232(1), 139-147.

- [2.69] Talibi, M., Hellier, P., Balachandran, R., & Ladommatos, N. (2014). Effect of hydrogen-diesel fuel co-combustion on exhaust emissions with verification using an in-cylinder gas sampling technique. *International journal of hydrogen energy*, 39(27), 15088-15102.
- [2.70] Saravanan, N., & Nagarajan, G. (2009). Performance and emission study in manifold hydrogen injection with diesel as an ignition source for different start of injection. *Renewable Energy*, 34(1), 328-334.
- [2.71] Saravanan, N., & Nagarajan, G. (2010). Performance and emission studies on port injection of hydrogen with varied flow rates with Diesel as an ignition source. *Applied Energy*, 87(7), 2218-2229.
- [2.72] Ahlvik, P. J., & Brandberg, Å. R. (2000). Relative impact on environment and health from the introduction of low emission city buses in Sweden. SAE transactions, 1317-1333.
- [2.73] Oyama, K., & Kakegawa, T. (2000). Japan Clean Air Program-Step I Study of Diesel Vehicle and Fuel Influence on Emissions. SAE transactions, 1821-1847.
- [2.74] Takada, K., Yoshimura, F., Ohga, Y., Kusaka, J., & Daisho, Y. (2003). Experimental study on unregulated emission characteristics of turbocharged DI diesel engine with common rail fuel injection system (No. 2003-01-3158). SAE technical paper.
- [2.75] Haupt, D., Nord, K., Egebäck, K. E., & Ahlvik, P. (2004). Hydrocarbons and aldehydes from a diesel engine running on ethanol and equipped with EGR, catalyst and DPF (No. 2004-01-1882). SAE Technical Paper.
- [2.76] Merritt, P. M., Ulmet, V., McCormick, R. L., Mitchell, W. E., & Baumgard, K. J. (2005). Regulated and unregulated exhaust emissions comparison for three tier II non-road diesel engines operating on ethanol-diesel blends. SAE transactions, 1111-1122.
- [2.77] Natti, K. C., Bhattacharyya, A., Kastury, A., Henein, N. A., & Bryzik, W. (2007). An analysis of regulated and unregulated emissions in an HSDI diesel engine under the LTC regime (No. 2007-01-0905). SAE technical paper.
- [2.78] Ogawa, H., & Taga, F. (2009). Unregulated harmful substances in exhaust gas from diesel engines. SAE International Journal of Fuels and Lubricants, 2(1), 870-876.
- [2.79] Wang, X., Ge, Y., Liu, L., & Gong, H. (2015). Regulated, carbonyl emissions and particulate matter from a dual-fuel passenger car burning neat methanol and gasoline (No. 2015-01-1082). SAE Technical Paper.
- [2.80] Liu, J., Liu, Z., Wang, L., Wang, P., Sun, P., Ma, H., & Wu, P. (2022). Numerical simulation and experimental investigation on pollutant emissions characteristics of PODE/methanol dual-fuel combustion. Fuel Processing Technology, 231, 107228.
- [2.81] Arias, S., Botero, M. L., Molina, F., & Agudelo, J. R. (2022). Pentanol/diesel fuel blends: Assessment of inhalation cancer risk and ozone formation potential from carbonyl emissions emitted by an automotive diesel engine. Fuel, 321, 124054.
- [2.82] Saxena, M. R., & Maurya, R. K. (2020). Influence of direct injection timing and mass of port injected gasoline on unregulated and nano-particle emissions from RCCI engine. *Fuel*, 282, 118815.
- [2.83] Heywood, J. B. (1988). Internal combustion engine fundamentals.

- [2.84] Pundir, B. P. (2007). Engine emissions: pollutant formation and advances in control technology. Alpha Science International, Limited.
- [2.85] Agarwal, A. K., Sharma, N., Singh, A. P., Kumar, V., Satsangi, D. P., & Patel, C. (2019). Adaptation of methanol-dodecanol-diesel blend in diesel genset engine. *Journal of Energy Resources Technology*, 141(10), 102203.
- [2.86] Chen, C., Yao, A., Yao, C., Wang, B., Lu, H., Feng, J., & Feng, L. (2019). Study of the characteristics of PM and the correlation of soot and smoke opacity on the diesel methanol dual fuel engine. *Applied Thermal Engineering*, 148, 391-403.
- [2.87] Chen, H., Su, X., He, J., & Xie, B. (2019). Investigation on combustion and emission characteristics of a common rail diesel engine fueled with diesel/n-pentanol/methanol blends. *Energy*, *167*, 297-311.
- [2.88] Geng, P., Yao, C., Wei, L., Liu, J., Wang, Q., Pan, W., & Wang, J. (2014). Reduction of PM emissions from a heavy-duty diesel engine with diesel/methanol dual fuel. *Fuel*, *123*, 1-11.
- [2.89] Saxena, M. R., & Maurya, R. K. (2017). Effect of premixing ratio, injection timing and compression ratio on nano particle emissions from dual fuel non-road compression ignition engine fueled with gasoline/methanol (port injection) and diesel (direct injection). *Fuel*, 203, 894-914.
- [2.90] Storey, J. M., Curran, S. J., Lewis, S. A., Barone, T. L., Dempsey, A. B., Moses-DeBusk, M., ... & Northrop, W. F. (2017). Evolution and current understanding of physicochemical characterization of particulate matter from reactivity controlled compression ignition combustion on a multicylinder light-duty engine. *International Journal of Engine Research*, 18(5-6), 505-519.
- [2.91] de Souza, C. V., & Corrêa, S. M. (2016). Polycyclic aromatic hydrocarbons in diesel emission, diesel fuel and lubricant oil. *Fuel*, *185*, 925-931.
- [2.92] Lim, M. C., Ayoko, G. A., Morawska, L., Ristovski, Z. D., & Jayaratne, E. R. (2005). Effect of fuel composition and engine operating conditions on polycyclic aromatic hydrocarbon emissions from a fleet of heavy-duty diesel buses. *Atmospheric Environment*, 39(40), 7836-7848.
- [2.93] Mi, H. H., Lee, W. J., Chen, C. B., Yang, H. H., & Wu, S. J. (2000). Effect of fuel aromatic content on PAH emission from a heavy-duty diesel engine. *Chemosphere*, 41(11), 1783-1790.
- [2.94] Alkurdi, F., Karabet, F., & Dimashki, M. (2013). Characterization, concentrations and emission rates of polycyclic aromatic hydrocarbons in the exhaust emissions from in-service vehicles in Damascus. *Atmospheric Research*, 120, 68-77.
- [2.95] Alves, C. A., Barbosa, C., Rocha, S., Calvo, A., Nunes, T., Cerqueira, M., ... & Querol, X. (2015). Elements and polycyclic aromatic hydrocarbons in exhaust particles emitted by light-duty vehicles. *Environmental science and pollution research*, 22, 11526-11542.
- [2.96] Kweon, C. B., Okada, S., Foster, D. E., Bae, M. S., & Schauer, J. J. (2003). Effect of engine operating conditions on particle-phase organic compounds in engine exhaust of a heavy-duty direct-injection (DI) diesel engine. *SAE transactions*, 460-476.
- [2.97] Hu, S., Herner, J. D., Robertson, W., Kobayashi, R., Chang, M. C. O., Huang, S. M., ... & Ayala, A. (2013). Emissions of polycyclic aromatic hydrocarbons (PAHs) and nitro-PAHs from heavy-duty diesel vehicles with DPF and SCR. *Journal of the Air & Waste Management Association*, 63(8), 984-996.

- [2.98] Zhang, Z. H., Cheung, C. S., Chan, T. L., & Yao, C. D. (2011). Experimental study on particulate emissions of a methanol furnigated diesel engine equipped with diesel oxidation catalyst. *Aerosol Science and Technology*, 45(2), 262-271.
- [2.99] Shukla, P. C., Gupta, T., Labhsetwar, N. K., & Agarwal, A. K. (2017). Trace metals and ions in particulates emitted by biodiesel fuelled engine. *Fuel*, *188*, 603-609.
- [2.100] Cheung, K.L., Ntziachristos, L., Tzamkiozis, T., Schauer, J.J.et al., "Emissions of Particulate Trace Elements, Metals and Organic Species from Gasoline, Diesel, and Biodiesel Passenger Vehicles and Their Relation to Oxidative Potential," Aerosol Science and Technology 44(7):500-513, 2010.
- [2.101] Verma, V., Shafer, M.M., Schauer, J.J., and Sioutas, C., "Contribution of Transition Metals in the Reactive OxygenSpecies Activity of PM Emissions from Retrofitted Heavy Duty Vehicles," Atmospheric Environment 44(39):5165-5173, 2010.
- [2.102] Wang, Y.F., Huang, K.L., Li, C.T., Mi, H.H. et al., "Emissionsof Fuel Metals Content from a Diesel Vehicle Engine," Atmospheric Environment 37(33):4637-4643, 2003.
- [2.103] Maurya, R. K., & Agarwal, A. K. (2014). Particulate morphology and toxicity of an alcohol fuelled HCCI engine. *SAE International Journal of Fuels and Lubricants*, 7(1), 323-336.
- [2.104] Yadav, N. K., Saxena, M. R., & Maurya, R. K. (2021). A review of toxicity analysis of particulate emissions from conventional and low-temperature combustion engines.
- [2.105] Park, M., Joo, H. S., Lee, K., Jang, M., Kim, S. D., Kim, I., ... & Park, K. (2018). Differential toxicities of fine particulate matters from various sources. *Scientific reports*, 8(1), 17007.
- [2.106] Lademann, J., Schaefer, H., Otberg, N., Teichmann, A., Blume-Peytavi, U., & Sterry, W. (2004). Penetration of microparticles into human skin. *Der Hautarzt*, 55, 1117-1119.
- [2.107] Vierkötter, A., & Krutmann, J. (2012). Environmental influences on skin aging and ethnic-specific manifestations. *Dermato-endocrinology*, 4(3), 227-231.
- [2.108] https://www.epa.gov/pm-pollution/particulate-matter-pmbasics.
- [2.109] Puri, P., Nandar, S. K., Kathuria, S., & Ramesh, V. (2017). Effects of air pollution on the skin: A review. *Indian journal of dermatology, venereology and leprology*, 83, 415.
- [2.110] Møller, P., Jacobsen, N. R., Folkmann, J. K., Danielsen, P. H., Mikkelsen, L., Hemmingsen, J. G., ... & Loft, S. (2010). Role of oxidative damage in toxicity of particulates. *Free radical research*, 44(1), 1-46.
- [2.111] Wu, W., Graves, L.M., Jaspers, I., Devlin, R.B. et al., "Activation of the EGF Receptor Signaling Pathway in Human Airway Epithelial Cells Exposed to Metals," American Journal of Physiology-Lung Cellular and Molecular Physiology 277(5):L924-L931, 1999
- [2.112] Smith, K. R., & Aust, A. E. (1997). Mobilization of iron from urban particulates leads to generation of reactive oxygen species in vitro and induction of ferritin synthesis in human lung epithelial cells. *Chemical research in toxicology*, 10(7), 828-834.
- [2.113] Smith, K. R., & Aust, A. E. (1997). Mobilization of iron from urban particulates leads to generation of reactive oxygen species in vitro and induction of ferritin synthesis in human lung epithelial cells. *Chemical research in toxicology*, 10(7), 828-834.

- [2.114] Ris, C. (2007). US EPA health assessment for diesel engine exhaust: a review. *Inhalation toxicology*, 19(sup1), 229-239.
- [2.115] Maynard, A. D., & Aitken, R. J. (2007). Assessing exposure to airborne nanomaterials: current abilities and future requirements. *Nanotoxicology*, *I*(1), 26-41.
- [2.116] Knaapen, A. M., Borm, P. J., Albrecht, C., & Schins, R. P. (2004). Inhaled particles and lung cancer. Part A: Mechanisms. *International journal of cancer*, *109*(6), 799-809.
- [2.117] Seagrave, J., McDonald, J. D., Gigliotti, A. P., Nikula, K. J., Seilkop, S. K., Gurevich, M., & Mauderly, J. L. (2002). Mutagenicity and in vivo toxicity of combined particulate and semivolatile organic fractions of gasoline and diesel engine emissions. *Toxicological Sciences*, 70(2), 212-226.
- [2.118] Seagrave, J., Mauderly, J. L., & Seilkop, S. K. (2003). In vitro relative toxicity screening of combined particulate and semivolatile organic fractions of gasoline and diesel engine emissions. *Journal of Toxicology and Environmental Health, Part A*, 66(12), 1113-1132.
- [2.119] Seagrave, J., Knall, C., McDonald, J. D., & Mauderly, J. L. (2004). Diesel particulate material binds and concentrates a proinflammatory cytokine that causes neutrophil migration. *Inhalation toxicology*, *16*(sup1), 93-98.
- [2.120] McDonald, J. D., Harrod, K. S., Seagrave, J., Seilkop, S. K., & Mauderly, J. L. (2004). Effects of low sulfur fuel and a catalyzed particle trap on the composition and toxicity of diesel emissions. *Environmental health perspectives*, 112(13), 1307-1312.
- [2.121] McDonald, J. D., Eide, I., Seagrave, J., Zielinska, B., Whitney, K., Lawson, D. R., & Mauderly, J. L. (2004). Relationship between composition and toxicity of motor vehicle emission samples. *Environmental Health Perspectives*, *112*(15), 1527-1538.
- [2.122] Seagrave, J., McDonald, J. D., & Mauderly, J. L. (2005). In vitro versus in vivo exposure to combustion emissions. *Experimental and Toxicologic Pathology*, 57, 233-238.
- [2.123] Seagrave, J., Dunaway, S., McDonald, J. D., Mauderly, J. L., Hayden, P., & Stidley, C. (2007). Responses of differentiated primary human lung epithelial cells to exposure to diesel exhaust at an air-liquid interface. *Experimental lung research*, 33(1), 27-51.
- [2.124] McDonald, J. D., Reed, M. D., Campen, M. J., Barrett, E. G., Seagrave, J., & Mauderly, J. L. (2007). Health effects of inhaled gasoline engine emissions. *Inhalation toxicology*, *19*(sup1), 107-116.
- [2.125] Agarwal, A. K., Singh, A. P., Gupta, T., Agarwal, R. A., Sharma, N., Rajput, P., ... & Ateeq, B. (2018). Mutagenicity and cytotoxicity of particulate matter emitted from biodiesel-fueled engines. *Environmental science & technology*, 52(24), 14496-14507.
- [2.126] Calabrese, E. J., Moore, G. S., Guisti, R. A., Rowan, C. A., & Schulz, E. N. (1981). A review of human health effects associated with exposure to diesel fuel exhaust. *Environment International*, 5(4-6), 473-477.
- [2.127] Yu CP and Xu GB. (1986) Predictive Models for Deposition of Diesel Exhaust Particulates in Human and Rat Lungs. Aerosol Sci Technol. 5 3337-347
- [2.128] Yu CP and Xu GB (1987) Predictive models for deposition of inhaled diesel exhaust particles in humans and laboratory species. Res Rep Health Eff Inst: (10):3-22

- [2.129] Yu, C. P., Yoon, K. J., & Chen, Y. K. (1991). Retention modeling of diesel exhaust particles in rats and humans. *Journal of aerosol medicine*, 4(2), 79-115.
- [2.130] Gradon L, Pratsinis SE., Podgorski A, Scott SJ and Panda S (1996). Modeling retention of inhaled particles in rat lungs including toxic and overloading effects. J. Aerosol Sci., 27(3), 487-503
- [2.131] Brown JS, Wilson WE, Grant LD (2005) Dosimetric comparisons of particle deposition and retention in rats and humans. Inhal Toxicol. 17(7-8):355-85
- [2.132] Penconek A and Moskal A (2013) Deposition of diesel exhaust particles from various fuels in a cast of human respiratory system under two breathing patterns. J. Aerosol Sci. 63, 48-59.
- [2.133] Rissler J, Swietlicki E, Bengtsson A, Boman C, Pagels J, Sandström T and Löndahl J. (2012) Experimental determination of deposition of diesel exhaust particles in the human respiratory tract. J. Aerosol Sci., 48, 18-33.
- [2.134] Oravisjärvi K, Pietikäinen M., Ruuskanen J, Niemi S, Laurén M, Voutilainen A and Rautio A (2014). Diesel particle composition after exhaust after-treatment of an off-road diesel engine and modeling of deposition into the human lung. J. Aerosol Sci. 69, 32-47
- [2.135] Sturm R. (2017). Deposition of diesel exhaust particles in the human lungs: theoretical simulations and experimental data. J Public Health Emerg.
- [2.136] Daniel S, Phillippi D, Schneider LJ, Nguyen KN, Mirpuri J, and Lund AK (2021). Exposure to diesel exhaust particles results in altered lung microbial profiles, associated with increased reactive oxygen species/reactive nitrogen species and inflammation, in C57Bl/6 wildtype mice on a high-fat diet. Part Fibre Toxicol 18, 3
- [3.1] Heywood, J. B. (2018). Internal combustion engine fundamentals. McGraw-Hill Education
- [3.2] Gatowski, J. A., Balles, E. N., Chun, K. M., Nelson, F. E., Ekchian, J. A., & Heywood, J. B. (1984). Heat release analysis of engine pressure data. SAE transactions, 961-977.
- [3.3] Hohenberg, G. F. (1979). Advanced approaches for heat transfer calculations. SAE Transactions, 2788-2806
- [3.4] Cambustion Ltd. (2015). DMS 500 User Manual, Version 4.04.
- [3.5] https://www.avl.com/en-in/testing-solutions/all-testing-products-and-software/emission-analysis-and-measurement/avl-sesam-i60
- [3.6] Heller, B., Klingenberg, H., Lach, G., & Winckler, J. (1990). Performance of a new system for emission sampling and measurement (SESAM). SAE transactions, 126-136.
- [3.7] Funkenbusch, E. F., Leddy, D. G., & Johnson, J. H. (1979). The characterization of the soluble organic fraction of diesel particulate matter. *SAE Transactions*, 1540-1560.
- [3.8] Mouli, P. C., Mohan, S. V., Balaram, V., Kumar, M. P., & Reddy, S. J. (2006). A study on trace elemental composition of atmospheric aerosols at a semi-arid urban site using ICP-MS technique. *Atmospheric Environment*, 40(1), 136-146.
- [3.9] Chawla, V., Sharma, S., & Singh, Y. (2023). Yttrium Oxide Nanoparticle-Loaded, Self-Assembled Peptide Gel with Antibacterial, Anti-Inflammatory, and Proangiogenic Properties for Wound Healing. *ACS Biomaterials Science & Engineering*, 9(5), 2647-2662.

- [3.10] Andrews, A. W., Thibault, L. H., & Lijinsky, W. (1978). The relationship between carcinogenicity and mutagenicity of some polynuclear hydrocarbons. *Mutation Research/Fundamental and Molecular Mechanisms of Mutagenesis*, 51(3), 311-318.
- [3.11] U.S. EPA. Integrated Risk Information System US EPA. Environ Prot Agency 2018. https://www.epa.gov/iris (accessed October 14, 2021)
- [3.12] Rousseau, M. C., Straif, K., & Siemiatycki, J. (2005). IARC carcinogen update. *Environmental Health Perspectives*, 113(9), A580-A581.
- [3.13] Means, B. (1989). Risk-assessment guidance for superfund. Volume 1. Human health evaluation manual. Part A. Interim report (Final) (No. PB-90-155581/XAB; EPA-540/1-89/002). Environmental Protection Agency, Washington, DC (USA)
- [3.14] U.S. EPA. Integrated Risk Information System US EPA. Environ Prot Agency 2018
- [3.15] Błaszczyk, E., Rogula-Kozłowska, W., Klejnowski, K., Fulara, I., & Mielżyńska-Švach, D. (2017). Polycyclic aromatic hydrocarbons bound to outdoor and indoor airborne particles (PM2. 5) and their mutagenicity and carcinogenicity in Silesian kindergartens, Poland. Air Quality, Atmosphere & Health, 10(3), 389-400.
- [3.16] Yu CP and Yoon KJ (1991) Retention modeling of diesel exhaust particles in rats and humans. Res Rep Health Eff Inst.;(40):1-24. PMID: 1716915
- [3.17] Yu CP and Xu GB (1987) Predictive models for deposition of inhaled diesel exhaust particles in humans and laboratory species. Res Rep Health Eff Inst: (10):3-22
- [3.18] Stocker, T., Plattner, G. K., & Dahe, Q. (2014, May). IPCC climate change 2013: the physical science basis-findings and lessons learned. In EGU general assembly conference abstracts (p. 17003).
- [3.19] Vallero, D. A. (2019). Air pollution calculations: Quantifying pollutant formation, transport, transformation, fate and risks. Elsevier.
- [3.20] National Research Council. (1999). Ozone-forming potential of reformulated gasoline. National Academies Press.
- [3.21] Carter, W. P. (2009). Updated maximum incremental reactivity scale and hydrocarbon bin reactivities for regulatory applications. California Air Resources Board Contract, 339, 2009.
- [3.22] Arias, S., Botero, M. L., Molina, F., & Agudelo, J. R. (2022). Pentanol/diesel fuel blends: Assessment of inhalation cancer risk and ozone formation potential from carbonyl emissions emitted by an automotive diesel engine. *Fuel*, 321, 124054
- [3.23] Yoshikawa, T., & Reitz, R. D. (2009). Validation of a grid independent spray model and fuel chemistry mechanism for low temperature diesel combustion. *International Journal of Spray and Combustion Dynamics*, 1(3), 283-316.
- [3.24] Ansys, 2019, ANSYS ® Forte. Release 2019 R3. Forte Theory, Ansys Inc., Canonsburg, PA.
- [3.25] DESIGNS, M. E. (2011). Chemkin-pro. Ansys.
- [3.26] Beale, J. C., & Reitz, R. D. (1999). Modelling spray atomization with the Kelvin-Helmholtz/Rayleigh-Taylor hybrid model. Atomization and sprays, 9(6).

- [3.27] Abani, N., & Reitz, R. D. (2007). Unsteady turbulent round jets and vortex motion. Physics of Fluids, 19(12), 125102.
- [3.28] Abani, N., Munnannur, A., & Reitz, R. D. (2007, January). Reduction of numerical parameter dependencies in diesel spray models. In Internal Combustion Engine Division Fall Technical Conference (Vol. 48116, pp. 163-174).
- [3.29] Hou, S., & Schmidt, D. P. (2006). Adaptive collision meshing and satellite droplet formation in spray simulations. International Journal of Multiphase Flow, 32(8), 935-956
- [3.30] Ra, Y., & Reitz, R. D. (2009). A vaporization model for discrete multi-component fuel sprays. International Journal of Multiphase Flow, 35(2), 101-117.
- [3.31] Han, Z., & Reitz, R. D. (1997). A temperature wall function formulation for variable-density turbulent flows with application to engine convective heat transfer modeling. International journal of heat and mass transfer, 40(3), 613-625.
- [3.32] Yakhot, V., & Orszag, S. A. (1986). Renormalization group analysis of turbulence. I. Basic theory. Journal of scientific computing, 1(1), 3-51.
- [3.33] Han, Z., & Reitz, R. D. (1995). Turbulence modeling of internal combustion engines using RNG κ - ϵ models. Combustion science and technology, 106(4-6), 267-295.
- [3.34] Kong, S. C., Han, Z., & Reitz, R. D. (1995). The development and application of a diesel ignition and combustion model for multidimensional engine simulation. SAE transactions, 502-518.
- [3.35] Singh, S., Reitz, R., and Musculus, M., "Comparison of the Characteristic Time (CTC), Representative Interactive Flamelet (RIF), and Direct Integration with Detailed Chemistry Combustion Models against Optical Diagnostic Data for Multi-Mode Combustion in a Heavy-Duty DI Diesel Engine," SAE Technical Paper -01-0055, 2006
- [3.36] Musculus, M. P., Dec, J. E., & Tree, D. R. (2002). Effects of fuel parameters and diffusion flame lift-off on soot formation in a heavy-duty DI diesel engine. SAE Transactions, 1467-1489.
- [3.37] Gainey, B., Longtin, J. P., & Lawler, B. (2019). A guide to uncertainty quantification for experimental engine research and heat release analysis. SAE International Journal of Engines, 12(5), 509-290.
- [3.38] Petitpas, G., McNenly, M. J., & Whitesides, R. A. (2017). A framework for quantifying measurement uncertainties and uncertainty propagation in HCCI/LTGC engine experiments. SAE International Journal of Engines, 10(3), 1275-1296.
- [3.39] Maurya, R. K., & Agarwal, A. K. (2013). Investigations on the effect of measurement errors on estimated combustion and performance parameters in HCCI combustion engine. Measurement, 46(1), 80-88.
- [3.40] Holmén, B. A., & Qu, Y. (2004). Uncertainty in particle number modal analysis during transient operation of compressed natural gas, diesel, and trap-equipped diesel transit buses. Environmental science & technology, 38(8), 2413-2423.
- [3.41] Giechaskiel, B., Lähde, T., Melas, A. D., Valverde, V., & Clairotte, M. (2021). Uncertainty of laboratory and portable solid particle number systems for regulatory measurements of vehicle emissions. Environmental Research, 197, 111068.

- [3.42] Hall, D. E., Stradling, R. J., Zemroch, P. J., Rickeard, D. J., Mann, N., Heinze, P., ... & Szendefi, J. (2000). Measurement of the number and size distribution of particle emissions from heavy duty engines (No. 2000-01-2000). SAE Technical Paper.
- [3.43] Saxena MR and Maurya RK (2017) Effect of premixing ratio, injection timing and compression ratio on nano particle emissions from dual fuel non-road compression ignition engine fueled with gasoline/methanol (port injection) and diesel (direct injection). Fuel, 203, 894-914
- [4.1] Verhelst, Sebastian, James WG Turner, Louis Sileghem, and Jeroen Vancoillie. "Methanol as a fuel for internal combustion engines." *Progress in Energy and Combustion Science* 70 (2019): 43-88.
- [4.2] Bejan, A. (2016). Advanced engineering thermodynamics. John Wiley & Sons.
- [4.3] Anderson, J. E., Kramer, U., Mueller, S. A., & Wallington, T. J. (2010). Octane numbers of ethanol–and methanol– gasoline blends estimated from molar concentrations. *Energy & Fuels*, 24(12), 6576-6585.
- [4.4] Agarwal, A. K., Srivastava, D. K., Dhar, A., Maurya, R. K., Shukla, P. C., & Singh, A. P. (2013). Effect of fuel injection timing and pressure on combustion, emissions and performance characteristics of a single cylinder diesel engine. *Fuel*, *111*, 374-383.
- [4.5] Westbrook, C. K., & Dryer, F. L. (1979). Comprehensive mechanism for methanol oxidation. *Combustion Science and Technology*, 20(3-4), 125-140.
- [4.6] Sarathy, S. M., Oßwald, P., Hansen, N., & Kohse-Höinghaus, K. (2014). Alcohol combustion chemistry. *Progress in energy and Combustion Science*, 44, 40-102